LANDSCAPE CONTROLS ON SEDIMENT SUPPLY AND STREAM CHANNEL MORPHO-DYNAMICS IN THE NORTHERN ROCKY MOUNTAINS

by

ERICH RAYMOND MUELLER

B.S., University of Wisconsin, 2000

M.A., University of Colorado, 2002

A thesis submitted to the

Faculty of the Graduate School of the

University of Colorado in partial fulfillment

of the requirement for the degree of

Doctor of Philosophy

Department of Geography

2012

This thesis entitled:
Landscape controls on sediment supply and stream channel morpho-dynamics in the northern Rocky Mountains
written by Erich Raymond Mueller
has been approved for the Department of Geography

____
John Pitlick

____
Jonathan M. Nelson

Date_________________

The final copy of this thesis has been examined by the signatories, and we find that both the content and the form meet acceptable presentation standards of scholarly work in the above mentioned discipline.

Abstract

Mueller, Erich Raymond (Ph.D. Geography)

Landscape controls on sediment supply and stream channel morpho-dynamics in the northern Rocky Mountains

Thesis directed by Professor John Pitlick

Quantifying landscape variations in sediment supply to streams and rivers is fundamental to our understanding of both denudational processes and stream channel morpho-dynamics. Previous studies have linked a variety of sediment supply proxies to climatic, topographic or geologic factors, but few have connected these directly to the characteristics of fluvial systems draining these landscapes. Using measurements of water and sediment fluxes for over 80 basins in the northern Rocky Mountains, USA, it is shown that the sediment supply signal is dominated by basin lithology, while exhibiting little correlation to factors such as relief, mean basin slope, and drainage density. Bankfull sediment concentrations (bed load and suspended load) increase as much 100-fold as basin lithology becomes dominated by softer sedimentary and volcanic rocks, at the expense of more resistant lithologies.

Downstream hydraulic geometry relations for single-thread reaches in these basins are remarkably similar and reasonably well predicted based on a channel forming Shields number; yet this simple model cannot capture the 2-3 order of magnitude range in sediment flux for a given discharge. In these streams the difference in the magnitude of bed load flux is modulated regionally by changes in bed armoring, resulting in a non-unique Shields number for a given channel configuration. As a result, single-thread reaches can absorb a wide range in sediment concentration, but at very high concentrations, bed surface, subsurface and bed load grain sizes converge and a transition from single-thread to to braided channel patterns is commonly observed. A physically-based sediment concentration braiding – single-thread discriminant function is derived and tested using the empirical data, appropriately classifying 50 of 53 pattern types. Flow modeling shows that 2-dimensional variability in flow properties in braided reaches may become equal to or dominate over changes in slope in response to high sediment supply. The resilience of single-thread channels to morphologic change thus reflects the degree to which textural changes can modulate variations in sediment supply, and a transition to a braided planform likely represents a dynamic equilibrium form in the face of high sediment supply.

Acknowledgements

First and foremost I would like to thank my advisor John Pitlick. John has always encouraged me to pursue my own interests in the field, while providing excellent direction, advice, and resources; this has led to the successful completion of both my Master's and Ph.D. degrees. My idea for a dissertation five years ago was quite wide-ranging, and despite grizzlies, wolves, and relentless rain (and snow), John always came to the field and was paramount in shaping the data collection process. The success of this work would not have occurred without John's discerning guidance during all phases of the project, and I look forward to future collaborations along some remote western river. Jon Nelson served on both by Master's and Doctoral committees, and my career has been forwarded by his continued guidance and support. The rest of my committee – Bob Anderson, Suzanne Anderson, and Greg Tucker – have been inspirations as teachers and researchers and I greatly appreciate their insight on this work.

Field work for this study would not have been possible without the help and good attitudes of several individuals (in alphabetical order): Wade Grewe, Jason Hoefer, Tony LaGreca, John Schrader, Mike Smith, Derek Weller, and Aaron Zettler-Mann. Rich McDonald and Paul Kinzel provided useful insight on modeling using iRIC. Access for this research was generously provided by a variety of agencies: Sawtooth National Forest/Recreation Area, Salmon-Challis National Forest, Bridger-Teton National Forest, Shoshone National Forest, Grand Teton National Park, and John D. Rockefeller National Parkway. And an extra thanks to Wyoming Fish and Game for keeping us up to date on the grizzly status at Sunlight Creek. The Department of Geography has provided funding for many years during my Master's and Ph.D. work, and for that I am extremely appreciative. Funding for field work was provided from a variety of sources: a Geological Society of America graduate student research grant, a CU-

Boulder Beverly Sears graduate student grant, the CU-Geography Gary Gaile Graduate Fellowship, the CU-Geography Gilbert F. White Fellowship, and two CU-Boulder UROP Grants.

Finally, I would like to thank my friends and family for support over the years. Jordan Clayton, Tony LaGreca, Catalina Segura, and Don Rosenberry have been great colleagues in the Pitlick lab. Mike Smith, thanks for driving to Idaho to identify rocks – it seems to have been worthwhile. My mom and dad, Don and Sue, have always encouraged (and often funded) my geological exploits and continued schooling; thank you so much for all the years of love and support. To my brother Craig, next time please offer to fund the trip to Patagonia when it is not the final semester of my dissertation. And let us not forget the dogs: Sequoia (RIP) – loyal companion and gravel-bed stream enthusiast; Sierra (RIP) – three-legged muse and archetype of perseverance; and Cody – the up-and-comer. Last, I would like to thank my beautiful and wonderful wife Megan for years of encouragement, especially over these last few months. You are a model for hard work and dedication, while maintaining incredibly good spirits, and I am deeply grateful for your love and presence in my life.

Table of Contents

List of Figures

Introduction

Chapter 1

Chapter 2

Chapter 3

Chapter 4

List of Tables

Chapter 1

Chapter 2

Chapter 3

Chapter 4

INTRODUCTION

Downstream changes in channel morphology result from the physical adjustment of streams and rivers to an imposed water and sediment supply. While the water supply component of the problem is easily measured and tightly coupled to climate, there is less agreement as to what controls sediment supply. The influences of climate, geology, and topographic relief are likely important, but the true variability as a function of these parameters is unclear – particularly for the bed load component of the supply. A full understanding of natural variability in channel form and pattern is thus limited by the lack of measured sediment transport rates (e.g. Parker et al., 2008). For example, hydraulic geometry relations coupling downstream changes in discharge to channel dimensions (Leopold and Maddock, 1953) tend to be relatively invariant over a wide range of climate and physiography (Knighton, 1998), masking what are likely significant differences in supply. Yet stream channels also exhibit threshold behavior (Schumm, 1979), and multi-threaded braided patterns are common in some settings. The controls on this transition from single-thread to braided are not entirely clear, but the importance of sediment supply on channel pattern is somewhat implicit as braided reaches are often considered to convey high bed loads. However, no quantitative estimate of a sediment supply braiding threshold has been proposed, largely due to the lack of data to test any such threshold. As a result, channel pattern is typically discriminated based on more easily-measured channel properties (e.g. Leopold and Wolman, 1957; Eaton et al., 2010), which often act as surrogates for sediment transport capacity (e.g. slope, grain size).

The basic problem is shown in Figure I.1, where different landscapes are expected to deliver different sediment (size and quantity) and water loads due to climate and physiography. At any point in the stream network, both the quantity and composition of the sediment flux will be influenced by upstream erosion, transport, and abrasion processes conditioned by the basin architecture. The morphology and sedimentology of the channels draining these landscapes should therefore reflect these basin-conditioned processes, and in some cases may result in changes in channel planform. From a downstream hydraulic geometry perspective, the scaling relation between discharge (Q) and sediment load (Q_s) – reflecting how a watershed has organized to deliver sediment downstream (Parker et al., 2008) – represents a fundamental constraint for predicting changes in width, depth or slope.

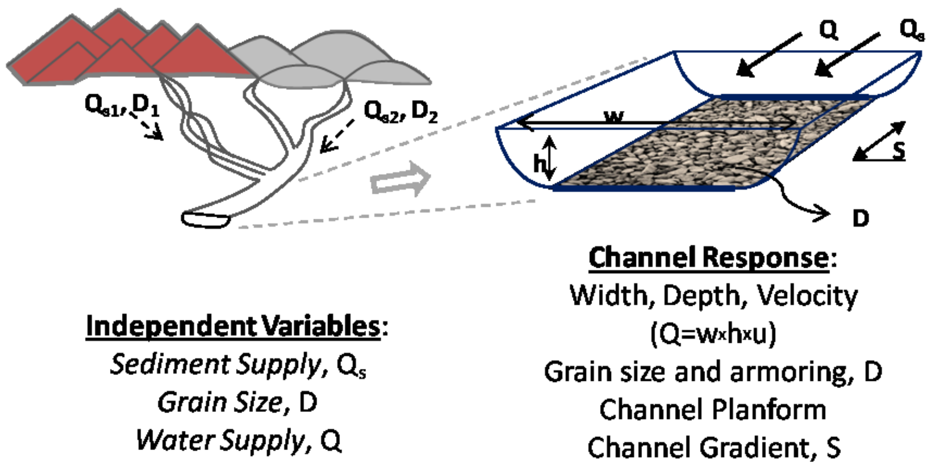

Figure I.1. Cartoon illustrating relationship between landscape conditioned independent variables and adjustable components of the fluvial system.

The generality of downstream hydraulic geometry relations reported in the literature masks potentially wide variation in sediment supply, indicating that simple adjustments of width or depth may not be indicative of actual differences in sediment transport rates. For example, sediment supply has been shown to exert a strong control on the degree of stream bed armoring in flume and field studies (Dietrich et al., 1989; Buffington and Montgomery, 1999; Eaton and Church, 2009). Without consideration of sediment textures the relation between sediment transport and channel geometry is somewhat obscured, largely due to the sensitivity of transport to small changes in transport intensity. Expressed as the ratio between the shear stress, τ, and some reference stress near the threshold for motion, τ_r, sediment transport is a strong non-linear function of transport intensity in typical formulations (e.g. Parker, 1979; Wilcock and Crowe, 2003). A decrease in surface grain size (or armoring) likely leads to a reduction in τ_r due to reduced hiding effects, decreased bed roughness, and the inherent higher mobility of smaller grains (Kirchner et al., 1990). As a result, surface textural changes and attendant hydraulic modifications may regulate significant variations in sediment loads – either spatially between streams or within a given reach in response to sediment perturbations.

While single-thread channels appear to be relatively resilient to a fairly wide range in sediment supply, there must be some limit at which changes in bed armoring can no longer accommodate increasing supply. Figure I.2 shows potential textural and morphologic adjustments across a sediment supply spectrum. In this simple conceptual model, single-thread reaches respond to changes in supply solely through changes in bed armoring, altering the reach-averaged transport intensity. But at some supply rate armoring is exhausted and a transition to a braided channel pattern occurs; at this point, spatial variability in shear stress may come to dominate the transport signal. This also suggests that braided channels convey higher sediment

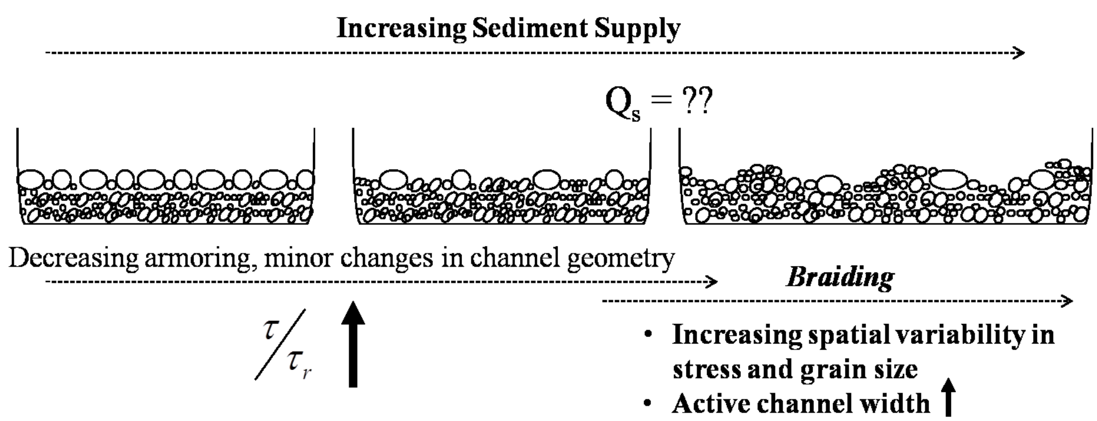

Figure I.2. Potential changes in channel morphology as a function of sediment supply loads for a given discharge, and, in multi-thread channels, several authors have proposed that greater lateral variance in shear stress and transport intensity enhances sediment transport (e.g. Paola, 1996; Nicholas, 2003). This provides a physical explanation for a supply-driven braiding threshold, but little insight into the exact nature of this threshold given the limited data on sediment transport rates. Nevertheless, braided streams may represent a pseudo-equilibrium channel form in the face of high sediment supply (Leopold and Wolman, 1957; Carson, 1984a), where dynamic channel change maintains zones of enhanced transport.

OVERVIEW

Several research questions emerge from the above considerations:

1) What are the physiographic controls on regional sediment supply?
2) How do bed and suspended load fluxes evolve downstream, and is this consistent with watershed-scale sediment delivery and abrasion processes?
3) Can the observed scaling between discharge and sediment flux be linked in a physically-based way to downstream changes in hydraulic geometry?
4) How do channels regulate regional variations in supply, and, in particular, what drives a transition to a dynamic braided channel pattern?

Using a unique data set on bed load and suspended sediment transport rates in the Rocky Mountains of Idaho and Wyoming and focused regional field studies, the research presented herein attempts to bridge the gap between physiographic controls on landscape scale variations in sediment supply and associated morphologic response of streams and rivers. This work is presented in four related components. First, the physiographic and climatic controls on regional variations in sediment supply are investigated through a GIS analysis for over 80 watersheds.

These data place the regional variations in hydraulic geometry and channel pattern within a sediment supply context. Then, in Chapter 2, a simple erosion-abrasion model is developed for two adjacent watersheds and tested using measurements of bed sediment size and lithology. In this case, sediment is input downstream from tributaries and hillslopes, conditioned by basin lithology, and modified by abrasion during downstream transport. This offers insight both on the degree of hillslope-channel coupling in these basins as well as how local differences in rock type influence the observed sediment flux. Additionally, this model provides a physical linkage between watershed-scale sediment delivery and the downstream evolution of bed and suspended loads, and can be compared to the independent empirical results below.

In Chapter 3, I present the measured downstream scaling patterns between discharge and both bed and suspended load sediment fluxes. A physically-based hydraulic geometry formulation based on a channel-forming Shields number is compared to observed channel geometry and sediment load scaling relations. These downstream scaling relations are then considered in terms of regional sediment delivery patterns using the results from the erosion-abrasion model in Chapter 2 as a guide. Both the regional analysis and a paired-watershed study highlight bed armoring as vital to modulating 2-3 orders of magnitude in bed load transport.

Finally, Chapter 4 focuses on braided channel development in the context of sediment supply, using the Yellowstone region – and the relatively common occurrence of braided streams in this region of the Rocky Mountains – as a natural experiment. This work can be broken into two related components: 1) a regional analysis discriminating channel patterns using physically-based braiding criteria, and presenting for the first time a sediment concentration discriminant function; 2) a detailed analysis in the Sunlight Creek basin addressing the geomorphic controls on longitudinal pattern changes, in addition to flow and sediment transport modeling between reach types. The goal of this chapter is to link large scale controls on braided channel occurrence to associated changes in flow and sediment transport dynamics at the reach scale.

Chapter 1 - Landscape controls on sediment supply and channel pattern: northern Rocky Mountains, USA

SUMMARY

Quantifying landscape variations in sediment supply to streams and rivers is fundamental to our understanding of both denudational processes and stream channel morpho-dynamics. Previous studies have linked a variety of sediment supply proxies to climatic, topographic or geologic factors (Schumm, 1967; Ahnert, 1970; Schaller et al., 2001; Montgomery and Brandon, 2002; Aalto et al., 2006; Moon et al., 2011; Portenga and Bierman, 2011), but few have connected these directly to the characteristics of fluvial systems draining these landscapes. Here we correlate landscape controls on sediment supply to observed sedimentology and channel patterns through direct measurements of water and sediment fluxes for over 80 basins in the northern Rocky Mountains, USA. These data show that the signal of sediment supply is dominated by basin lithology, while exhibiting little correlation to factors such as relief, mean basin slope, and drainage density. Bankfull sediment concentrations (bed load and suspended load) increase as much 100-fold as basin lithology becomes dominated by softer sedimentary and volcanic rocks, at the expense of more resistant lithologies. As sediment concentrations increase, stream beds become less armored, and bed load grain size coarsens. At very high concentrations, bed surface, subsurface and bed load grain sizes converge and a transition from single-thread to to braided channel patterns is commonly observed.

INTRODUCTION

Stream channels function to convey both sediment and water from the landscape, and while the water supply component of the problem is easily measured, spatial variability in sediment supply is often poorly constrained. It is generally accepted that climate exerts the dominant control on water supply, however, there is no consensus on what controls sediment supply. Climate is likely important here as well (Moon et al., 2011; Portenga and Bierman, 2011), but the influences of geology and topographic relief could be equally important. Indeed, topographic indices such as relief and hillslope angle have been linked to enhanced denudation and sediment yields in numerous studies (Schumm, 1967; Ahnert, 1970; Schaller et al., 2001; Montgomery and Brandon, 2002; Aalto et al., 2006), though not uniformly (Matmon et al, 2003; von Blanckenburg, 2006). Additionally, several authors have shown a clear relationship between lithology and sediment fluxes through cosmogenic radionuclide (CRN) analyses (Schaller et al., 2001; Morel et al., 2003; Portenga and Bierman, 2011), sedimentary basin modeling and stratigraphy (Tucker and Slingerland, 1996; Carroll et al., 2006), and sediment transport measurements (Aalto et al., 2006; Ryan, 2007; Syvitski and Milliman, 2007). Importantly, none of the above examples correlating landscape characteristics to sediment production explicitly address the delivery of coarse sediment (bed load) and its effect on stream channel morphology. From both theoretical and practical perspectives, quantifying the relation between sediment supply and channel morphology represents one of the biggest challenges in attempting to predict channel behavior.

STUDY AREA AND METHODS

In this study, we focus on contemporary sediment supply through the analysis of suspended and bed load transport measurements made at 83 sites in the northern Rocky Mountains (Figure1.1; Supplementary Table S1.1). Streams in this region exhibit a snowmelt-dominated hydrograph, and bankfull flow is highly correlated with the 1.5-yr flood (Castro and

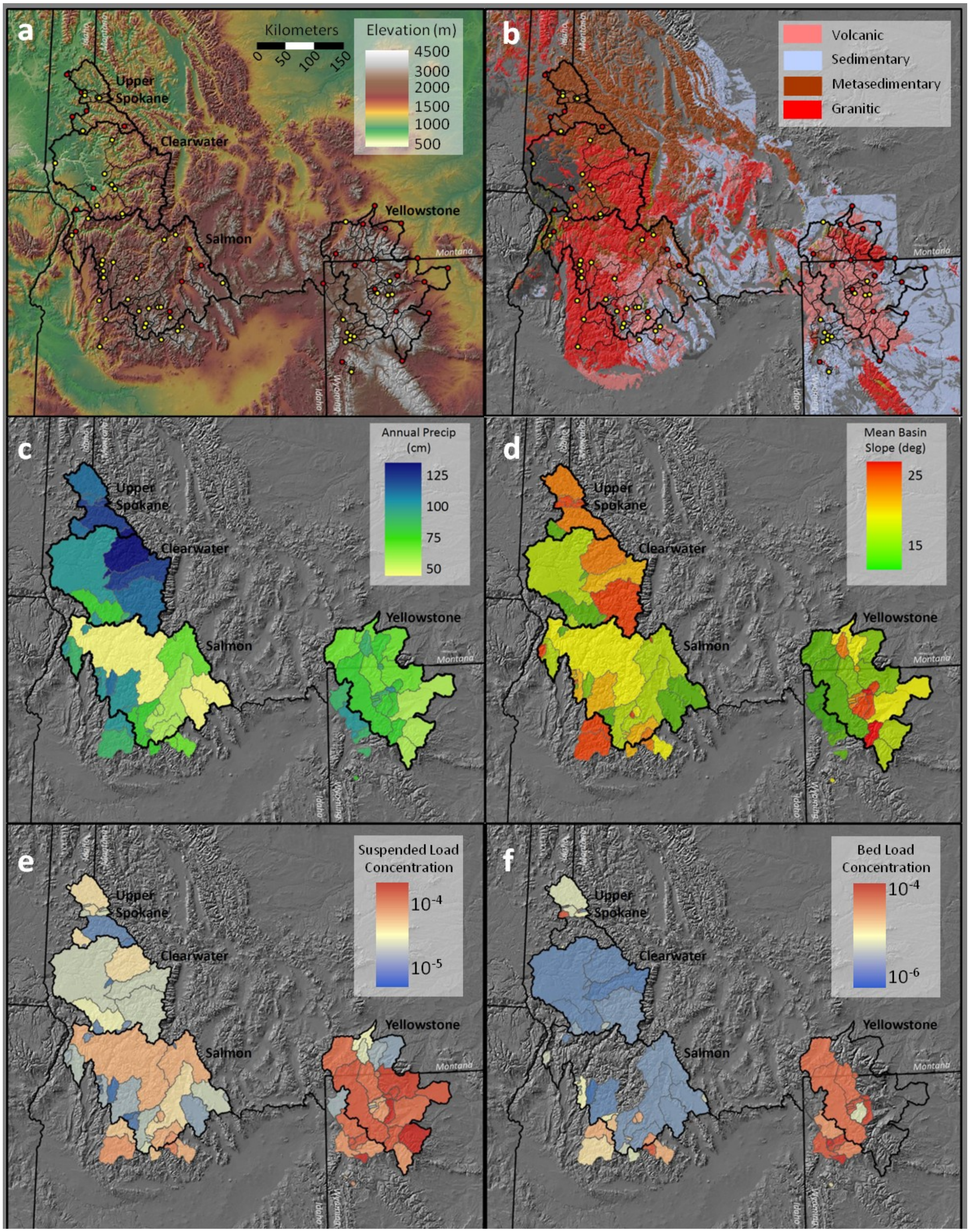

Figure 1.1. Map of study sites in Idaho, Wyoming, and Montana. Yellow dots indicate locations of bed and suspended load data, and red dots only suspended load. Watersheds draining to major river basins are outlined in bold. **a**) Elevation; **b**) Simplified geologic map; Study basins color-coded by **c**) Annual Precipitation; **d**) Mean Slope; **e**) suspended load concentration; **f**) Study basins color-coded by bed load concentration.

Jackson, 2001; King et al, 2004). In order to isolate landscape characteristics from climate, we estimate bankfull bed load and suspended load concentrations for each site as the ratio of the volumetric sediment discharge to the water discharge at bankfull: $Q_{s,bf}/Q_{bf}$. Normalizing the bankfull transport rate by the bankfull flow results in a dimensionless number (concentration) that very simply expresses the fundamental balance between sediment and water crucial to the form of a given stream reach (see Supplemental Discussion).

Bankfull flow was determined through field measurements or as the 1.5 year flood where field measurements were unavailable. In a few cases where hydrologic records were insufficient, bankfull discharge was calculated via a regional relation. In order to compute bankfull bed and suspended load concentrations, coupled measurements of flow and sediment transport from a variety of sources were used to develop discharge-transport relations (Table S1.1, Figure S1.1). A power-law equation fit to these data was used to compute the bankfull transport rate if it provided a good fit, and in some cases low flow data (<25% bankfull) were eliminated in order to give greater weight to measurements made at higher discharges. In several cases, the bankfull transport rate was chosen by eye as the central value of near-bankfull measurements (Figure S1.1).

Grain size data were obtained from a variety of sources (Supplementary Table S1.1), including field data by the authors. Surface grain size distributions were determined by pebble counts of 100 or more particles (Wolman, 1954). Subsurface size distributions were obtained through bulk sampling of the stream substrate, where the surface layer has been removed (Church et al., 2007). Bankfull bed load grain size was determined as the mean size of all samples collected within 25% of bankfull discharge. In cases where this criterion was not met, the mean bed load size of the two largest discharges was used.

In order to explore the influence of landscape properties on regional sediment concentrations, landscape metrics were determined from GIS analysis of 30-m digital elevation models (DEMs) of the study basins. 10-m DEMs were available but the added resolution did not change the results when tested, and greatly increased processing time. Basin slope was calculated as the average of all grid cells, where the slope of each cell was calculated as the steepest drop using a 3x3 cell window (Figure 1.1d). Relief ratio is calculated as total relief scaled by mean distance to the basin outlet. In these cases, the basin slope parameter shows a wider range and tends to reflect the steeper portions of the landscape (as each cell is defined by the maximum drop), whereas the relief ratio is more indicative of overall basin steepness. Drainage density was determined using the highest resolution hydrography from the National Hydrologic Data set equivalent to 1:24,000 scale maps, and mean annual precipitation was calculated for each basin using the PRISM data set (Figure 1.1c). See Supplementary Table S1.1 for data and sources.

Basin lithology was simplified from detailed digital geologic maps (Figure 1.1b) (Green and Drouillard, 1994; Zeinteck et al., 2005). Within each basin, rock types were lumped into four major groups – granitic, metasedimentary, volcanic, and sedimentary – broadly reflecting a change from harder to softer rock types. Basins consisting of ≥75% of a single rock type were assigned that rock type, otherwise they were simply designated “mixed”. Granitic rocks consist primarily of coarse-grained igneous rocks associated with the Idaho Batholith and other plutonic rocks, but include some Precambrian crystalline metamorphic rocks (e.g. basement rocks of the Beartooth Plateau). The meta-sedimentary category is almost singularly associated with the Belt Supergroup that makes up much of northern Idaho and western Montana. These rocks are weakly metamorphosed argillites and quartzites that retain their original bedding, but are relatively hard. Volcanic rocks here refer to extrusive rocks (volcaniclastic, rhyolite, andesite, ash flows, etc) associated with major eruptive centers which produced the Challis, Absaroka and Yellowstone volcanic fields. Sedimentary rocks are generally Paleozoic formations ranging from shale to sandstone and limestone, but including younger unconsolidated material. Large-scale basalt flows (e.g. Columbia River basalts) were treated separately but are significant in only two instances, and those watersheds are "mixed" regardless. Surficial deposits were ignored and basin lithology was based on the proportions solely of bedrock geology. For the purposes of this study volcanic and sedimentary rocks behaved similarly and were lumped so as to increase the sample size of these soft rock landscapes. Rock types broadly transition from predominantly metasedimentary in northern Idaho, to granitic rocks of the Idaho Batholith, south and east to Paleozoic sedimentary lithologies, and finally to the volcanic rocks of the Yellowstone region (Figure 1.1). See Supplementary Discussion for more detail on the lithology of the major river basins.

Study sites cover a range in geologic structures, including the Northern Rockies fold and thrust belt, the Idaho Batholith, Laramide uplifts, and volcanic terranes from the Eocene Challis to the Yellowstone caldera. The result is diverse, though locally consistent, variations in topography and lithology that provide an ideal opportunity to explore landscape drivers of sediment supply (Figure 1.1). Modern topography has largely resulted from late Cenozoic erosional exhumation due to downcutting of mainstem rivers (Meyer and Leidecker, 1999; Dethier, 2001) and sculpting by Quaternary glaciations (Pierce, 2003). Much of the topography in central and northern Idaho is dominated by deeply incised canyons separated by rugged but relatively low elevation mountains. Topography in the southeast portion of the Salmon River basin, as well as portions of the Yellowstone region, is influenced by Basin and Range faulting which has broken up the landscape into block-faulted mountain ranges with wide valleys. The

Yellowstone volcanic center has locally swelled the crust, enhancing relief in adjacent ranges such as the Absaroka Mountains (Pierce and Morgan, 1992).

RESULTS

Landscape Controls on Sediment Supply

Our basin-wide estimates of bed load and suspended load concentration follow a clear trend from consistently high values of ~10^{-4} in the Yellowstone region to lower values of 10^{-5} – 10^{-6} in the major river basins of central and northern Idaho (Figure 1.1e-f). Relations between drainage area, discharge, and relief ratio are consistent across these basins (Figure 1.2) and suggest that the climate and topography of the region are relatively homogeneous. However, stratifying these data by sediment concentration does not reveal the expected trend wherein sediment loads decrease with increasing drainage area (Syvitski and Milliman, 2007) or increase

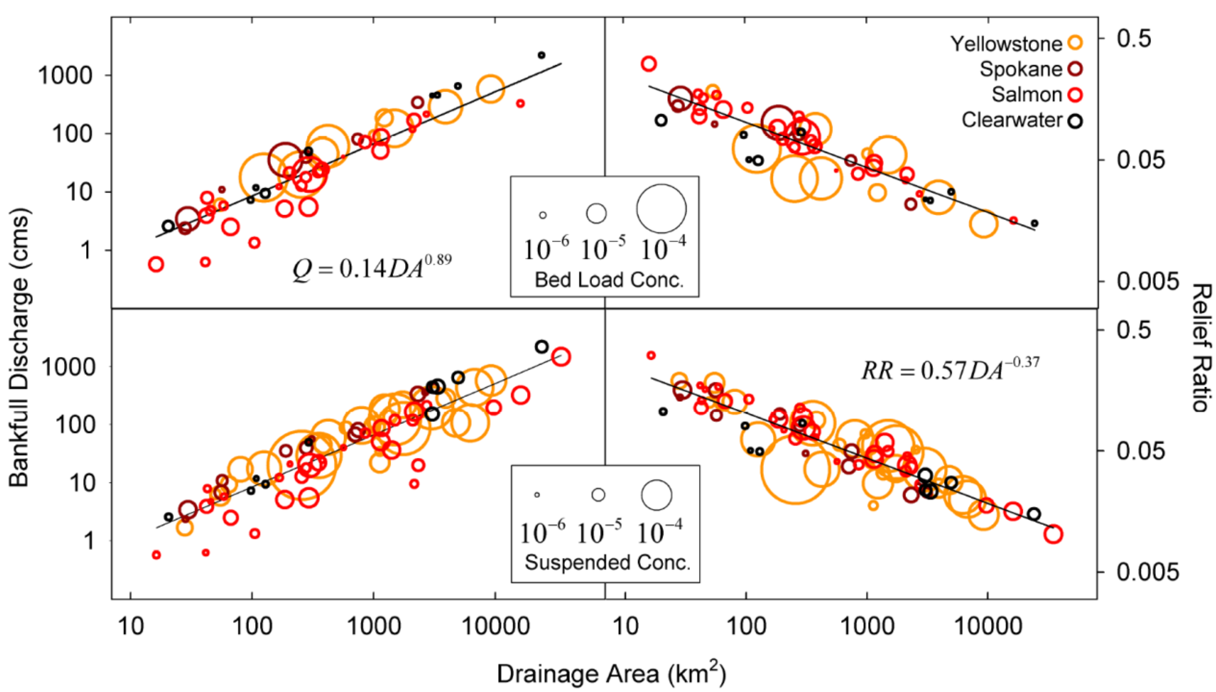

Figure 1.2. Drainage area versus discharge (left) and relief ratio (right) where colors represent different drainage basins from Figure 1. The size of each point is scaled to the bed load concentration (top) and the suspended load concentration (bottom).

with increasing relief ratio (Schumm, 1963; Ahnert, 1970). Rivers with high and low sediment concentrations are scattered somewhat randomly throughout the data set. In fact, some of the highest sediment concentrations ($Q_{s,bf}/Q_{bf} \approx 10^{-4}$) occur in some of the largest basins with some of the lowest relief (Figure 1.2).

Figure 1.3 shows a series of box plots comparing sediment concentrations for different categories of (a) mean basin slope, (b) annual precipitation, (c) drainage density, (d) relief ratio, and (e) rock type. The first of these plots (Figure 1.3a) shows that there is essentially no correlation between sediment concentration and mean basin slope, despite a range in slope from 6 to 28 degrees (Table 1.2); separating the data by rock type does not improve the correlation (Supplementary Figure S1.2). Similarly, we find that annual precipitation shows little systematic correlation with sediment concentration, although this may be expected given the inherent scaling between precipitation, water discharge and sediment concentration (Figure 1.3b). Precipitation does vary from north to south across the region, primarily because of the trajectories of maritime air masses (Figure 1.1c), but in this case the net effect of storm tracks is to produce the highest amounts of precipitation in the lowest elevation mountains of northern Idaho. Precipitation in the higher-elevation mountain ranges of central Idaho and northwest Wyoming is consistently lower and does not appear to be a principal driver of variations in sediment supply. Further, measures of landscape dissection such as relief ratio or drainage density show no distinct relation with sediment concentration (Figure 1.3c-d).

Ultimately, sediment concentration is most strongly correlated to basin lithology (Figure 1.3e), and where annual sediment yields and erosion rates could be calculated, a nearly identical trend is evident (Supplementary Figure S1.3). Between these individual rock types, relief ratio and drainage density are quite similar, and differences in slope and precipitation between

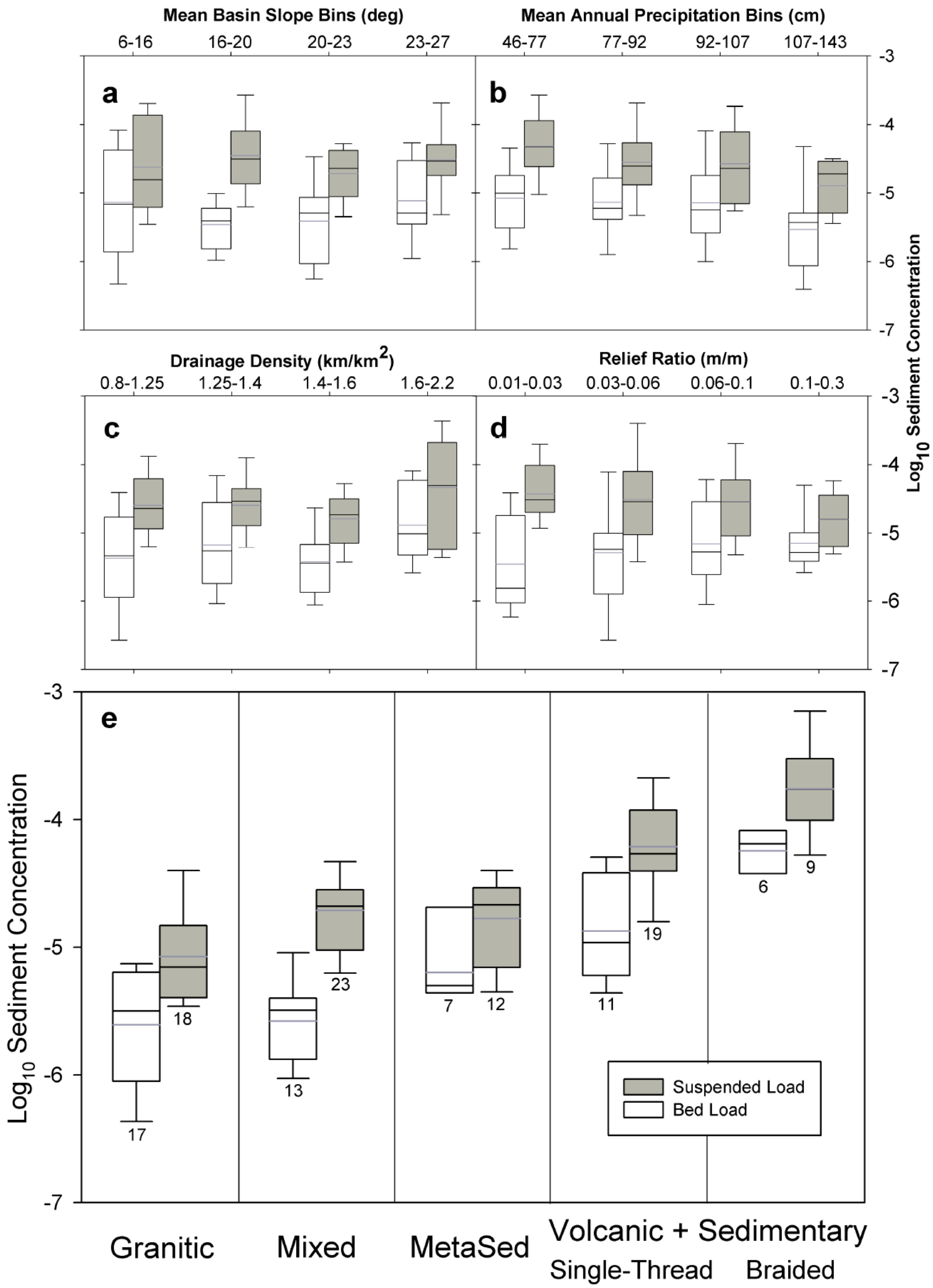

Figure 1.3. Box plots of sediment concentration for four equal-quantity bins of basin slope (**a**), mean annual precipitation (**b**), drainage density (**c**), and relief ratio (**d**) defined by the quartiles of the distribution. **e**) Box plots showing the variation in sediment concentration across different rock types. Braided and single-thread reaches are separated in the sedimentary/volcanic data. Box plots show the 10^{th}, 25^{th}, 50^{th}, 75^{th}, and 90^{th} percentiles (of the log-transformed data), the gray line is the mean, and sample size is listed below each plot for the rock type data.

Suspended Load	Slope (deg) 6-16	16-20	20-23
6-16	---		
16-20	0.84	---	
20-23	0.59	0.08	---
23-27	0.6	0.7	0.16

Suspended Load	Precip (cm) 46-77	77-92	92-107
46-77	---		
77-92	0.16	---	
92-107	0.16	0.9	---
107-143	0.0002	0.024	0.06

Bed Load	Slope (deg) 6-16	16-20	20-23
6-16	---		
16-20	0.22	---	
20-23	0.36	0.82	---
23-27	0.93	0.08	0.2

Bed Load	Precip (cm) 46-77	77-92	92-107
46-77	---		
77-92	0.78	---	
92-107	0.77	0.98	---
107-143	0.09	0.15	0.09

Table 1.1. Significance testing (t-tests) of differences between population means for log-transformed sediment concentration data grouped by slope (top) and precipitation (bottom) bins defined by the 25th, 50th, and 75th percentiles of the distributions. Dark pink areas are significant at p<0.05, light pink at p<0.10, and white are not significant. Numbers are the individual p values.

Suspended Load	Granitic	Mixed	MetaSed	Sed + Volc (S-T)
Granitic	---			
Mixed	0.003	---		
MetaSed	0.035	0.61	---	
Sed + Volc (All)	<0.00001	<0.00001	<0.00001	
Sed + Volc (S-T)	<0.00001	0.0001	0.0002	---
Sed + Volc (Braided)	<0.00001	<0.00001	<0.00001	0.0054

Bed Load	Granitic	Mixed	MetaSed	Sed + Volc (S-T)
Granitic	---			
Mixed	0.86	---		
MetaSed	0.083	0.064	---	
Sed + Volc (All)	<0.00001	<0.00001	0.017	
Sed + Volc (S-T)	0.003	<0.00001	0.15	---
Sed + Volc (Braided)	<0.00001	<0.00001	0.0017	0.0021

Table 1.2. Significance testing (t-tests) of differences between population means for log-transformed sediment concentration data. Dark pink areas are significant at p<0.05, light pink at p<0.10, and white are not significant. (S-T = single-thread). Numbers are the individual p values.

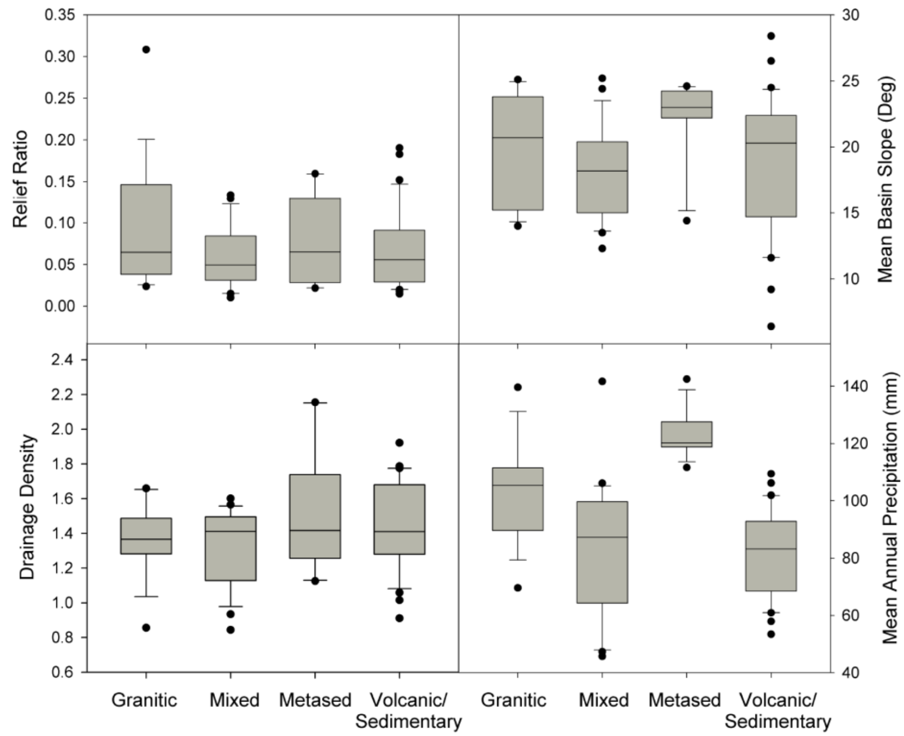

Figure 1.4. Variation in landscape metrics and mean annual precipitation among basins dominated by a particular rock type. Box plots show the 10th, 25th, 50th, 75th, and 90th percentiles, with outliers as black dots.

lithologies generally reflect the spatial variations in geologic history and storm tracks discussed above (Figure 1.4). Thus there does not appear to be a distinct coupling between landscape metrics and contemporary sediment production within or between rock types (Figure 1.4 and Supplementary Figure 1.2). Instead the lithology signal dominates such that sediment concentration tends to be lowest in streams draining more resistant granitic landscapes, and highest in softer sedimentary and volcanic landscapes, although there is a considerable range. Significance testing shows that splitting the data by rock type almost uniformly separates the data into different populations of sediment concentration (Table 1.2). In general, bed load and suspended load concentrations increase slightly as meta-sedimentary rocks come to dominate over more resistant granitic rocks in basins of northern Idaho. As granitic rocks in the Idaho

Batholith give way to the sedimentary and volcanic landscapes of the eastern Salmon River and Yellowstone regions, bed load and suspended load concentrations can increase by as much as two orders of magnitude (Figure 1.3e). These data are broadly consistent with chemical weathering rates for the Clark's Fork Yellowstone River, one of the streams in this study, which show that volcanic and carbonate rocks weather respectively ~1.5-5 and ~12-35 times faster than granitic rocks (Horton et al, 1999). Our data show that concentrations of bed load and suspended load in streams draining volcanic and sedimentary lithologies are on average 10 times the loads derived from granitic rocks. Metasedimentary basins supply sediment at 2-3 times the rate of granitic basins.

Sediment Supply Effects on Stream Channels

Alluvial stream channels generally adjust on relatively short timescales (10^0 – 10^2 yrs) to sediment and water inputs, and we may expect the wide range in sediment concentrations to result in substantial morphologic differences between stream channels. This turns out not to be the case, as most streams in this study are relatively stable single-thread channels, which tend to exhibit a quasi-universal scaling of hydraulic geometry (Parker et al., 2008). Notable exceptions are the morphologically dynamic braided channels of the Yellowstone region (Supplementary Figure S1.4). Data from nine braided sites in this region allow us to address a long standing question in geomorphology – the braided, single-thread transition (Leopold and Wolman, 1957) – from a sediment supply perspective. While it is often assumed that braided streams carry high sediment loads, very few data exist to test this assumption, and theory does not require it (Parker, 1976). Here we show that indeed braided channels have the highest concentrations of bed load ($> 4x10^{-5}$) and suspended load ($> 10^{-4}$) of streams in the study area (defined by the 25^{th} percentile of the distribution in Figure 1.3e). In particular, braided streams drain basins underlain by

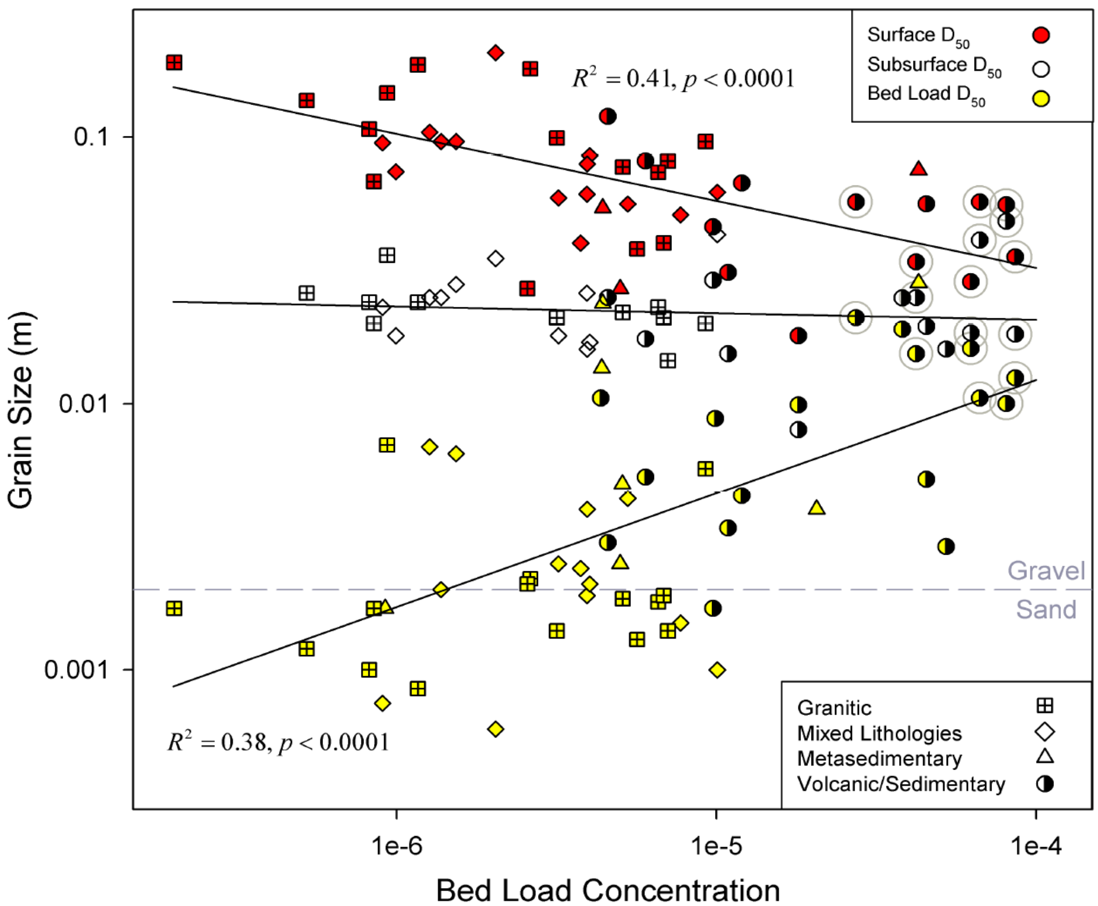

Figure 1.5. Relation between bed load concentration and the median grain size of three different sediment populations: surface, subsurface, and bed load. Symbols represent the different rock types. Braided channels are circled in light gray. Correlation and probabilities shown for significant relations.

specific lithologies – coarse clastic sedimentary and volcanic rocks – that result in some of the highest measured bed load transport rates in the Rocky Mountains.

Lithology influences not only the sediment supply and the magnitude of sediment transport, but also the size of the bed load and streambed sediment. Figure 1.5 shows the trend in three different grain size populations – the bed surface, the subsurface, and the bed load – as a function of bankfull bed load sediment concentration. As bed load concentration increases, the surface layer (armor) becomes finer, the bed load becomes coarser, while the subsurface sediment size remains essentially unchanged. This pattern reflects a transition from highly armored streams in basins dominated by granitic lithologies, to weakly armored streams in basins dominated by sedimentary and volcanic lithologies. For the 34 sites where we have complimentary data, the ratio of surface median grain size to subsurface median grain size decreases from about 5 to 1.5 as concentration increases. A striking result is the nature in which these sediment populations converge at high sediment concentrations: at the upper end armoring is nearly eliminated, and channels are predominantly braided. These trends explain to some extent how relatively stable single-thread channels can absorb a wide range in sediment supply, principally through changes in armoring (Dietrich, et al, 1989). At very high sediment supply rates, however, changes in bed surface texture are no longer a viable mechanism to enhance sediment transport (Eaton and Church, 2009), leading to avulsion and the development of a more complex braided channel pattern (Murray and Paola, 2003; Eaton et al, 2010).

CONCLUSION

While the long-term erosion of these landscapes is likely tied to an array of factors, including tectonics (Pierce and Morgan 1992), glaciations (Pierce, 2003), river incision and landsliding (Meyer and Leidecker, 1999; Dethier, 2001), wildfire (Kirchner et al., 2001; Meyer et al., 2001), and human land use (Megahan et al., 1992), contemporary sediment supply to stream channels in the northern Rocky Mountains is governed primarily by lithology. Both suspended and bed load concentrations increase as basins transition from granitic or hard rock dominated to sedimentary and volcanic or soft rock dominated. The morphology of streams in the region reflects this such that as sediment concentration increases, streams become less armored and the grain size of the bed load approaches the grain size of the bulk streambed sediment. In the face of very high concentrations a transition from single-thread to dynamic braided channels is commonly observed.

SUPPLEMENTAL INFORMATION

Discussion of Sediment Concentration

There are several reasons for choosing sediment concentration and bankfull transport rate to assess sediment supply. Sediment concentration provides a simple variable to describe the amount of sediment a given stream must transport in relation to its water supply. This is particularly relevant from a channel geometry perspective, where channels adjust based on the balance between water and sediment fluxes. In a classic paper, Lane (1955) showed that channels should adjust such that $Q_sD \alpha QS$, where Q_s is the quantity of sediment, D is the grain size of the bed material, Q is the quantity of water, and S is slope. Sediment concentration, $C=Q_s/Q$, can then be related directly to changes in channel morphology as $C \alpha S/D$. In this sense, sediment concentration provides a metric for the relative sediment loading, or supply, to a given channel thereby modulating for differences in the discharge across a range of scales. While this is a very simple physical model with unknown proportionalities, it is a useful demonstration on the fundamental relation between sediment and water supply and associated changes in channel morphology. Our results are broadly consistent with this conceptual model such that grain size of surface bed material decreases as sediment concentration increases despite a similar range in channel slope between basins.

We use the bankfull transport rate to define sediment supply in this study. Bankfull flow is commonly used in the development of downstream hydraulic geometry relations (Parker et al, 2008), and correlates quite well with the effective sediment discharge for streams in this area

(Whiting et al., 1999; Emmett and Wolman, 2001). Effective discharge considers both the magnitude and frequency of transport, and thus sediment transport rates at this discharge are likely a reasonable proxy for annual sediment yields. Calculating an annual sediment yield introduces uncertainty associated with the length and quality of the hydrologic records, as well as the choice of a representative sediment rating curve. Where hydrologic records permit, we find that bankfull transport rates are well correlated with annual sediment yields (see Chapter 3). Ultimately, flow and sediment transport at bankfull generally correspond to channel formative conditions (Wolman and Miller, 1960), and allow for a larger data set as several streams do not have sufficient hydrologic records for yield calculations. Where yield calculations were possible, the results were largely unaffected (Supplementary Figure S1.3).

Geology of Major River Basins

The upper Spokane River basin in the Northern Rockies fold and thrust belt is dominated by Proterozoic metasedimentary rocks of the Belt Supergroup. These rocks were deposited in an intracratonic basin resulting in a massive thickness of fine-grained and weakly metamorphosed rocks such as siltites, argillites, and quartzites that retain their original bedding, but are relatively hard and dense (Harrison and Grimes, 1970). The Clearwater River basin in north-central is largely composed of granitic rocks of the Cretaceous Idaho Batholith with lesser Belt rocks and flay-lying Miocene Columbia River Basalt flows. The Salmon River basin and adjacent streams are composed of mixed lithologies, stratified such that the Idaho Batholith is exposed in the western half of the basin, with a mixture of Eocene Challis Volcanics and Paleozoic sedimentary rocks to the east. The Challis Volcanics are dominantly rhyolitic and volcaniclastic, but contain an abundant intrusive suite ranging from granitic to dioritic (Link and Hackett, 1988; Digital Geology of Idaho, Idaho State University: geology.isu.edu/Digital_Geology_Idaho/) which were grouped in with granitic rock types. Paleozoic sedimentary rocks in southeast Idaho formed in a passive margin setting and range from shales to sandstones, and include thick sequences of carbonate rocks.

The streams draining the Yellowstone Region of Wyoming and Montana are dominated by volcanic rocks of the Yellowstone Plateau and the Eocene Absaroka Volcanic Province, with lesser sedimentary rocks ranging in age from Paleozoic to Cenozoic. Additionally, the Laramide Beartooth Plateau is cored with crystalline Precambrian igneous and metamorphic basement rocks which were lumped with granitic rocks in this study. Several of the braided streams in this study originate in the Absaroka mountains, which are dominated by andesitic volcaniclastic rocks (Nelson and Pierce, 1968: Love and Christiansen, 1985), many of which are breccias and conglomerates that supply ample coarse material to streams and rivers. The remaining braided streams originate from Paleozoic rocks of the Washakie Range in the upper Snake River basin. The headwaters of these basins contain abundant sequences of coarse quartzite conglomerate (Love, 1973; Love and Christiansen, 1985) such that braided stream reaches are dominated by quartzite clasts derived from rapid erosion of conglomerate beds (see Chapter 4). See references Green and Drouillard (1994) and Zeinteck et al. (2005) for information on the geologic maps used in the analysis.

Supplementary Tables and Figures

Table S1.1. Site data.

	Source[a]	Drainage Area (km²)	Bankfull Q (cms)	Guage Record (yrs)	Number of Samples: Susp Load	Number of Samples: Bed Load	Bankfull Sediment Load: Susp Conc (Qs/Q)	Bankfull Sediment Load: Bed Conc (Qs/Q)	Bankfull Sediment Load: Susp Qs (m³/s)	Bankfull Sediment Load: Bed Qs (m³/s)	Surface D_{50} (m)	Sub-Surface D_{50} (m)	Bedload D_{50} (m)	Bedrock Lithology[b]: Granitic %	Bedrock Lithology[b]: MetaSed %	Bedrock Lithology[b]: Volc/Sed %	Bedrock Lithology[b]: Other[c] %	Total Relief (m)	Relief Ratio (m/m)	Drainage Density (km/km²)	Mean Slope (deg)	Mean Annual Precip[d] (cm)
Upper Spokane Basin																						
Cat Spur Creek	9,9	28	2.4	8	32	35	5.0E-06	5.0E-06	1.2E-05	1.2E-05	0.027		0.003	0	100	0	0	620	0.139	2.1	17	119
Ninemile Creek	1,6	30	3.4	8	10	16	4.4E-05	2.1E-05	1.5E-04	7.0E-05			0.004	24	76	0	0	1170	0.160	1.1	23	120
Hayden Creek	2,1	56	6.8	37	151	---	2.9E-05		2.0E-04					0	100	0	0	988	0.159	1.4	23	118
Canyon Creek	1,6	57	11	9	11	16	1.8E-05	9.2E-07	2.0E-04	1.0E-05			0.002	5	95	0	0	1211	0.098	1.1	24	130
Pine Creek	1,6,13	189	35	13	12	15	2.0E-05	4.3E-05	7.0E-04	1.5E-03	0.075		0.028	0	100	0	0	1236	0.101	1.3	25	122
South Fork Coeur d'Alene River	2,6	279	39	20	12	20	2.3E-05	5.1E-06	9.1E-04	2.0E-04			0.005	4	96	0	0	1277	0.081	1.2	25	126
St. Joe River	1,1	310	56	13	54	---	4.3E-06		2.4E-04					0	100	0	0	1201	0.047	1.8	22	143
St. Maries River	2,1	706	67	44	14	---	2.9E-05		1.9E-03					4	93	0	3	1152	0.037	2.2	14	112
South Fork Coeur d'Alene River	2,6	744	80	23	12	19	2.9E-05	4.4E-06	2.3E-03	3.5E-04			0.014	1	99	0	0	1414	0.049	1.3	24	119
North Fork Coeur d'Alene River	2,6,14	2315	340	71	8	10	3.2E-05	4.4E-06	1.1E-02	1.5E-03	0.054		0.024	0	100	0	0	1416	0.022	1.5	23	120
St. Joe River	2,1	2653	366	90	38	---	5.4E-06		2.0E-03					5	95	0	0	1631	0.025	1.6	23	128
Coeur d'Alene River	2,1	3126	431	76	61	---	1.5E-05		6.3E-03					1	99	0	0	1427	0.023	1.5	23	119
Clearwater River Basin																						
Trapper Creek	9,9	21	2.6	---	143	167	7.8E-06	4.0E-06	2.0E-05	1.0E-05	0.085	0.017	0.002	21	68	12	0	520	0.105	1.1	12	104
South Fork Red River	9,9	98	7.3	35	136	202	6.0E-06	1.4E-06	4.4E-05	1.0E-05	0.096	0.025	0.002	40	57	3	0	938	0.080	1.3	14	95
Lolo Creek	9,9	108	12	35	135	112	3.6E-06	8.5E-07	4.2E-05	1.0E-05	0.068	0.020	0.002	84	11	0	5	918	0.050	1.3	15	140
Main Fork Red River	9,9	129	9.4	36	136	198	6.8E-06	3.2E-06	6.3E-05	3.0E-05	0.059	0.018	0.003	52	48	0	0	699	0.049	1.5	14	99
Johns Creek	9,9	292	49	10	46	122	6.0E-06	2.0E-06	2.9E-04	1.0E-04	0.207	0.035	0.001	51	49	0	0	1811	0.084	1.2	19	101
South Fork Clearwater River	2,1	3027	152	46	45	---	2.6E-05		4.0E-03					38	36	1	25	2308	0.031	1.4	14	87
Lochsa River	9,9	3052	446	77	36	72	2.0E-05	5.2E-07	8.9E-03	2.3E-04	0.137	0.026	0.001	79	20	1	0	2234	0.024	1.1	21	129
North Fork Clearwater River	9,9	3354	453	40	36	70	3.0E-05	9.0E-07	1.4E-02	4.1E-04	0.095	0.023	0.001	43	56	1	0	1891	0.023	1.5	22	142
Selway River	9,9	4962	652	78	36	72	2.0E-05	1.2E-06	1.3E-02	7.6E-04	0.186	0.024	0.001	85	15	0	0	2375	0.027	1.4	24	111
Clearwater River	10,10	24065	2210	85	47	78	2.0E-05	1.0E-06	4.5E-02	2.2E-03	0.074	0.018		46	30	1	23	2608	0.015	1.4	18	106
Salmon River Region																						
Eggers Creek	9,9	1.4	0.05	32	130	137	4.2E-06	6.1E-06	2.0E-07	2.9E-07				100	0	0	0	589	0.420	1.7	21	80
Little Buckhorn Creek	9,9	16	0.6	5	73	72	6.4E-06	7.1E-06	3.6E-06	4.0E-06	0.081	0.015	0.001	100	0	0	0	1308	0.308	1.7	21	82
Squaw Creek (USFS)	9,9	42	0.6	---	89	42	4.8E-06	2.6E-06	3.0E-06	1.6E-06	0.027		0.002	94	3	2	0	1498	0.174	1.7	25	70
Fourth of July Creek	9,9	42	3.9	---	25	79	2.6E-05	7.7E-06	1.0E-04	3.0E-05	0.051		0.002	30	15	55	0	1096	0.114	1.1	21	101
Dollar Creek	9,9	43	7.8	5	76	85	7.6E-06	5.1E-06	6.0E-05	4.0E-05	0.077	0.022	0.002	100	0	0	0	950	0.131	1.3	17	107
Blackmare Creek	9,9	46	4.7	5	83	88	3.6E-06	3.2E-06	1.7E-05	1.5E-05	0.099	0.021	0.001	100	0	0	0	1376	0.162	1.5	25	112
West Fork Buckhorn Creek	9,9	59	5.7	5	68	85	5.4E-06	2.6E-06	3.1E-05	1.5E-05	0.180		0.002	100	0	0	0	1544	0.170	1.4	22	105
Thompson Creek	9,9	67	2.5	38	24	84	2.8E-05	1.0E-05	7.0E-05	2.5E-05	0.062	0.043	0.001	4	27	69	0	1147	0.129	1.6	25	64
Hawley Creek	9,9	105	1.3	---	82	85	1.1E-05	3.8E-06	1.5E-05	5.0E-06	0.040		0.002	1	25	74	0	1216	0.134	1.1	18	47
Little Slate Creek	9,9	167	12	46	80	157	8.2E-06	8.2E-07	1.0E-04	1.0E-05	0.107	0.024	0.001	97	2	0	1	1344	0.091	1.5	15	110
Squaw Creek (USGS)	9,9	186	5.1	38	32	62	4.3E-05	9.7E-06	2.2E-04	5.0E-05	0.046	0.029	0.002	0	4	96	0	1248	0.091	1.7	20	61
Marsh Creek	9,9	205	21	---	27	98	3.5E-06	5.3E-06	7.2E-05	1.1E-04	0.056		0.004	75	3	22	0	954	0.074	1.5	14	107

	Source[a]	Drainage Area (km²)	Bankfull Q (cms)	Guage Record (yrs)	Number of Samples: Susp Load	Number of Samples: Bed Load	Bankfull Sediment Load: Susp Conc (Qs/Q)	Bankfull Sediment Load: Bed Conc (Qs/Q)	Bankfull Sediment Load: Susp Qs (m^3/s)	Bankfull Sediment Load: Bed Qs (m^3/s)	Surface D_{50} (m)	Sub-Surface D_{50} (m)	Bedload D_{50} (m)	Bedrock Lithology[b]: Granitic %	Bedrock Lithology[b]: MetaSed %	Bedrock Lithology[b]: Volc/Sed %	Bedrock Lithology[b]: Other[c] %	Total Relief (m)	Relief Ratio (m/m)	Drainage Density (km/km²)	Mean Slope (deg)	Mean Annual Precip[d] (cm)
Salmon River Region (cont.)																						
Salmon River	9,9	255	13	12	23	50	2.4E-05	3.9E-06	3.0E-04	5.0E-05	0.061	0.026	0.002	37	0	63	0	1069	0.063	1.4	18	88
Rapid River	9,9	278	18	88	85	190	1.2E-05	3.9E-06	2.2E-04	7.0E-05	0.079	0.016	0.004	7	43	0	51	2189	0.113	1.3	24	100
Herd Creek	9,9	293	5.5	---	23	72	5.4E-05	1.2E-05	3.0E-04	6.6E-05	0.067		0.005	0	0	100	0	1571	0.094	1.4	23	61
North Fork Big Lost River	2,7,17	298	20	66	23	23	8.1E-05	4.5E-05	1.6E-03	9.0E-04	0.056	0.020	0.005	6	1	93	0	1536	0.077	1.1	23	71
Big Wood River	9,9	351	22	23	26	100	3.4E-05	4.6E-06	7.5E-04	1.0E-04	0.119	0.025	0.003	25	0	75	0	1493	0.072	1.4	22	87
Valley Creek	9,9	377	24	66	71	192	4.6E-06	6.8E-06	1.1E-04	1.7E-04	0.040	0.021	0.002	92	7	1	0	1356	0.065	1.5	14	88
Johnson Creek	9,9	564	40	79	36	72	3.3E-06	2.0E-07	1.3E-04	8.0E-06	0.190		0.002	90	10	0	0	1366	0.041	1.1	16	112
South Fork Salmon River	9,9	854	71	35	92	130	1.3E-05	5.6E-06	9.5E-04	4.0E-04	0.038		0.001	100	0	0	0	1646	0.038	1.3	21	100
Big Lost River	2,7	1142	50	62	21	21	4.8E-05	9.9E-06	2.4E-03	5.0E-04			0.009	11	5	84	0	1608	0.043	1.0	20	69
South Fork Payette River	9,9	1157	86	66	37	72	3.9E-05	9.3E-06	3.4E-03	8.0E-04	0.096	0.020	0.006	99	0	0	0	2090	0.047	1.3	25	100
East Fork Salmon River	2,8	1401	36	19	21	---	4.4E-05		1.6E-03					5	1	94	0	1918	0.058	1.4	21	65
Little Salmon River	2,1	1493	118	57	33	---	1.6E-05		1.9E-03					31	11	0	59	2330	0.049	1.4	18	91
Salmon River	9,9	2092	118	74	30	60	1.7E-05	1.3E-06	2.0E-03	1.5E-04	0.104	0.025	0.007	56	2	42	0	1525	0.034	1.5	18	81
Pahsimeroi River	1,1	2151	9.5	26	32	---	9.5E-06		9.0E-05					0	34	66	0	2437	0.045	1.5	15	49
Boise River	9,9	2154	167	96	40	82	5.1E-05	6.6E-06	8.5E-03	1.1E-03	0.074	0.023	0.002	99	0	1	0	2197	0.038	1.5	24	92
Lemhi River	2,1	2326	20	51	30	---	2.1E-05		4.2E-04					2	35	63	0	1963	0.036	1.2	14	46
Middle Fork Salmon River	9,9	2726	214	17	31	64	1.3E-05	9.3E-07	2.7E-03	2.0E-04	0.146	0.036	0.007	77	2	21	0	1663	0.026	1.3	21	102
Salmon River	2,1	9707	196	95	31	---	3.1E-05		6.1E-03					16	15	69	0	2660	0.018	1.5	18	58
Salmon River	9,9	16166	326	42	21	61	4.6E-05	1.5E-06	1.5E-02	5.0E-04	0.096	0.028	0.007	16	31	53	0	2884	0.016	1.4	18	74
Salmon River	2,1	34773	1479	98	201	---	4.7E-05		7.0E-02					46	20	31	3	3416	0.010	1.4	20	56
Yellowstone Region																						
Cache Creek	4,1	28	1.7	48	240	---	3.6E-05		6.0E-05					0	0	100	0	1086	0.190	1.6	22	92
Crow Creek	1,1,15	50	6.3	10	196	---	1.6E-05		1.0E-04		0.038			0	0	100	0	1190	0.126	1.4	22	87
Little Granite Creek	12,12	55	6.0	10	152	280	5.8E-05	6.0E-06	3.4E-04	3.6E-05	0.081	0.018	0.005	6	0	94	0	1354	0.183	1.4	20	82
Jones Creek	1,1,15	65	9.4	5	63	---	4.0E-05		3.7E-04		0.058			0	0	100	0	1184	0.126	1.3	21	90
Sode Butte Creek	1,1	80	17	12	34	---	8.9E-05		1.5E-03					5	0	95	0	1179	0.127	0.9	21	96
Sunlight Creek	4/17,1	113	16	29	---	21		6.2E-05		1.0E-03	0.029	0.018	0.016	2	0	98	0	1466	0.152	1.3	28	109
Pilgrim Creek	16,1	126	17	---	31	53	1.7E-04	8.6E-05	3.0E-03	1.5E-03	0.036	0.018	0.013	0	0	100	0	899	0.062	1.4	14	102
Spread Creek	1,1	256	20	4	45	39	7.1E-04	8.1E-05	1.4E-02	1.6E-03	0.056	0.048	0.010	0	0	100	0	1059	0.035	1.8	14	93
North Fork Shoshone River	16,1	381	45	---	16	14	4.5E-05	3.8E-05	2.0E-03	1.7E-03		0.025	0.019	0	0	100	0	1623	0.089	1.4	22	89
Pacific Creek	2,1/11	423	60	63	39	41	1.8E-04	6.7E-05	1.1E-02	4.0E-03	0.057	0.041	0.011	0	0	100	0	1147	0.035	1.6	12	96
Boulder River	3,1	591	87	27	366	---	2.3E-05		2.0E-03					56	22	22	0	1936	0.056	0.8	22	89
South Fork Shoshone River	4,1	794	97	53	62	---	2.1E-04		2.0E-02					7	0	93	0	1910	0.063	1.8	27	83
Buffalo Fork	11,11	845	111	45	---	39		1.8E-05		2.0E-03	0.018	0.008	0.010	3	0	97	0	1394	0.029	1.5	15	97
Stillwater River	3,1	966	105	18	731	---	1.2E-05		1.3E-03					78	2	20	0	2439	0.069	0.9	20	88
North Fork Shoshone River	16,1	1016	92	---	14	13	6.2E-05	4.3E-06	5.7E-03	4.0E-04			0.011	0	0	100	0	1819	0.056	1.6	24	85

Table S1.1 (cont.). Site data.

Table S1.1 (cont.). Site data.

	Source[a]	Drainage Area (km^2)	Bankfull Q (cms)	Guage Record (yrs)	Number of Samples Susp Load	Number of Samples Bed Load	Bankfull Sediment Load Susp Conc (Qs/Q)	Bankfull Sediment Load Bed Conc (Qs/Q)	Bankfull Sediment Load Susp Qs (m^3/s)	Bankfull Sediment Load Bed Qs (m^3/s)	Surface D_{50} (m)	Sub-Surface D_{50} (m)	Bedload D_{50} (m)	Bedrock Lithology[b] Granitic %	Bedrock Lithology[b] MetaSed %	Bedrock Lithology[b] Volc/Sed %	Bedrock Lithology[b] Other[c] %	Total Relief (m)	Relief Ratio (m/m)	Drainage Density (km/km^2)	Mean Slope (deg)	Mean Annual Precip[d] (cm)
Yellowstone Region (cont.)																						
East Fork Wind River	4,1	1121	22	28	124	---	5.7E-05		1.3E-03					7	0	93	0	1864	0.043	1.7	18	63
Madison River	2,1	1124	34	83	38	---	1.2E-05		4.0E-04					0	0	100	0	853	0.018	1.2	6	90
Snake River	2,1	1230	184	27	152	16	1.4E-04	1.1E-05	2.5E-02	2.0E-03	0.031	0.015	0.003	0	0	100	0	1063	0.027	1.3	9	106
Boulder River	3,1	1358	133	61	32	---	2.6E-05		3.5E-03					48	12	40	0	2205	0.033	0.9	19	77
North Fork Shoshone River	16,1	1496	123	36	21	14	4.1E-04	5.2E-05	5.0E-02	6.4E-03		0.016	0.003	2	0	98	0	1889	0.055	1.6	25	82
Lamar River	4,1	1731	218	68	1180	---	1.1E-04		2.4E-02					11	0	89	0	1593	0.036	1.2	16	75
Greybull River	4,1	1757	86	41	60	---	4.3E-04		3.7E-02					1	0	99	0	2256	0.049	1.9	18	58
Stillwater River	3,1	2530	157	70	21	---	9.5E-06		1.5E-03					56	1	43	0	2707	0.051	1.0	17	76
Clarks Fork Yellowstone River	4,1	2989	194	89	178	---	2.8E-04		5.5E-02					33	0	67	0	2662	0.035	1.6	17	71
Snake River	11,11	3916	285	16	85	60	5.3E-05	4.2E-05	1.5E-02	1.2E-02	0.034	0.025	0.015	2	3	95	0	1822	0.024	1.4	12	102
Shoshone River	16,1	4743	106	3	33	---	1.2E-04		1.3E-02					2	0	98	0	2397	0.029	1.8	20	63
Shoshone River	1,1	6207	106	44	125	---	2.1E-04		2.3E-02					2	0	98	0	2604	0.022	1.8	16	53
Yellowstone River	4,1	6784	436	100	84	---	2.1E-04		9.0E-02					5	4	89	2	2125	0.020	1.3	13	80
Yellowstone River	5,5	9210	575	73	129	47	1.4E-04	2.7E-05	7.9E-02	1.6E-02	0.057		0.021	7	4	86	3	2293	0.015	1.2	15	76

Notes:

a: First number refers to discharge source, second number to sediment transport data source, third number to additional grain size data source.

b: Green, G.N., & Drouillard, P.H. The Digital Geologic Map of Wyoming in ARC/INFO Format: U.S. Geol. Surv. Open-File Rep. 94-0425 (1994).

Zienteck et al. Spatial databases for the geology of the Northern Rocky Mountains – Idaho, Montana, and Washington. U.S. Geol. Surv. Open-File Rep. 2005-1235 (2005).

c: Other lithology refers to basalt flows (largely from Columbia River Basalts and Yellowstone caldera), tectonite, and metamorphic rocks of the Seven Devils complex.

d: PRISM, United States Anuual Precipitation 1971-2000. The PRISM Climate Group at Oregon State University (2006).

1: USGS NWIS; 2: Hortness and Berenbrock, 2004; 3: Parrett and Johnson, 2004; 4: Miller, 2003; 5: Holnbeck, 2005; 6: Clarck and Woods, 2001; 7: Williams and Krupin, 1984; 8: Emmett, 1975;

9: King et al., 2004; 10: Jones and Seitz, 1980; 11: Erwin et al., 2011; 12: Ryan and Emmett, 2002; 13: Kondolf et al., 2002; 14: Berenbrock and Tranmer, 2008; 15: Zelt, 2001;

16: Bankfull discharge estimated from a regional relationship as $Q=aDA^b$, where Q is discharge, DA is drainage area, and a and b are empirical power-law parameters;

17: Determined from field measurements by the authors.

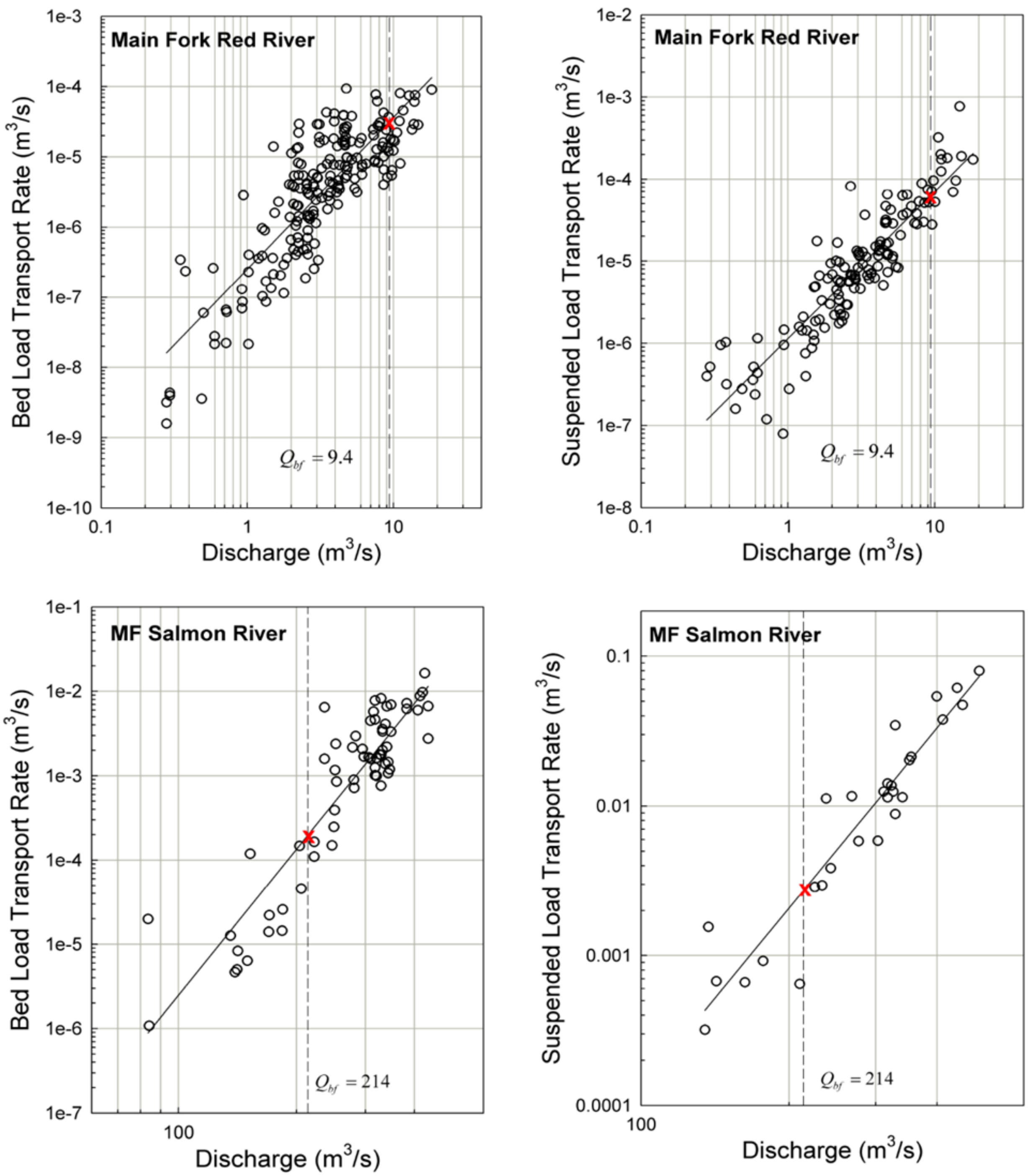

Figure S1.1. Examples of sediment transport relations used to determine bankfull transport rate with power law relations shown in black. Red X's represent reported values. Gray vertical dashed line represents bankfull discharge. In the above examples, a power-law fit provides a good estimate for both bed load and suspended load.

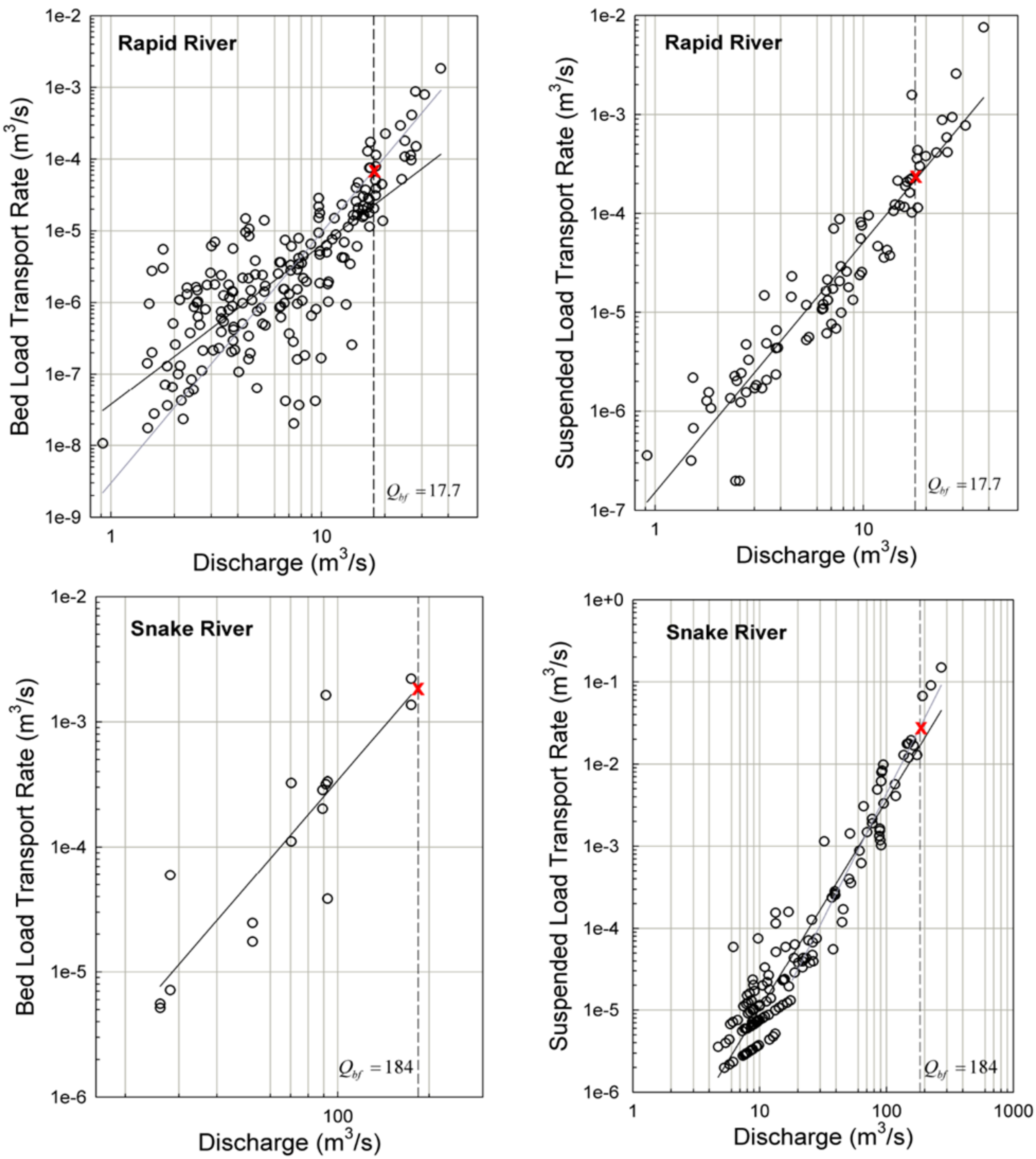

Figure S1.1 (continued). Top: Power-law does not follow the bed load data trend well, so a by-eye fit (gray) was used. Power-law provides good fit for suspended load. Bottom: Example with relatively few data points in the case of bed load. Here a power-law fit is in good agreement with measurements near bankfull. In the case of suspended load, measurements less than 10% bankfull were eliminated providing a better fit to high flow data (gray line).

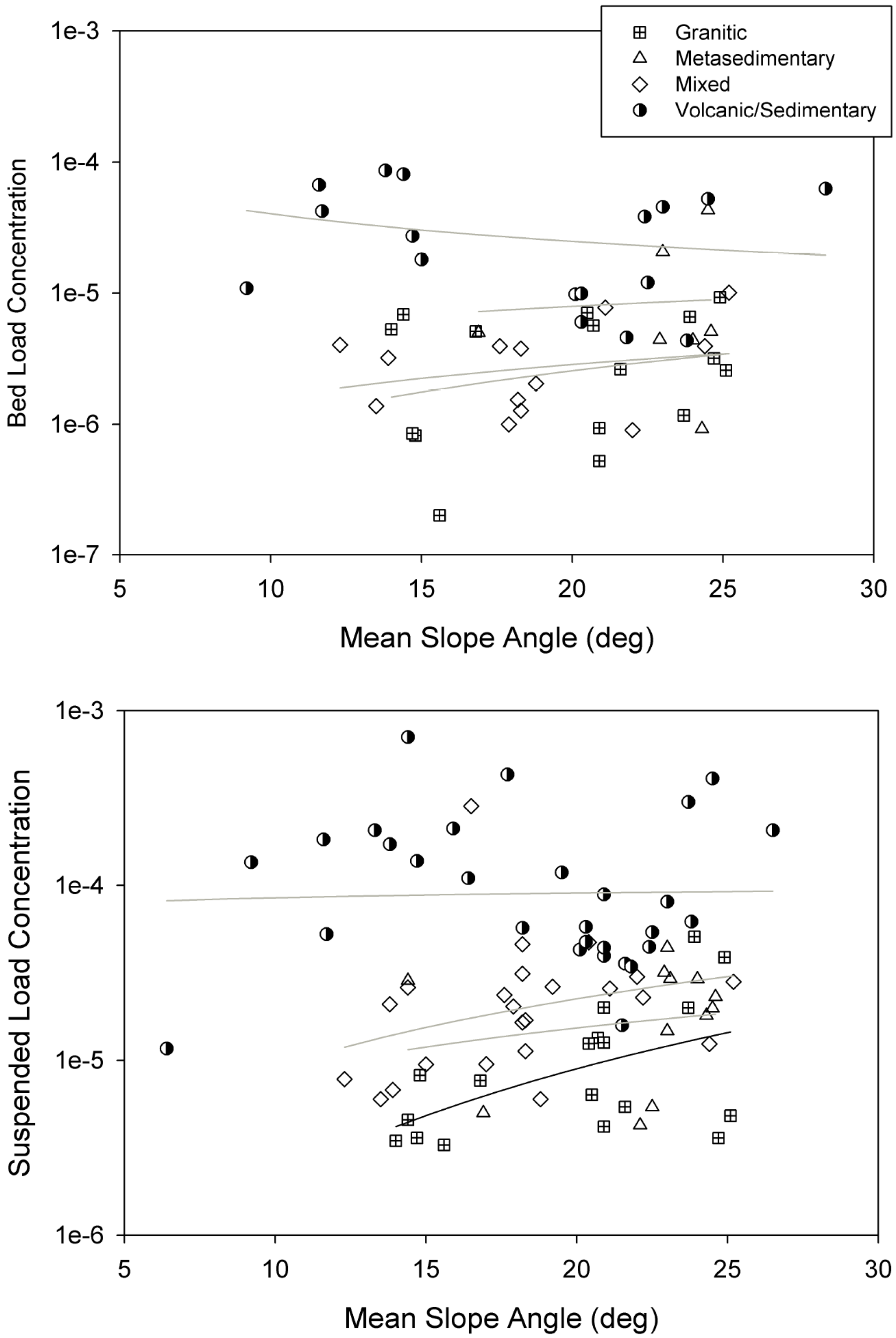

Figure S1.2. Relation between bed load and suspended load concentration and mean slope angle within individual lithologies. The only significant power-law relation is indicated by the black line.

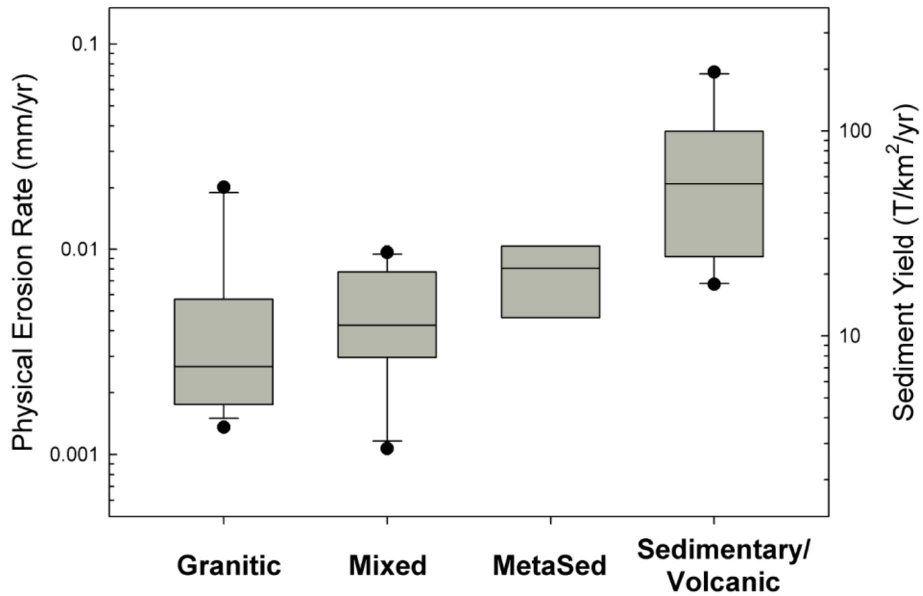

Figure S1.3. Box plots showing the variation in physical erosion rate and sediment yields across different rock types. These data are derived from computing annual bed and suspended sediment fluxes for sites with sufficient hydrologic data. Box plots show the 10th, 25th, 50th, 75th, and 90th percentiles, with outliers as black dots.

Figure S1.4. Example single-thread reaches near sampling locations. Flow is from left to right and scale is identical in all photos. All images from *Google Earth*.

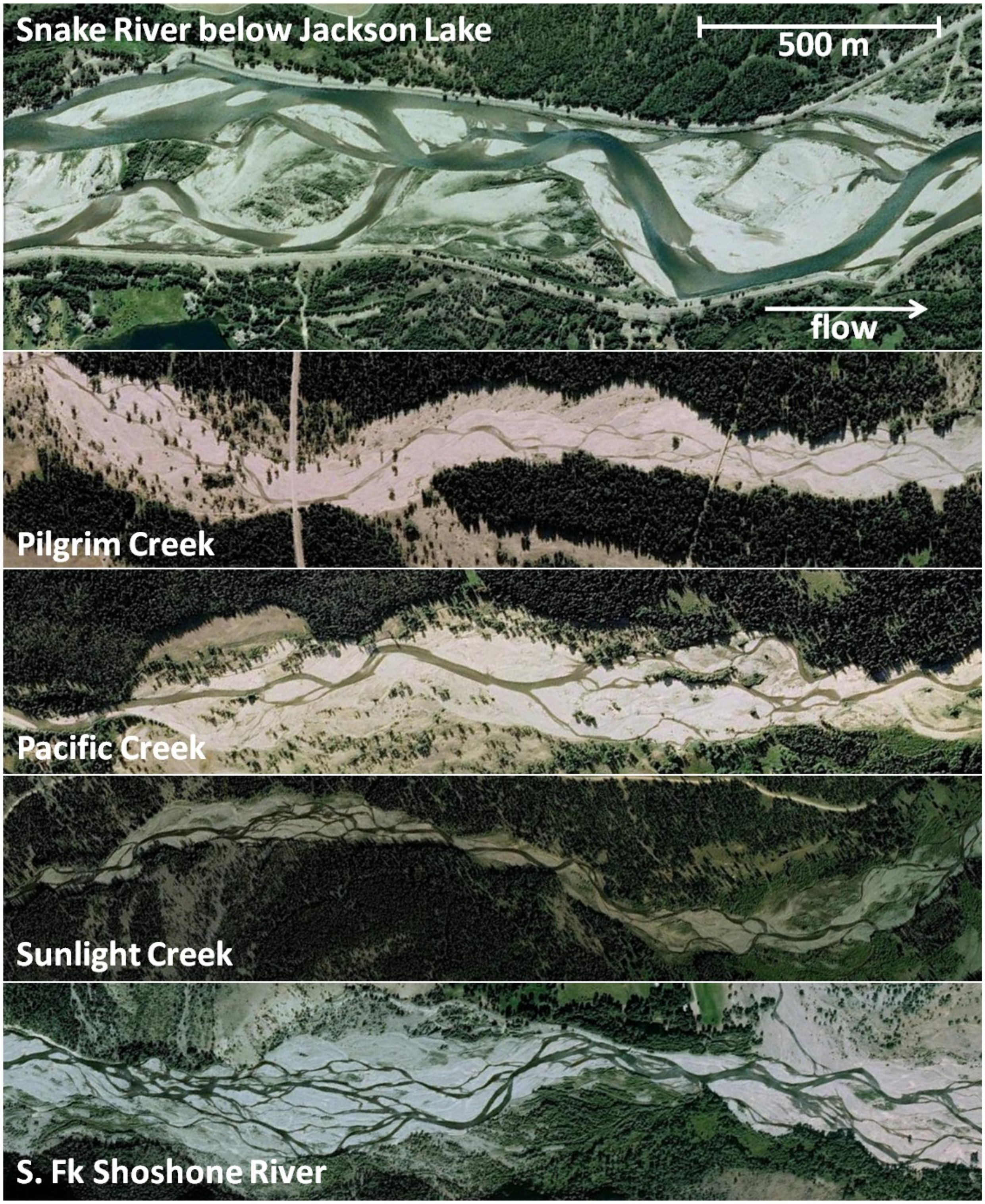

Figure S1.4 (cont.). Example braided reaches near sampling locations. Flow is from left to right and scale is identical in all photos. All images from *Google Earth*.

Chapter 2 - An erosion-abrasion mixing model of sediment flux: using stream sediment lithology as a signature of watershed processes

ABSTRACT

Both the flux and characteristics of sediment in the bed of a river should reflect spatial variations in supply, rock strength, and channel network structure. Stream sediment both decays in size and changes in its lithologic composition downstream. We use a simple erosion-abrasion mass balance to model the downstream evolution of the bed and suspended load flux, and composition in two adjacent watersheds draining differing mixtures of soft and resistant rock types in the Northern Rocky Mountains. Measurements of bed sediment grain size and lithology are used in conjunction with measured bed load and suspended load sediment fluxes to constrain the model. Our results demonstrate that the downstream evolution in bed load composition can be strongly influenced by subtle differences in underlying geology. In the Big Wood basin, abrasion rapidly reduces the size of fine-grained sedimentary and volcanic rocks, concentrating plutonic rocks in the stream bed and depressing bed load in favor of suspended load. In contrast, in the North Fork Big Lost basin the bed sediment becomes dominated by more resistant quartzitic sandstones whose size evolution is best modeled with modest abrasion rates. In both cases, the best-fit model can reproduce within 5% the composition of the stream bed substrate using realistic erosion and abrasion parameters constrained by observed sediment fluxes. These results illustrate strong linkages between modern hillslope-channel systems where the sediment signature of the primary streams reflects the systematic tapping of distinct source areas.

INTRODUCTION

In geomorphic systems individual sediment grains evolve as they migrate through components of the earth's surface, from weathering and entrainment on hillslopes, through transport and abrasion in channels, and eventual deposition. Further, most sediment particles contain information about their origin, including a unique geologic or chemical signature, and can thus be used as tracers of landscape processes. Longitudinal sediment evolution can reveal process connections in a variety of settings including littoral (Perg et al., 2003), eolian (Jerolmack et al., 2011), or paleo-sedimentary systems (Chetel et al., 2011) using tracers such as cosmogenic radionuclides, particle size and shape, or lithologic composition. In fluvial systems, a long history of studies on downstream fining addresses the relative importance of factors such as abrasion and lithology (Krumbein, 1941; Bradley, 1970; Kodama, 1994), selective transport (Parker, 1991; Ferguson et al., 1996), or punctuation by tributary inputs (Rice, 1999; Ferguson et al., 2006). Generally, these studies have focused solely on grain size; only recently have workers begun to examine how variations in source area lithology and channel network structure influence the size, flux, and composition of stream sediments (Pizzuto, 1995; Attal and Lave, 2006; Sklar et al., 2006; Chatanantavet et al., 2010). Viewed in reverse, the mixture of lithologies at a given location in the channel network should reveal information about upstream hillslope-channel coupling given a known spatial distribution of individual rock types within the basin (Sklar et al., 2006).

Here we take a similar network-based approach as the above authors, setting up a simple mass balance mixing model, and employ two new unique data sets on the size and composition of sediments in two adjacent watersheds with different rock type distributions and network structures. The primary objective is to examine how variations in rates of erosion and abrasion influence downstream changes in the quantity and composition of the sediment flux. In contrast to previous studies, the model results can be verified using measured bed load and suspended load sediment fluxes.

METHODS

Study Area

Field data were obtained from two adjacent, similarly sized watersheds (~300 km^2) in the Northern Rocky Mountains of Idaho – the upper Big Wood (BW) and North Fork Big Lost (NBL) Rivers (Figure 2.1). The BW and NBL basins have similar relief, with mean elevations of 2508 and 2640 meters, respectively, and a snowmelt-dominated hydrology. Underlying bedrock consists of imbricated thrust sheets of Paleozoic strata intruded by Eocene plutons, overlain by volcanic rocks of the Eocene Challis Volcanic Group; in the NBL, gneissic rocks have been exposed by the Pioneer Core Complex (Figure 2.1) (Worl et al., 1995; Zienteck et al., 2005). Sedimentary rocks in the BW catchment consist predominantly (>90%) of micritic silty carbonates of the Wood River Formation, whereas >60% of the sedimentary strata in the NBL catchment are carbonate and quartzose siliciclastic rocks of the Copper Basin Formation (Zienteck et al., 2005). Plutonic rocks of granitic to quartz monzodioritic composition were subsequently intruded during the Eocene with associated Challis volcanics consisting of aphyric to sparsely porphyritic flows, flow breccias, and vent deposits (Worl et al., 1995). Both of these basins were glaciated in the Quaternary, and we consider mapped surficial deposits to contain a mixture of adjacent rock types. At their outlets, the basins are underlain by differing proportions of sedimentary (BW: 23%; NBL: 48%), volcanic (BW: 52%; NBL: 45%), and granitic/plutonic/gneissic (BW: 25%; NBL: 7%) rocks.

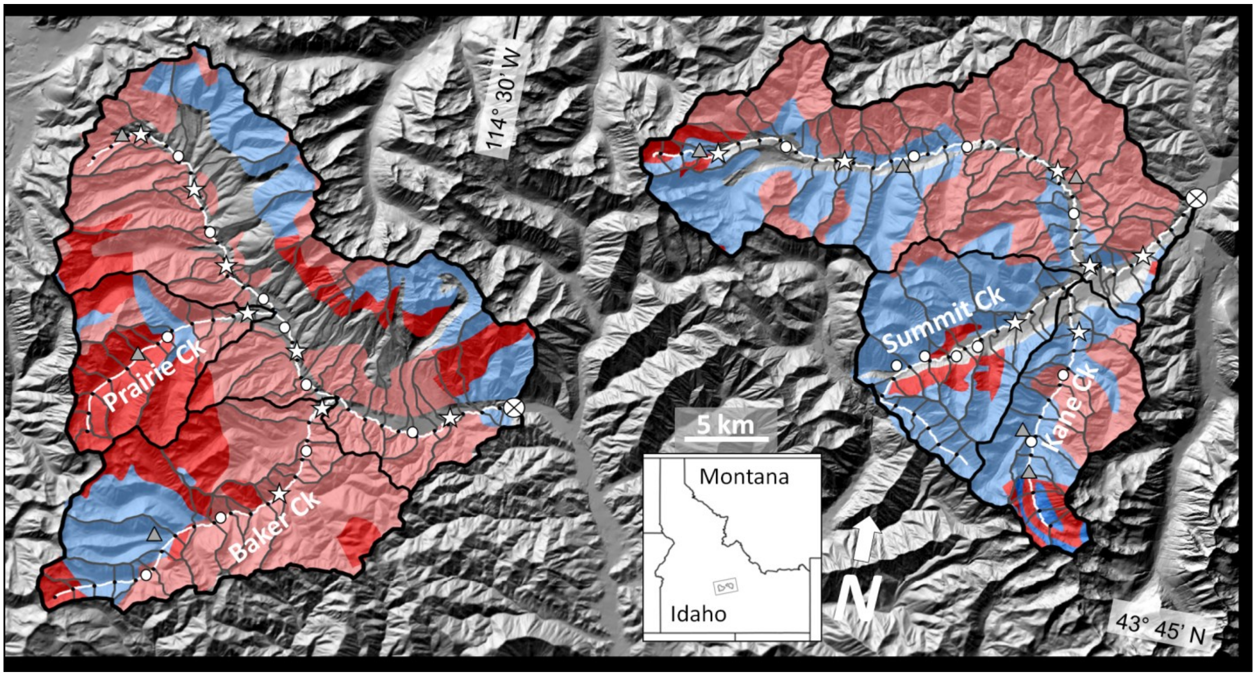

Figure 2.1. Big Wood basin (left) and North Fork Big Lost basin (right) indicating distribution of major rock types (blue: sedimentary; pink: volcanic; red: granitic/plutonic; dark blue: gneissic; no color: surficial) and locations of sediment sampling (stars: surface, subsurface, and morphologic measurements; circles: surface sample; triangles: headwater subsurface sample; circles with cross: gauging station). The main channel is the top most channel in both cases and major tributaries are labeled with their drainage areas outlined in bold. Small black dots represent computation nodes, where the gray lines outline the associated incremental drainage area.

Sediment Sampling

A unique aspect of this study is incorporation of measured bed load and suspended load transport rates at the basin outlets (King et al., 2004; Williams and Krupin, 1984), supplemented by our own bed load measurements. Sediment rating curves combined with hydrological records from stream gauges at the basin outlets suggest that sediment transport in the BW is dominated by suspended load (~3000 m^3/yr) relative to bed load (~500 m^3/yr). Likely owing to differences in lithology, tectonic history, and vegetation cover (Figure DR2.1), sediment loads in the NBL are roughly 40% greater; the difference is largely due to enhanced bed load transport (~2000 m^3/yr bed load; ~3000 m^3/yr suspended load).

Surface pebble counts and subsurface bulk samples were used to document downstream trends in the size and proportion of individual lithologies at 45 sites along the main channel and tributaries (Figure 2.1). The grain size and lithology of the bed surface were determined in the field from point counts of 200 clasts ranging in size from 4 to 256 mm. For the subsurface, the lithology of approximately 1000 individual grains was characterized using hand samples (>4 mm) and a petrographic microscope (<4 mm) in the field and lab. For subsurface samples, the lithologic proportions were determined by weighting the composition of individual size classes by their weight-proportion in the substrate. Rock types were simplified to sedimentary, volcanic, and granitic/plutonic; gneissic rocks were lumped with the latter based on their limited exposure and crystalline texture.

Erosion-Abrasion Model

Our model is formulated for a simple watershed where eroded sediment is supplied directly from hillslopes to channels, being modified during transport through abrasion, and supplemented downstream by lateral inputs (Figure DR2.2). In the case of a uniformly eroding watershed in steady-state, where sediment production equals sediment output with no storage change, the total sediment flux, Q_t, at some downstream distance, x, can be expressed simply as erosion or sediment production rate, ε, times contributing area at that distance, A(x):

$$Q_t(x) = \varepsilon A(x)\,. \tag{1}$$

Sediment passing through the channel network is reduced in size by abrasion, converting some of the bed load to suspended load. The sediment flux at distance x is thus apportioned between bed load, Q_b, and suspended, Q_{susp}, loads:

$$Q_t(x) = Q_{susp}(x) + Q_b(x)\,. \tag{2}$$

The downstream changes in grain size are assumed to follow Sternberg's (1875) Law:

$$D(x) = D_o e^{-\alpha x} \tag{3}$$

where D is grain diameter, D_o is the initial grain size, and α is an abrasion parameter (km^{-1}). Assuming spherical grains, the volume, V, at distance x is therefore given as:

$$V(x) = V_o e^{-3\alpha x} \tag{4}$$

where V_o is the initial volume. In the absence of storage, the total sediment flux will increase downstream (equation 1), and as a result, the relative proportion of bed load versus suspended load (equation 2) will be directly related to the efficiency of abrasion and travel-path lengths of individual grains (equation 4). Attal and Lave (2006) and Sklar et al. (2006) both consider the special case of a monotonically eroding linear watershed ($x \sim A^1$) where the downstream unit supply rate, $q=Q_t(x)/x$, is uniform. In this case the volumetric bed load flux, Q_b, can be evaluated at any distance as the integral of supply less abrasion losses:

$$Q_b(x) = \int_0^x q e^{-3\alpha x} dx = \frac{q}{3\alpha}\left(1 - e^{-3\alpha x}\right). \tag{5}$$

Of course, in reality we expect variability in both q and α as a function of network geometry and spatial differences in rock types or erodibility.

In order to account for such variability, the BW and NBL watersheds were broken into discrete sediment input slices containing some mixture of the above lithologies in 1 km links along the main channel and major tributaries (Figures 2.1 and DR2.2). The bed load flux of several lithologies at the outlet ($Q_{b,out}$) of a stream link is given as the incoming bed load flux to the given link less abrasion losses, plus hillslope/small tributary inputs across the link:

$$Q_{b,out} = \sum_a^n \left\{ Q_{b,in,n} e^{-3\alpha_n \Delta x} + \varepsilon_n A_{n,x} \right\} \tag{6}$$

where the subscript n corresponds to different lithologies that may vary in ε or α, $Q_{b,in,n}$ is the input flux of a given lithology, $A_{n,x}$ is the area of an individual lithology within a link, and Δx=1 km is the link length.

In links where major tributaries (>20km^2) enter, another component is added to the above equation:

$$Q_{b,out} = \sum_{a}^{n} \left\{ Q_{b,in,n} e^{-3\alpha_n \Delta x} + Q_{h,n} + Q_{trib,n} \right\} \tag{7}$$

where $Q_{trib,n}$ is the bed load flux of an individual lithology delivered from the major tributaries to the main channel, modeled prior to arriving using the approach above. Major tributaries are outlined in bold in Figure 2.1. Suspended loads for individual lithologies are simply found as the residual of total flux less the bed load component by rearranging equation 2. The modeled lithologic proportion of the stream bed sediment at a given location is then found as the ratio of the bed load flux for a given lithology to the total bed load flux: $Q_{b,n}/Q_b$.

Assumptions

In order to use the constraint provided by bed and suspended load measurements at the basin outlet, we assume that the initial sediment input, $\varepsilon_n A_{n,x}$, to contain 30% suspended load and 70% bed load, which is broadly consistent with sediment transport data from Idaho streams (King et al., 1994), and within the range reported in the recent compilation by Turowski et al. (2009). We assume that Sternberg's Law applied to the median grain size of the bed load sediment (D_{50}) is representative of the abrasion processes of the entire sediment size distribution, and is represented by a characteristic α. All losses due to abrasion are simply added to the suspended load flux. We also assume that these streams are in equilibrium with sediment production from the landscape so that there is neither net deposition nor erosion. Analysis of aerial photos reveals that channel migration has not been significant over several decades. Given an average bed load yield of order 1000 m^3/yr, the entire stream bed over the 30 km main channel could be recycled to a depth of 1 m in several hundred years, and bed sediments thus likely represent modern (~10s-100s years) sediment delivery and transport regimes. While selective transport likely plays some role in altering grain size with distance downstream, particularly the sizes of surface grains, here we focus on compositional changes due to abrasion and downstream mixing, and target our results to match the subsurface sediment as more representative of the bed load.

Erosion and Abrasion Parameters

As a baseline to compare to more complex watersheds, we use the simplified linear model (equation 5), with major tributaries, calibrated so that distance and total drainage area matches the study basins. The primary model runs then follow equations 6 and 7 with increasing parameter variability (Table 2.1), in order to test the interplay between erosion and abrasion in matching the observations. We start by assuming (a) constant erosion rate with no abrasion (run 1), which results in sediment composition that is equal to the proportions of the lithologies in the basin; then (b) constant erosion rate and constant abrasion rates (run 2); and (c) several runs in which the parameters are varied based on rock type as shown in Table 2.1 (runs 3-6), including a best-fit (run 5) and reversed parameter scenario (run 6).

Parameters were scaled so that the erosion or sediment production rate reasonably matched the observed total sediment flux. Overall basin-averaged abrasion rates were set based on the measured bed load ratio at the basin outlet, and, as complexity was added, erosion and/or abrasion rates for individual rock types were tuned to best match the measured substrate composition. The α values considered are consistent with the recent compilation of Attal and

TABLE 1. MODEL PARAMETERS AND RESULTS

run #	Location/model scenario	Erosion rate, ε (m/yr)			Abrasion parameter, α (km^{-1})			m.a.e.*	r.m.s.e.†	Modeled sediment yield (m^3/yr)			Deviation from measured yield (m3/yr)		
	Big Wood R	sed	volc	gran	sed	volc	gran	composition		Q_b	Q_{susp}	Q_{tot}	Q_b	Q_{susp}	Q_{tot}
1	ε=const; α=0	1.0E-05	1.0E-05	1.0E-05	0	0	0	0.087	0.104	2454	1052	3506	1954	-1948	6
2	ε=const; α=const	1.0E-05	1.0E-05	1.0E-05	0.04	0.04	0.04	0.092	0.116	495	3011	3506	-5	11	6
3	ε=const; α=variable	1.0E-05	1.0E-05	1.0E-05	0.07	0.04	0.02	0.052	0.066	565	2941	3506	65	-59	6
4	ε=variabe; α=const	5.0E-06	1.0E-05	1.5E-05	0.04	0.04	0.04	0.055	0.080	487	3041	3527	-13	41	27
5	ε=variable; α=variable	1.15E-05	1.15E-05	5.0E-06	0.0885	0.0625	0.0030	0.044	0.059	486	3005	3491	-14	5	-9
6	best-fit for other basin	1.3E-05	1.3E-05	7.5E-06	0.013	0.011	0.0011	0.099	0.117	1818	2282	4100	1318	-718	600
	North Fork Big Lost R														
1	ε=const; α=0	1.7E-05	1.7E-05	1.7E-05	0	0	0	0.084	0.101	3478	1565	5043	1478	-1435	43
2	ε=const; α=const	1.7E-05	1.7E-05	1.7E-05	0.011	0.011	0.011	0.089	0.106	2070	2972	5043	70	-28	43
3	ε=const; α=variable	1.7E-05	1.7E-05	1.7E-05	0.009	0.018	0.0015	0.074	0.092	2038	3004	5043	38	4	43
4	ε=variabe; α=const	2.0E-05	1.5E-05	1.0E-05	0.011	0.011	0.011	0.076	0.096	2017	2990	5007	17	-10	7
5	ε=variable; α=variable	1.3E-05 (2.25e-5)§	1.3E-05	7.5E-06 (2.25e-5)#	0.013	0.011	0.0011	0.057	0.068	2006	3019	5024	6	19	24
6	best-fit for other basin	1.15E-05	1.15E-05	5.0E-06	0.0885	0.0625	0.0030	0.132	0.156	267	3055	3322	-1733	55	-1678

* Mean absolute error of measured subsurface versus modeled bed load compostion

† Root mean squared error of measured subsurface versus modeled bed load compostion

§ Erosion rate specifically for the Copper Basin Formation (CBF)

\# Erosion rate specifically for the Pioneer Core Complex (PCC)

Table 2.1. Model parameters and results.

Lave (2009) on lithology-modulated abrasion rates. These range from 0.5-25% volume loss per km; choices for individual lithologies are discussed in more detail below.

RESULTS AND DISCUSSION

Figure 2.2 shows a subset of the model runs compared to the measured downstream change in the proportion of individual lithologies in the stream bed. In all cases, variation in modeled proportions chiefly reflects the downstream sourcing of different rock types by tributaries and hillslopes (Figure 2.1). This is illustrated in the case of no abrasion (run 1), the model here simply reflects basin proportions and matches within 10% the changes in measured subsurface sediment composition (Figure 2.2, Table 2.1). When abrasion is incorporated (run 2), the model results diverge, particularly downstream, as clasts with long travel paths are slowly lost to suspension. As more variability in erosion and abrasion are added (runs 3-5), the fit improves, reducing the mean absolute error (m.a.e) to about 5% (Table 2.1). Similar to Attal and Lave (2006), we find the best-fit (run 5) result is obtained when we include both differential erosion and differential abrasion. This corresponds to a more realistic scenario in which softer lithologies (sedimentary/volcanic) are both more erodible and more easily abraded relative to resistant rock types (granitic/ plutonic) (Table 2.1). But we also find important differences in these parameters between the two watersheds, such that when the best fit parameters from one basin are applied to the other basin (reversed - run 6), the result is the poorest fit of any of the model scenarios (Figure 2.2, Table 2.1).

Figure 2.3a shows the downstream trends in bed load flux for the different model scenarios. These range from a monotonically increasing trend where abrasion is non-existent or limited (e.g. run 1; NBL best-fit), to a highly variable trend where abrasion losses act strongly in opposition to bed load inputs (e.g. BW best-fit). In both cases the linear watershed model

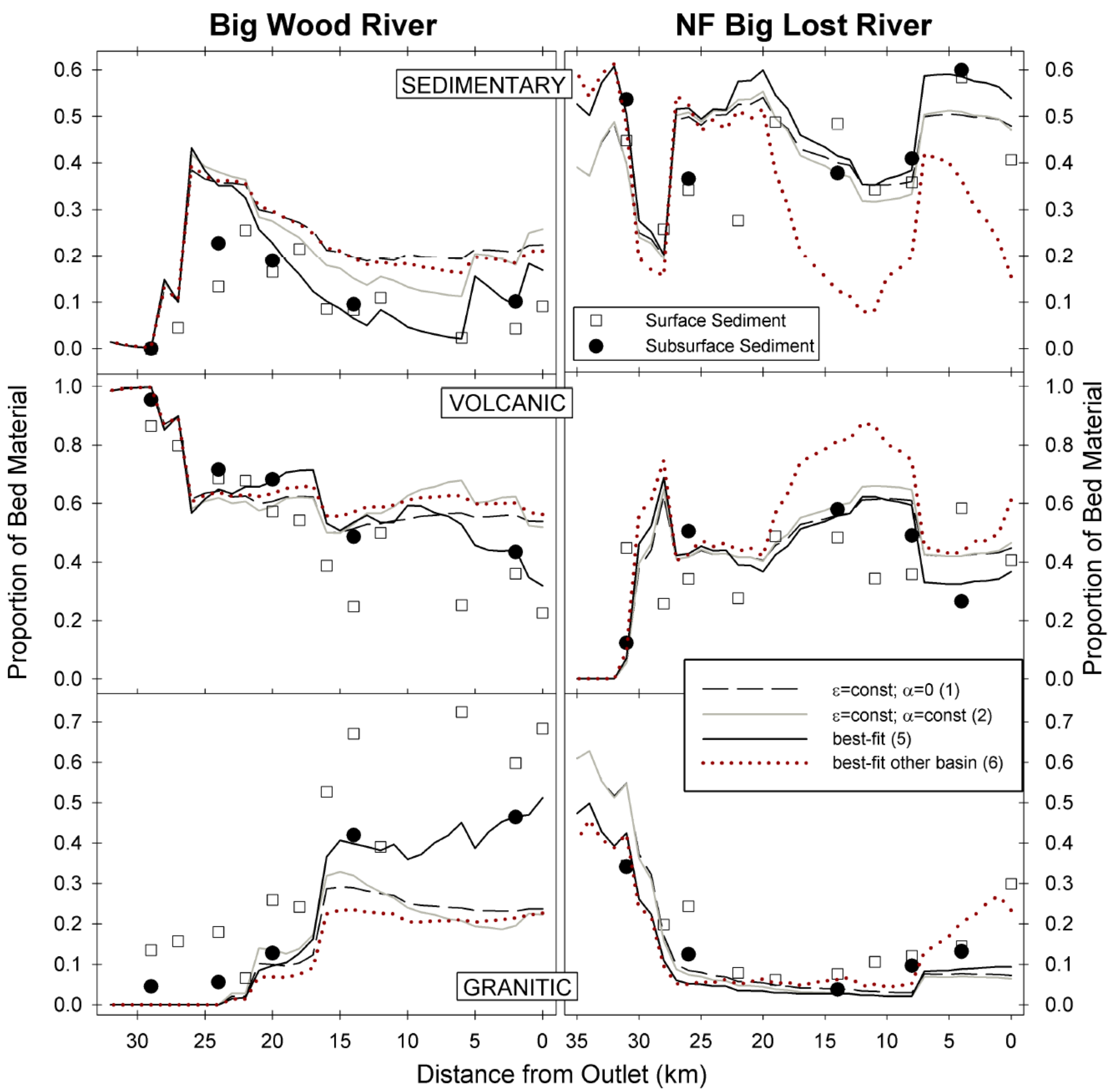

Figure 2.2. Modeled versus measured bed material proportions subdivided by lithology for a subset of the runs detailed in Table 2.1. Run numbers in parentheses.

follows the overall trend quite well (Figure 2.3a) – consistent with the lack of a downstream trend in incremental area in these basins (Figure DR2.1b) – but the best-fit model in the BW shows a much stronger sensitivity to network structure. This occurs because abrasion rates in the BW basin are necessarily higher in order to match the observed bed load proportion (Table 2.1). By contrast, the best-fit model in the NBL requires much lower abrasion rates in order to match

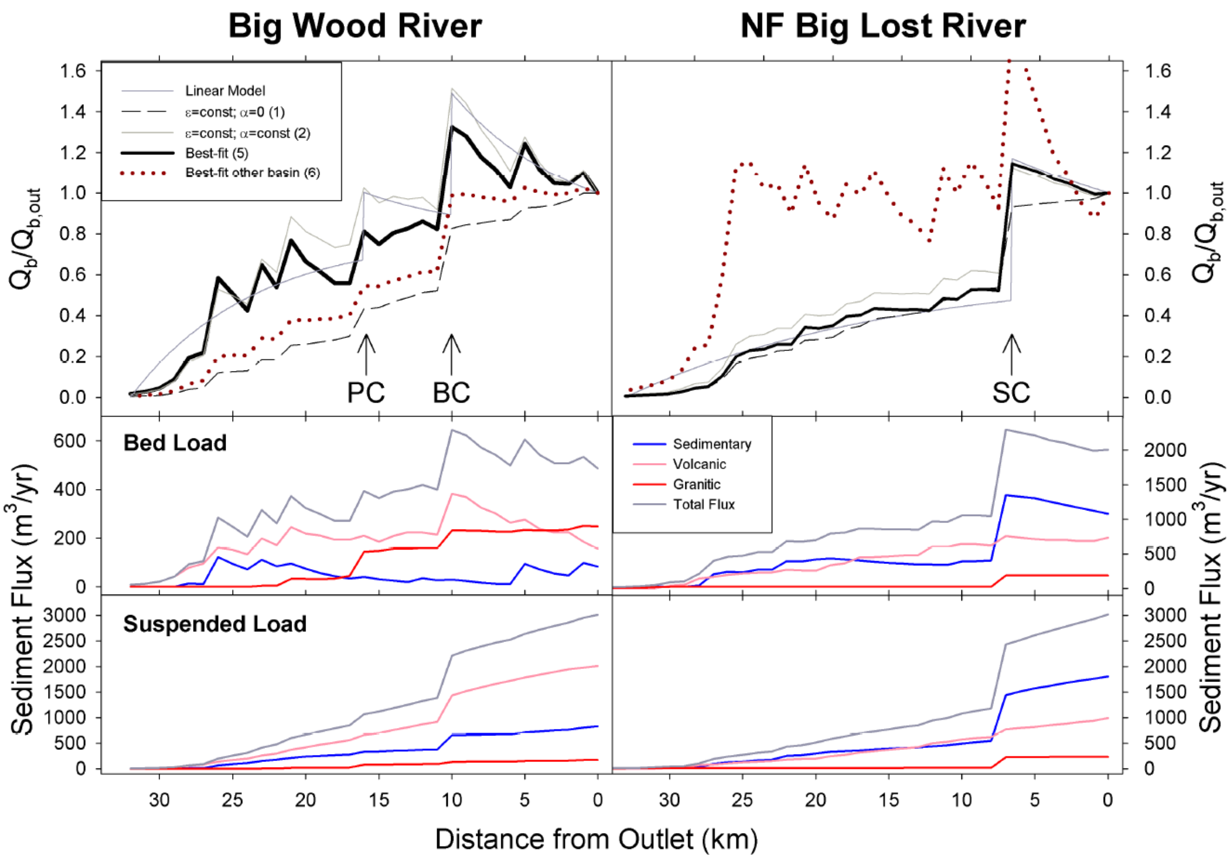

Figure 2.3. Downstream evolution of bed and suspended load fluxes. **a)** Bed load flux, Q_b, scaled to the bed load flux at the basin outlet, $Q_{b,\ out}$, highlighting the downstream trend of different parameter sets in Table 2.1. Major tributaries noted as PC: Prairie Creek, BC: Baker Creek, and SC: Summit Creek. Downstream trends in the **b)** bed and **c)** suspended load fluxes of individual lithologies for the best-fit model. Run numbers in parentheses.

observations, and the downstream bed load flux increases more steadily until a major tributary (Summit Creek) enters (Figure 2.3a). The influence of these differences in abrasion is borne out in the modeled composition of bed load versus suspended load between the basins for the best-fit scenarios (Figure 2.3b,c). Despite representing roughly 1/3 of the total sediment discharge from the BW, sedimentary rocks tend to have long travel paths and make up a tiny fraction of the bed load component, almost disappearing in some locations. A similar effect is seen with volcanic lithologies such that resistant plutonic rocks appear to grind away the softer lithologies and come to dominate the bed material (Figures 2.2 and 2.3b). In contrast, in the NBL, where abrasion is apparently more limited, stream bed material compositions are more faithful to the upstream watershed proportions (Figures 2.2 and 2.3b). In both cases, resistant granitic rocks compose a very small fraction of the modeled suspended sediment load – due to low values of α. As a result, the composition of the suspended load may be quite similar to that of the bed load (NBL) or very different from it (BW) contingent upon abrasion rates and travel path lengths (Figure 2.3b,c). Again, when the best-fit parameters are reversed between basins (run 6), sediment yields are very poorly predicted (Table 2.1), and the downstream trends in bed load flux are distinctly altered (Figure 2.3a).

The above results suggest abrasion rates in the NBL are 3-7 times less than in the BW, within the 1 to 2 order magnitude variation observed for individual rock types from experimental studies (Lewin and Brewer, 2002; Attal and Lave, 2009). In fact, the basic difference between watersheds is supported by the fact that abrasion rates can increase up to 3-fold as the proportion of resistant lithologies increases (as in the BW), but also that abrasion can be suppressed under conditions of high bed load flux by limiting impacts with resistant grains (as in the NBL) (Attal and Lave, 2009). While bed load clasts in the BW are likely to interact with immobile or resistant particles in potentially high energy collisions, sedimentary and volcanic lithologies in the NBL are more likely to be moving in higher concentrations as bed load sheets in which clast-clast collisions may be less effective (Lewin and Brewer, 2002). Indeed, grain size measurements show the bed sediment in the BW actually coarsens downstream as granitic rocks come to dominate the stream bed. This is consistent with the modeled grain size (Figure DR2.3) and is further evidence of depressed bed load transport through bed armoring (Dietrich et al., 1989).

Differences in sedimentary strata between basins also point to an obvious explanation for reduced abrasion rates in the NBL; silty carbonates dominate the Wood River Formation in the BW while more lithified sandstones and conglomerates dominate the Copper Basin Formation in the NBL. Field evidence is consistent with this interpretation, as sedimentary rocks dominate all size classes in the NBL, but are essentially absent from the coarse fraction in the BW (Figure DR2.4). Furthermore, the erosion rates of the basins in the best fit model can be set quite similar for individual lithologies with the exception of the Copper Basin Formation and the Pioneer Core Complex. In both cases these rocks are strongly deformed, and geologic mapping shows extensive faulting in the NBL associated with the Pioneer Thrust sheet, where by contrast very few faults are mapped in the BW (Worl et al., 1995). The Pioneer Core Complex is located in the most rugged, high relief portion of either watershed. A high erosion rate there better mimics the observed stream bed composition, but in general has a small influence because of its limited area. Thus the crux of the difference in sediment loads between basins appears to lie in the ubiquitous presence of the Copper Basin Formation in the NBL, coupled with limited exposures of resistant rock types.

Finally, the faithfulness of stream bed composition to our simple equilibrium model is somewhat striking, particularly in watersheds that have been glaciated. The accommodation space created by glaciers has been shown to trap sediment supplied from headwater areas, limiting the sediment connectivity between upstream hillslopes and downstream channels (e.g. Dühnforth et al., 2008). Yet our data show a strong downstream signature of successive lithologies consistent with their mapped (hillslope) proportions. The majority of the source areas in these basins show active hillslopes that clearly supply sediment directly to moderate-sized tributary channels, which act as the primary sediment point sources to the main channel (Figure 2.1 and DR2.5). The main channel sediment thus strongly reflects these source areas despite being locally disconnected from hillslopes by a floodplain. As a result, this simple method has promise for untangling the degree of channel-hillslope coupling in a variety of settings, provided that the spatial distribution of lithologies (or some other tracer) is sufficiently diverse.

CONCLUSIONS

The results of this study show that abrasion processes, which have likely been underestimated in the field (Lewin and Brewer, 2002), can dramatically alter the downstream evolution of bed and suspended load fluxes, even across relatively short distances and between basins draining a similar suite of rock types. The model results thus offer an explanation for the large difference in bed load flux between these basins. Such conclusions require attention to both abrasion processes and the distribution of travel path lengths of the major rock types in a basin. The model results demonstrate a strong linkage between modern hillslopes and channel systems even in these formerly glaciated landscapes, as the sediment signature of the primary streams reflects the systematic tapping of distinct source areas. While this work shows promise, it highlights the need for more detailed studies of such hillslope-channel interactions, which require measurement of the spatial patterns in the size and composition of bed and suspended load fluxes at locations throughout a channel network.

DATA REPOSITORY

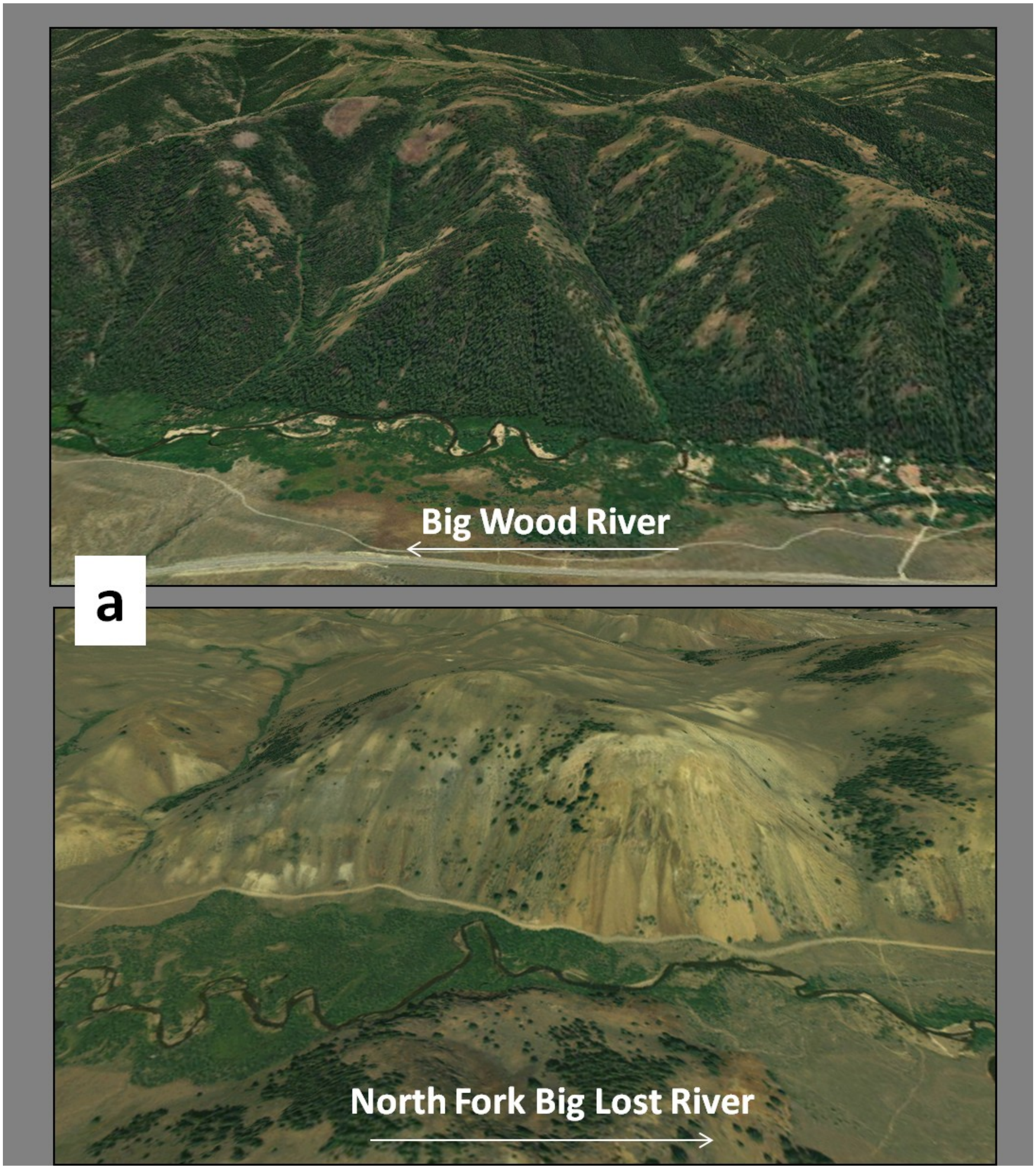

Figure DR2.1. **a)** Differences in vegetation cover in volcanic terrain between the basins, highlighting the more semi-arid vegetation cover in the NBL basin resulting in more active hillslopes. Field of view is roughly 1.5 kilometers.

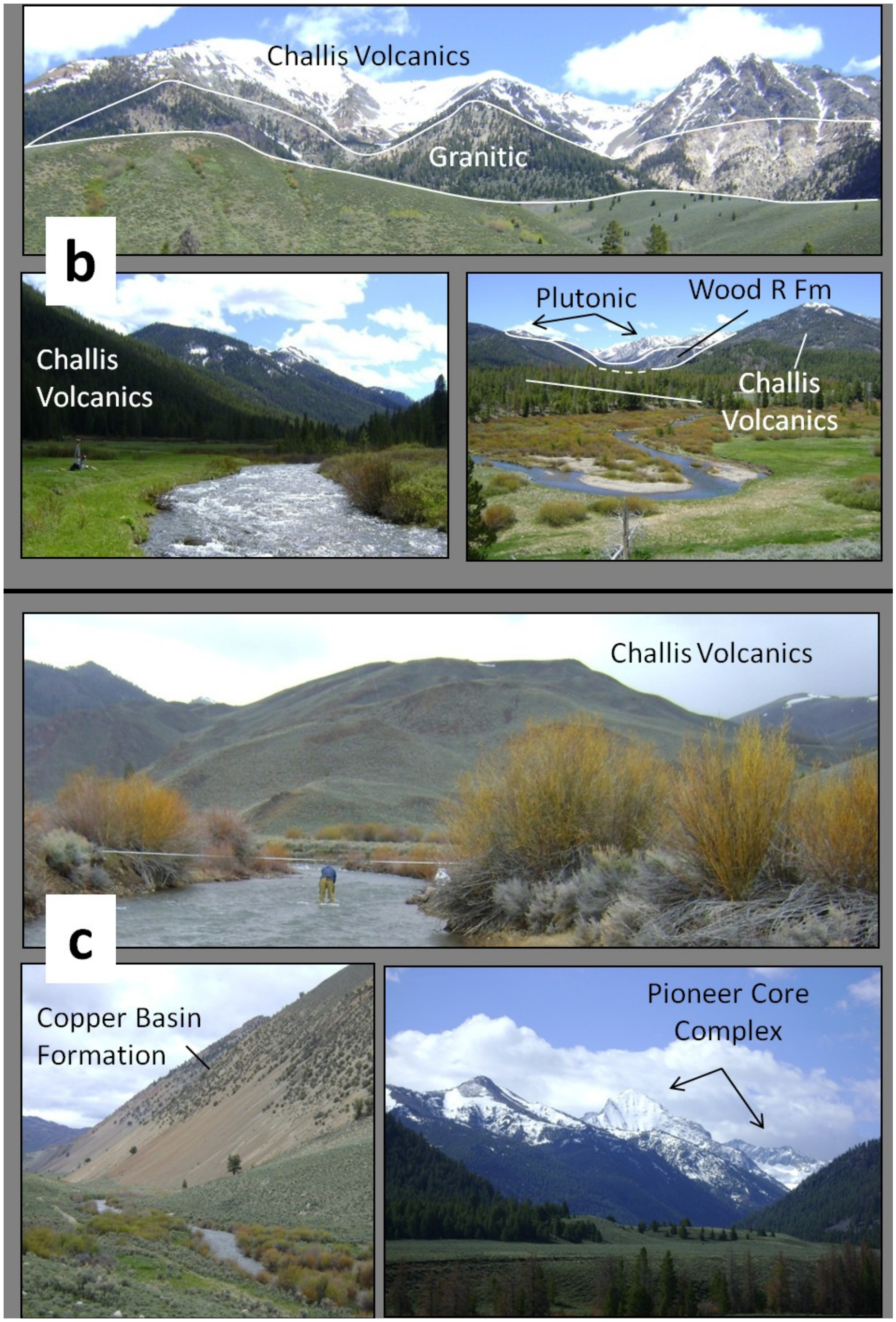

Figure DR2.1 (cont.). Exposures of different lithologies in the **b)** Big Wood basin and **c)** the Big Lost basin.

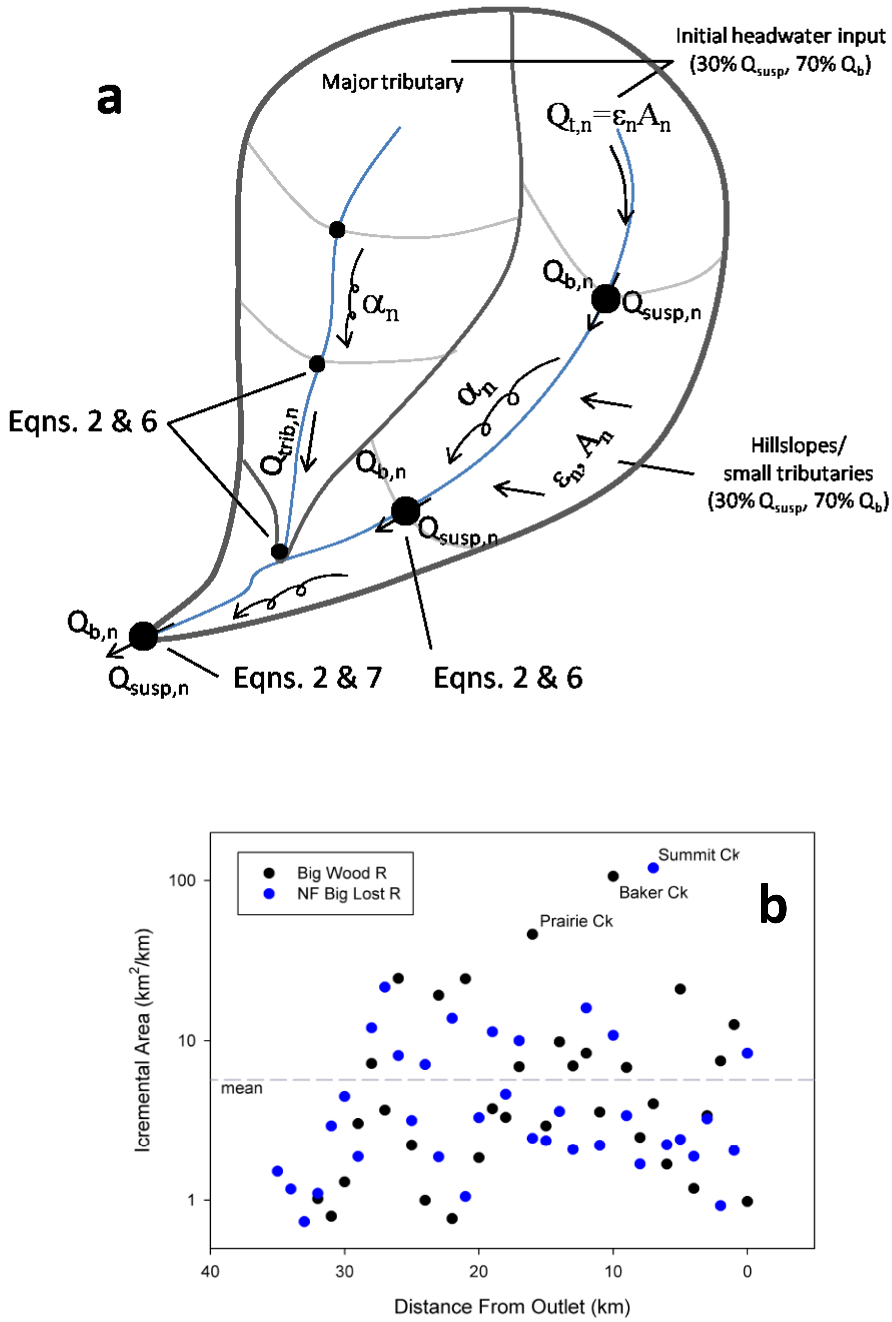

Figure DR2.2. **a)** Schematic of erosion abrasion model. At the initial upstream calculation node, sediment is delivered to the channel through a simple erosion rate, proportioned as 30% suspended load and 70% bed load. At downstream nodes, bed load fluxes are computed via equation 6, with abrasion losses added to the suspended load as in equation 2. Below major tributaries, an additional component is added as in equation 7. **b)** Incremental area added downstream at 1 kilometer increments in both basins. The major tributaries where the model was run independently are labeled, and note that another major tributary (Kane Creek) joins Summit Creek just upstream of the confluence with the main channel.

Grain Size Calculation

The median grain size of the bed load for a given lithology at the outlet of a link can be calculated as a simple combination of the input hillslope grain size and the evolved incoming bed load grain size:

$$D_{50,out;n} = D_{50,h;n}\left(\frac{Q_{h;n}}{Q_{s,out;n}}\right) + D_{50,in;n}e^{-\alpha_n L}\left(\frac{Q_{s,in;n}e^{-3\alpha L}}{Q_{s,out;n}}\right)$$

where the first term represents the grain size of the hillslope/tributary input, and the second term represents the grain size of the incoming sediment from upstream, in both cases scaled by their relative proportions. The median grain size of the bed load can then be calculated by averaging the grain size of individual lithologies weighted by their proportion in the bed load:

$$D_{50,out} = \sum_{a}^{n} D_{50,n}\left(\frac{Q_{s,out;n}}{Q_{s,out;tot}}\right)$$

In this case, the input grain size from hillslopes was defined by independent measurements of the grain size of different lithologies from small tributary (<10 km^2) basins scattered throughout both watersheds (Figure 2.1). The results from the above median grain size model are in generally good agreement with the measured size of the subsurface sediment (Figure DR2.3).

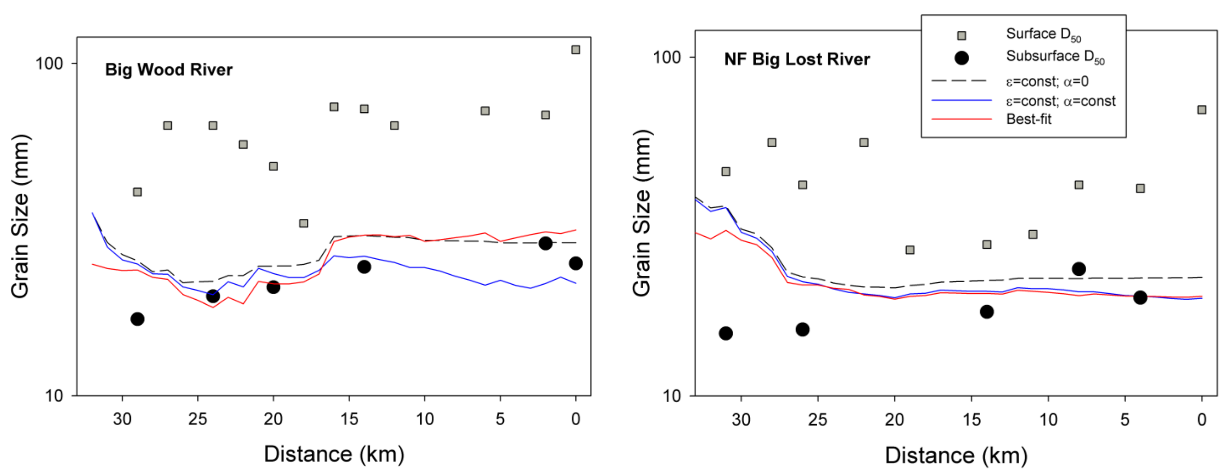

Figure DR2.3. Modeled versus measured change in grain size between the basins, where the model should best match the subsurface material.

Figure DR2.4. Field examples of different lithologies showing size and texture of subsurface bed sediment. A) Sedimentary, B) volcanic, and C) plutonic rocks in the Big Wood basin. 32mm sieve is shown for scale. D) Sedimentary, E) volcanic, and F) plutonic hand samples from the Big Wood basin. G) Wide view of samples A,B, and C from above. Note the much coarser grain size of the plutonic rocks. H) Sample dominated by quartzitic sandstones and conglomerates of the Copper Basin Formation, with fewer lighter-colored metamorphic rocks. Note channel proximal erodilble hillslope of the same material in the background. Sedimentary clasts of this formation are much coarser than found in the Big Wood Basin. Gravelometer for scale where largest opening is 180 mm. I) Close up view of pebble-conglomerate of the Copper Basin Formation.

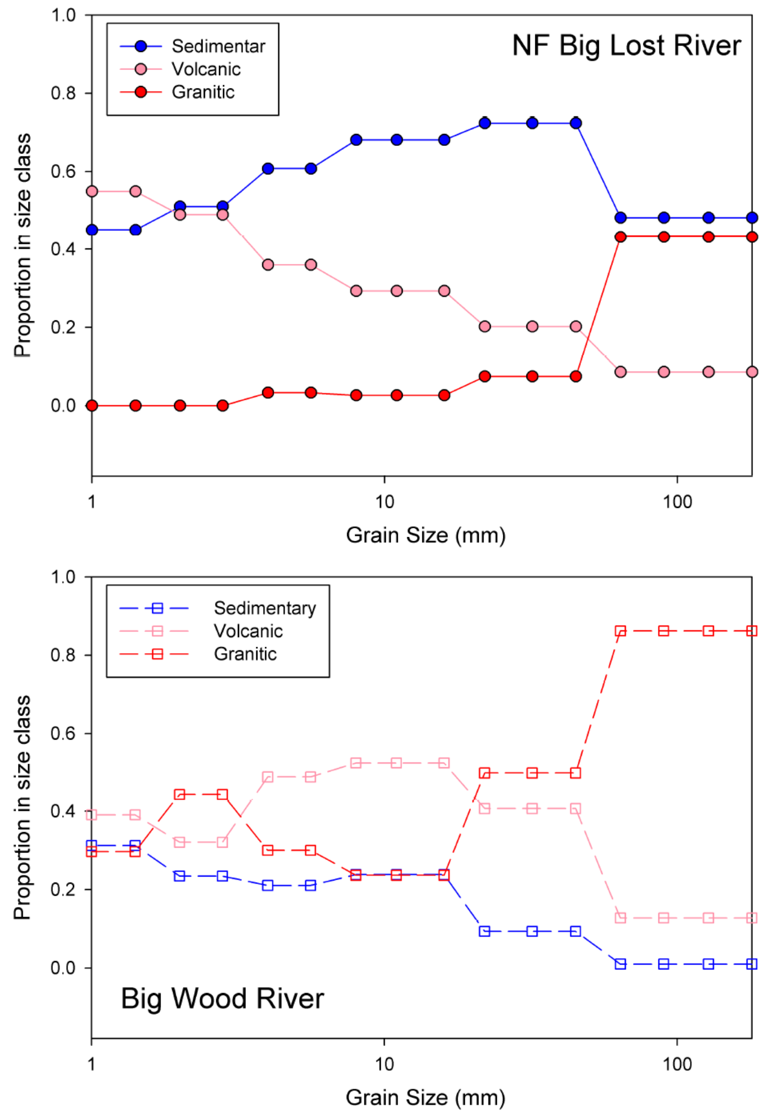

Figure DR2.4 (cont.). Plots of relative proportion of different lithologies across all size classes in the subsurface sediment near the basin outlets. Sedimentary lithologies in the NBL, which are dominated by the CBF, are ubiquitous across all size classes. In the BW, sedimentary lithologies are essentially absent from the coarse fraction, whereas volcanic rocks behave somewhat similarly between basins. The coarse nature of granitic rocks is also evident.

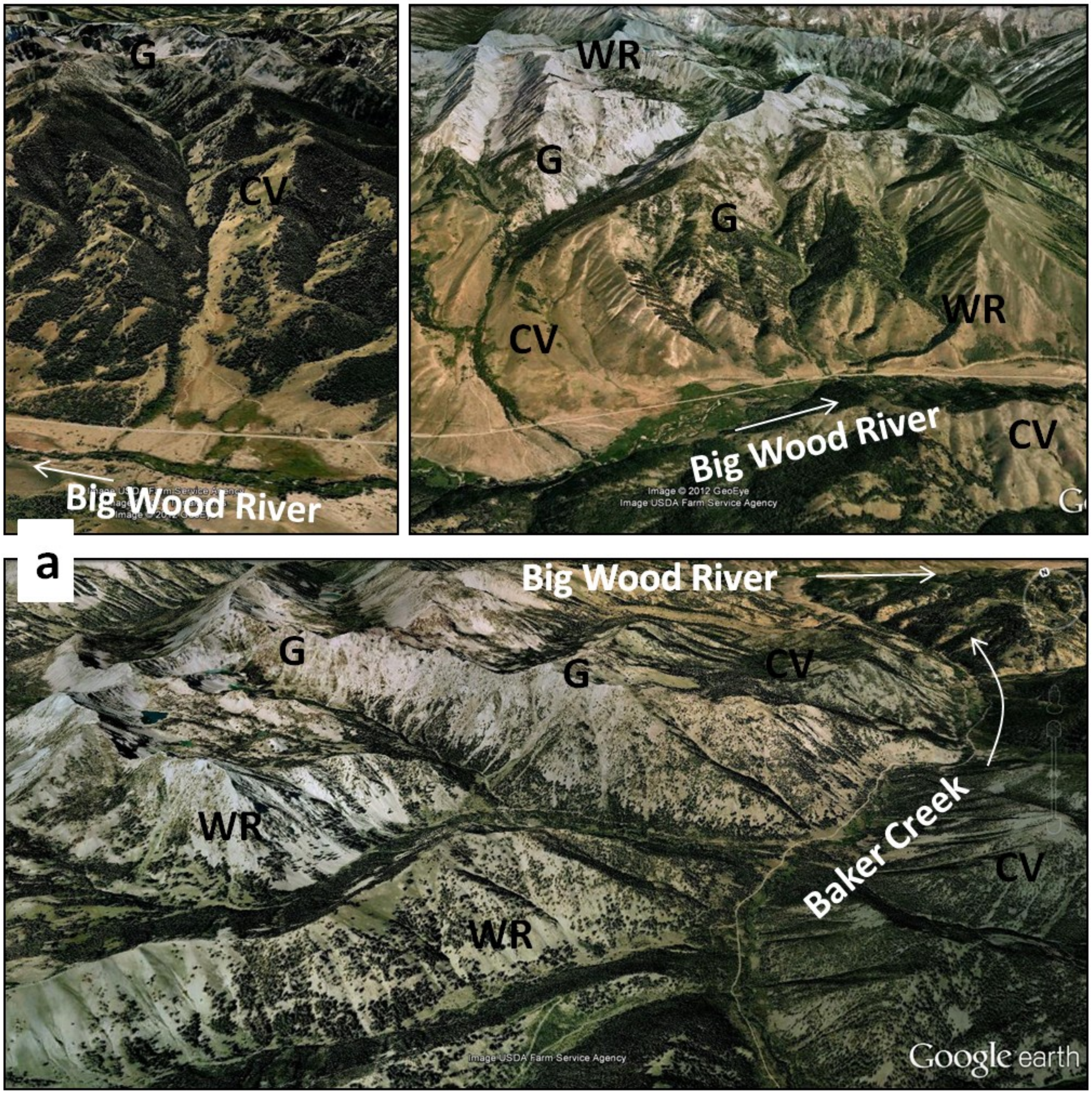

Figure DR2.5. Google Earth images showing hillslope-channel connectivity in a variety of settings; note narrow two-lane road for scale along main channel in each photo. **a)** Big Wood basin where labels show general rock types; G: granitic/plutonic; WR: Wood River Formation (sedimentary); CV: Challis volcanics. In general hillslopes and tributary channels are relatively well connected, except perhaps in the most glaciated portions of the basin. While the main channel of these basins can be disconnected from local hillslopes, point source tributary inputs dominate sediment delivery to the main channel.

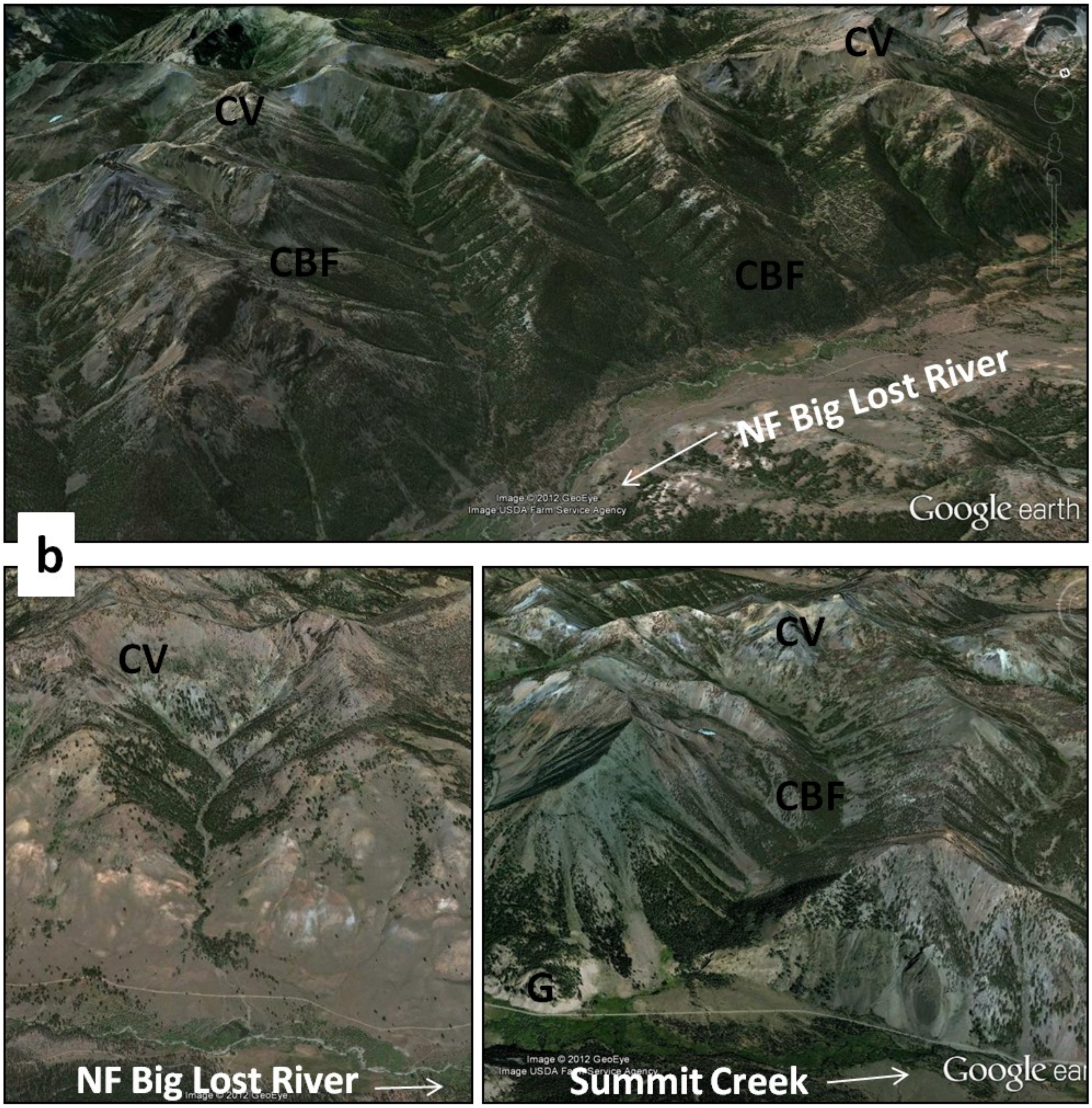

Figure DR2.5 (cont.). Google Earth images showing hillslope-channel connectivity in a variety of settings; hillslopes and debris flow channels in smaller basins feed directly to larger tributaries that enter the main channel. Note road for scale along main channel in each photo. **b)** North Fork Big Lost basin where labels show general rock types; G: granitic/plutonic; CBF: Copper Basin Formation (sedimentary); CV: Challis volcanics. Hillslope-channel coupling is perhaps even stronger in the NBL due to the soft lithologies and reduced vegetation cover, but sediment is delivered to the main channel by small tributary point sources, as in the BW.

Chapter 3 - Downstream hydraulic geometry and sediment yields in the northern Rocky Mountains, USA

INTRODUCTION

Stream channel form results from the conveyance of sediment and water, and a fundamental problem in fluvial geomorphology remains the prediction of downstream changes in channel dimensions as a function of the governing variables. In this case a suite of landscape-conditioned independent variables including discharge (Q), sediment load (Q_s), and grain size (D), are related to the adjustable characteristics of the stream channel: width (w), depth (h), velocity (u) and slope (S). In a classic paper, Leopold and Maddock (1953) introduced the empirical hydraulic geometry approach to describe the downstream scaling of channel characteristics. In this approach, bankfull discharge, Q, is assumed to be the primary independent variable and bankfull channel properties are described by a series of power-law relations:

$$w = a_w Q^{b_w} , \tag{1a}$$

$$h = a_h Q^{b_h} , \tag{1b}$$

$$u = a_u Q^{b_u} , \tag{1c}$$

and

$$S = a_S Q^{b_S} , \tag{1d}$$

where a is a coefficient, b is an exponent, and the subscripts refer to the specific variable. Many analyses of hydraulic geometry have shown the exponents in the above relations are relatively constant over a range of scales with typical values of b_w=0.4-0.5, b_h=0.3-0.4, and b_u=0.1-0.2

(Park, 1977; Hey and Thorne, 1986; Church, 1992; Knighton, 1998), although changes in slope tend to be more variable and conditioned by geologic history (Ferguson, 1986).

There is a long standing debate as to what yields these quasi-universal relations, and analytical approaches provide a physically-based framework for predicting channel dimensions using equations for flow and sediment transport. For a determinate solution, four relations are needed to define the channel dimensions (w, h, u, S) in terms of the independent variables (Q, Q_s, D) (Parker, 1979; Ferguson, 1986; Pizzuto, 1992; Millar and Quick, 1998; Eaton et al., 2004). Three of these relations are given through flow continuity (Q=whu), a flow resistance equation, and a bed load transport equation (Griffiths, 1983, 1984). Yet the solution to the problem requires some additional closure such as a channel stability relation (Ferguson, 1986). Some workers have attempted to avoid this problem by adopting some optimality criterion or extremal hypothesis (e.g. minimum slope, maximum transport efficiency) to select from the range of possible channel dimensions for a given set of input conditions (White et al., 1982; Eaton et al., 2004; Millar, 2005), although these approaches have been criticized as lacking a physical basis (Griffiths, 1984). Alternatively, Parker (1978) showed that lateral momentum diffusion and stress reduction near the banks results in a stable channel width with active bed load transport. Expressed in terms of the dimensionless Shields number:

$$\tau^* = \frac{\tau}{(\rho_s - \rho) g D_{50}} \tag{2}$$

where τ is the bankfull shear stress, ρ_s is the sediment density, ρ is water density, g is gravitational acceleration , and D_{50} is the median grain diameter, Parker (1978) originally proposed that at bankfull, $\tau^*=1.2\tau^*_r$, where τ^*_r is a reference shear stress near the threshold for motion. In the more recent work of Parker et al. (2008), they suggest that at bankfull $\tau^*=1.67\tau^*_r$. This simple shear stress rule provides a physical basis for stable channel form, though measurements from natural rivers show considerable variability in both τ^* and τ^*_r (e.g. Mueller et al., 2005; Church, 2006; Pitlick et al., 2008; Recking, 2009).

No matter the approach, prediction of downstream hydraulic geometry fundamentally rests on appropriate specification of Q, Q_s, and D. Because there is rarely any information on the bed load flux, slope is often treated as independent and the sediment load is then calculated (Ferguson, 1986). While field measurements of channel geometry can be used to assess the predictions for width and depth, the lack of information on sediment loads represents a primary empirical void for testing physically-based approaches describing bankfull hydraulic geometry (e.g. Millar, 2005). This led Parker et al. (2008) to suggest that the real missing component from previous analyses is a relation that describes how a catchment has organized to deliver sediment downstream. In fact, Leopold and Maddock's (1953) original formulation included such a function for sediment load of the form:

$$Q_s = cQ^d \tag{3}$$

where Q_s is the sediment flux and c and d are a power-law coefficient and exponent respectively. Defining concentration as Q_s/Q, an exponent greater than 1 indicates increasing downstream sediment concentrations and less than 1 decreasing concentrations. This basin-conditioned relation between discharge and sediment load should be borne out in the downstream hydraulic geometry. Griffiths (1983), for example, assumes constant downstream bed load concentration (d=1) to close the hydraulic geometry problem. Alternatively, Eaton and Church (2007) use an optimality criterion and suggest that sediment concentration should decrease downstream.

Despite the implications for the hydraulic geometry problem, very little data exist to evaluate the true value of d, despite multitudes of studies on channel geometry. Mueller and

Pitlick (2005) used measured channel geometry to calculate sediment loads and found that annual $Q_{bed} \propto Q^{0.96}$ for a small watershed in the Colorado Rocky Mountains. Alternatively, Parker et al. (2008) used a similar, although dimensionless, approach with a larger data set and found that bankfull $Q_{bed} \propto Q^{0.55}$. In both cases the magnitude of the exponent is strongly dependent on the ratio τ^*/τ^*_r, or transport intensity. Parker et al. (2008) treat this as a constant and a property of stable channels (see above). On the other hand, τ^*_r has been shown to depend strongly on slope and attendant changes in flow hydraulics (Mueller et al., 2005; Lamb et al., 2008; Recking, 2009; Ferguson, 2012). Mueller and Pitlick (2005) use a slope-dependent τ^*_r resulting in a downstream increase in transport intensity. In combination, these studies show that, depending on the formulation, authors have variously suggested a near linear scaling (Griffiths, 1983; Mueller and Pitlick, 2005), a square-root scaling (Parker et al., 2008), or even a negative scaling of Q_{bed} and Q (Eaton and Church, 2007). Ultimately, all of these scenarios are possible, as the downstream sediment flux is ultimately conditioned by climate and basin properties (as are Q and D).

In contrast to bed load, there is considerable empirical data for suspended load which can provide some insight on the variability in scaling patterns. For example, Leopold et al. (1964), in terms of the suspended load transport rate, Q_{susp}, give exponents of 0.8 and 1.3 in equation 3 for Midwestern streams and semiarid ephemeral streams respectively, while Emmett (1975) in the upper Salmon River basin found an exponent of 0.75. Several other authors have explored the scaling of specific suspended sediment yields (yield scaled by drainage area) as drainage area increases downstream and found that – almost uniformly – specific sediment yield decreases downstream (e.g. Walling, 1983; Syvitski and Milliman, 2007). This implies an exponent less than one in equation 3 (given that discharge typically scales with drainage area to some exponent less than or equal to 1). This could indicate less intense erosion as streams flow from mountains to plains, or that sediment is being stored in the system in depositional basins (Aalto et al., 2006). Alternatively, Church et al. (1989,1999) and Schiefer et al. (2001) using suspended sediments and lake sediments respectively, find that specific sediment yield increases downstream in many regions of Canada which they attribute to degradation of glacial valley fill deposits. The above studies indicate a range of scaling shaped by regional physiography and geologic history. We would therefore expect landscapes of different climate and geologic history to exhibit potentially very different coefficients and exponents in equation 3. In fact, the universality of downstream hydraulic geometry relations tends to obscure variations in sediment supply between basins, and suggests that simple adjustments of width or depth may not be indicative of actual differences in sediment transport rates.

Objectives

In this study we address the sediment component of the hydraulic geometry problem in the context of a unique sediment transport data set for over 80 streams and rivers in the northern Rocky Mountains of Idaho, Montana, and Wyoming, coupled with measurements of channel geometry and grain size from a variety of sources. These data sets are used to address three primary research questions:

1) What are the regional scaling patterns between sediment load and discharge?

2) Can a predictive approach based on a channel-forming Shields number reproduce the observed channel dimensions and sediment scaling relations?

3) Are the observed scaling patterns consistent with watershed-scale sediment delivery considerations, and can the inherent spatial variability in sediment supply be reconciled with the apparent uniformity of hydraulic geometry?

In order address these questions, bankfull and annual sediment loads are calculated to describe the downstream scaling in both bed and suspended loads for four major river basins: Upper Spokane, Clearwater, Salmon, and Yellowstone. We then explore the relationship between channel geometry and sediment flux in the context of theoretical hydraulic geometry relations based on a channel-forming Shields number. Last, a paired-watershed study of two basins with a 10-fold difference in bed load concentrations is used to document on a smaller scale the local variations in channel geometry and bed sediment texture between basins due to sediment supply. In this case, field measurements are used to model longitudinal bed load fluxes at the reach scale and are then compared to measurements at the basin outlet. In the paired basins, the hydraulic geometry approach is compared with an independent erosion-abrasion model of bed and suspended load flux (see Chapter 2), providing a context for the observed scaling patterns. These coupled analyses show that the quasi-universal nature of hydraulic geometry disguises orders of magnitude variability in regional sediment flux, and reach-scale transport intensity may vary considerably both downstream and regionally as a function of bed texture.

STUDY AREA

Regional Analysis

This study focuses on streams and rivers draining the northern Rocky Mountains in Idaho and the greater Yellowstone Region in Wyoming and Montana (Figure 3.1). The study sites encompass four major river basins: from north to southeast these are the Upper Spokane, Clearwater, Salmon, and Yellowstone Rivers. It should be noted that the sites in this study are scattered throughout these basins, and in the Salmon and Yellowstone regions several sites just

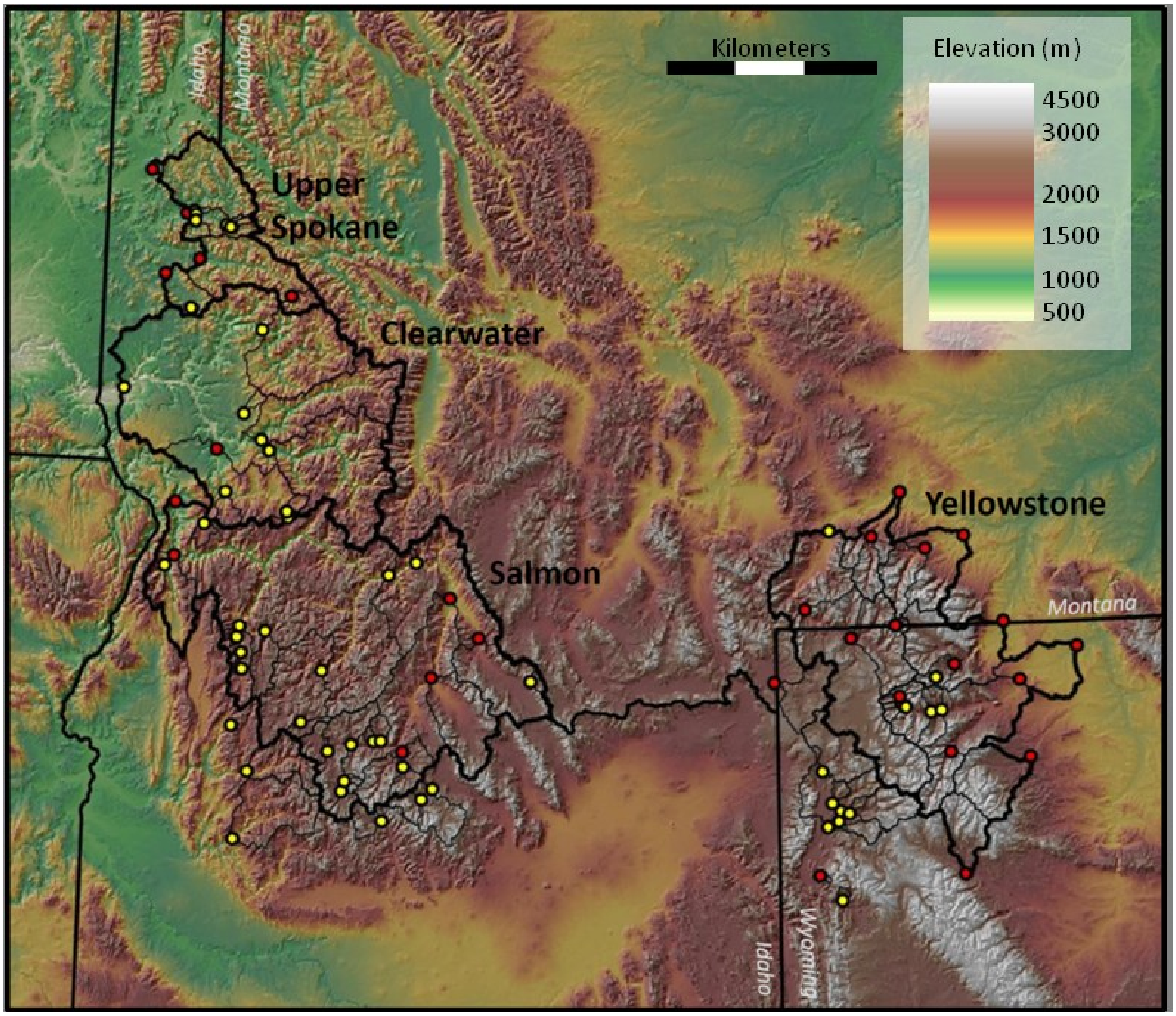

Figure 3.1. Map of study area. Outlined in bold are major river basins referred to in the study. Lighter outlines delineate individual basins. Yellow dots: bed load and suspended load samples; Red dots: suspended load samples.

outside the drainage boundary are lumped within these basins. As a result, the data presented here are regional trends. The physiography of the region is typified by a topographic gradient where elevation generally increases from north to south. Conversely, precipitation tends to decrease from north to south, particularly in Idaho, with slightly higher precipitation in the Yellowstone region of Wyoming and Montana. All of the basins are dominated by snowmelt, though rain-on-snow events do occur, particularly in lower elevation basins in Idaho. The entire region was previously glaciated in the higher elevations (Pierce, 2003), but with substantial local variation in extent. Vegetation is dominated by coniferous forest but gives way to more semi-arid land cover at lower elevations – specifically in wide valleys more common to the upper Salmon and Yellowstone regions.

Basin lithology plays an important role in sediment production, discussed in detail in Chapter 1. The basic regional geology is as follows: The upper Spokane River basin in northern Idaho lies in the Northern Rockies fold and thrust belt and is dominated by Proterozoic metasedimentary rocks of the Belt Supergroup. The Clearwater River basin in north-central Idaho is largely composed of granitic rocks of the Cretaceous Idaho Batholith with lesser Belt rocks and flat-lying Miocene Columbia River Basalt flows. The Salmon River basin and adjacent streams are composed of mixed lithologies; the Idaho Batholith is exposed in the eastern half of the basin, with a mixture of Eocene Challis volcanics and Paleozoic sedimentary rocks to the west. Finally, the streams draining the Yellowstone Region of Wyoming and Montana are dominated by volcanic rocks of the Yellowstone Plateau and the Eocene Absaroka Volcanic Province, with lesser amounts of sedimentary rocks. Both the Salmon and Yellowstone regions have been broken up to some degree by basin and range faulting, and the Yellowstone hot spot has locally uplifted the crust (Pelton and Smith, 1982; Pierce and Morgan, 1992). Because rock type and climate are broadly consistent within a given basin, these delineations provide an ideal test for the influence of regional physiographic controls on observed hydraulic geometry and sediment transport scaling relations.

Paired Watershed Study

From the broader data set above two watersheds in the Idaho study area, the Big Wood River (BW) and North Fork Big Lost River (NBL) (Figure 3.2), were selected for a paired

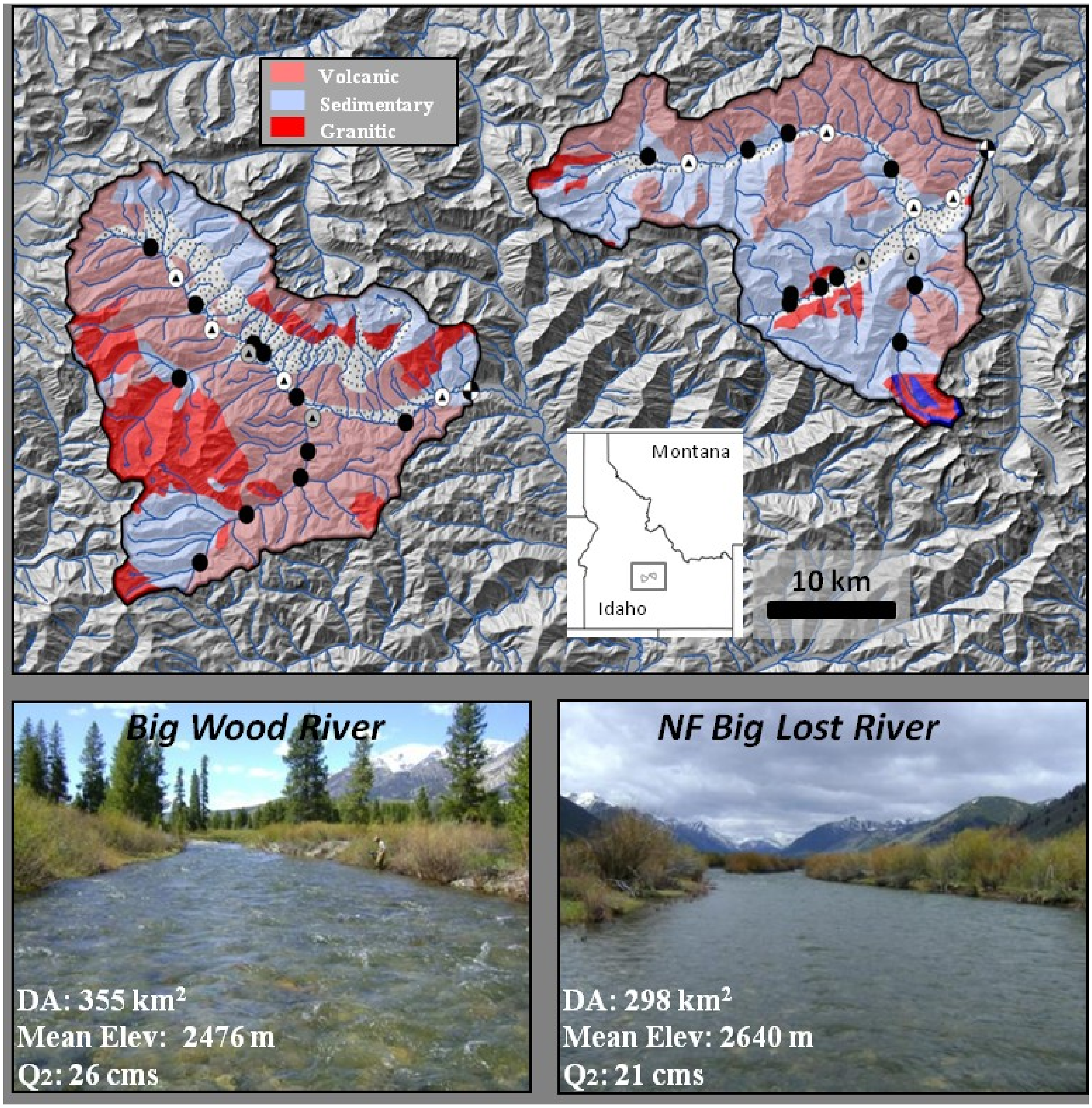

Figure 3.2. Location map for paired watershed study, with the Big Wood basin on the left, and the North Fork Big Lost basin on the right. Black circles indicate locations of morphological measurements and surface sediment samples; sites with subsurface samples are shown as white or gray circles with triangles. Photos and characteristics of the basin near the downstream end of the study area are shown at bottom. DA: drainage area; Q_2: 2-year recurrence flow.

watershed study of the influence of sediment supply on network-scale hydraulic geometry. These basins are very consistent in their hydrology (dominated by snowmelt), span a similar elevation range, are of comparable drainage area, but differ markedly in sediment loads – overall measured bed and suspended load sediment concentration are 5-10 times greater in the NBL. In these basins, variation in sediment yields is likely driven by differences in basin-wide lithology, both in the proportion of granitic rocks as well as erodibility of sedimentary rock types (see Chapter 2). Field measurements described below are used to document differences in channel morphology and sedimentology between these basins.

METHODS

Regional Analysis

Coupled measurements of flow and sediment transport were used to develop transport relations between discharge and sediment load for each site where the data were available; 80 streams and rivers had suspended sediment measurements, and 52 had bed load measurements. Sediment transport (bed load and suspended load) measurements were obtained from a variety of sources (Table 3.1), and the sampling protocol in the majority of these studies followed the USGS procedures outlined in Edwards and Glysson (1999). Bed load samples were typically obtained with a Helley-Smith or Elwha sampler employed by wading, or from a bridge. In nearly all cases sediment samples were obtained within a kilometer of a USGS or USFS gauging station. Instantaneous measurements of bed load and suspended load were plotted versus discharge for each site, and fit with a power-law relation of the form:

$$Q_s = \alpha Q^{\beta} \tag{4}$$

where α and β are a coefficient and exponent respectively. In several cases where a power-law

	Source[a]	Drainage Area (km^2)	Bankfull Q (cms)	Guage Record (yrs)	Bankfull Width (m)	Bankfull Depth (m)	Slope (m/m)	Number of Samples Susp Load	Number of Samples Bed Load	Bankfull Sediment Load Q_{tot} (m^3/s)	Bankfull Sediment Load Q_{susp} (m^3/s)	Bankfull Sediment Load Q_{bed} (m^3/s)	Bankfull Sediment Load Q_{grav} (m^3/s)	Bankfull Sediment Load Q_{sand} (m^3/s)	Annual Sediment Load Q_{tot} (m3/yr)	Annual Sediment Load Q_{susp} (m3/yr)	Annual Sediment Load Q_{bed} (m3/yr)	Annual Sediment Load Q_{grav} (m3/yr)	Annual Sediment Load Q_{sand} (m3/yr)	Surface D_{50} (m)	Sub-Surface D_{50} (m)
Upper Spokane Basin																					
Cat Spur Creek	9,9	28	2.4	8	5.5	0.45	0.0111	32	35	2.4E-05	1.2E-05	1.2E-05	4.0E-06	6.0E-06	35	22	13	3	8	0.027	---
Ninemile Creek	1,6	30	3.4	8	5	---	---	10	16	0.00022	1.5E-04	7.0E-05	3.6E-05	1.6E-05	307	209	98	65	22	---	---
Hayden Creek	2,1	56	6.8	37	13.8	0.4	---	151	---	---	2.0E-04	---	---	---	---	49	---	---	---	---	---
Canyon Creek	1,6	57	11	9	10.5	---	---	11	16	0.00021	2.0E-04	1.0E-05	3.4E-06	5.2E-06	263	252	11	4	5	---	---
Pine Creek	1,6,13	189	35	13	25	---	0.0160	12	15	0.0022	7.0E-04	1.5E-03	1.2E-03	1.1E-04	1126	677	449	1125	106	0.075	---
South Fork Coeur d'Alene River	2,6	279	39	20	16.5	---	---	12	20	0.00111	9.1E-04	2.0E-04	1.6E-04	3.2E-05	2453	2237	216	476	66	---	---
St. Joe River	1,1	310	56	13	---	---	---	54	---	---	2.4E-04	---	---	---	---	358	---	---	---	---	---
St. Maries River	2,1	706	67	44	36.6	1.3	---	14	---	---	1.9E-03	---	---	---	---	3938	---	---	---	---	---
South Fork Coeur d'Alene River	2,6	744	80	23	41.7	---	---	12	19	0.00268	2.3E-03	3.5E-04	2.4E-04	1.0E-04	5992	5114	878	639	219	---	---
North Fork Coeur d'Alene River	2,6,14	2315	340	71	84	---	---	8	10	0.0123	1.1E-02	1.5E-03	1.2E-03	1.2E-04	26847	23404	3442	3265	209	0.054	---
St. Joe River	2,1	2653	366	90	78.4	2.1	---	38	---	---	2.0E-03	---	---	---	---	2910	---	---	---	---	---
Coeur d'Alene River	2,1	3126	431	76	---	---	---	61	---	---	6.3E-03	---	---	---	---	9237	---	---	---	---	---
Clearwater River Basin																					
Trapper Creek	9,9	21	2.6	---	5.9	0.4	0.0414	143	167	3E-05	2.0E-05	1.0E-05	5.0E-06	5.0E-06	---	---	---	---	---	0.085	0.017
South Fork Red River	9,9	98	7.3	35	8.9	0.6	0.0146	136	202	5.4E-05	4.4E-05	1.0E-05	2.5E-06	5.0E-06	198	156	42	8	19	0.096	0.025
Lolo Creek	9,9	108	12	35	12.2	1	0.0097	135	112	5.2E-05	4.2E-05	1.0E-05	1.3E-06	6.0E-06	270	216	54	6	28	0.068	0.020
Main Fork Red River	9,9	129	9.4	36	11.5	0.6	0.0059	136	198	9.3E-05	6.3E-05	3.0E-05	6.5E-06	2.0E-05	425	286	138	31	90	0.059	0.018
Johns Creek	9,9	292	49	10	18.2	1.1	0.0207	46	122	0.00039	2.9E-04	1.0E-04	7.0E-06	8.0E-05	312	274	38	2	15	0.207	0.035
South Fork Clearwater River	2,1	3027	152	46	---	---	---	45	---	---	4.0E-03	---	---	---	---	6070	---	---	---	---	---
Lochsa River	9,9	3052	446	77	77.3	2.7	0.0023	36	72	0.00916	8.9E-03	2.3E-04	3.1E-05	1.8E-04	14997	14462	535	74	421	0.137	0.026
North Fork Clearwater River	9,9	3354	453	40	84	2.8	0.0005	36	70	0.01401	1.4E-02	4.1E-04	6.0E-05	3.0E-04	32327	31220	1107	180	816	0.095	0.023
Selway River	9,9	4962	652	78	89.2	2.5	0.0021	36	72	0.01376	1.3E-02	7.6E-04	6.0E-05	5.3E-04	22838	21548	1290	104	871	0.186	0.024
Clearwater River	10,10	24065	2210	85	145	5.3	0.0003	47	78	0.0472	4.5E-02	2.2E-03	7.5E-04	1.3E-03	185620	180400	5220	1093	4682	0.074	0.018
Salmon River Region																					
Little Buckhorn Creek	9,9	16	0.6	5	4.3	0.3	0.0509	73	72	7.6E-06	3.6E-06	4.0E-06	1.6E-06	2.6E-06	31	18	13	4	9	0.081	0.015
Squaw Creek (USFS)	9,9	42	0.6	---	2.8	0.24	0.0240	89	42	4.6E-06	3.0E-06	1.6E-06	7E-07	7.7E-07	---	---	---	---	---	0.027	---
Fourth of July Creek	9,9	42	3.9	---	8.2	0.46	0.0202	25	79	0.00013	1.0E-04	3.0E-05	1.5E-05	1.4E-05	---	---	---	---	---	0.051	---
Dollar Creek	9,9	43	7.8	5	10.8	0.43	0.0146	76	85	0.0001	6.0E-05	4.0E-05	2.5E-05	2.5E-05	116	87	28	8	19	0.077	0.022
Blackmare Creek	9,9	46	4.7	5	6.8	0.56	0.0299	83	88	3.2E-05	1.7E-05	1.5E-05	5E-06	6.5E-06	75	56	19	5	14	0.099	0.021
West Fork Buckhorn Creek	9,9	59	5.7	5	9.4	0.57	0.0320	68	85	4.6E-05	3.1E-05	1.5E-05	5.2E-06	7.7E-06	80	58	22	8	13	0.180	---
Thompson Creek	9,9	67	2.5	38	6.4	0.33	0.0153	24	84	9.5E-05	7.0E-05	2.5E-05	5.5E-06	1.5E-05	522	361	161	38	114	0.062	0.043
Hawley Creek	9,9	105	1.3	---	6.5	0.24	0.0233	82	85	0.00002	1.5E-05	5.0E-06	1.3E-06	2E-06	---	---	---	---	---	0.040	---
Little Slate Creek	9,9	167	12	46	14.2	0.66	0.0268	80	157	0.00011	1.0E-04	1.0E-05	1E-06	9E-06	299	263	36	3	24	0.107	0.024
Squaw Creek (USGS)	9,9	186	5.1	38	11.3	0.44	0.0100	32	62	0.00027	2.2E-04	5.0E-05	1.5E-05	0.00003	1251	1093	158	63	64	0.046	0.029
Marsh Creek	9,9	205	21	---	12.3	0.84	0.0060	27	98	0.00018	7.2E-05	1.1E-04	6.7E-05	4.6E-05	---	---	---	---	---	0.056	---

Table 3.1. Site characteristics and sediment transport data for individual study basins.

Table 3.1. (continued)

	Source[a]	Drainage Area (km^2)	Bankfull Q (cms)	Guage Record (yrs)	Bankfull Width (m)	Bankfull Depth (m)	Slope (m/m)	Number of Samples Susp Load	Number of Samples Bed Load	Bankfull Sediment Load Q_{tot} (m^3/s)	Q_{susp} (m^3/s)	Q_{bed} (m^3/s)	Q_{grav} (m^3/s)	Q_{sand} (m^3/s)	Annual Sediment Load Q_{tot} (m3/yr)	Q_{susp} (m3/yr)	Q_{bed} (m3/yr)	Q_{grav} (m3/yr)	Q_{sand} (m3/yr)	Surface D_{50} (m)	Sub-Surface D_{50} (m)
Salmon River Region (cont.)																					
Salmon River	9,9	255	13	12	10.2	0.8	0.0066	23	50	0.00035	3.0E-04	5.0E-05	1.6E-05	2.6E-05	849	734	115	36	63	0.061	0.026
Rapid River	9,9	278	18	88	18.5	0.64	0.0108	85	190	0.00029	2.2E-04	7.0E-05	0.00003	0.00002	1390	1010	380	66	50	0.079	0.016
Herd Creek	9,9	293	5.5	---	9	0.48	0.0077	23	72	0.00036	3.0E-04	6.6E-05	0.00005	0.00003	---	---	---	---	---	0.067	---
North Fork Big Lost River	2,7,17	298	20	66	7.6	1.02	0.0063	23	23	0.0025	1.6E-03	9.0E-04	0.0004	0.0002	4812	2886	1926	782	305	0.056	0.020
Big Wood River	9,9	351	22	23	12.8	0.89	0.0092	26	100	0.00085	7.5E-04	1.0E-04	4.7E-05	4.8E-05	3443	2913	530	222	187	0.119	0.025
Valley Creek	9,9	377	24	66	24.7	0.79	0.0040	71	192	0.00028	1.1E-04	1.7E-04	7.6E-05	8.2E-05	998	443	555	251	281	0.040	0.021
Johnson Creek	9,9	564	40	79	24	1	0.0040	36	72	0.00014	1.3E-04	8.0E-06	1.4E-06	5.5E-06	928	857	71	21	48	0.190	---
South Fork Salmon River	9,9	854	71	35	34.2	1.72	0.0025	92	130	0.00135	9.5E-04	4.0E-04	7.1E-05	0.0003	5567	3842	1726	425	1205	0.038	---
Big Lost River	2,7	1142	50	62	15.5	1.56	---	21	21	0.0029	2.4E-03	5.0E-04	0.0003	0.00015	8347	7236	1112	656	454	---	---
South Fork Payette River	9,9	1157	86	66	51.5	0.95	0.0040	37	72	0.00415	3.4E-03	8.0E-04	0.0003	0.0006	23315	20065	3249	1265	1792	0.096	0.020
East Fork Salmon River	2,8	1401	36	19	38.7	1.3	---	21	---	---	1.6E-03	---	---	---	---	4887	---	---	---	---	---
Little Salmon River	2,1	1493	118	57	21.1	0.9	---	33	---	---	1.9E-03	---	---	---	---	5541	---	---	---	---	---
Salmon River	9,9	2092	118	74	36.3	1.82	0.0034	30	60	0.00215	2.0E-03	1.5E-04	0.0001	6.4E-05	9569	7993	1576	1481	245	0.104	0.025
Pahsimeroi River	1,1	2151	9.5	26	---	---	---	32	---	---	9.0E-05	---	---	---	---	1160	---	---	---	---	---
Boise River	9,9	2154	167	96	59	1.38	0.0038	40	82	0.0096	8.5E-03	1.1E-03	0.00009	0.001	38248	34726	3522	224	2756	0.074	0.023
Lemhi River	2,1	2326	20	51	---	---	---	30	---	---	4.2E-04	---	---	---	---	2523	---	---	---	---	---
Middle Fork Salmon River	9,9	2726	214	17	61.1	1.43	0.0041	31	64	0.0029	2.7E-03	2.0E-04	5.4E-05	0.0001	14806	12185	2621	2330	835	0.146	0.036
Salmon River	2,1	9707	196	95	65.5	1.3	---	31	---	---	6.1E-03	---	---	---	---	28417	---	---	---	---	---
Salmon River	9,9	16166	326	42	85.2	1.84	0.0019	21	61	0.0155	1.5E-02	5.0E-04	0.0002	0.0003	63771	60654	3117	1370	713	0.096	0.028
Salmon River	2,1	34773	1479	98	121	4.4	---	201	---	---	7.0E-02	---	---	---	---	237584	---	---	---	---	---
Yellowstone Region																					
Cache Creek	4,1	28	1.7	48	---	---	---	240	---	---	6.0E-05	---	---	---	---	71	---	---	---	---	---
Crow Creek	1,1,15	50	6.3	10	8.6	---	---	196	---	---	1.0E-04	---	---	---	---	95	---	---	---	0.038	---
Little Granite Creek	12,12	55	6.0	10	9.8	0.42	0.0190	152	280	0.00038	3.4E-04	3.6E-05	0.00002	0.00002	1059	919	139	33	19	0.081	0.018
Jones Creek	1,1,15	65	9.4	5	11.2	---	---	63	---	---	3.7E-04	---	---	---	---	835	---	---	---	0.058	---
Sode Butte Creek	1,1	80	17	12	---	---	---	34	---	---	1.5E-03	---	---	---	---	973	---	---	---	---	---
Sunlight Creek	4/17,1	113	16	29	35	0.36	0.0075	---	21	0.001		1.0E-03	0.00073	0.00016	---	---	741	566	140	0.029	0.018
Pilgrim Creek	16,1	126	17	---	55	0.33	0.0091	31	53	0.0045	3.0E-03	1.5E-03	0.00134	0.00015	---	---	---	---	---	0.036	0.018
Spread Creek	1,1	256	20	4	54	0.31	0.0158	45	39	0.0156	1.4E-02	1.6E-03	0.00057	0.00059	---	---	---	---	---	0.056	0.048
North Fork Shoshone River	16,1	381	45	---	25	0.91	---	16	14	0.00368	2.0E-03	1.7E-03	0.0015	0.00037	---	---	---	---	---	---	0.025
Pacific Creek	2,1/11	423	60	63	43	---	0.0035	39	41	0.015	1.1E-02	4.0E-03	0.004	0.0005	24757	20524	4232	3534	506	0.057	0.041
Boulder River	3,1	591	87	27	---	---	---	366	---	---	2.0E-03	---	---	---	---	3101	---	---	---	---	---
South Fork Shoshone River	4,1	794	97	53	56.9	0.86	---	62	---	---	2.0E-02	---	---	---	---	16344	---	---	---	---	---
Buffalo Fork	11,11	845	111	45	45	---	0.0025	---	39	---	---	2.0E-03	0.0013	0.00047	---	---	5690	8896	2384	0.018	0.008
Stillwater River	3,1	966	105	18	---	---	---	731	---	---	1.3E-03	---	---	---	---	2359	---	---	---	---	---
North Fork Shoshone River	16,1	1016	92	---	30	---	---	14	13	0.0061	5.7E-03	4.0E-04	0.00023	8.5E-05	---	---	---	---	---	---	---

Table 3.1. (continued)

	Source[a]	Drainage Area (km^2)	Bankfull Q (cms)	Guage Record (yrs)	Bankfull Width (m)	Bankfull Depth (m)	Slope (m/m)	Number of Samples Susp Load	Number of Samples Bed Load	Bankfull Sediment Load Q_{tot} (m^3/s)	Bankfull Sediment Load Q_{susp} (m^3/s)	Bankfull Sediment Load Q_{bed} (m^3/s)	Bankfull Sediment Load Q_{grav} (m^3/s)	Bankfull Sediment Load Q_{sand} (m^3/s)	Annual Sediment Load Q_{tot} (m3/yr)	Annual Sediment Load Q_{susp} (m3/yr)	Annual Sediment Load Q_{bed} (m3/yr)	Annual Sediment Load Q_{grav} (m3/yr)	Annual Sediment Load Q_{sand} (m3/yr)	Surface D_{50} (m)	Sub-Surface D_{50} (m)
Yellowstone Region (cont.)																					
East Fork Wind River	4,1	1121	22	28	38.7	0.84	---	124	---	---	1.3E-03	---	---	---	---	14353	---	---	---	---	---
Madison River	2,1	1124	34	83	28.7	---	---	38	---	---	4.0E-04	---	---	---	---	1879	---	---	---	---	---
Snake River	2,1	1230	184	27	58.5	1.15	0.0013	152	16	0.027	2.5E-02	2.0E-03	0.00125	0.001	28967	26173	2794	1717	1560	0.031	0.015
Boulder River	3,1	1358	133	61	---	---	---	32	---	---	3.5E-03	---	---	---	---	6040	---	---	---	---	---
North Fork Shoshone River	16,1	1496	123	36	53	0.95	---	21	14	0.0564	5.0E-02	6.4E-03	0.0044	0.003	109196	57824	51372	99191	15881	---	0.016
Lamar River	4,1	1731	218	68	50.6	1.98	---	1180	---	---	2.4E-02	---	---	---	---	41055	---	---	---	---	---
Greybull River	4,1	1757	86	41	26.5	0.4	---	60	---	---	3.7E-02	---	---	---	---	46173	---	---	---	---	---
Stillwater River	3,1	2530	157	70	---	---	---	21	---	---	1.5E-03	---	---	---	---	4134	---	---	---	---	---
Clarks Fork Yellowstone River	4,1	2989	194	89	57.1	1.91	---	178	---	---	5.5E-02	---	---	---	---	121931	---	---	---	---	---
Snake River	11,11	3916	285	16	70	---	0.0025	85	60	0.027	1.5E-02	1.2E-02	0.02	0.003	119654	51810	67844	181965	16015	0.034	0.025
Shoshone River	16,1	4743	106	3	---	---	---	33	---	---	1.3E-02	---	---	---	---	---	---	---	---	---	---
Shoshone River	1,1	6207	106	44	---	---	---	125	---	---	2.3E-02	---	---	---	---	91369	---	---	---	---	---
Yellowstone River	4,1	6784	436	100	73.8	1.0	---	84	---	---	9.0E-02	---	---	---	---	100398	---	---	---	---	---
Yellowstone River	5,5	9210	575	73	95	---	0.0028	129	47	0.09502	7.9E-02	1.6E-02	---	---	207032	185951	21081	---	---	0.057	---

Notes:

a: First number refers to discharge source, second number to sediment transport data source, third number to additional grain size or channel geometry data source.

1: U.S.G.S. National Water Information System (NWIS) accessed between 1/2008-7/2011; 2: Hortness and Barenbrock, 2004; 3: Parrett and Johnson, 2004; 4: Miller, 2003; 5: Holnbeck, 2005; 6: Clark and Woods, 2001; 7: Williams and Krupin, 1984; 8: Emmett, 1975; 9: King et al., 2004; 10: Jones and Seitz, 1980; 11: Erwin et al., 2011; 12: Ryan and Emmett, 2002; 13: Kondolf et al., 2002; 14: Barenbrock and Tranmer, 2008; 15: Zelt, 2001; 16: Bankfull discharge estimated from a regional relationship as Q=aDAb, where Q is discharge, DA is drainage area, and a and b are empirical power-law parameters; 17: Determined from field measurements by the authors.

gave a poor fit, either very low flow values (<20% bankfull) were eliminated or a power-law relation was fit by eye giving emphasis to measurements at higher stages where most transport occurs. Because discharge is commonly expressed in m^3/s, a dimensionally correct relation would relate to some instantaneous transport rate in the same units. For reasons implicit in the hydraulic geometry formulation, we choose to relate the instantaneous transport rate at bankfull to the bankfull discharge to generate the downstream sediment load scaling relations as in equation 3.

Given the ubiquity of studies that link sediment yields to a variety of factors, and acknowledging that channel morphology is reflective of all sediment transporting flows, here we also document the scaling relation between drainage area and total annual sediment yields. Annual sediment yields were computed by combining the above power-law relation between discharge and sediment load with an average annual hydrology based on stream gauging records (available for 69 suspended load and 43 bed load sites). Discharge data were broken into 30 bins of differing flow frequency, and for each flow bin the instantaneous sediment transport rate was calculated via equation 4. These values were then simply multiplied by the frequency of a given flow (d/yr) and summed across all discharge bins to arrive at an annual yield:

$$Q_{s,ann} = k\sum_{i}^{30} Q_{si} f(Q) \tag{5}$$

where the constant k=86,400 s/day, i refers to a discharge bin, and f(Q) is the frequency of a given flow in d/yr (Table 3.1). It should be noted that errors may compound in the computation of annual yields, as small variations in the shape of the transport curve or in the length of the hydrologic record can have large impacts on the modeled annual average sediment yield. For this reason, we suggest that bankfull transport values are more reliable as these are estimated directly from the data with no further manipulation, but we also address the relation between bankfull values and annual yields. Previous authors have computed annual yields for some of the same basins using a similar approach and their results are consistent with ours (Whiting et al., 1999; Kirchner et al., 2001). In the case of both bankfull fluxes and annual yields the sediment transport data were calculated for both suspended load and bed load, and summed for the total load (Table 3.1).

Measurements of channel geometry, slope and grain size were obtained from a number of sources, including surveys by the authors. Several of the sediment transport measurements had little or partial documentation of channel dimensions (Table 3.1). These data are therefore supplemented with other regional measurements of channel geometry as available (Leopold and Maddock, 1953; Harenberg, 1980; Legleiter et al., 2003; Zelt and Wohl, 2004; Greg Bevenger, Shoshone National Forest, Personal Communication, 2010). From this data set, downstream hydraulic geometry relations for channel width and depth of the form of equation 1 were made for 93 sites across the region. While several braided reaches exist in the Yellowstone region (Chapter 4), the focus here is on single-thread hydraulic geometry, and thus braided reaches were not included. Direct velocity measurements were available for the King et al. (2004) data set representing 32 sites. Bankfull discharge was determined in the field through a distinct break in slope toward the floodplain, or in some cases by vegetation changes where distinct floodplains did not exist (Harenberg, 1980; King et al., 2004). For several sites where no bankfull stage was defined, we assume the 1.5-year flood is representative and has proven reasonable for this region (Castro and Jackson, 2001). In a few cases, bankfull flow was determined from a regional relation between discharge and drainage area (Table 3.1). Where available, measurements of slope and grain size were also related to bankfull discharge as in equation 1. Median grain size of the surface bed material was typically determined with a pebble count (Wolman, 1954), whereas subsurface sediment was analyzed using a bulk sampling procedure (e.g. King et al., 2004).

The measured hydraulic geometry relations (w, h, u, Q_s) are compared to the results from a predictive approach based on a channel-forming Shields number and measured relations for discharge, slope, and grain size. This approach is described following presentation of the sediment scaling results.

Paired Watershed Study

The primary objective of this portion of the study is to document in more detail differences in hydraulic geometry and stream bed characteristics between basins that are physiographically similar and regionally adjacent, but with very different sediment supply rates. Field measurements of channel morphology (width, depth, slope) and characterization of the size and lithology of bed sediments (surface and subsurface) were made along 18 reaches in the Big Wood (BW) basin and 17 reaches in the North Fork Big Lost (NBL) basin (Figure 3.2; Table 3.2). Measurements of channel dimensions involved surveys of a minimum of three cross-sections at each reach spaced about one channel width apart, and the width and depth for each reach was computed from the average of these cross-sections. Slope was determined from a linear regression of longitudinal water-surface elevations over at least 10 times the channel width. Pebble counts (Wolman, 1954) were used to document the surface grain size at all sites, and subsurface samples were obtained at six locations in each basin. Subsurface sampling involved removing the surface layer armor, and sorting by weight enough sediment so that the largest particle made up less that 5% of the total sample size (Church et al., 1987). Sediment coarser than 32 mm was sorted and weighed in the field, and a subsample of the finer material was sieved in the lab. Determination of the lithology of the bed sediment is explained in Chapter

	DA	Q_{bf}	w	h	u (est.)	S	τ	τ*	Subsurface Grain Size			Surface Grain Size		
									D_{16}	D_{50}	D_{84}	D_{16}	D_{50}	D_{84}
	(km^2)	(m^3/s)	(m)	(m)	(m/s)	(m/m)	(N/m^2)		(mm)	(mm)	(mm)	(mm)	(mm)	(mm)
NF Big Lost Basin														
NBL1 (gauge)	297	20.2	7.6	1.29	2.33	0.0063	80	0.070				20	70	174
NBL2	283	19.5	19.4	0.67	1.85	0.0078	51	0.077	1.6	20	114	16	41	93
NBL3	157	12.4	11.8	0.67	1.66	0.0079	52	0.076	2.4	24	109	18	42	133
NBL4	141	11.4	13.3	0.52	1.53	0.0061	31	0.064				15	30	59
NBL5	120	10.1	11.5	0.55	1.49	0.0063	34	0.075	1.4	18	75	14	28	79
NBL6	97	8.5	10.2	0.54	1.52	0.0059	31	0.071				12	27	62
NBL7	82	7.4	10.9	0.47	1.53	0.0130	60	0.066				16	56	142
NBL8	55	5.5	10	0.42	1.46	0.0125	52	0.076	2.0	16	91	15	42	118
NBL9	25	3.0	5.8	0.36	1.46	0.0217	77	0.085				18	56	160
tributaries														
Summit1	52	5.2	9.9	0.45	1.48	0.0116	51	0.055	1.2	12	58	24	57	119
Summit2	42	4.4	8.2	0.44	1.40	0.0096	41	0.055				20	46	102
Summit3	29	3.4	7.2	0.35	1.14	0.0050	17	0.053				10	20	39
Summit4	16	2.1	5.3	0.27	0.95	0.0085	22	0.041				12	34	78
Little Fall	8	1.3	3.7	0.3	1.68	0.0305	90	0.113				14	49	116
Kane1	45	4.7	9.1	0.42	1.49	0.0133	55	0.065	1.5	16	90	22	52	120
Kane2	31	3.5	6.5	0.48	1.63	0.0142	67	0.059				25	70	142
Kane3	13	1.8	4.2	0.28	1.10	0.0185	51	0.051				30	62	147
Big Wood Basin														
BW1 (gauge)	356	23.3	12.8	0.89	1.84	0.009	79	0.045		25		32	110	240
BW2	337	22.3	21.3	0.78	1.66	0.007	55	0.048	1.7	29	156	31	70	168
BW3	304	20.6	19.4	0.69	1.50	0.008	54	0.046				19	72	191
BW4	178	13.6	13	0.63	1.51	0.007	45	0.043				19	65	135
BW5	164	12.7	14.2	0.62	1.40	0.008	50	0.042	1.7	24	82	20	73	186
BW6	150	11.9	13.1	0.56	1.55	0.013	69	0.057				26	74	194
BW7	98	8.6	9.4	0.58	1.23	0.004	24	0.044				15	33	86
BW8	90	8.1	10.5	0.49	1.36	0.008	37	0.046	2.4	21	98	19	49	106
BW9	64	6.2	6.6	0.56	1.57	0.009	48	0.057				20	57	117
BW10	45	4.6	9.6	0.39	1.26	0.014	54	0.051	2	20	96	24	65	163
BW11	17	2.2	4.9	0.36	1.33	0.017	60	0.058				19	65	151
tributaries														
Baker1	104	8.9	9.5	0.6	1.78	0.014	79	0.068	2	17	97	16	72	175
Baker2	80	7.4	8.9	0.48	1.51	0.013	61	0.064				17	59	152
Baker3	55	5.5	8.2	0.37	1.40	0.018	65	0.062				19	65	151
Baker4	44	4.6	6.8	0.37	1.55	0.019	67	0.066				23	63	124
Baker5	9	1.3	3.5	0.33	1.49	0.025	79	0.109				17	45	145
Prairie1	45	4.7	7.3	0.39	1.47	0.017	66	0.059	2.1	18	76	24	70	145
Prairie2	19	2.4	3.9	0.36	2.02	0.032	111	0.111				19	62	117

Table 3.2. Site characteristics for the Big Wood and North Fork Big Lost River basins.

2. Bankfull discharge was estimated for each site as Q=whu, where the mean velocity was estimated as:

$$u = \frac{u_*}{\kappa} \ln\left(11\frac{h}{k_s}\right) \tag{6}$$

where u_* is shear velocity $\left(\sqrt{\tau/\rho}\right)$, κ is von Karman's constant, and k_s is a characteristic roughness height here taken to be equal to $3D_{84}$ where D_{84} is the 84^{th} percentile of the surface grain size distribution (Kuelegan, 1938; Whiting and Dietrich, 1990). The basin-wide estimates of bankfull discharge were smoothed with a power-law fit, but this has little effect on the results. In order to understand how reach scale channel and textural adjustments modulate the scaling and magnitude of the sediment flux downstream, a simple 1-D model (explained below) was used to compute bankfull bed load transport rates at each reach along the main channel in the paired basins.

RESULTS

Regional Sediment Scaling

Figure 3.3 shows the regional scaling relations between bankfull discharge and drainage area relative to bankfull and annual sediment fluxes for 3 different sediment populations: total load (suspended + bed load), suspended load, and bed load. Sediment loads vary by 1-3 orders of magnitude regionally, with clearly the highest sediment fluxes derived from erodible volcanic and sedimentary rocks in the Yellowstone region. Despite differences in the magnitude of sediment transport regionally, all of these river systems exhibit similar near-linear sediment scaling exponents (Table 3.3). Focusing on the hydraulic geometry relations correlating bankfull discharge and transport rates, we find that in general the total sediment load tends to exhibit a

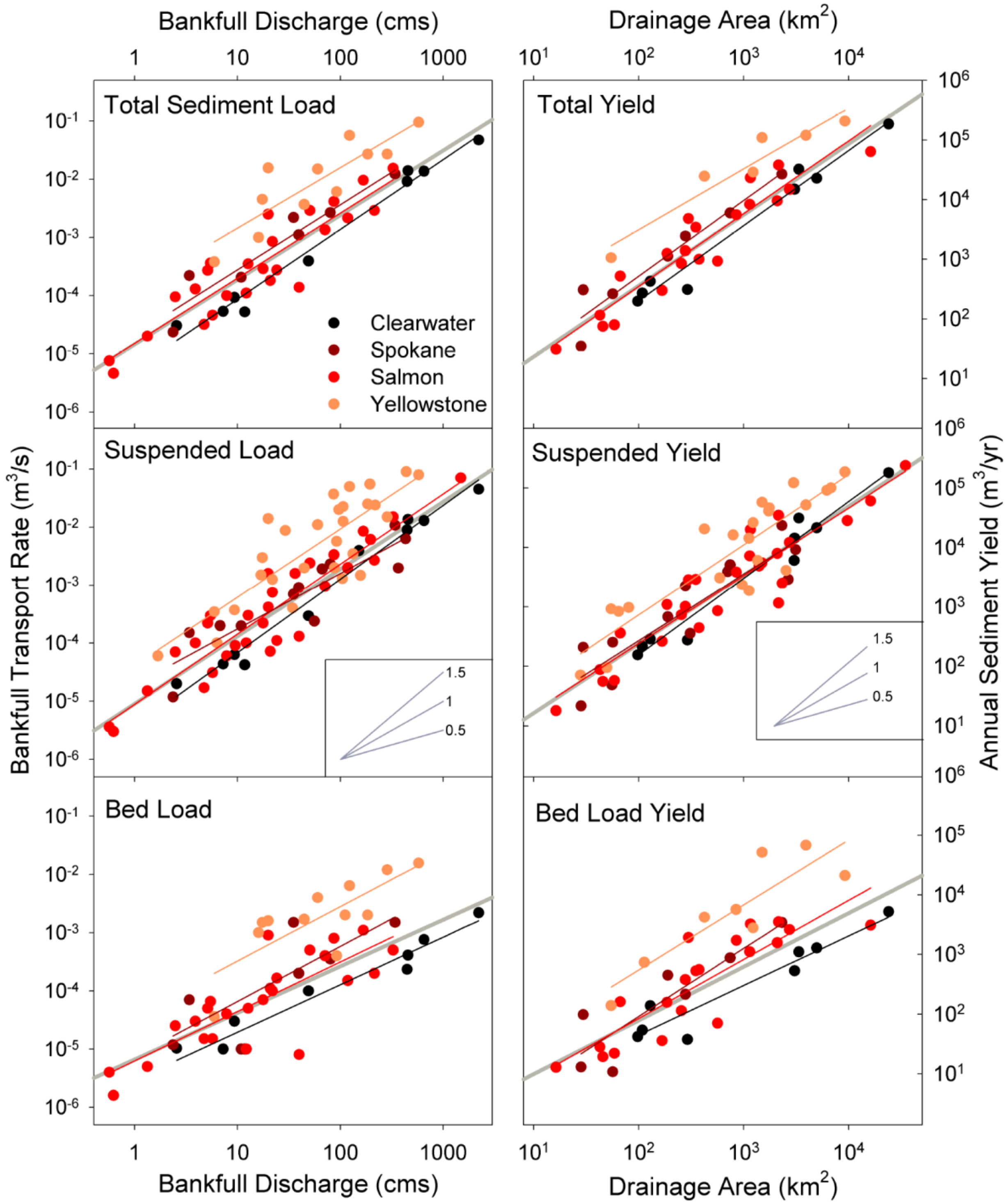

Figure 3.3. Bankfull sediment load versus bankfull discharge and annual sediment yield versus drainage area for total, suspended, and bed loads. Power-law relations are shown for each data set, with the parameters shown in table 3.1, and power-law exponent slopes inset in the middle plots. The gray line represents the average of the Idaho basins.

	c	d	R^2	n	lin	c_{da}	d_{da}	R^2	n	lin
	Q_{bf} v Q_{tot}					**DA v $Q_{tot,ann}$**				
Yellowstone	1.3E-04	1.04	0.74	11	o	28.60	1.02	0.92	6	o
Salmon	1.5E-05	1.12	0.89	20	o	1.28	1.22	0.89	20	x
Clearwater	5.5E-06	1.20	0.98	9	x	0.61	1.26	0.97	8	x
Spokane	2.1E-05	1.12	0.91	11	o	1.50	1.27	0.92	7	o
Idaho	1.5E-05	1.10	0.90	40	o	1.50	1.19	0.90	35	x
	Q_{bf} v Q_{susp}					**DA v $Q_{susp,ann}$**				
Yellowstone	4.1E-05	1.18	0.70	28	o	3.21	1.18	0.79	22	o
Salmon	8.8E-06	1.21	0.87	31	x	1.27	1.14	0.87	26	o
Clearwater	3.7E-06	1.27	0.98	10	x	0.41	1.29	0.97	9	x
Spokane	1.9E-05	0.96	0.90	11	o	1.55	1.12	0.82	11	o
Idaho	9.1E-06	1.16	0.90	52	x	1.14	1.16	0.88	46	x
	Q_{bf} v Q_{bed}					**DA v $Q_{bed,ann}$**				
Yellowstone	3.8E-05	0.94	0.61	11	o	3.64	1.09	0.78	8	o
Salmon	6.3E-06	0.85	0.66	25	o	0.89	1.00	0.75	20	o
Clearwater	3.0E-06	0.82	0.94	9	x	0.98	0.83	0.91	8	o
Spokane	7.5E-06	0.95	0.65	7	o	0.48	1.14	0.80	7	o
Idaho	6.6E-06	0.80	0.68	41	x	1.25	0.90	0.74	35	o

Table 3.3. Power-law coefficients, c, and exponents, d, for the plots in Figure 3.3, where the subscript da refers to drainage area. R^2 is the coefficient of determination and n is the number of sites. The column lin indicates whether these exponents are significantly different from 1; x: yes, o: no. The data were de-trended linearly in log-space, and t-tests were used to test whether the residual slope of the log-transformed data was significantly different from zero at p=0.05. Note that in addition to individual basins, the average for Idaho set is shown. Q_{bf}: bankfull discharge; Q_{tot}: total bankfull sediment load; Q_{susp}: bankfull suspended load; Q_{bed}: bankfull bed load; DA: drainage area; $Q_{tot,ann}$: total annual sediment yield; $Q_{susp,ann}$: annual suspended load yield; $Q_{bed, ann}$: annual bed load yield.

scaling exponent slightly greater than one, indicating increasing sediment concentrations moving downstream (Figure 3.3, Table 3.3). This signal is generally dominated by increasing suspended sediment loads which comprise about 50% of the total sediment flux in headwater streams, increasing to greater than 90% in trunk channels (Figure 3.4). Conversely, the bed load signal is such that the scaling exponents are typically less than one, indicating a slight decrease in concentrations downstream. On average, bankfull bed load scales as roughly $Q_{bed} \propto Q^{0.8\text{-}0.95}$ and

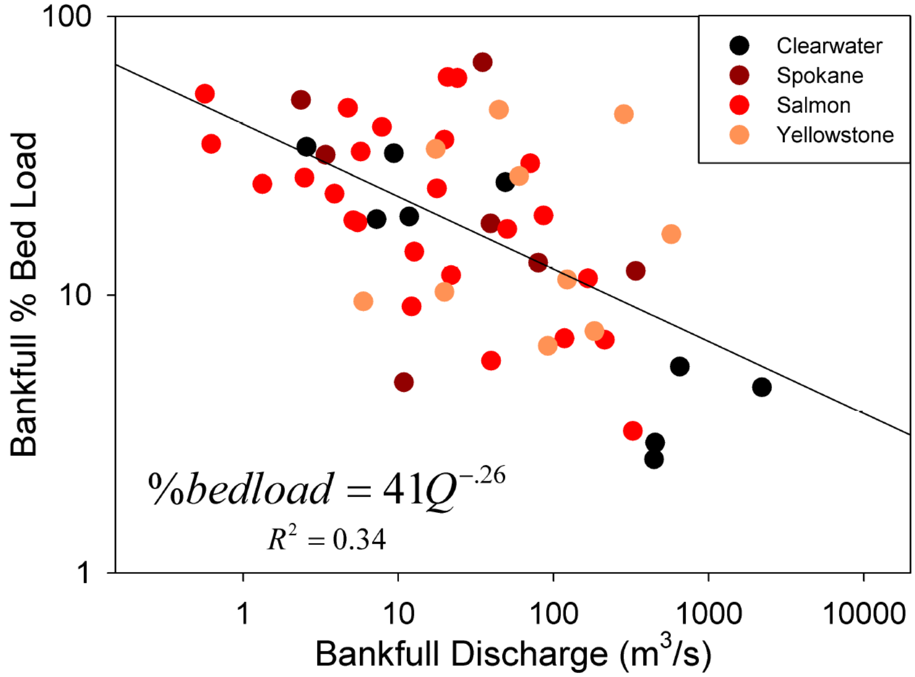

Figure 3.4. Bankfull percent bed load as a function of bankfull discharge.

suspended load as $Q_{susp} \propto Q^{1\text{-}1.2}$, although only half of these are significantly different from 1 (Table 3.3). Given the relatively similar trends and in order to increase the sample size the entire Idaho data set was lumped together, showing a similar overall trend as the individual basins.

In the context of drainage area versus sediment yields (Figure 3.3), an overall similar pattern emerges as the suspended yield exponents are nearly identical as in the bankfull relations, although there is a slight increase in the bed load exponent. This may be expected given the correlation between discharge and drainage area (Figure 3.5a):

$$Q = 0.14DA^{0.9}\,. \tag{7}$$

This also implies a strong relationship between the instantaneous bankfull sediment fluxes and annual yields. Parker et al. (2008), for example, suggest that we are truly interested in a yield relation, as stream channels result from all sediment transporting flows, but admit the relation between bankfull and annual sediment fluxes is not known. Here we show that in these basins

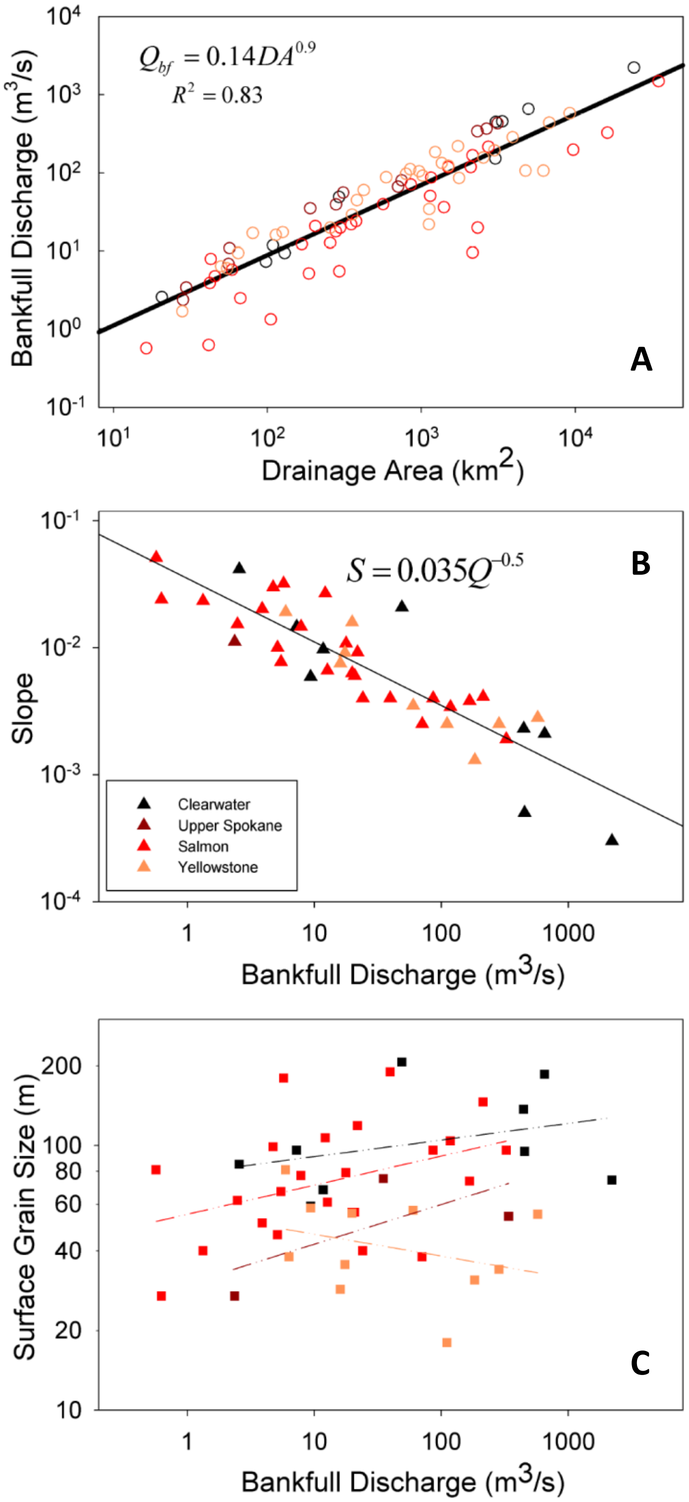

Figure 3.5. A) Drainage area versus bankfull discharge. B) Bankfull discharge versus slope. C) Bankfull discharge versus surface grain size. Relations in A and B are significant, whereas relations in C are not. Color coding as in B across all plots.

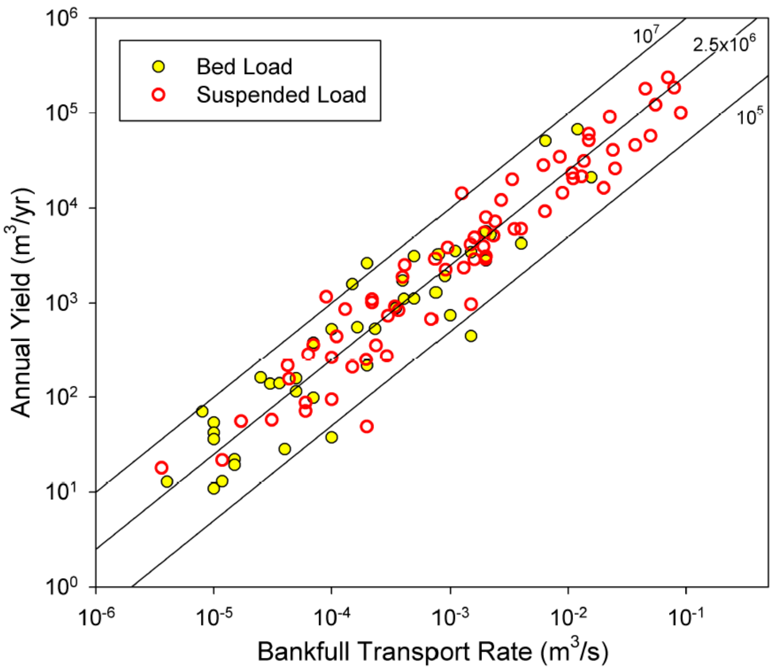

Figure 3.6. Bankfull sediment transport rate versus annual yield for study basins. The lines show the linear scaling multiple for annual yield as a function of bankfull flux.

there is a nearly linear relationship between the bankfull transport rate and the annual yield for both suspended load and bed load (Figure 3.6). The results indicate that for both bed and suspended loads, the annual yield in m^3/yr is approximately $2.5x10^6$ times greater than the instantaneous bankfull transport rate given in m^3/s; this is equivalent to several weeks of bankfull flow and is of the same order as the number of days above the threshold for bed load motion in a typical year. For these snowmelt-dominated basins with relatively regular inter-annual hydrographs this is perhaps not unexpected, as the transport maxima and centroid of the annual sediment flux tend to occur consistently near bankfull flow (Whiting et al., 1999). Nevertheless, there is a two order of magnitude range in scatter about this linear relation, likely reflecting local differences in hydrology, sediment supply, or period of record.

Ultimately the data show that bed load concentrations and specific yields decrease slightly downstream, possibly related to particle abrasion or decreasing sediment production.

Conversely, suspended load concentrations and specific yields increase downstream, likely due in part to the conversion of bed load particles to suspended load (Figure 3.4). Yet the total sediment concentration also increases downstream, as the increase in suspended load concentrations slightly outpace the decrease in bed load. This may point to some enhanced sediment production as drainage area increases, such as the degradation of alluvial deposits. This would echo the results of Church et al. (1999) and Schiefer et al. (2001) for the nearby Canadian Cordillera and Rocky Mountain regions. In any case, overall sediment concentrations are not changing decidedly downstream; for these basins assuming a near-linear scaling between discharge or drainage area and sediment flux provides a reasonable first-order approximation.

Downstream Hydraulic Geometry

Regional Analysis

In order to relate the observed sediment loads to downstream changes in channel properties and associated flow and sediment transport processes, we attempt to predict the downstream hydraulic geometry and sediment scaling relations using an empirical channel-forming Shields number closure. In this case, downstream changes in discharge, slope and grain size are prescribed, and width, depth, velocity, and sediment load are predicted. Slope is thus set here based on the measured relation (Figure 3.5b):

$$S = 0.035Q^{-0.5}. \tag{8}$$

Surface grain size does not vary considerably downstream and is set to the median value of 67 mm, although there is significant regional variability (Figure 3.5c). In order to close the problem, we assume that the bankfull Shields number follows a power-law relation with slope and is modeled as an empirical function:

$$\tau^* = 0.25S^{0.3} \tag{9}$$

that is derived from data from 126 gravel-bed streams in rivers in North America and Europe (R^2=0.55) (Charlton et al., 1978; Kellerhals et al., 1972; Andrews, 1984; Pitlick and Cress, 2002; Ryan et al., 2002; Torizzo and Pitlick, 2004; Mueller and Pitlick, 2005). Importantly, these data are independent from those used to test the model. Downstream changes in depth are simply determined by setting $\tau=\rho ghS$ in equation 2 and rearranging as:

$$h = \frac{\tau^*(s-1)D}{S} \tag{10}$$

where s is sediment specific gravity. After solving for depth, velocity was first estimated using a Manning-Strickler relation after Parker (1990) of the form:

$$\mathrm{u} = 8.1u_*\left(\frac{h}{k_s}\right)^{1/6} \tag{11}$$

where k_s in this case was set to $5D_{50}$, an approximation of $3D_{84}$ (data on D_{84} were not widely available for the regional analysis). For the streams in this study, the Manning-Strickler and other flow resistance equations (e.g. equation 6) tend to overestimate velocity at slopes greater than 0.5%. Alternatively, the Jarrett (1984) steep-slope approximation of the Manning equation performed well and is given by:

$$\mathrm{u} = 3.1h^{0.83}S^{0.12}\,. \tag{12}$$

The best fit is obtained using equation 11 where S<0.5% and equation 12 where S>0.5%. Width is then simply calculated from flow continuity as:

$$w = \frac{Q}{hu}\,. \tag{13}$$

Finally, because slope is considered an independent variable, the final unknown in the hydraulic geometry formulation – bed load transport – can be calculated. Here we use the

Wilcock and Crowe (2003) surface-based relation which is cast in terms of a dimensionless transport rate:

$$W^* = 0.002\phi^{7.5} \qquad \text{for } \phi < 1.35 \tag{14a}$$

$$W^* = 14\left(1 - \frac{0.894}{\phi^{0.5}}\right)^{4.5} \qquad \text{for } \phi \geq 1.35 \tag{14b}$$

where

$$W^* = \frac{(s-1)gq_b}{u_*^3}, \tag{15}$$

$\phi = \tau^*/\tau_r^*$ and q_b is the unit transport rate. τ^*_r is assumed to vary with slope following the Pitlick et al. (2007) power-law fit of the Mueller et al. (2005) relation:

$$\tau_r^* = 0.36S^{0.46}. \tag{16}$$

While other sediment transport equations of similar form could be used (e.g. Parker, 1979), this equation was selected as it gave results most consistent with observations, and required no tuning when applied in conjunction with equation 16. Bankfull values of W* for each reach were transformed to a dimensional sediment discharge by solving for the unit transport rate in equation 11 and multiplying by width as:

$$Q_{bed} = \frac{W^* u_*^3 w}{(s-1)g} . \tag{17}$$

As a result, given discharge, slope and grain size, the downstream hydraulic geometry is predicted through equations 10, 11/12, 13, and 17.

Figure 3.7 shows the downstream hydraulic geometry relations for the regional data set compared to that predicted in the above formulation. The modeled depth relation, based simply on a channel-forming Shields number and typical grain size, very closely matches the observed depths (Figure 3.7a). The modeled versus measured relations are given, respectively, as:

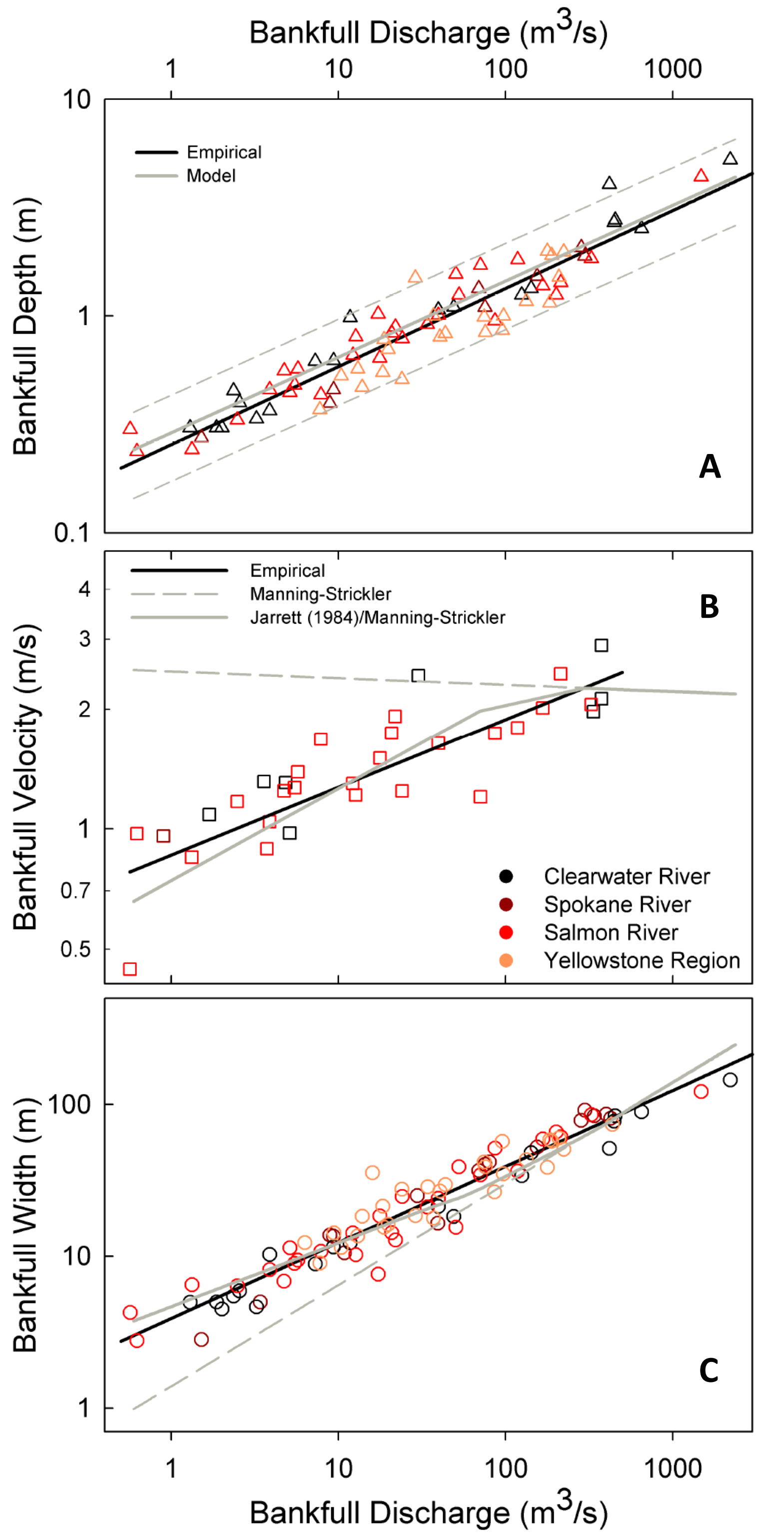

Figure 3.7. Modeled and measured hydraulic geometry relations for bankfull depth (A), velocity (B), and width (C). Dashed lines in A show the envelope predictions for D=40 mm and D=100 mm.

$$\hat{h} = 0.29Q^{0.35} \tag{18a}$$

and

$$h = 0.25Q^{0.36} \tag{18b}$$

where the carat refers to the modeled values. This result can be quite sensitive to the chosen grain size as is explicit in equation 10, and varying D from 40-100 mm (the range in average grain size between basins) envelopes the scatter in the observed data set (Figure 3.7a). Because the Shields number is specified for a given slope, the depth prediction is entirely contingent on the downstream trends in slope and grain size, and fits the data in this study quite well. As mentioned above, modeled velocity tends to be over-predicted by the Manning-Strickler relation (equation 11), but is well modeled by the Jarrett (1984) approximation at steeper slopes (Figure 3.7b). The modeled result using equation 11 at slopes less than 0.5%, and equation 12 at steeper slopes, is not a perfect power law, but one that fits the data reasonably well. Fitting a power-law to the model and field data yields:

$$\hat{u} = 0.78Q^{0.17} \tag{19a}$$

and

$$u = 0.87Q^{0.17} \tag{19b}$$

Given the similarity of the above relations for depth and velocity, width is also well predicted (Figure 3.7c):

$$\hat{w} = 4.17Q^{0.5} \tag{20a}$$

and

$$w = 3.91Q^{0.5}. \tag{20b}$$

If the Manning-Strickler velocity approximation is used at all slopes, velocity is over-predicted and width is under-predicted in small streams (Figure 3.7b). The implication is that at smaller discharges and steeper slopes, flow resistance may not be fully represented by some multiple of grain size. This is similar to the conclusion reached by Jarrett (1984) as flow resistance is likely enhanced by bed structuring and changing flow hydraulics in steeper streams (Church et al., 1998; Recking, 2009).

Finally, the downstream modeled bed load flux is approximated by the power-law:

$$\hat{Q}_{bed} = 6.8 \cdot 10^{-5} Q^{0.72} \tag{21}$$

which is slightly less steep than the measured values (Figure 3.8,Table 3.3). This results from the fact that at smaller discharges and steeper slopes the modeled depths predicted from equation 10 are slightly greater than observed. This subtle difference results in higher modeled bed load

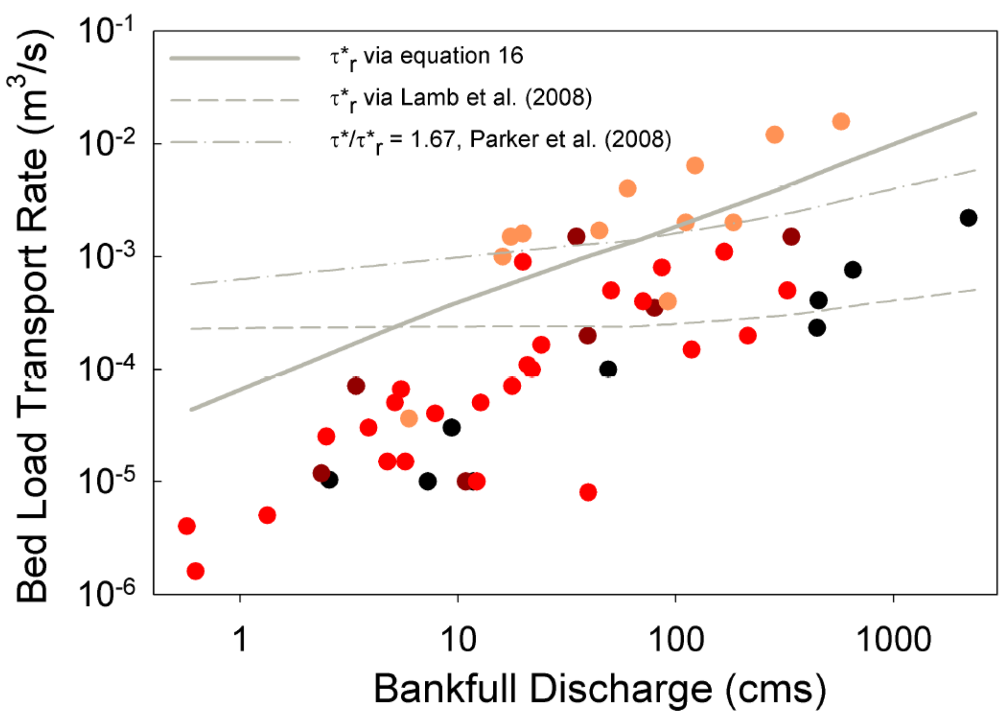

Figure 3.8. Modeled and measured discharge versus sediment load relations.

transport rates in these smaller streams producing a less steep downstream trend and smaller exponent. The magnitude of the modeled sediment flux plots between the Idaho and Yellowstone data sets and generally suggests that the bankfull τ^* values given in equation 10 are reasonable – on average – for these streams, though perhaps too high for the Idaho streams where bed load flux is over-predicted. But this relation is also sensitive to equation 16 which governs downstream changes in τ^*_r. As 33 of the 45 streams used to make this relation come from the streams in this study, it is not wholly independent. For example, using the Lamb et al. (2008) relation, $\tau^*_r=0.15S^{0.25}$, would result in almost no downstream change in Q_{bed} and an exponent near zero in the Q-Q_{bed} scaling relation (Figure 3.8). Similarly, simply assuming that $\tau^*/\tau^*_r=1.67$ as in Parker et al. (2008), results in a scaling exponent of 0.27 (Figure 3.8). The observed sediment scaling pattern is clearly better predicted using equation 16, and this choice has no effect on the hydraulic geometry model. But these results also suggest that while the slope versus τ^* relation works on average for these streams, the variability in sediment load between basins is not captured solely by the average hydraulic geometry.

Paired Watershed Study

Sediment transport rates in the adjacent Big Wood (BW) and North Fork Big Lost (NBL) Rivers differ markedly (Figure 3.9), and provide an opportunity to isolate in more detail channel response to differences in sediment supply. The highest measured bed load transport rate on the NBL was 1.72 kg/m/s, although transport rates were highly variable and as low as 0.068 kg/m/s at flows greater than bankfull. Alternatively, measured bankfull bed load transport rates in the BW range from 0.0085-0.31 kg/m/s. These data reflect the order of magnitude variation in both between site rates and temporally within individual sites. Suspended load

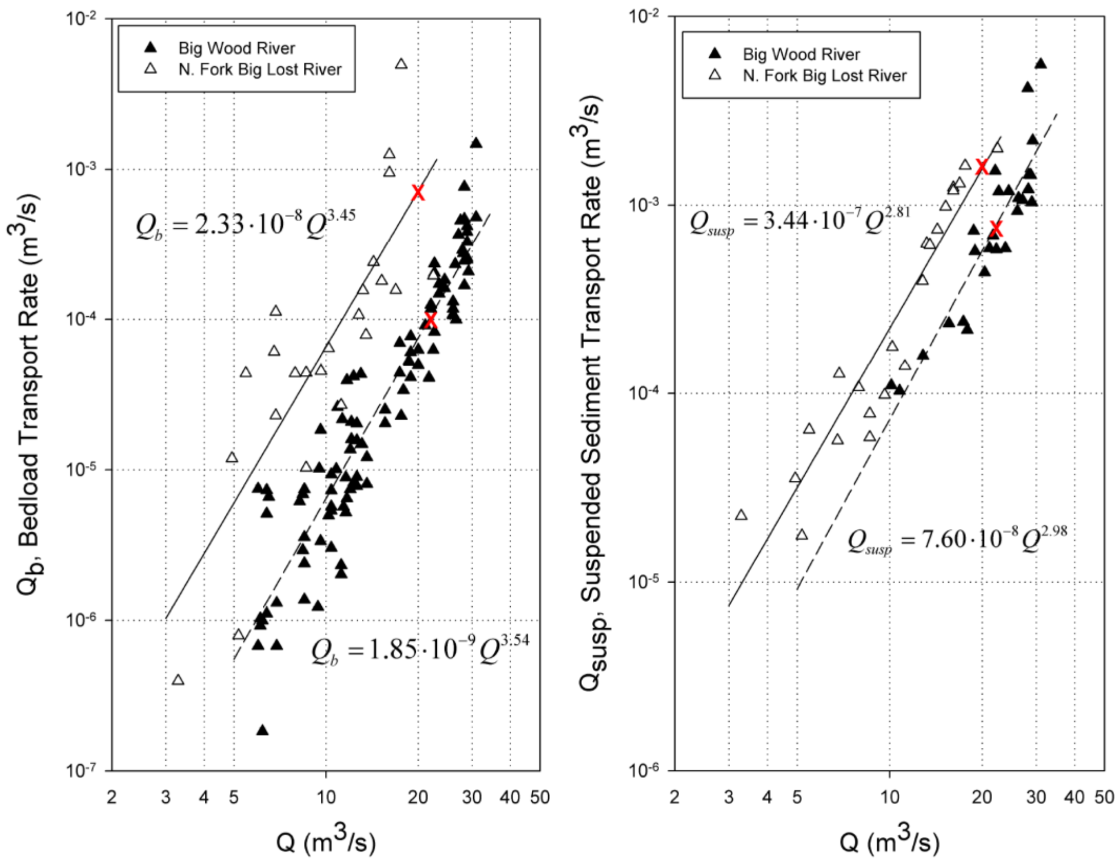

Figure 3.9. Bed and suspended load transport rate as a function of discharge for the Big Wood and North Fork Big Lost Rivers. Red x's represent bankfull values. Power-law relations shown were used to compute annual yields.

measurements show a similar pattern, with fluxes roughly five times greater in the NBL (Figure 3.9). Nevertheless, as in the regional analysis, the hydraulic geometry relations for width, depth, and slope are quite similar between these basins despite a ten-fold difference in bed load sediment concentration. Downstream hydraulic geometry relations (Figure 3.10) for the BW basin are given as:

$$w = 2.7Q^{0.63}, \tag{22a}$$

$$h = 0.26Q^{0.32}, \tag{22b}$$

$$S = 0.03Q^{-0.48}; \tag{22c}$$

and for the NBL basin as:

$$w = 3.4Q^{0.57}, \quad (23a)$$

$$h = 0.25Q^{0.35}, \quad (23b)$$

$$S = 0.024Q^{-0.47}. \quad (23c).$$

Surveyed reaches in the NBL are slightly wider and less steep, but the difference in grain size between the basins is marked (Figure 3.10c). Focusing on the main channel of each basin, longitudinal changes in grain size along the BW are characterized by increasing proportions of resistant granitic rocks in the substrate, reflecting enhanced armoring of the bed surface such that D_{50} actually increases downstream to an average of about 70mm (Figure 3.11). Alternatively, the NBL becomes dominated by erodible extrusive volcanic and sedimentary rocks, resulting in a

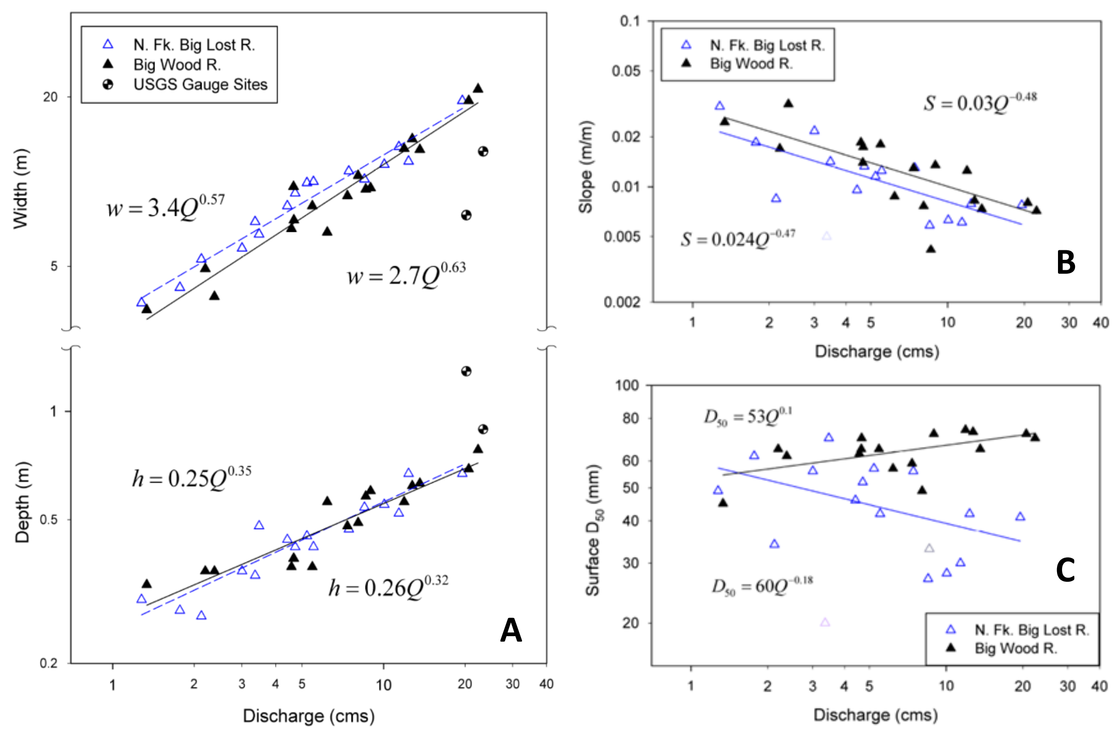

Figure 3.10. Hydraulic geometry relations as a function of bankfull discharge for (A) width and depth, (B) slope, and (C) surface grain size along the Big Wood and North Fork Big Lost River basins.

more typical downstream fining with an average D_{50} of 40mm (Figure 3.11). In both cases, downstream variability in surface grain size is coupled to downstream changes in slope, and scatter in the data largely reflects local hydraulic adjustments between slope, grain size, and transport capacity. This is shown in Figure 3.12a, in which both watersheds show a strong relation between shear stress and grain size, but for a given stress in the BW, the surface sediment size is approximately 50% greater. The result is a bankfull Shields stress that is roughly 50% lower in the BW for a given slope or discharge (Figure 3.12b).

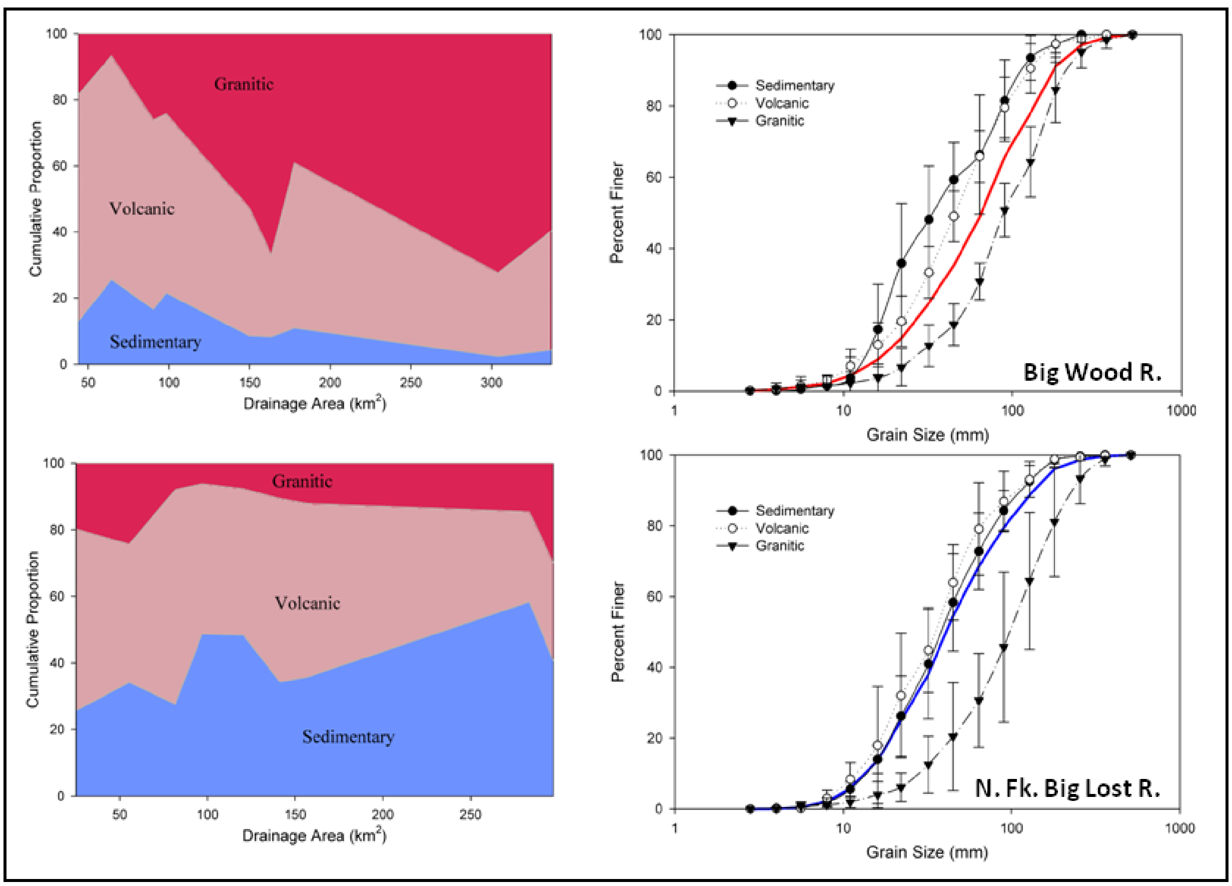

Figure 3.11. Cumulative proportion of different lithologies in the surface sediment (left) for the Big Wood (top) and North Fork Big Lost (bottom) basins. Composite size distribution of surface sediment shown as a red and blue line (right) for the Big Wood (top) and North Fork Big Lost (bottom) basins. Note that the size distributions and range for individual lithologies are shown, indicating the strong relation between lithology and grain size.

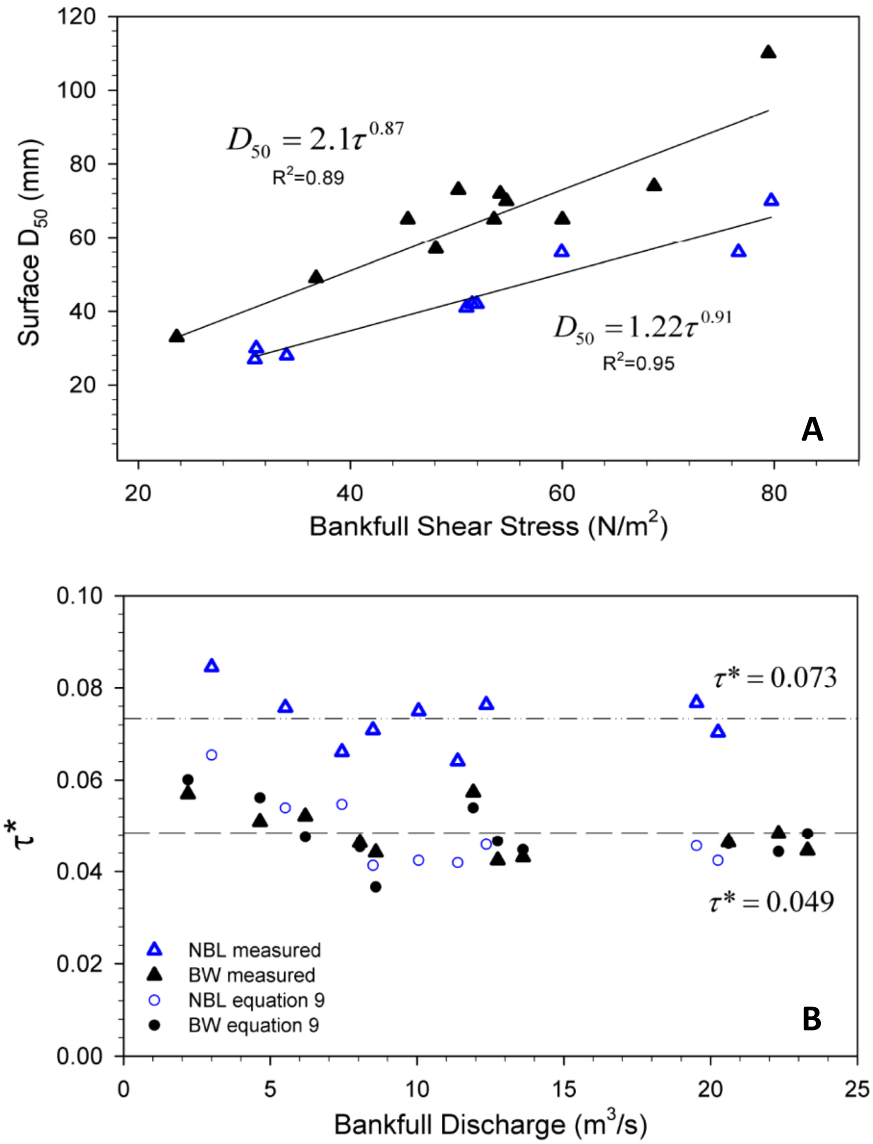

Figure 3.12. A) Relation between bankfull shear stress and surface grain size for the main channel of each river. B) Relation between bankfull discharge and dimensionless bankfull shear stress downstream along the main channel for each river.

This result counters the idea of a constant channel-forming Shields number for a given slope. For example, Figure 3.12b also shows the Shields stress predicted by equation 9 for each reach, and while the BW mimics the trend extremely well, the measured NBL data plots much higher. As a result, using the measured Q, D, and S for these reaches, predicted channel geometry using equation 9 works well in the BW but would suggest much shallower and wider channels in the

NBL (Figure 3.13) (note: in this case u was determined with equation 6 following from the original Q estimates in these basins). While this would enhance sediment transport due to a larger width for the same transport intensity, this is not consistent with observations. Instead, finer surface grain size for a give stress results in a modeled transport intensity that is considerably higher in the NBL for a given slope. Using the Wilcock and Crowe (2003) relation (equation 14) and measured τ^*, bankfull bed load flux in the NBL is about 10 times greater than in the BW, and very consistent with measurements at the basin outlet (Figure 3.14). Because channel dimensions are nearly identical, this effect is due almost entirely to the influence of grain size in the formulation of τ^* and τ^*_r. As τ^*_r is only a function of slope in the model, the effect of a decrease in grain size for a given slope (and shear stress) is to reduce the *dimensional* reference shear stress as $\tau_r \propto \tau^*_r D_{50}$. This makes physical sense in that for a given channel configuration and bankfull shear stress, surface fining results in a more mobile bed and enhanced transport intensity.

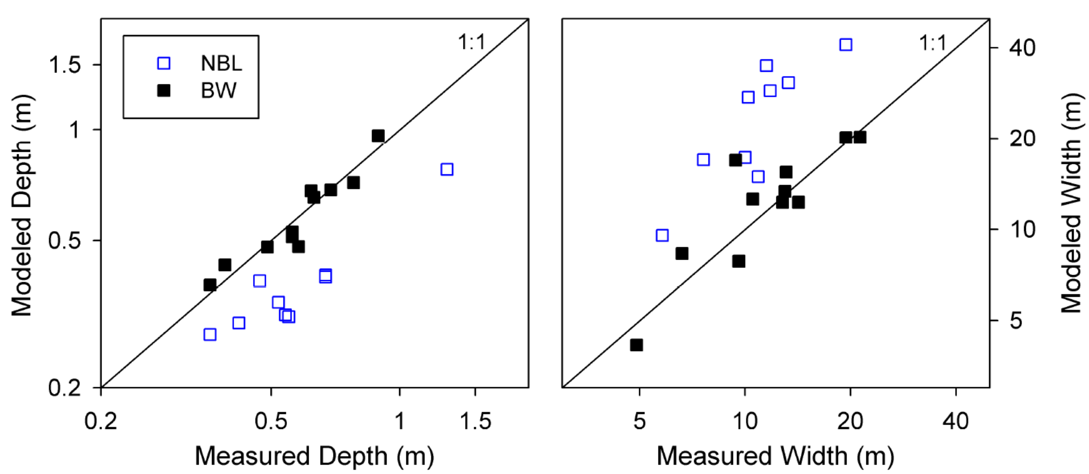

Figure 3.13. Modeled versus measured width and depth for the Big Wood and North Fork Big Lost Rivers.

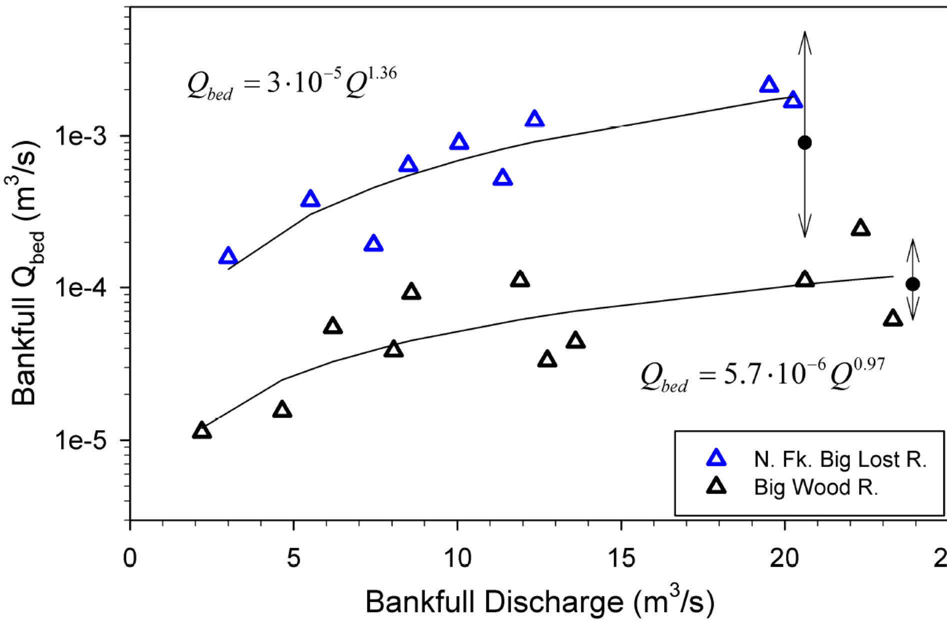

Figure 3.14. Downstream changes in modeled bed load flux between basins, showing a power-law relation fit to these data. Range in measured bed load flux at the basin outlets shown by the arrow, where the black dot represents the bankfull value from the rating curve (see Figure 3.9).

Linkage to Erosion-Abrasion Model

The model results also suggests a downstream scaling between discharge and bed load transport with exponents of 1.36 and 0.97 for the NBL and BW, respectively. This is broadly consistent with the regional analysis and the results from Mueller and Pitlick (2005) for a small mountain watershed. In order to link the hydraulic geometry approach to landscape scale considerations, an independent erosion-abrasion model developed for the BW and NBL basins (Chapter 2) is compared to the results from the modeling approach described above. While these types of watershed-scale erosion-abrasion models have often been used to understand the longitudinal evolution of the size and characteristics of stream bed sediment (Pizzuto, 1995; Attal and Lave, 2006; Sklar et al., 2006; Chatanantavet et al., 2010), this approach also has important implications for downstream bed and suspended load scaling relations (e.g. Attal and

Lave, 2009). In the erosion-abrasion model presented in Chapter 2, sediment (bed and suspended load) is input to the channel network at distinct 1 kilometer intervals, then allowed to abrade downstream (and converted to suspended load) as a function of rock type and travel distance. Meanwhile, sediment continues to be supplied downstream as a function of network topology and basin area. Given an equilibrium assumption, we can then calculate the bed and suspended load fluxes downstream through the channel network. In order to compare the instantaneous fluxes with annual yields (the output of the two approaches), the sediment flux at a given drainage area is scaled by the flux at the basin outlet. This is a reasonable comparison given the relation between bankfull and annual sediment loads (Figure 3.10).

Figure 3.15 shows drainage area versus sediment flux using the two methods, and the results are quite consistent in both watersheds. In the erosion-abrasion model, both suspended and bed load fluxes are considered, and the results are also very similar to the empirical results. In both cases, suspended load concentrations tend to increase downstream (NBL: $Q_{susp} \propto DA^{1.25}$; BW: $Q_{susp} \propto DA^{1.14}$) while bed load concentrations remain constant or decrease slightly (NBL: $Q_{bed} \propto DA^{1.01}$; BW: $Q_{bed} \propto DA^{0.68}$). This arises primarily due to abrasion losses from bed load to suspended load during downstream transport in the model. The exponent also reflects the spatial organization and abrasion characteristics of rock types in each basin, leading to a considerable difference in the observed bed load scaling. For example, in the NBL, a large tributary draining erodible lithologies enters near the basin outlet, leading to an exponent close to one. In the BW, soft lithologies found in headwater areas are easily abraded downstream, resulting in an overall decrease in bed load concentration downstream and a coarsening of the stream bed surface. In combination, these results indicate that in gravel-bed streams the flux of sediment through the channel network is governed as much by textural changes as by morphological changes, and that

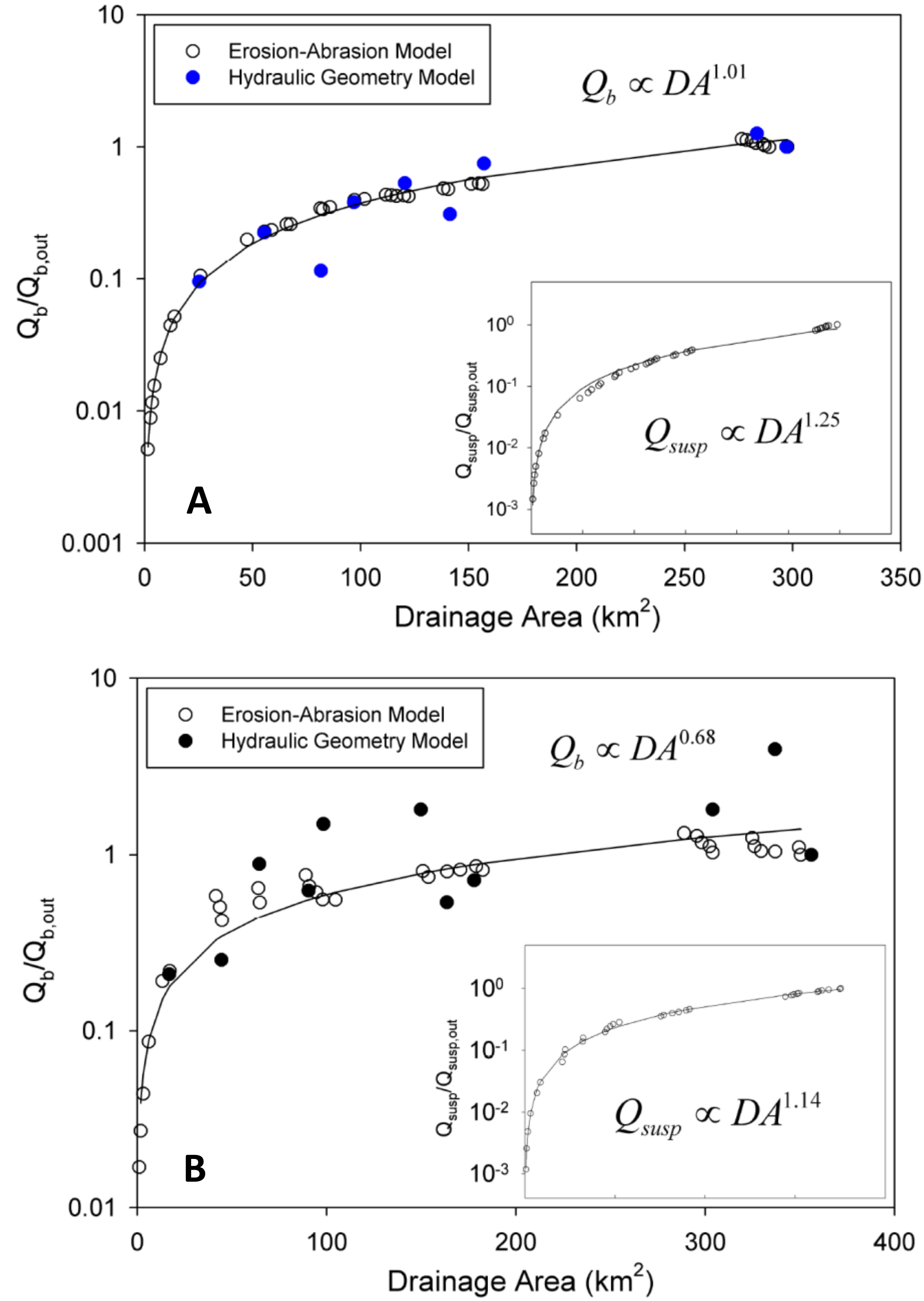

Figure 3.15. Downstream changes in bed and suspended load flux scaled by the flux at the basin outlet for (A) the North Fork Big Lost River and (B) the Big Wood River. Open circles show results from an erosion-abrasion model solved at 1-km increments along the main channel. Closed circles show results from morphologically-based model as shown in Figure 3.14.

downstream sediment scaling relations will reflect the interaction between source areas and channel network structure.

DISCUSSION

For these watersheds, a near-linear scaling between bankfull or annual sediment loads and discharge or drainage area is evident, with a tendency for suspended load concentrations to increase slightly while bed load concentrations decrease slightly. This result is generally consistent with the erosion-abrasion model in the NBL and BW basins, and provides physical reasoning for the observed scaling. If these streams are considered to be in relative equilibrium with sediment delivery – as is commonly assumed in hydraulic geometry studies – the sediment flux at any given point in the network is determined simply by the erosion rate of the watershed and the upstream drainage area, although modified through downstream transport and abrasion processes (e.g. Sklar et al., 2006). Considering a monotonically eroding linear watershed, in which discharge increases exactly with drainage area, and in which no abrasion occurs, then the exponent in equation 3 would simply be 1. Depending on the true abrasion rates of sediment during downstream transport, we would expect the exponent to be something less than 1 for bed load. Using this approach, Attal and Lave (2009) show that for a range in basin shapes (i.e. Hack's Law), the downstream scaling of bed load with drainage area should have an exponent between 0.5 and 1, being higher for more resistant rock types. At long distances (of order 100s of km), abrasion eventually balances with resupply resulting in an asymptotic behavior (Sklar et al., 2006; Attal and Lave, 2009), although this is not evident in our regional analysis. Importantly this also implies an exponent greater than 1 for the suspended load as abrasion losses from bed load are added to the suspended component downstream. This is consistent with the regional trends presented here. That the exponents are only slightly less than one for bed load suggests either relatively resistant bed load particles, which is likely true of many of the granitic basins, or re-supply of coarse particles downstream through mining of stored sediment in floodplains or terraces**.** Considering physiography, much of the Idaho and Yellowstone regions are dominated by consistently rugged topography longitudinally, such that many of these streams are located in areas where even the larger trunk channels continue to drain steep, high elevation mountains. This is evidenced to some extent by the nearly linear relation between discharge and drainage area. Furthermore, because rock type is reasonably uniform within a given basin, sediment supply or erosion rate may not vary considerably. A near-linear scaling between discharge/drainage area and sediment flux may thus be quite reasonable in this region.

Despite the similar trends, bed and suspended load concentrations are 1-3 orders of magnitude greater in the Yellowstone region, while the regional hydraulic geometry relations that are consistent across all regions mask these differences in supply. The slope-based channel-forming Shields criterion employed above predicts the average hydraulic geometry features well, but fails when comparing basins of widely different sediment supply and grain size, as in the BW and NBL. Instead, it seems likely that transport intensity (τ^*/τ^*_r) varies considerably for a given set of channel dimensions. Consider, for example, the special case of a constant downstream sediment concentration; the expected downstream trend in transport intensity can be solved in a fairly straightforward manner given a few simplifying assumptions. If sediment load scales linearly with discharge, we can write:

$$Q_{bed} = CQ \tag{24}$$

where C is the sediment concentration to be prescribed. The above equation can be written in terms of equations for bed load transport (equation 17) and flow continuity as:

$$\frac{W^* u_*^3 w}{(s-1)g} = Cwhu\,. \tag{25}$$

If the bed load transport rate is given by the simpler first portion of the Wilcock and Crowe (2003) equation (equation 14a) and u is replaced with the Manning-Strickler relation (equation 11), equation 25 can then be solved for transport intensity, ϕ, in terms of h, S, and k_s. After gathering constants, the resulting equation can be written as:

$$\phi = 3.24\left[\frac{C}{S}\right]^{2/15}\left[\frac{h}{k_s}\right]^{1/45} \approx 3.24\left[\frac{C}{S}\right]^{2/15} \tag{26}$$

where the simplified approximation results because the h/k_s term in the above equation is raised to the $1/45^{th}$ power and is always within about 5% of 1.

Assuming $C=2.5\times10^{-5}$ and given that slope varies as in equation 8, this independently derived relation shows a very similar downstream trend to the empirical relation given by dividing equations 9 and 16 (Figure 3.16). The result is not strongly influenced by different

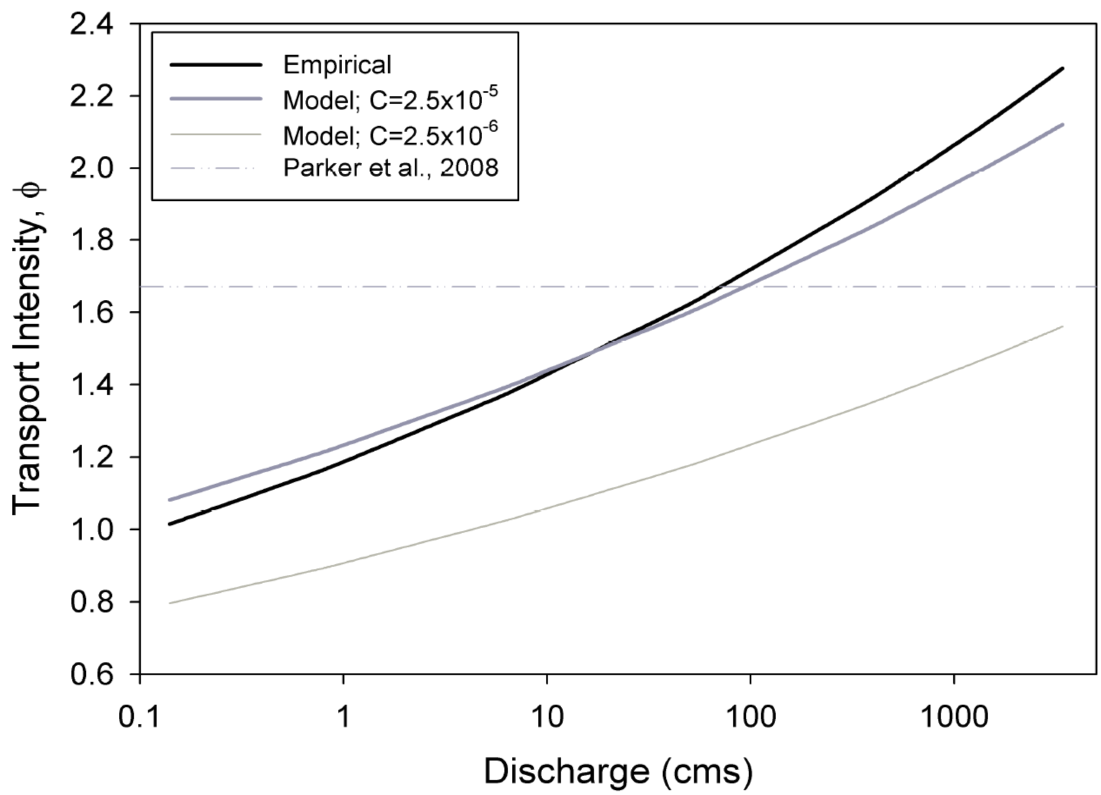

Figure 3.16. Downstream changes in transport intensity as a function of discharge for model and empirical data.

velocity or sediment transport relations. As slope decreases and discharge increases downstream, transport intensity must increase in order to maintain a constant sediment concentration. According to the empirical data, this represents a coincident decrease in both τ^* and τ^*_r downstream with slope. In this analysis, no account was made for the changes in velocity structure that are associated with shallow flows in high-gradient streams (Wiberg and Smith, 1991). For example, the recent work of Recking (2009) suggests that the appropriate roughness layer thickness (multiple of k_s) in flow resistance considerations should increase with slope. Additionally, Lamb et al. (2008) argue that the magnitude of turbulent fluctuations is suppressed in steep, shallow flows, and thus higher average stresses are necessary to entrain particles. Simple measures of grain size also do not reflect bed structuring and stabilization features that are common in high gradient streams; these too can greatly increase the threshold for motion (Church et al., 1998). The velocity predictions support this to some extent; velocities in steeper reaches are considerably smaller than would be expected based on standard approaches based on a uniform k_s. As a result, moving downstream, depth becomes large relative to roughness elements, turbulent intensities increase, and the bed material becomes less structured or "loosens", all of which would have the potential to enhance transport intensity. Changes in sediment patchiness or lateral flow properties as channels become less confined downstream could also have a marked effect on the effective transport capacity (e.g. Ferguson, 2003), as all considerations here are 1-D.

Equation 26 also suggests an intuitive result: for a given slope, if concentration increases, then transport intensity must also increase. In this case, an order of magnitude difference in concentration only requires a 50% change in transport intensity (Figure 3.16). This is the basic result of the analysis in the BW and NBL basins, where subtle changes in bed armoring modulate a 10-fold range in bed load concentration through changes in transport intensity. There is growing literature to support the idea that transport intensity may vary considerably both spatially and temporally in response to sediment supply, and perhaps τ^* can be viewed as a sediment supply-controlled bed state parameter (Dietrich et al., 1989; Church, 2006; Eaton et al., 2010; Church, 2011). This is consistent with the regional trends in grain size, where streams in the Clearwater Basin are the most armored (Figure 3.17a), and likewise convey the least sediment for a given discharge. Alternatively, bed loads in the Yellowstone region are 1-2 orders of magnitude greater, and the streambed is weakly armored and in some cases braided channels emerge (Chapter 4). As a result, the degree of armoring is tightly coupled to changes in bed load concentration, such that surface grain size and armoring decrease about 3-fold as concentration increases by two orders of magnitude (Figure 3.17b). For a given channel geometry, this implies a 3-fold increase in transport intensity, which, considering the exponents in typical transport relations such as equation 14, can easily accommodate the observed range in concentrations.

In both the regional data set and the paired watershed study, changes in surface grain size are typically not reflected in changes in channel dimensions. As a result, approaches based on a channel-forming Shields number are likely only accurate where sediment supply is relatively uniform, bed armoring is consistent regionally, and a regional Shields relation is available. Further, the exact relationship between τ^* and τ^*_r in natural stream channels remains uncertain, although there is a clear linkage with bank stability (Parker, 1978; Millar, 2005; Eaton and Church, 2009). Given sufficient bank strength, textural adjustments of the bed sediment resulting in variation in transport intensity could allow for a large range in sediment transport rates for a given channel geometry. Recent studies have shown that bank stability may be more

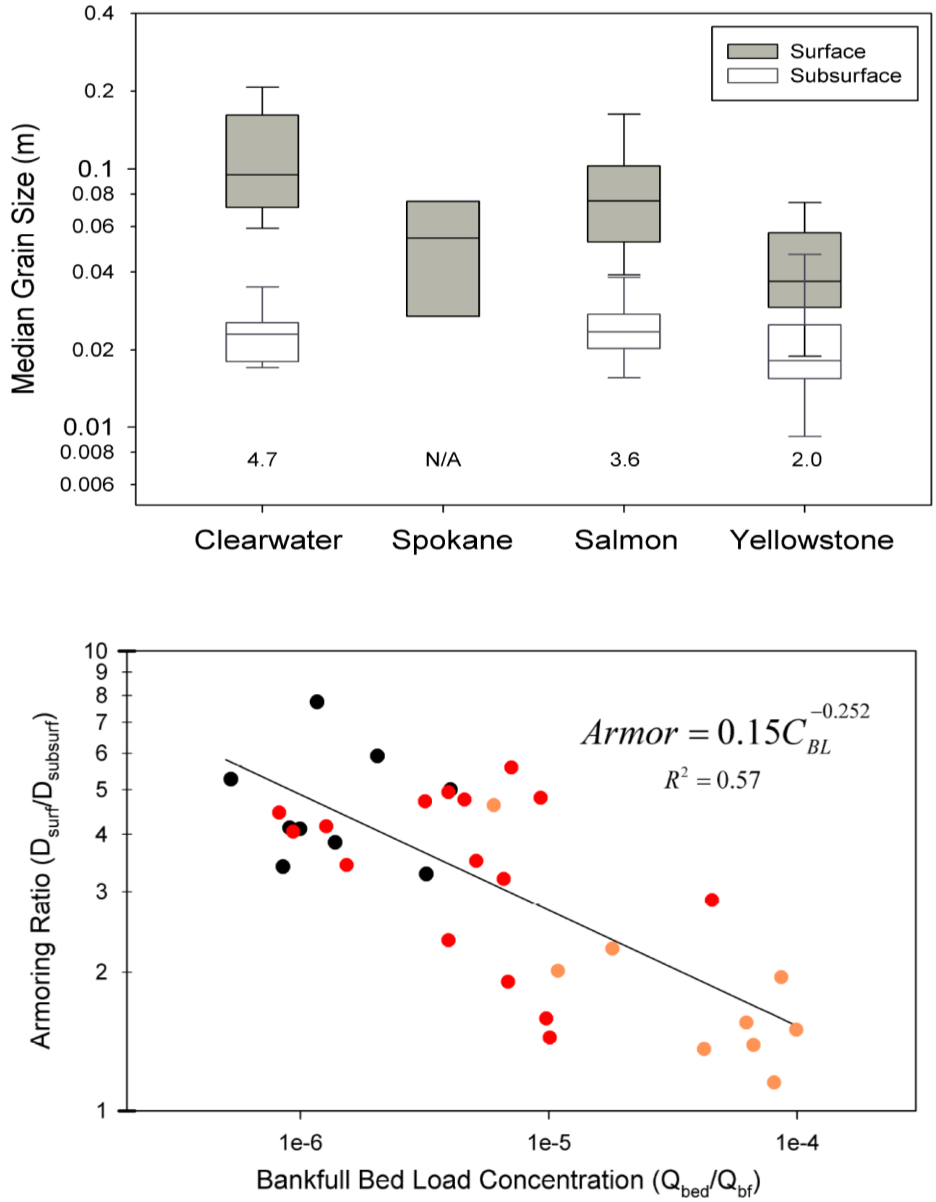

Figure 3.17. A) Range in surface and subsurface grain size for the study basins, with the average armoring ratio labeled below. Box plots show the 10th, 25th, 50th,75th and 90th percentiles. B) Armoring ratio as a function of bankfull bed load concentration.

tightly coupled to interactions with coarse particles near the stream banks, even as armoring or bed state changes in response to supply (Eaton and Church, 2006; Nelson et al., 2009; Madej et al., 2009; Venditti et al., 2010). The implication of these results is that textural changes modulate the transport intensity – both spatially and temporally – so as to maintain equilibrium transport of a given supply in the absence of significant morphologic change.

CONCLUSIONS

Despite being one of the three fundamental independent variables in the hydraulic geometry problem (in addition to water discharge and grain size), quantifying both the magnitude and downstream change in sediment flux has remained largely elusive – particularly for bed load. Downstream changes in sediment load are ultimately determined by longitudinal variations in landscape erodibility, climate, topography, and network topology, and there is no reason why any specific scaling relation should hold. Nevertheless, the empirical data, sediment transport modeling, and erosion-abrasion model presented here all show similar downstream trends. This supports the idea that these landscapes are sufficiently mountainous that downstream changes in specific sediment delivery are rather subtle overall, at least within a given basin. Interestingly, the long-term erosion rates (Late Pleistocene to Holocene) determined by Kirchner et al. (2001) show an almost identical trend ($Q_{tot} \propto DA^{1.03}$), pointing to a near linear increase in sediment yield per drainage area at both decadal and millennial timescales.

Downstream hydraulic geometry relations in these basins are reasonably well predicted based on a channel-forming Shields number, but cannot capture the 2-3 order of magnitude range in sediment flux for a given discharge. In these streams, the difference in the magnitude of bed load flux is controlled regionally by changes in bed armoring, resulting in a non-unique τ^* for a given channel configuration. Furthermore, while these streams show increasing downstream transport intensity, other regions with different sediment transport scaling relations may not exhibit similar behavior. The quasi-universal nature of hydraulic geometry relations thus obscure the true variability in sediment supply regionally, as small changes in armoring and transport intensity can translate to large changes in bed load flux.

Chapter 4 - Braided streams in the greater Yellowstone region: linking sediment supply to pattern and process

INTRODUCTION

Untangling the controls on transitions between a single-thread or meandering to braided channel pattern remains one of the classic problems in geomorphology (Leopold and Wolman, 1957; Parker, 1976; Ashmore, 1991; Lewin and Brewer, 2001; Kleinhans, 2010). Channel form and pattern results from the conveyance of water and sediment through stream systems, and the balance between them is accommodated by changes in morphology (width, depth and slope), bed sediment properties, and planform. Underlying a change in planform must be some change in the governing variables of the system, which then result in alterations in the hydraulic and sediment transport characteristic due to the pattern change itself. Generally these problems have been addressed separately. For example, sediment transport data, bed load in particular, is relatively sparse and much of the literature concerning the controls on braided channel formation therefore focuses on more easily measured parameters (e.g. slope, grain size, discharge, width/depth ratio) (e.g. Leopold and Wolman, 1957; Parker, 1976, Van de Berg, 1995), rather than sediment supply. Studies of sediment transport dynamics in braided reaches have demonstrated the importance of spatially variable flow (Paola, 1996; Nicholas, 2003), but generally do not couple this to pattern transitions which often occur longitudinally, or to braiding criteria in general. Thus the sediment transport component has not been fully linked to the sediment supply component of the problem, despite the obvious relation.

While braided rivers can be aggradational due to sediment overloading (Millar, 2005; Hoffman and Gabet, 2007), it has long been noted that braided channels often represent an equilibrium form where this dynamic channel pattern likely reflects high sediment transport rates (e.g. Leopold and Wolman, 1957; Carson, 1984a; Eaton et al., 2010). In other words, if the sediment supply to a single-thread channel is increased eventually the channel must either aggrade or adjust its planform so as to maintain equilibrium transport (Murray and Paola, 2003; Eaton and Church, 2009). The importance of high supply rates was suggested by Carson (1984a) who states "that the real prerequisite for braiding appears to be high loads of bed-calibre material". Several other authors have noted that pattern transitions are often associated with distinct sediment inputs from stream banks (e.g. Carson, 1984b; Smith and Smith, 1984) or tributaries (e.g. Harvey, 1991, 2001; Hoffman and Gabet, 2007). In fact Schumm (1979) argues that many New Zealand rivers are near a pattern threshold, and that longitudinal variation in supply due to bank erodibility may result in transitions between patterns. This caused Carson (1984b) to respond that this "begs the question: What is the pattern threshold?" From a sediment supply perspective, this question remains largely unaddressed.

Controls on Single-Thread/Braiding Transitions

Knighton (1998) lists several commonly cited conditions conducive to braided channel development including abundant bed load, erodible banks, and steep slopes (thus high energy). The fundamental work by of Leopold and Wolman (1957) addressed the latter of these components, first proposing a simple slope-discharge discriminant relation, indicating braided streams occupy steeper valleys for a given discharge:

$$S^* = 0.0125 Q_{bf}^{-0.44} \tag{1}$$

where S* is the threshold slope, and Q_{bf} is the bankfull discharge. Subsequently several authors have noted that bed particle size, which acts as a source of resistance to flow, must likewise be taken into account such that the discrimination of channel pattern should also reflect sediment properties (Osterkamp, 1978; Carson, 1984a). van den Berg (1995) uses a specific stream power approach that indicates that braided channels can be discriminated as possessing a greater power (discharge times slope) for a given grain size. Lewin and Brewer (2001) raise issue with van den Berg's (1995) reliance on regime-based width equations rather than actual measured widths, though recent work has tied this approach to bar theory (Kleinhans and van den Berg, 2010), and Anisimov et al. (2008) find very good discrimination using an independent data set. Essentially these approaches must relate back to sediment transport dynamics, and plotting slope, stream power or shear stress relative to some grain size gives some insight into bed mobility. While these empirical approaches provide reasonable discrimination, they lack a physical foundation to provide a direct link to flow and sediment transport processes.

In a classic paper, Parker (1976) used a stability analysis based on equations for flow and sediment transport to show that while sediment transport is important for inducing instability in the flow leading to alternate bar formation, the threshold itself is independent of the sediment load. Rather, braided channels are preferred at high slopes and high width/depth ratios, and as these increase the pattern configuration leads to more bars and thus more braids. Subsequently several other authors have used a similar approach concluding that braiding is the favored pattern at width/depth ratios greater than roughly 50 (e.g. Fredsoe, 1978; Crosato and Musselman, 2009), and consistent with field observations (Métivier and Barrier, 2012). While these analytical approaches produce meandering or braided forms based on the application of physically-based equations of flow and sediment transport, a significant drawback is that they require a priori knowledge of channel dimensions – in other words stating that braided channels develop at high width to depth ratios does not necessarily reveal why these dimensions were initially established, only that extensive bar formation and channel bifurcation is likely to occur at these dimensions.

While both empirical and analytical approaches provide insight on channel pattern discrimination, most approaches ignore the details of bank stability, instead using some excess shear stress criteria as closure to the stable width problem (e.g. Parker, 1979; Paola, 1996). But bank strength may vary considerably downstream, and several flume studies have documented the importance of the stabilizing characteristics of riparian vegetation in maintaining a single-thread or meandering planform (Schumm, 1985; Nanson and Knighton, 1996; Murray and Paola, 2003; Tal and Paola, 2007; Braudrick et al., 2009; Davies and Gibling, 2011). Intuitively it has long been recognized that erodible banks are necessary for channel migration, as well as providing a source of additional bed material (Schumm, 1979: Carson, 1984b).

Recently Millar (2005) and Eaton *et al*. (2010) have attempted to link a regime approach which includes a bank stability criterion, with the simple assumption that braided channel patterns will develop at width/depth ratios greater than 50 as suggested by analytical stability analyses and field studies. Millar (2005) uses a minimum slope optimality criterion to predict downstream dimensionless hydraulic geometry parameters for a variety of combinations of discharge, grain size, bed load concentration, and bank strength using equations for flow and bed load transport. From this analysis an expression for the width to depth ratio was obtained as:

$$w/h = 155 Q^{*0.53} S^{1.23} \mu'^{-1.74} \tag{2}$$

where w is width, h is depth, S is slope, and μ' is the relative erodibility of the bank versus bed material. Q* is dimensionless discharge defined as:

$$Q^* = \frac{Q_{bf}}{\sqrt{(s-1)gD_{50}}D_{50}^2} \tag{3}$$

where Q_{bf} is bankfull discharge, s is the specific gravity of sediment, g is gravitational acceleration, and D_{50} is the median diameter of the surface bed material (Millar, 2005). Solving for the threshold case where w/h=50, the critical slope is found as:

$$S^* = 0.4Q^{*-0.43}\,\mu'^{1.41} \quad (4)$$

which is the discriminant function of Eaton et al. (2010), where a value of μ'=1 would indicate no stabilizing effect of bank vegetation and "Parker-like" (1979) channels. Because Q* includes grain size, equation 4 is similar in essence to that of van den Berg (1995) in that the important variables are discharge, grain size, and slope, while including consideration of bank stability, and is comparable in form to the original Leopold and Wolman (1957) formulation.

Sediment Transport in Braided Channels

Equation 4 was formulated using equations for flow and bed load transport, and enhanced sediment transport at higher slopes and finer grain sizes is implicit in the relation (Millar, 2005; Eaton et al., 2011). Yet Millar (2005) uses a 1-D flow assumption, masking the importance of deviations about the mean state in flow and transport fields (Ferguson, 2003). This may blur the exact nature of the channel pattern transition as 1-D approaches for modeling sediment transport have long been considered inappropriate for braided reaches (Griffiths, 1989; Nicholas, 2000). A related aspect of the problem thus concerns how multi-thread channels convey potentially higher sediment loads for a given discharge, as lateral variations in flow may affect transport as much as differences in channel slope or grain size (Paola, 1996; Ferguson, 2003; Nicholas, 2003). Consider a typical bed load transport function of the form:

$$Q_b \propto \left(\tau^* / \tau_r^* \right)^{\beta} w \quad (5)$$

where the unit bed load transport rate is proportional to the transport intensity (τ^* / τ_r^*) raised to some power β greater than one, and the total transport rate is simply the unit transport rate times the width of the channel. Transport intensity is a function of dimensionless shear stress:

$$\tau^* = \frac{\tau}{(\rho_s - \rho) g D_{50}} \qquad (6)$$

relative to some reference value τ^*_r associated with a small transport rate, where τ is shear stress, ρ_s is sediment density, and ρ is water density. The implication for braided reaches is that transport intensity varies widely as a function of local shear stress and grain size, but is likewise strongly dependent on changes in the wetted width of the channel. Ashmore and Sauks (2006) show that increases in discharge are almost solely accounted for by changes in wetted width, essentially activating more threads for transport while depth or stress distributions may not vary much with discharge. Bertoldi et al. (2009) reaches a similar conclusion, and also shows that the mean stress field underestimates transport where the 80^{th} percentile of the distribution more accurately reflects total transport. This is consistent with a gamma-type distribution of shear stress (e.g. Paola, 1996; Nicholas, 2003), where a relatively small proportion of high stresses may dominate transport. Braided channels have also been shown to respond to changes in sediment supply through the degree of braiding intensity (Germanoski and Schumm, 1993; Chew and Ashmore, 2001; Ashworth et al., 2007), which likely affects this high stress tail of the distribution. By contrast, in single-thread reaches changes in bed load flux with discharge may be dominated simply through changes in the mean depth and velocity (stress) where a 1-D flow assumption is more accurate.

One of the primary difficulties in linking mophodynamic complexity to sediment transport in braided channels lies in the dearth of field data on actual flow and stress fields. Several authors have used local depth coupled with reach-averaged slope to compute shear stress distributions from the depth-slope product, under the assumption that the true stress distribution would be of similar form (Nicholas, 2000; Bertoldi et al., 2009). Only recently has some success been obtained using hydrodynamic models coupled to detailed measured topography to extract 2-D flow fields in real braided channels (Nicholas, 2003; Tunnicliffe et al., 2010). As a result, very few field data exist to explore the coupling between channel complexity, spatial variations in shear stress, and sediment loads as coincident measurements of these properties are difficult and time consuming.

Objectives

The objective of this study is to link the sediment supply controls on regional braided channel formation to the associated changes in flow and sediment transport processes at the watershed and reach scale. Braided streams are uncommon in the Rocky Mountains of the western U.S., except in the Yellowstone region of northwest Wyoming where many examples exist, commonly in conjunction with single-thread reaches. This provides a unique opportunity to investigate the conditions necessary for braided channel development across a large area of relatively similar hydrology and climate, supplemented by a data set of bed load transport from more than 50 streams and rivers including single-thread and braided reaches. A combination of data compilation and analysis, field measurements of braided morphology and sedimentology, and hydrodynamic and sediment transport modeling is used to link pattern and process through the following related analyses:

1) Regional controls on braided channel development are explored in terms of basin geology, measured sediment fluxes (i.e. sediment supply), morphologic characteristics, and associated braiding criteria. This portion of the study focuses on placing braided streams in the Yellowstone region within a broader channel pattern framework.
2) A more detailed analysis in an individual watershed – Sunlight Creek, WY – is used to explore the geomorphic controls on downstream transitions between single-thread and

braided reaches. Then, using bed load sampling and modeling between reach types, the associated changes in flow hydraulics and sediment transport dynamics are addressed, with implications for braided channels as an equilibrium form in these systems.

STUDY AREA AND METHODS

Regional Analysis

The greater Yellowstone region is dominated by volcanic and sedimentary rocks of Paleozoic to Holocene age, and bounded by ranges such as the Beartooth Plateau, Teton Range, and Wind River Mountains that are cored by resistant crystalline rocks. Braided reaches occur most prominently not in the modern Yellowstone Plateau, but in the adjacent Absaroka Mountains and Washakie Range in northwest Wyoming (Figure 4.1). The Absaroka Range is a thick Eocene volcanic pile composed of dominantly andesitic volcaniclastic deposits (Nelson and Pierce, 1968; Love and Christiansen, 1985), many of which are breccias and conglomerates deposited in volcanic debris flows. The Washakie Range lies east of Grand Teton National Park in the upper Snake River basin, and is typified by much lower relief than the adjacent Absaroka or Teton Ranges. Rocks here are composed of Paleozoic sedimentary lithologies, dominantly the Pinyon Conglomerate and the Bobcat Member of the Harebell Formation (Love, 1973) which are composed of thick (in some cases more than 1000m) sequences of quartzite conglomerate derived from western Montana via the paleo-Idaho River (Chetel et al., 2011). The entire area was covered by the Yellowstone ice cap (Pierce, 2004), and glacial deposits are quite common, although sediment delivery from hillslopes to channels remains high in areas of erodible bedrock. The modern Yellowstone volcanic plateau has locally swelled the crust enhancing relief in adjacent ranges, particularly the Absaroka Mountains which is a very rugged high relief

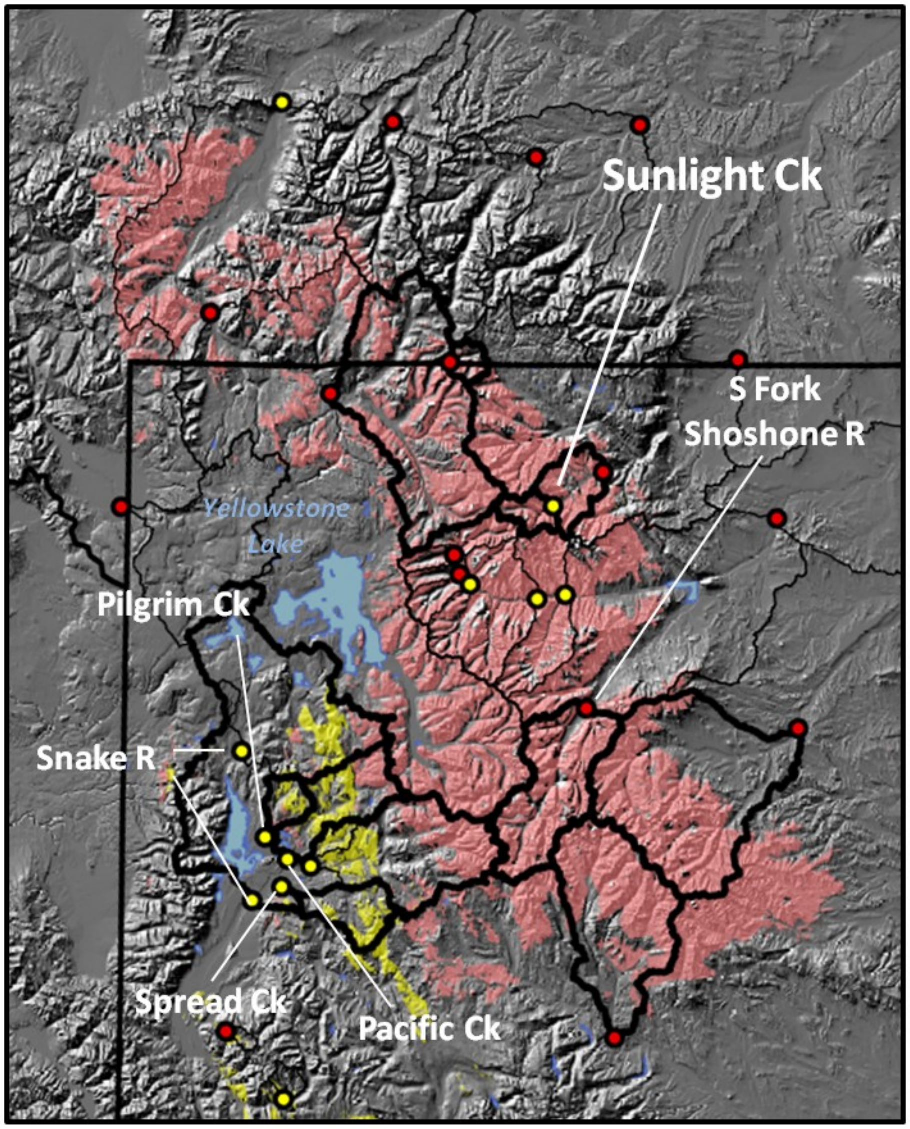

Figure 4.1. A) Map of study area showing bed load (yellow dots) and suspended load (yellow and red dots) sampling locations. Volcaniclastic rocks of the Absaroka Mountains (pink) and conglomerates of the Washakie Range (yellow) are overlain on the shaded relief. Outlined in bold are basins where sediment transport data has been collected and braided reaches are commonly observed. Labeled locations are field data collection sites discussed in the paper.

Location	Source
Sediment Transport	
Various Idaho Streams (33)	*King et al. (2004)*
Upper Spokane Basin, ID (2)	*Clark and Woods (2001)*
Big Lost River Basin, ID	*Williams and Krupin (1984)*
Sunlight Creek, WY^	*this study*
Snake River^, Buffalo Fork, WY	*Erwin et al. (2011)*
Little Granite Creek, WY	*Ryan and Emmett (2002)*
Spread^, Pacific^, Pilgrim Ck^, Snake R, WY	*USGS NWIS*
Yellowstone River, MT^	*Holnbeck (2005)*
East Fork San Juan R, CO^	*Ryan (2007)*
Ohau River, NZ^	*Thompson (1985)*
Toklat River, AK^	*Emmett et al. (1996)*
Susitna Basin, AK^ (4)	*Williams and Rosgen (1989)*
Tanana River, AK^	*Williams and Rosgen (1989)*
(^ braided)	
Supplemental Data	
Discharge	
Idaho	*Hortness and Barenbrock (2004)*
Wyoming	*Miller (2003)*
Alaska	*Curran et al. (2003)*
Channel Geometry	
Idaho	*Harenberg (1980)*
Montana	*Lawlor (2004)*
Wyoming	*Greg Bevenger, Shoshone NF, Pers. Comm. (2010)*
	Zelt (2001)
	Leopold and Maddock (1953)
Grain Size	
East Fork San Juan R, CO^	*Ryan et al. (2005)*
Pine Creek, ID	*Kondolf et al. (2002)*
North Fork Couer d'Alene, ID	*Barenbrock and Tranmer (2008)*

Table 4.1. Data sources for streams and rivers in this study. Supplemental data were used to define factors such as bankfull discharge or grain size where not available in the original sediment transport database. Channel geometry from a variety of regional single-thread reaches were used to complement data from the sediment sampling locations.

range deeply incised by streams (Pierce and Morgan, 1992). Modern streams drain a mixture of alpineto montane climate zones, with higher order streams typically bounded by an alluvial plain composed of Pleistocene and Holocene sediment.

While the focus of this study is on braided streams in the greater Yellowstone region, a compilation of bed load transport data for more than 50 streams and rivers in the Northern Rocky Mountains, Yellowstone region, and several additional braided streams worldwide is used to define a sediment supply context for the study (Table 4.1). For each site, a bankfull sediment concentration was calculated using site-specific relations between bed load transport and water discharge. A power-law relation was used to compute the bankfull transport rate, Q_b, if it provided a good fit, and in some cases low flow data (<25% bankfull) were eliminated or the value was chosen by eye in order to give greater weight to measurements made at higher discharges. Sediment concentration was then determined by scaling the bankfull transport rate by bankfull flow ($C=Q_b/Q_{bf}$), which was determined through field measurements or as the 1.5 year flood where field measurements were unavailable. Sediment concentration provides a simple variable to describe the amount of sediment a given stream must transport in relation to its water supply. In addition to sediment transport data, channel dimensions were obtained from over 100 single-thread reaches in the northern Rocky Mountains for comparison with the measured braided reaches described below (Table 4.1).

Field measurements of channel morphology and sediment characteristics were made on nine braided reaches in five braided streams: Sunlight Creek, South Fork Shoshone River, Pacific Creek, Pilgrim Creek, and Spread Creek (Figures 4.1 and 4.2, Table 4.2). For the latter four sites, surveys of channel geometry, in addition to surface and subsurface sampling were made near bed load sampling sites. Bed load samples were obtained from a variety of published

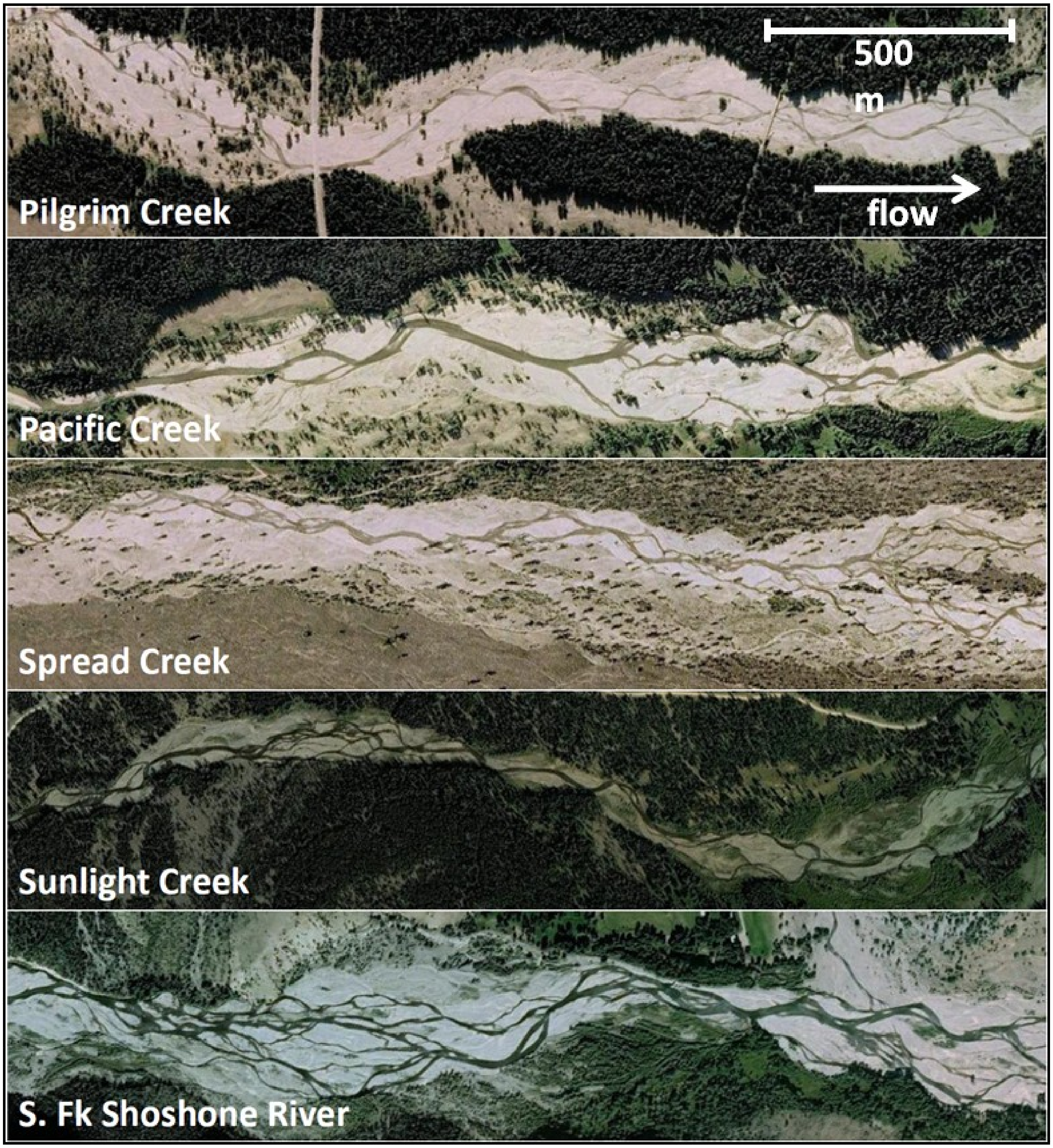

Figure 4.2. Google Earth images of the 5 braided stream reaches for which the authors collected field data. Scale is the same in all photos. Note that in the Sunlight Creek basin five distinct braided reaches were surveyed.

Site	Drainage Area (km2)	Bankfull Q (m3/s)	Bankfull Width (m)	Bankfull Depth (m)	Slope (m/m)	Surface D_{50} (mm)	Subsurface D_{50} (mm)
Braided							
South Fork Shoshone River	794	96.6	197	0.33	0.0113	38	28
Pacific Creek	423	60.1	77	0.50	0.0080	57	41
Spread Creek	256	19.8	54	0.31	0.0158	56	48
Pilgrim Creek	126	17.4	55	0.33	0.0091	36	18
Sunlight Creek-1	354	25.0	48	0.36	0.0051	25	12
Sunlight Creek-2	139	19.5	52	0.22	0.0057	26	16
Sunlight Creek-3	118	17.5	75	0.28	0.0086	32	17
Sunlight Creek-4	93	15.0	79	0.23	0.0095	30	18
Sunlight Creek-5	84	13.9	47	0.30	0.0091	32	25
Single-Thread							
Snake River abv Jackson Lake	1230	183.9	59	1.27	0.0013	31	15
Sunlight Creek-6 [a]	143	19.8	16	0.70	0.0061	49	24
Sunlight Creek-7 [a]	131	18.7	16	0.78	0.0054	60	22
Sunlight Creek-8	127	18.4	21	0.55	0.0070	43	29
Sunlight Creek-9	103	16.0	35	0.36	0.0075	43	12
Sunlight Creek-10	83	13.9	18	0.47	0.0091	36	25
Sunlight Creek-11	82	13.7	30	0.43	0.0087	40	22
Sunlight Creek-12	76	13.1	26	0.33	0.0110	47	24
Sunlight Creek-13	54	10.4	11	0.53	0.0110	57	38
Sunlight Creek-14	34	7.7	9	0.37	0.0160	53	---

Table 4.2. Characteristics of the reaches surveyed in this study. The superscript a indicates a transitional channel pattern, but dominated by a single thread. The width here refers to the entire braid plain.

sources (Table 4.1), except for Sunlight Creek where measurements were made by the authors (see below). For channel geometry, 3 cross-sections were chosen at representative locations along a roughly 400-500 meter long reach over which the longitudinal profile was measured. Average bankfull shear stress for the braided reaches was calculated simply as the depth-slope product:

$$\tau = \rho g h S \tag{7}$$

where ρ is water density, g is gravitational acceleration, h is reach-averaged depth, and S is slope. While reach-averaged depth values are not likely representative of true sediment transport processes (see discussion above), reach-averaged shear stress gives an assessment of the relative energy between braided systems (similar to unit stream power). Surface sediment samples were made using the standard pebble count procedure (Wolman, 1954) with a minimum of 100 particles chosen from an exposed bar, and another 100 particles from the main wetted channel. Samples were sorted at 1/2 phi intervals using a metal template (gravelometer) and merged for an average grain size. Subsurface samples were taken from exposed bars that visually appeared representative for the reach. Following removal of the surface armor, enough sediment (~100-300 kg) was sampled such that the largest particle was at a maximum 5% of the total weight and generally much less (e.g. Church et al., 1987). Particles coarser than 32mm were measured in the field, and a subsample of the finer material was sieved at 1/2 phi intervals in the lab.

Sunlight Creek

Geomorphic Measurements

A detailed analysis was performed over two years in the Sunlight Creek basin where channel pattern commonly alternates between braided and single-thread (Figure 4.3). First, surveys of 16 reaches distributed throughout the basin were used to document longitudinal changes in channel pattern (Figure 4.3a-c, Table 4.2). Of these 16 reaches, 9 are single-thread, 5 are braided, and 2 show a transitional pattern characterized by dynamic single-thread channels bounded by a gravel plain. Measurements at each site included surface and subsurface sediment samples (as above), a minimum of three cross-sections, and a longitudinal profile of order 10 times the channel width. More detailed measurements along a braided reach in the Sunlight Creek basin were used to document channel changes and sediment transport over a two year period which included three 1.5-year flood events (Figure 4.3d). Surveys were made at 9 cross-sections on four occasions along the braided reach to document channel change and aggradation or degradation associated with these flood events. Channel change was simply computed as the change in cross-sectional area for each cross-section spaced roughly 60 m apart. In order to understand the downstream controls on channel transitions, sediment samples from stream banks or tributary fans were made adjacent to each site (Figure 4.4a) using the subsurface sampling technique.

Bed Load Sampling

Bed load sampling was conducted in reaches upstream and downstream of the above braided reach during the 2009 season to both document overall bed load flux from the basin, in addition to quantifying the sediment flux to and from the braided reach (Figure 4.4). Sampling was performed by wading using a handheld Elwha bed load sampler (10x20 cm orifice) at 2 meter intervals across the bed (see Clayton and Pitlick (2007) for sampler discussion). Sampling times at individual points ranged from 30 seconds to 5 minutes depending on the transport rate. A total of 21 bed samples were taken, 10 at the upstream site and 11 at the downstream site, at a range of discharges over a two week period (5/29-6/11/2009) (Table 4.3). In all cases, the bed load samples were combined for each pass, returned to the lab, dried and sorted as in the subsurface samples described above. The unit bed load transport rate, q_b, was computed by dividing the total transport by the sampled width and sampling time per vertical following the approach of Edwards and Glysson (1999), then converted to a total transport rate, Q_b, by multiplying by the active channel width.

Immediately prior to or following bed load sampling, current-meter measurements of velocity at 1-m intervals across the channel at 0.4 of the water depth were used to calculate discharge following the mid-section method. Sampled discharges ranged from 4.5-12 cms at the

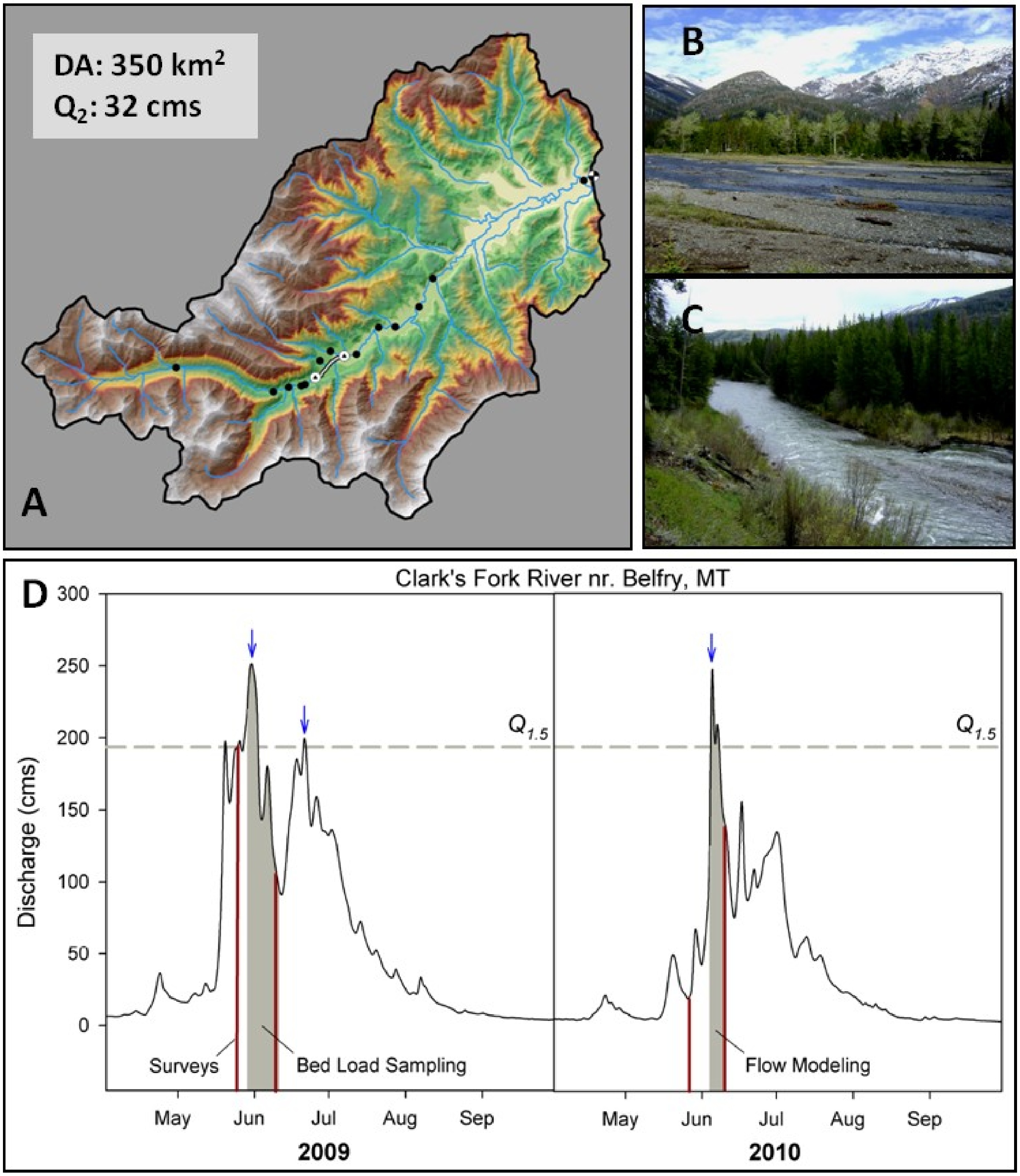

Figure 4.3. A) Shaded relief map of the Sunlight Creek basin with locations of morphologic measurements shown as black dots. White dots indicate bed load sampling sites. A stream gauge at the basin outlet operated from 1929-1971. Example braided reach (B) and single-thread reach (C). D) Proxy stream gauge from the nearby Clark's Fork River showing the timing of different measurements in the Sunlight basin. Blue arrows represent flow peaks greater than the 1.5-year recurrence interval.

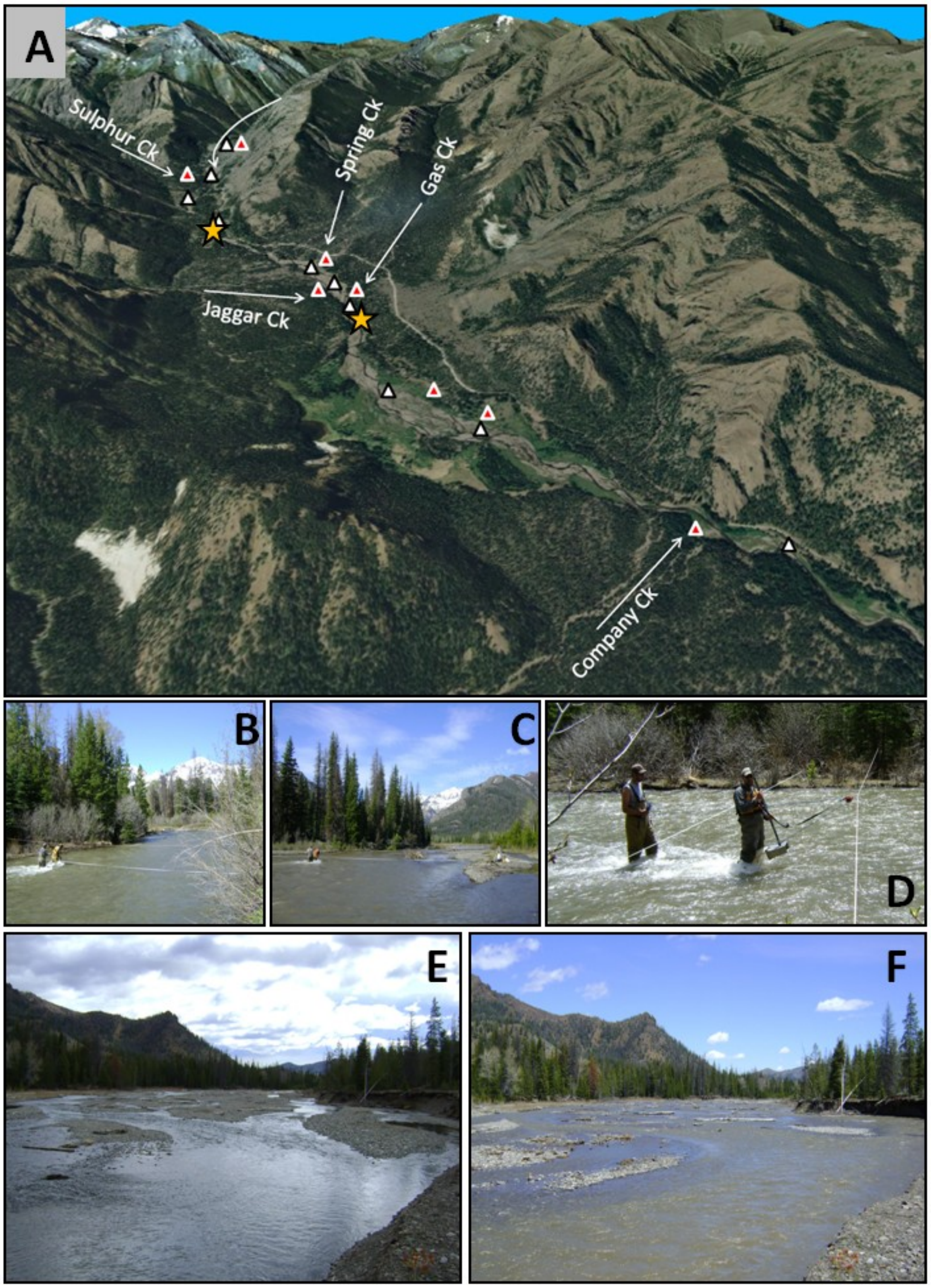

Figure 4.4. A) Oblique view of upper portion of Sunlight Creek basin showing bank/tributary fan sampling locations (red and white triangles), main channel surface and subsurface samples (black and white triangles), and bed load sampling locations (yellow stars). View of upstream (B) and downstream (C) bed load sampling sites. D) Image showing bed load sampling set up, where the Elwha sampler is attached to a static line via pully allowing for the sampler to be held in place by downstream person. Photos of the braided reach between bed load sampling locations taken on (E) 5/31/2010 at 2-3 cms and (F) 6/8/2010 at 8-10 cms.

Sample #	Date	Q	Q_i/Q_{bf}	τ	Sample Size	Number verticals	time/ vertical	q_b	Q_b	% sand	D_{16}	Grain Size D_{50}	D_{84}
		(cms)		(N/m^2)	(kg)		(min)	(kg/m/s)	(kg/s)			(mm)	
Upstream Site													
1	5/29/09	9.5	0.68	35	6.7	7	5	0.016	0.281	30	0.9	14.3	44.4
2	5/29/09	9.8	0.70	36	1.7	7	5	0.004	0.070	59	0.6	1.3	18.6
3	5/29/09	12.2	0.87	38	5.6	7	2	0.033	0.600	19	1.2	24.7	49.1
4	5/30/09	11.8	0.84	39	14.9	9	2	0.069	1.228	2	12.7	25.1	41.4
5	5/31/09	11.2	0.80	38	4.3	9	2	0.020	0.356	47	0.7	2.5	33.4
6	6/1/09	11.4	0.81	41	21.1	9	2	0.098	1.748	36	0.8	9.2	40.3
7	6/3/09	7.6	0.54	33	8.4	9	5	0.016	0.274	36	0.7	11.4	29.2
8	6/5/09	9.1	0.65	34	10.9	9	2	0.050	0.898	28	0.9	21.4	44.9
9	6/8/09	5.7	0.41	28	0.8	9	2	0.004	0.063	38	0.9	4.2	24.5
10	6/11/09	4.5	0.32	25	0.1	9	3	0.000	0.006	55	0.8	1.8	4.5
Downstream Site													
1	5/30/09	12.7	0.77	34	6.6	7	2	0.039	0.759	13	4.0	18.6	38.0
2	5/30/09	12.7	0.77	34	19.8	7	2	0.118	2.284	14	2.6	11.1	32.5
3a	5/30/09	14.7	0.89	38	11.8	9	1	0.109	2.145	27	1.1	9.4	32.2
3b	5/30/09	14.7	0.89	38	11.5	9	1	0.106	2.083	11	14.2	32.1	59.2
4	5/31/09	14.3	0.87	35	6.5	9	2	0.030	0.583	45	0.7	4.6	35.7
5	6/1/09	13.7	0.83	35	7.3	9	2	0.034	0.650	30	0.8	20.9	46.6
6a	6/3/09	8.5	0.51	26	1.1	10	2	0.005	0.096	93	0.6	0.9	1.4
6b	6/3/09	8.5	0.51	26	2.7	9	2	0.013	0.267	15	2.6	15.5	28.5
7	6/5/09	9.9	0.60	27	2.2	19^a	1	0.010	0.207	17	1.8	19.2	37.0
8	6/8/09	7.6	0.46	26	1.6	17^a	2	0.004	0.070	6	23.5	35.9	44.8
9	6/11/09	5.5	0.33	22	0.1	8	5	0.000	0.005	54	0.5	1.4	18.2

Table 4.3. Bed load sampling data for the Sunlight Creek basin. The superscript a indicates that the transport measurements consisted of two passes; Q_i/Q_{bf} is the flow level relative to bankfull discharge; q_b is the unit bed load transport rate; Q_b is the total bed load transport rate; and grain sizes are given for the 16^{th}, 50^{th}, and 84^{th} percentiles of the bed load.

upstream site and 5.5-15 cms at the downstream site which spans roughly 30-90% of bankfull discharge at these sites.

Flow and Sediment Transport Modeling

In order to quantify the influence of morphologic complexity on sediment transport, shear stress fields were derived at a range of flows along a braided reach using a 2-dimensional hydrodynamic model developed by the U.S. Geological Survey, Flow and Sediment Transport with Morphologic Evolution of Channels (FaSTMECH), using the iRIC user interface (Nelson et al., 2003) (Figures 4.4e,f and 4.5). Due to spatial variability in flow in both the lateral and streamwise directions, individual cross-sections are not likely to represent the time and space averaged flow properties in a braided reach. Alternatively, it is assumed that the flow distribution spatially over a long braided reach is more representative of the time-averaged conditions of an individual cross-section. The resulting probability distribution of shear stress can be divided by the reach length for a cross-sectional average, and then be coupled to a sediment transport equation to compute the bed load flux.

Primary input to the FaSTMECH model is accurate topographic data, which provides the computational boundary for flow calculations (Legleiter et al., 2011a), in addition to discharge and downstream stage. Detailed field surveys provided the initial topographic data set, which were then post-processed by interpolating points along the main channels so as to prevent irregular and inappropriate topography during triangulation within iRIC. Photographs, field analysis, and an aerial photo of the study reach provided the guidance on interpolating these channels within the constraint of the surveyed points (Figure 4.5). These data were then interpolated to a 1m x 1m grid using a nearest neighbor technique in ArcGIS, and then returned to iRIC to create the model topography. This resulted in a much smoother realistic boundary than triangulation of the raw data in iRIC.

FaSTMECH uses a channel-centered orthogonal curvilinear grid as computational nodes, where here the grid spacing is approximately 1m x 1m. The model solves the depth- and Reynolds-averaged momentum equations in the streamwise and cross-stream directions (Nelson et al., 2003; Legleiter et al., 2011b). Flow is assumed to be steady and hydrostatic and turbulence is treated by relating Reynolds stress to shear via an eddy viscosity (Barton et al., 2005; Legleiter et al., 2011b; Logan et al., 2011). Bed stresses are calculated via a drag coefficient closure (Nelson et al., 2003), and the drag coefficient can be either constant or spatially variable in the model domain. Lateral eddy viscosity, a measure of lateral momentum exchange, is a tunable parameter in the model. Calibration then consists of manipulating values of the drag coefficient and lateral eddy viscosity in order to best match the observed water-surface elevations – the primary verification target. The drag coefficient was set at a reach-averaged value of 0.02, which is equivalent to a Manning's n of 0.035-0.04 for a typical depth scale of the reach. Lateral eddy viscosity was set to 0.075 as representing the lowest value that resulted in a stable solution in agreement with measured water-surface elevations. Model results have been shown to be relatively insensitive to spatial variations in C_d (Segura et al., 2011) and over a 4-fold range in lateral eddy viscosity (Legleiter et al., 2011b), and the values here are within the range reported in other studies (Conaway and Moran, 2004; Barton et al., 2005; Legleiter et al., 2011a; Logan et al., 2011).

The flow model was run at four discharges: 10, 12, 14, and 16 cms representing a range of typical sediment transporting flows covering roughly 60-100% of bankfull flow. Smaller discharges were not feasible as the flow threads became too shallow for the topographic

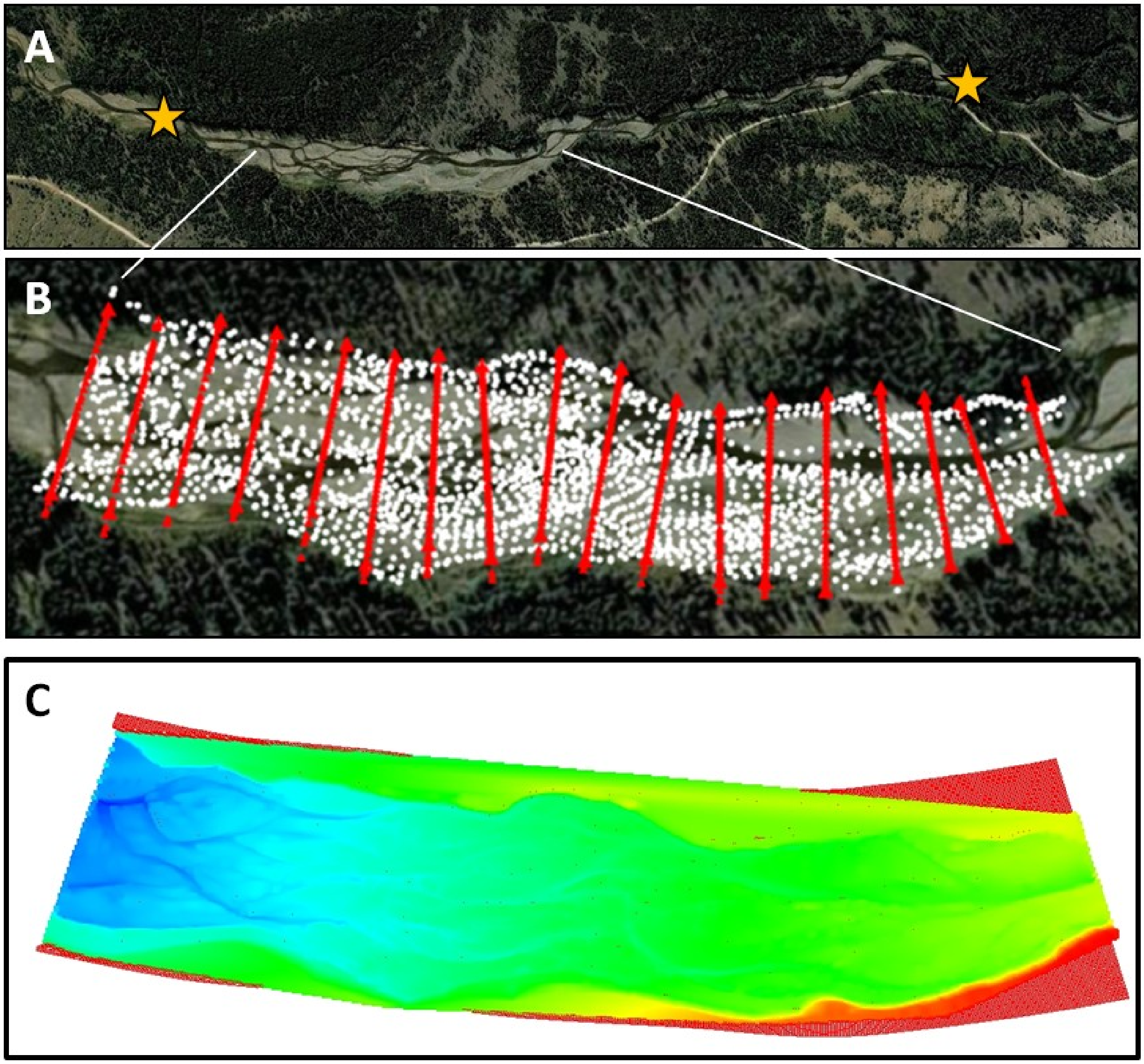

Figure 4.5. A) Google Earth image highlighting the location of bed load sampling sites (yellow stars) relative to the braided reach used for flow modeling. B) Survey density of braided reach used in flow modeling. Red points represent permanent cross-sections. C) Smoothed topography used as input into the FastMECH hydrodynamic model. Grid mesh is 1 m^2 and is shown in red near the edges of the model domain. Model reach is roughly 500 m for scale.

resolution of the reach, and the model would not converge on a solution. At the modeled discharges convergence was obtained in less than 1000 iterations, with discharge modeled within 1% of the normalized value at the higher flows, and within 5% at low flow though generally much less. Verification of the flow model comes from water surface measurements throughout the reach and generally showing very good agreement (Figure 4.6a). Water surface surveys were only available for 10 and 14 cms, but water-surface elevation does not change significantly with discharge at these flows (Figure 4.6b). As a result the model was run at 12 and 16 cms using the same parameters to allow for a broader range of flow computations, and the results are consistent with simple widening at these flows. Output from the model includes a number of 2-D scalars, and here we extract the shear stress field to model sediment transport. The reach-scale stress distribution was divided by the streamwise distance to produce a stress distribution for an average cross-section. These data were then scaled by the average channel width to compute the

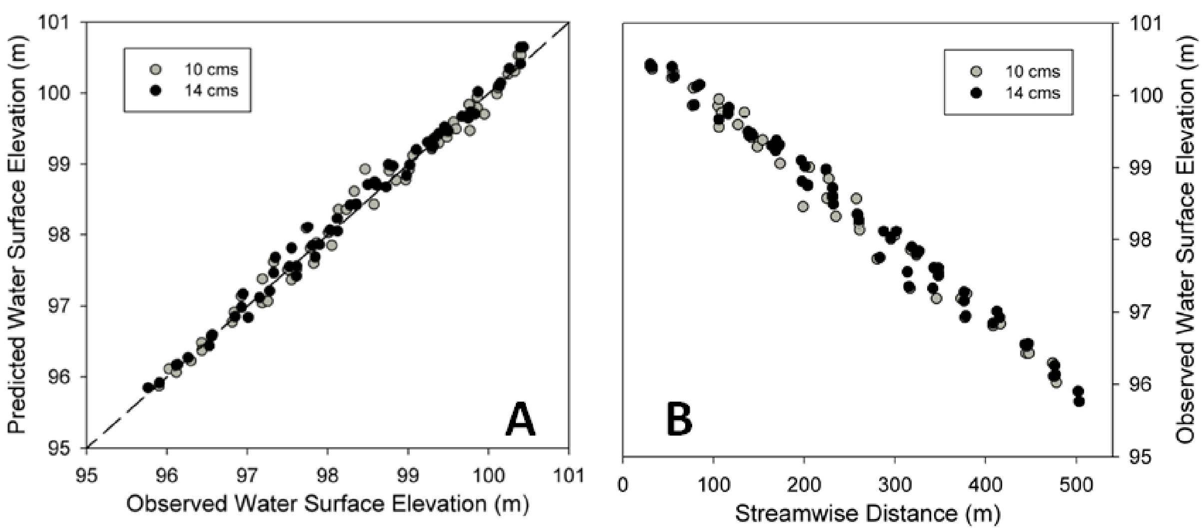

Figure 4.6. A) Observed versus predicted water-surface elevations for the braided reach modeled with FaSTMECH at 10 and 14 cms. B) Observed water-surface elevations versus streamwise distance at 10 and 14 cms.

fraction of the bed associated with different shear stress values for calculation of bed load transport described below

Shear stress estimates in the single-thread reach (Figure 4.4b) were made by relating mean velocity to shear via an assumption of a logarithmic velocity profile of the form:

$$u = \frac{u_*}{\kappa} \ln\left(11 \frac{h}{k_s}\right) \tag{8}$$

where u is mean velocity, u_* is shear velocity, κ is von Karman's constant, h is depth, and k_s is a characteristic roughness height here taken to be equal to $3D_{84}$ where D_{84} is the 84th percentile of the surface grain size distribution (Kuelegan, 1938; Whiting and Dietrich, 1990). From measurements of local depth and velocity, the above equation can be solved for u_* and thus shear stress as:

$$\tau = \rho u_*^2 \,. \tag{9}$$

Individual local values of shear stress estimated in this manner were made at 1 meter increments across the channel for discharges of roughly 8, 10, and 12 cms. Stress estimates obtained in this manner suggest a drag coefficient (C_d) averaging 0.016, very similar to the value used for stress calculations in the braided reach. Two suites of velocity measurements obtained on different occasions resulted in 34 unique shear stress values for each discharge, and these data were then scaled by the channel width to calculate stress bins as in the braided reach.

Sediment transport in the braided and single-thread reaches was then computed using the Parker and Klingeman (1982) substrate-based bed load transport model. While this equation is similar in its general form to several surface-based transport equations (e.g. Parker, 1990; Wilcock and Crowe, 2003), the substrate based approach accounts for sand, which is abundant, and resulted in better agreement between modeled and observed bed load sediment size. The Parker and Klingeman (1982) equation takes the form:

$$W_i^* = 11.2\left[1 - \frac{0.853}{\phi}\left(\frac{D_i}{D_{50s}}\right)^{\beta}\right]^{4.5} \tag{10}$$

where W_i* is a dimensionless bed load transport rate defined as:

$$W_i^* = \frac{(s-1)gq_{ij}}{u_*^3 f_i} \tag{11}$$

and ϕ_i is the transport intensity, $\left(D_i / D_{50s}\right)^{\beta}$ is a hiding function, D_i is an individual size class, D_{50s} is the subsurface median grain size, s is the specific gravity of sediment, f_i is the fraction of the bed occupied by a given grain size fraction i in the substrate, and q_{ij} is the unit transport rate of a given size class for a given stress level j. Here the transport intensity is cast as:

$$\phi = \frac{\tau_j^*}{\tau_r^*} \tag{12}$$

which is a function of both local dimensionless shear stress, $\tau*_j$, and $\tau*_r$. The hiding function adjusts the transport intensity for individual size classes, but the exponent of 0.018 results in a relatively small change in transport associated with particle exposure as this is a substrate-based approach. Parker and Klingeman (1982) suggest a value of 0.0876 for the subsurface-based $\tau*_r$, and here that value is tuned slightly to better match measured transport rates. As a result, the dimensionless transport rate is defined by the interaction of the stress field with the grain size distribution, and the total mass transport rate can be found by computing transport rates for each size class across the fraction of the bed experiencing a given stress level, f_j:

$$Q_b = w\rho_s \sum_i \sum_j q_{ij} f_i f_j \tag{13}$$

where w is width and ρ_s is sediment density. Verification and calibration of the sediment transport model comes in the form of bed load measurements in the single-thread reach described here, in addition to the downstream sampling location below the braid plain.

RESULTS

Regional Geology and Braided Stream Characteristics

Despite a wide range in rock types across the Rocky Mountains of the Western U.S., braided reaches are relatively rare and their occurrence in the Yellowstone Region is associated with very specific geologic formations in the Absaroka Mountains and Washakie Range. In both cases, the dominance of conglomeratic lithologies results in a high supply rate of bed load caliber material to the adjacent streams (Figure 4.7). For example, in the Washakie Range conglomerate beds readily supply pre-rounded, coarse quartzite clasts to the adjacent braided channels, and despite being exposed in only a portion of these catchments, quartzite clasts represent >95% of the bed sediment. Figure 4.8 shows the transition from a dynamic meandering single-thread channel to a braided channel pattern downstream from tributaries that drain these conglomerates. The channel pattern associated with these rocks is translated far downstream to the braided Snake River, as the primary sediment sources downstream of Jackson Lake are these Washakie Range streams. While the Absaroka Range exhibits much greater relief, the sediment weathered from these volcaniclastic rocks tends to be finer grained in both hillslope and stream deposits (Figure 4.7). Figures 4.4a and 4.9 typify the setting of braided reaches in the Absarokas such that as valleys become less restricted downstream, a braiding pattern often emerges, and in many cases transitions with single-thread reaches longitudinally. In both settings, the delivery of coarse sediment results in bed load transport rates that are high relative to other streams in the northern Rockies (see Chapter 1). Bankfull transport rates from 11 sites (Figure 4.1) draining these lithologies range from $4x10^{-4}$ to $2x10^{-2}$ m^3/s (1-42 kg/s) and bed load concentrations from $4x10^{-6}$ to $9x10^{-5}$, with the highest concentrations occurring in braided reaches (>3 $x10^{-5}$).

Along nine braided reaches near several of the above sites (Table 4.2), field surveys and measurements of bed sediment characteristics show that a significant range in slope and grain size exists among the channels. Surface grain size ranges from 25 to 57mm while subsurface

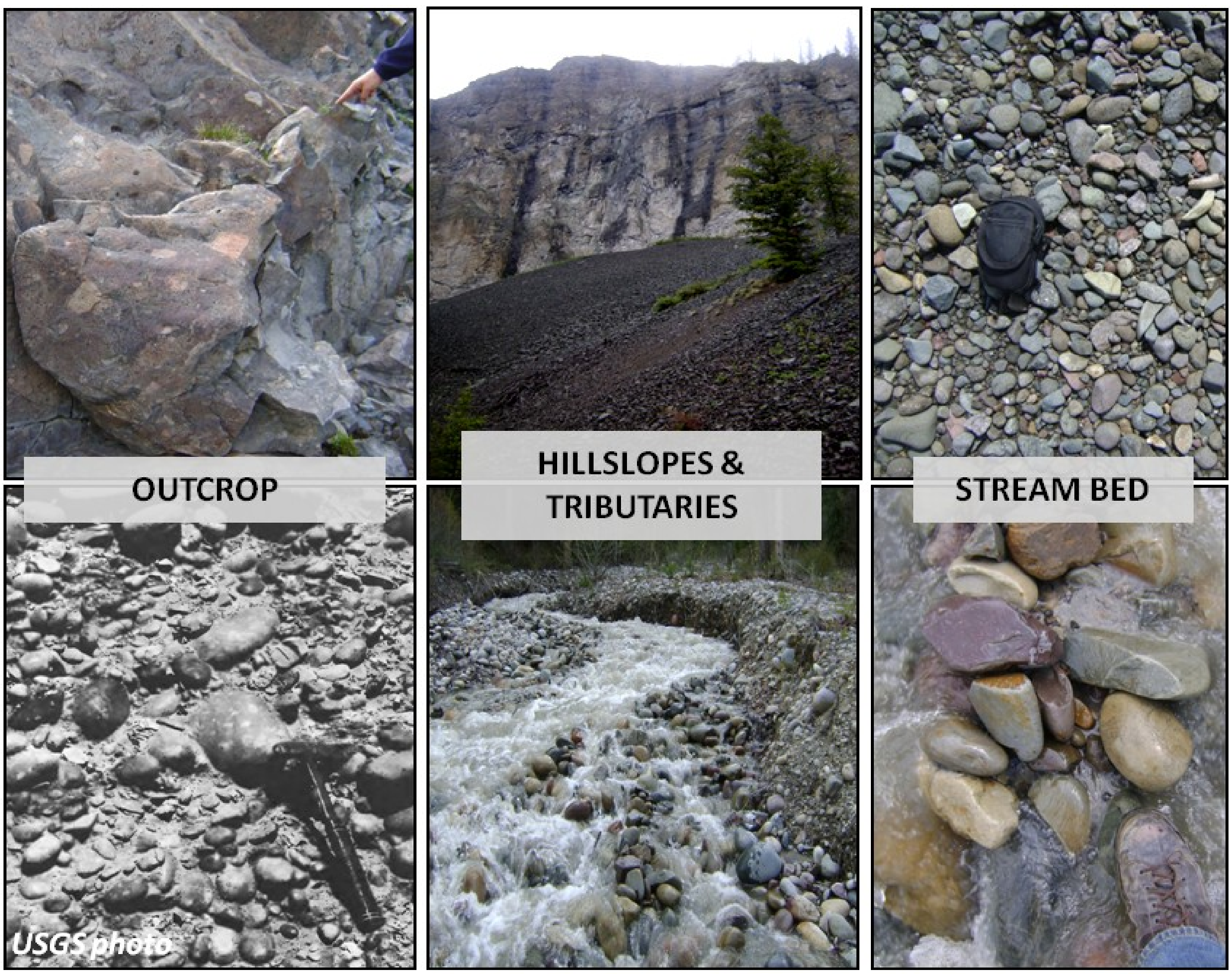

Figure 4.7. Examples of the Wapiti Formation in the Absaroka Mountains (top) and the Harebell and Pinyon Formations common in the Washakie range (bottom) in outcrop, weathered to hillslope scree and tributary material, and typical stream bed material.

Figure 4.8. Dynamic meandering single-thread to braided channel pattern transition along Pacific Creek; prominent transition occurs downstream of Gravel Creek. Sediment inputs from tributaries draining the Harebell and Pinyon formations presumably drive the bed load supply to a braided channel pattern which persists downstream as these formations continue to supply coarse sediment.

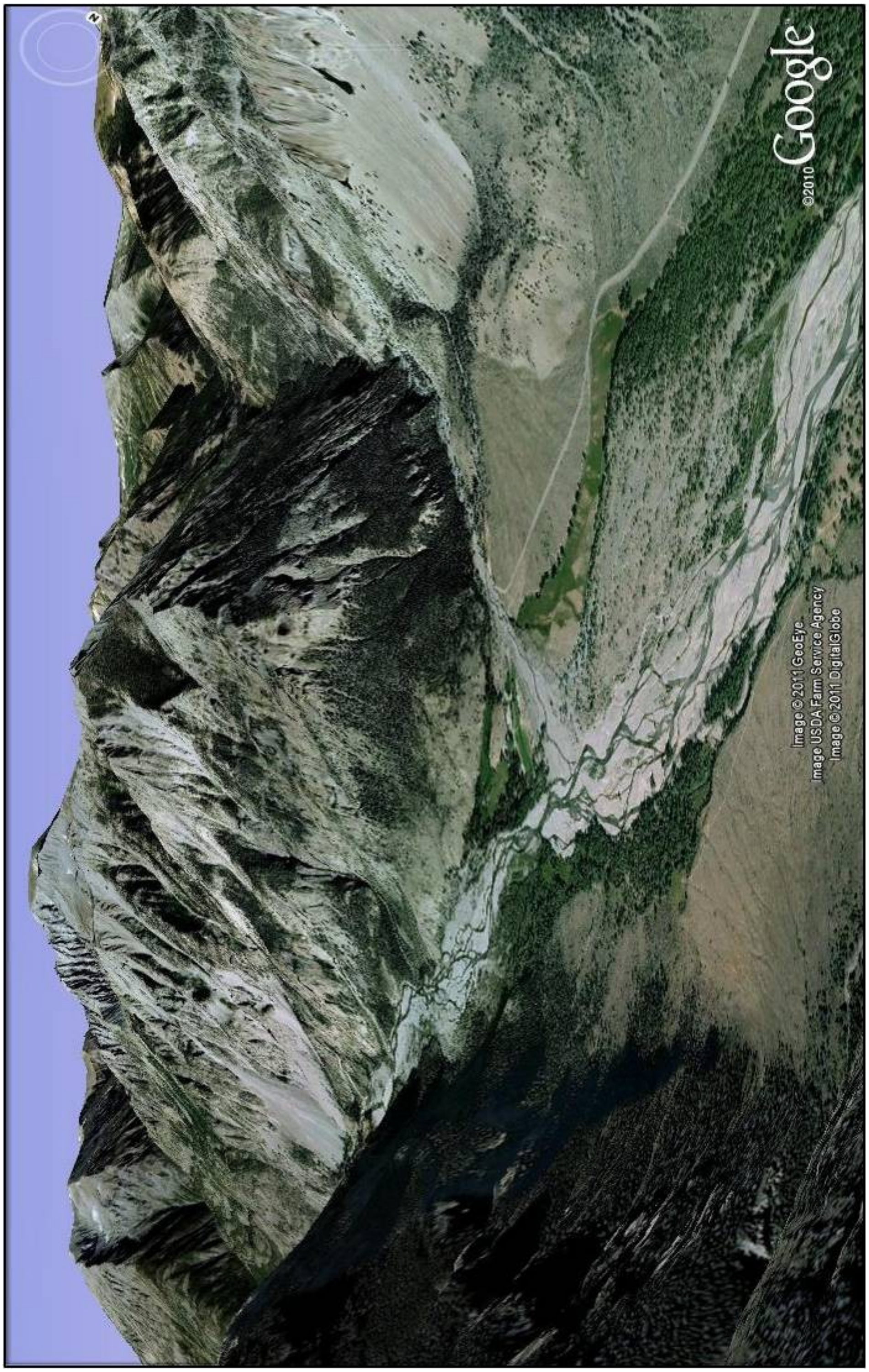

Figure 4.9. Braided channel of the South Fork Shoshone River emerging from the rugged Absaroka Mountains. Note tributary entering at right is also very dynamic. Braided patterns typically occur where valleys widen downstream, with downstream pattern transitions reflecting local geomorphic controls.

grain size ranges from 12 to 48mm, a fairly typical range for gravel-bed streams in the region, although the average armoring ratio of 1.6 is relatively low (Table 4.2). The range in grain size generally reflects source-area lithology as quartzite clasts derived from the Washakie Range conglomerates are decidedly coarser than the softer volcanic rocks making up clasts in the Absaroka Range. There is, however, a strong linear relation between the average shear stress and the median grain size of both the surface and subsurface material (Figure 4.10). While this largely reflects steeper gradients where grain size is coarse, some braided reaches are simply dominated by deeper, but fewer threads (e.g. Pacific Creek) which likewise enhances the available stress. From a hydraulic geometry perspective, braided reaches are on average much wider and shallower than single-thread channels (Figure 4.11a), with average width to depth ratios greater than 100 for all of the braided reaches surveyed. In the single-thread data set on the

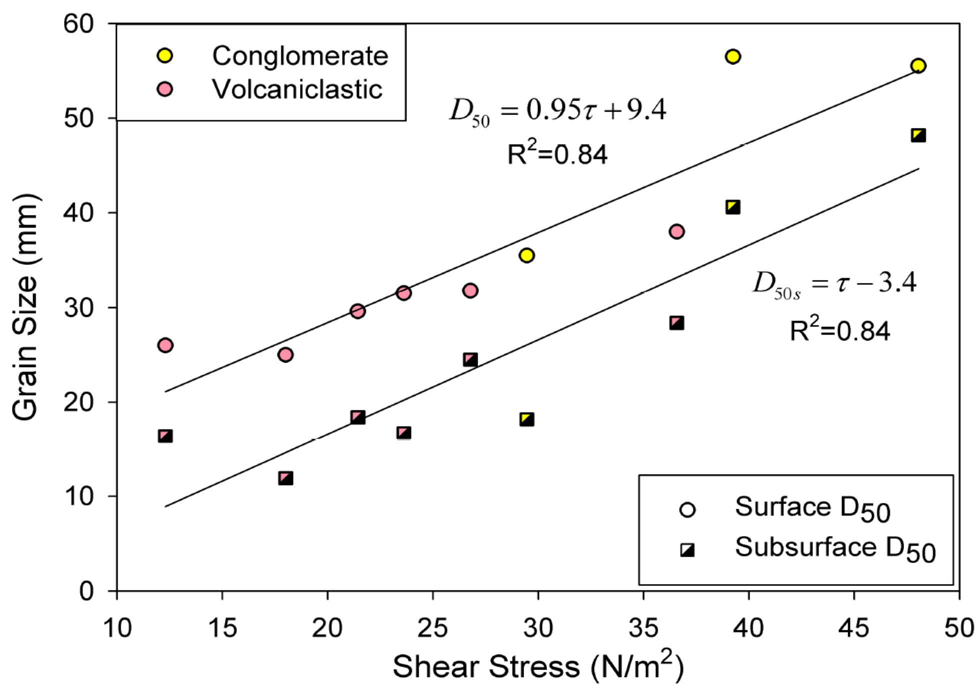

Figure 4.10. Average bankfull shear stress versus surface and subsurface grain size for braided reaches draining different rock types in this study.

other hand, only 6 of 119 reaches have width/depth ratios greater than 50. Slope varies more than three-fold in braided reaches from 0.005 to 0.016, which is not substantially different from single-threaded gravel-bed streams in the region. Plotting a subset of the single-thread data set where slope information was available in fact shows no difference in slope between braided and single-thread reaches (Figure 4.11b). The discriminant function originally proposed by Leopold and Wolman (1957) is shown for reference, and would imply that essentially all of the streams in this study should be braided.

Sediment Supply and Channel Pattern

While equation 1 presented by Leopold and Wolman (1957) performs poorly, the importance of grain size is clearly highlighted in the discriminant function of Eaton et al. (2010) which takes into account the surface grain size or "bed state" (sensu Church, 2006) by including a grain size scaling in Q*. When the Q*-S plot is used, the discriminant function proposed by Eaton et al. (2010) reasonably separates braided reaches from single-thread reaches (Figure 4.12a), where here the braided reaches include an additional 8 sites where bed load data are available. The light gray line on the plot shows the braiding threshold with a value of $\mu'=1.4$, indicating stronger banks and a typical value for well vegetated banks according to Millar (2005). In this case, all of the single-thread reaches plot below the braiding threshold while several of the braided reaches fall very near this line, consistent with these streams existing near the braiding threshold. This is illustrated further by considering the case of the Snake River above and below Jackson Lake. Below Jackson Lake bankfull bed load concentrations are roughly four times greater than further upstream, due in large part to sediment-laden tributaries that enter just below the lake (Pacific Creek, Buffalo Fork, and Spread Creek). The change in

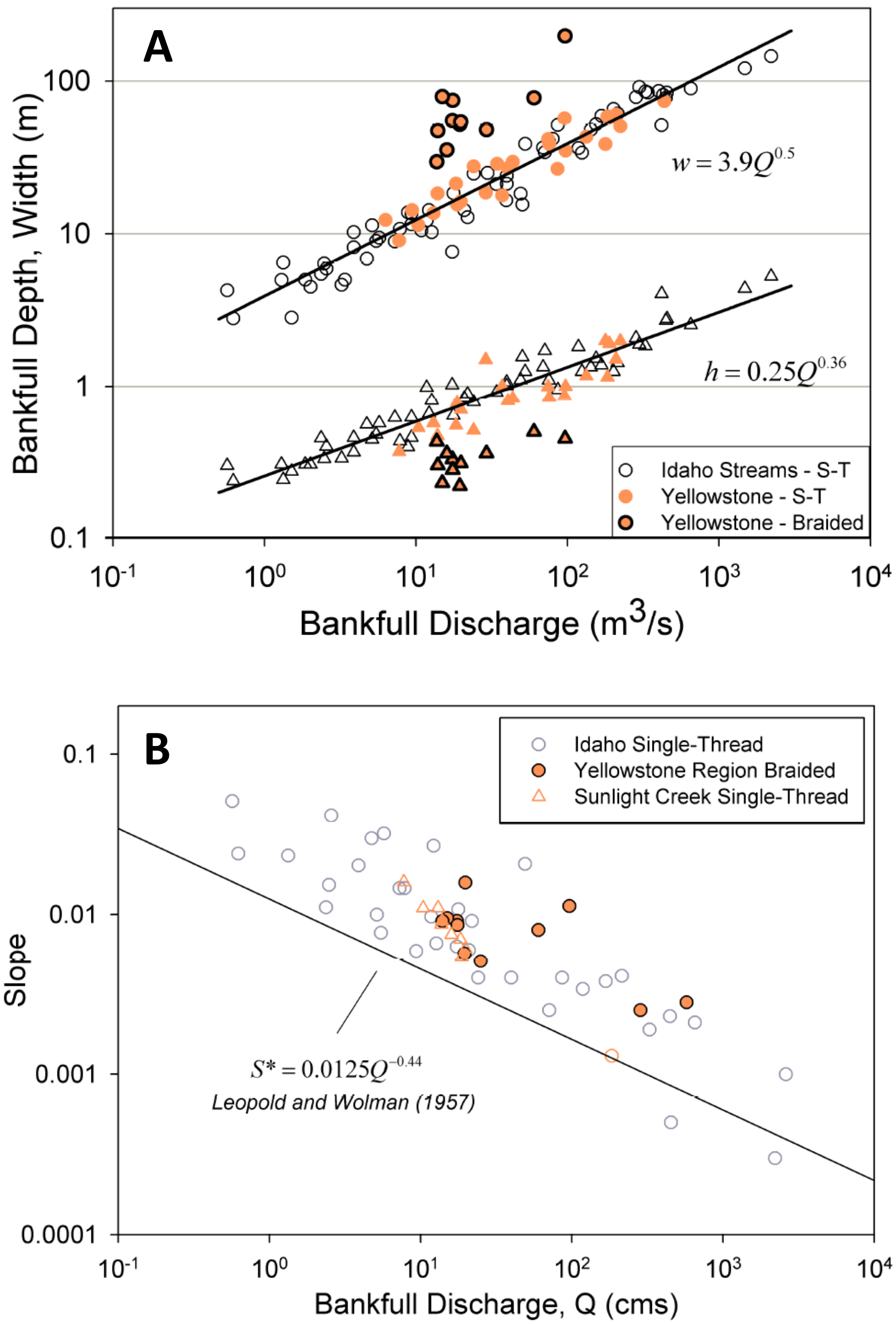

Figure 4.11. Hydraulic geometry plots for single-thread reaches in Idaho and the Yellowstone region, with braided streams outlined in bold. A) Changes in bankfull width and depth with bankfull discharge. B) Changes in slope with bankfull discharge showing the braided threshold proposed by Leopold and Wolman (1957).

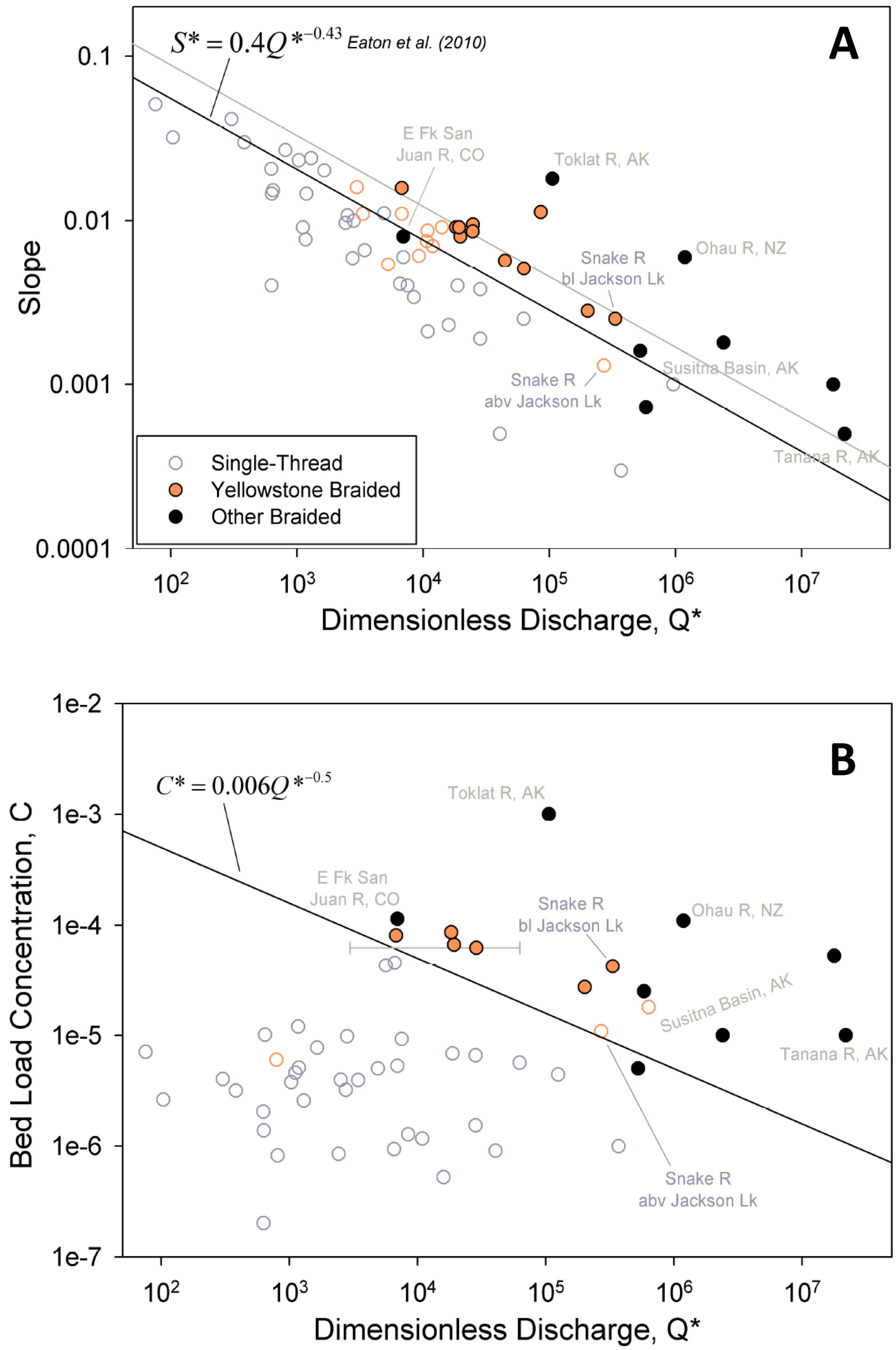

Figure 4.12. A) Bankfull discharge versus bankfull bed load concentration where the gray-line represents the transition to dominantly braided channels. B) Plot of dimensionless discharge versus slope showing the braided threshold proposed by Eaton et al., 2010.

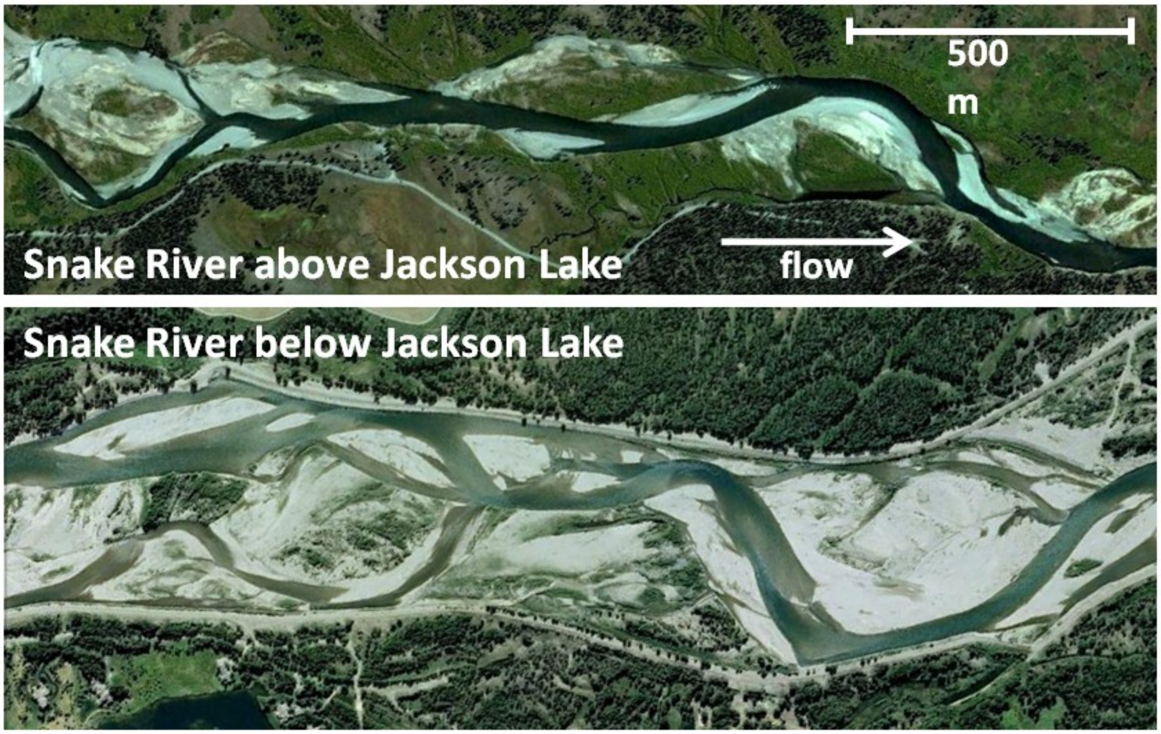

Figure 4.13. Change in channel pattern on the Snake River below Jackson Lake is consistent with Eaton et al. (2010) and is associated with an influx of bed load from braided tributaries draining the Washakie Range (see Figure 4.7).

channel pattern is consistent with the discriminant function of Eaton et al. (2010) (Figure 4.12a) such that the downstream channel is nearly twice as steep despite similar grain sizes, and the change in channel pattern from dynamic single-thread upstream to braided downstream is clearly observable (Figure 4.13). Further, the South Fork Shoshone River plots highest above the braiding threshold and aerial photos show this to be one of the most dynamic and multi-threaded of all the braided reaches in the region (Figure 4.2).

Because Q* is a function of $D^{-2.5}$, the separation of points on the Q*-S plot versus the Q-S plot is very sensitive to surface grain size, with the implication that this should reflect differences in sediment load. In fact in the original formulation, Millar (2005) solved for width, depth, and slope as a function of discharge, sediment concentration, and bank strength. However, given the lack of data on bed load flux, slope was treated as an independent variable and used in place of sediment concentration in order to test the model. But it is possible to use the same assumption of w/d=50, and solve for the critical sediment concentration, using equation 12d from Millar (2005):

$$w/h = 425Q^{*0.12}\, C'^{-2.30}\, \mu'^{-2.90} \tag{14}$$

where C'=-$\log_{10}$C and C is sediment concentration. For simplicity setting μ'=1, the above equation can be rearranged to form a braided-single thread discriminant relation as a function of sediment concentration:

$$C^* = 10^{\left(-2.54Q^{*0.052}\right)} \tag{15}$$

where C* is the critical bed load concentration. Equation 15 is well approximated over a wide range of Q* by the power-law:

$$C^* = 0.006Q^{*-0.5}. \tag{16}$$

Figure 4.12b shows that braided streams do indeed plot at much higher bed load concentrations than single-thread reaches, with the Q*-C plot showing an even greater divergence between reach types than the Q*-S plot. The discriminant function proposed in equation 16 performs very well, misclassifying two single-thread reaches and only one braided reach. It should be noted that because Q* and C* both contain Q, equation 16 could be influenced by spurious correlation. Yet because Q is in the numerator of Q* and denominator of C*, equation 16 can be written in dimensional terms as:

$$Q_b^* = 0.006\left(s-1\right)^{1/4} g^{1/4} D^{5/4} Q^{0.5} \tag{17}$$

where Q^*_b is the threshold bankfull bed load transport rate (m^3/s). This relation performs similarly well, misclassifying only 2 reaches in this study. The drawback of equation 17 is that any Q- Q^*_b discrimination is non-unique, as it varies as a function of surface grain size which is embedded in Q* in equation 16. In any case, both equations 16 and 17 suggest that the threshold sediment flux for a given discharge decreases slightly downstream. This makes intuitive sense in that as slope and bed load transport capacity decrease downstream, so does the threshold for sediment overloading and braided channel development. Irrespective of the exact form of equations 16 and 17, the above results show that braided streams and rivers have sediment concentrations up to several orders of magnitude greater than single-thread channels. As illustrated in the Q*-S plot, for a given discharge braided streams are either steeper (enhancing stress or stream power) or finer-grained (reducing resistance) or both, and the result is a more mobile stream bed with enhanced transport. This is well represented by the Q*-C* discriminant function, and quantification of a sediment concentration braiding threshold has not previously been proposed in the literature.

Sunlight Creek Basin

Geomorphic Controls on Channel Pattern Transitions

Braided streams in the greater Yellowstone region do not lie far above the supply driven braided threshold, as reflected in the Q*-C and Q*-S plots (Figure 4.12). Consequently it is common for braided channel segments to transition with single-thread segments. In Sunlight Creek, downstream changes in channel pattern reflect the interaction with tributary fans, in terms of both grain size and channel constriction, thereby influencing the reach-averaged Q* value and presumably bank strength. Figure 4.14 shows downstream changes in channel pattern – labeled as single-thread, transitional, or braided – for the roughly 15-km primary study reach. Upstream the channel is quite steep, remains single-thread, and is supplied with relatively coarse sediment

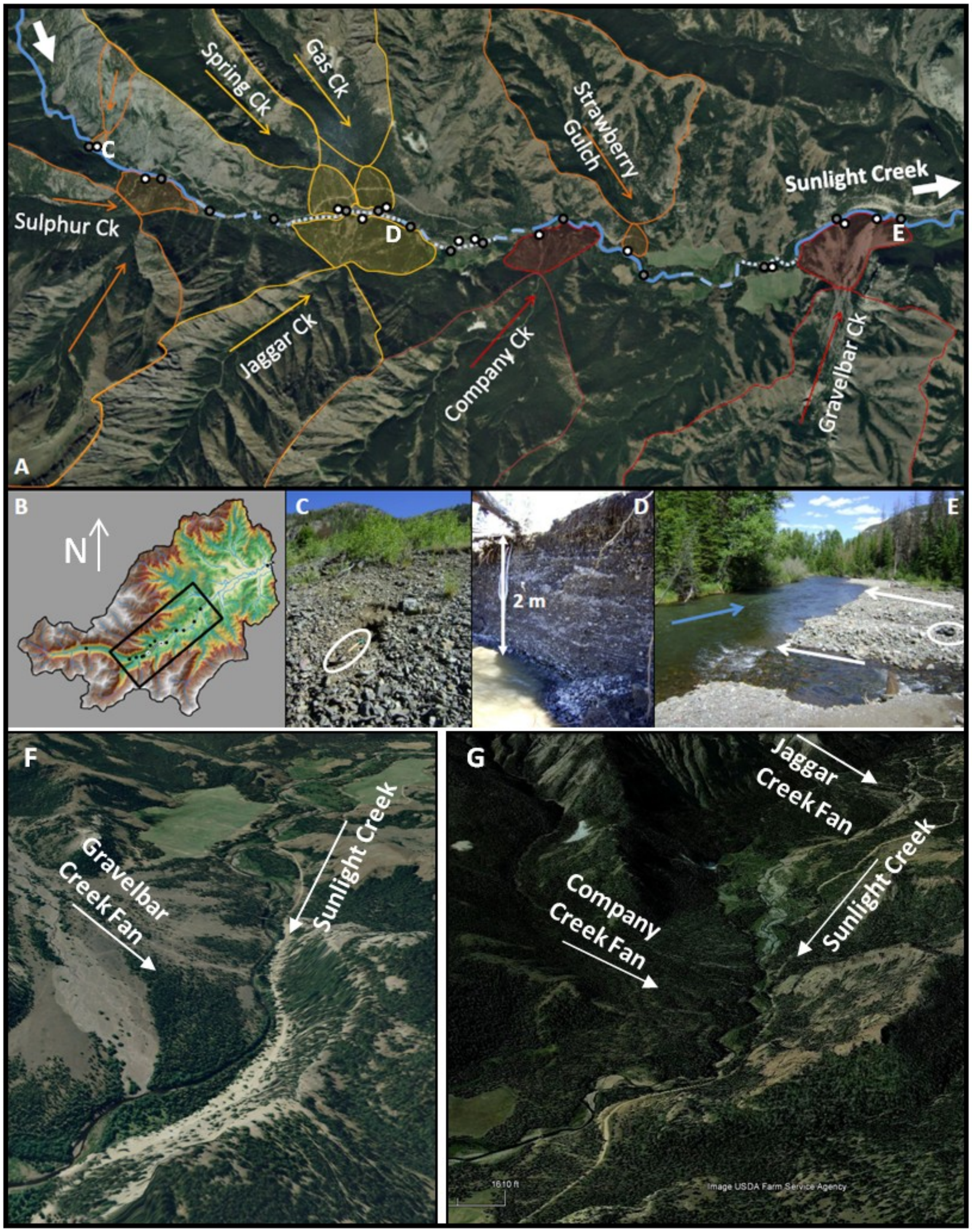

Figure 4.14. A) Aerial photo of region shown in (B) showing downstream changes in channel pattern (blue line: dotted=braided; dashed=transitional; solid=single-thread), sediment sampling locations (white dot: main channel; gray dot: banks/tributary fans), and outlines of major fans sampled (yellow: fine-grained; orange: intermediate; red: coarse-grained. Example sample sites for fan and bank material labeled in (A) are shown in C, D, and E. Note shovel (C) and backpack (E) circled for scale. F and G) Examples of channel constriction and narrowing associated with major fans.

from debris fans (Figure 4.14c). Moving downstream a braided pattern begins to emerge, with pattern transitions controlled by the interaction with larger-scale alluvial fan features. In general, single-thread reaches are associated with constrictions due to the input of major tributary fans (Figure 4.14f,g), but one of the most extensively braided reaches occurs at the confluence of three major fans: Jaggar, Spring, and Gas Creeks. The solution to this apparent dichotomy is in the grain size of the fan material. Where tributary fans are relatively fine grained (Figure 4.14d), bank erosion is obvious (μ'~1), and a braided channel pattern develops, but coarse-grained fans such as Gravelbar Creek (Figure 4.14e) tend to force a transition to a single-thread planform (μ'>1) (Figure 4.14a). As Sunlight Creek flows away from these constrictions a braided pattern re-emerges where the channel is bounded by finer grained alluvial sediments and possible lake deposits. These results are shown more explicitly in Figure 4.15, indicating that main channel sediment size strongly mimics tributary fan and bank materials, with the bed load size (discussed below) shown for reference. Further, the longitudinal profile of Sunlight Creek is incredibly

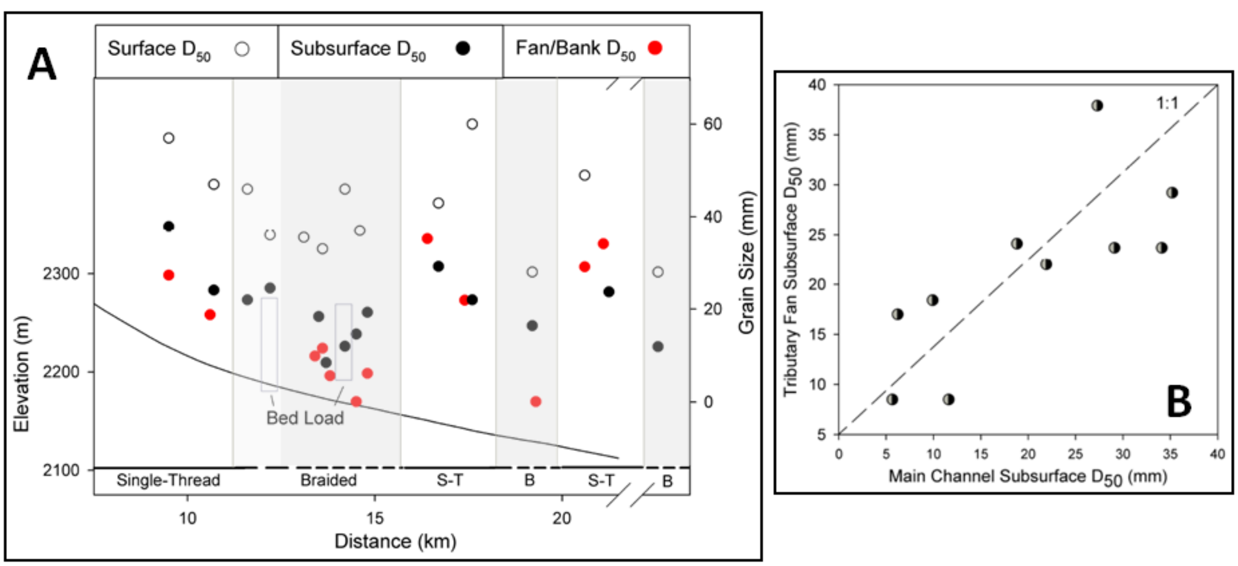

Figure 4.15. A) Downstream changes in grain size of surface, subsurface, and bank/fan sediment, with channel pattern indicated below and the longitudinal profiles shown for reference. B) Main channel subsurface versus bank/fan subsurface median grain size.

smooth and graded (Figure 4.15a), and downstream changes in slope do not reflect the changes in channel constriction and grain size associated with transitions between single-thread and braided reaches (Table 4.2). These results confirm that bank stability is an important component of the transitional nature of channel pattern, especially for streams near the supply threshold.

Bed Load Transport and Channel Change

Sediment flux downstream through a single-thread – braided – single-thread succession was investigated through bed load sampling at the upstream and downstream boundary. Bed load transport ranged from 0.01-1.75 kg/s at the upstream site, and 0.01-2.3 kg/s at the downstream site (Table 4.3), with discharge-transport relations that are quite similar (Figure 4.16) despite the roughly 1 km long intervening braid plain. While based on results from a single high flow event, there does not appear to be a marked difference in inputs or outputs to the braided reach. Multiple surveys over the study period allow us to address this to some degree (Figure 4.17), showing variability in scour and fill between reaches spatially, and within reaches temporally. In general, flow is more concentrated in a single channel at the upstream end of the study area, resulting in lateral erosion. Further downstream, flow disperses and aggradation was more common. Overall for these cross-sections, the first event caused slight aggradation (~1 m^2/section), the second event caused very slight degradation, and the final event was essentially neutral. Field observations of terraces and aerial photos suggest that while the channel is dynamic, there is little evidence of long-term aggradation. As a result, this particular braided reach appears in relative equilibrium with respect to sediment inputs and outputs. The median grain size of the bed load varied considerably, ranging from sand to gravel but again quite similar between reaches (Table 4.2). Figures 4.16 b and c show the overall composite bed load

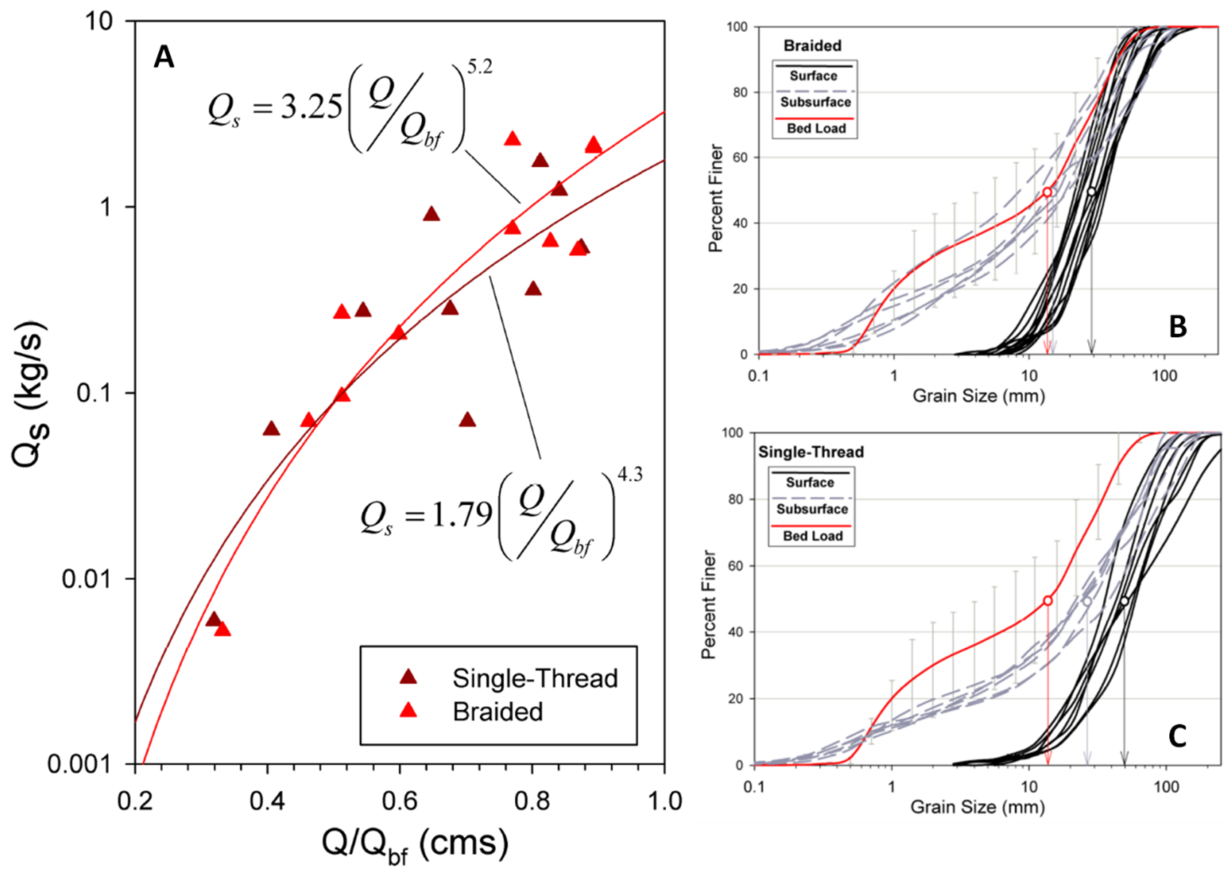

Figure 4.16. A) Discharge scaled by bankfull discharge versus measured bed load transport rate. Comparison between surface, subsurface and bed load size distributions between braided (B) and single-thread (C) reaches. Error bars on bed load distribution represent the 25th and 75th percentile of all samples; arrows indicate average D_{50} for different sediment populations.

size, with gray bars representing the 25th and 75th percentiles, relative to the subsurface and surface sediment sizes from braided and single-thread reaches in the basin. The plots show that bed load and subsurface grain size are quite similar in braided reaches, whereas the subsurface material of single-thread reaches is coarser than the bed load and similar in size to surface material in the braided reach (Figure 4.16b,c). Thus bed material in braided reaches is very

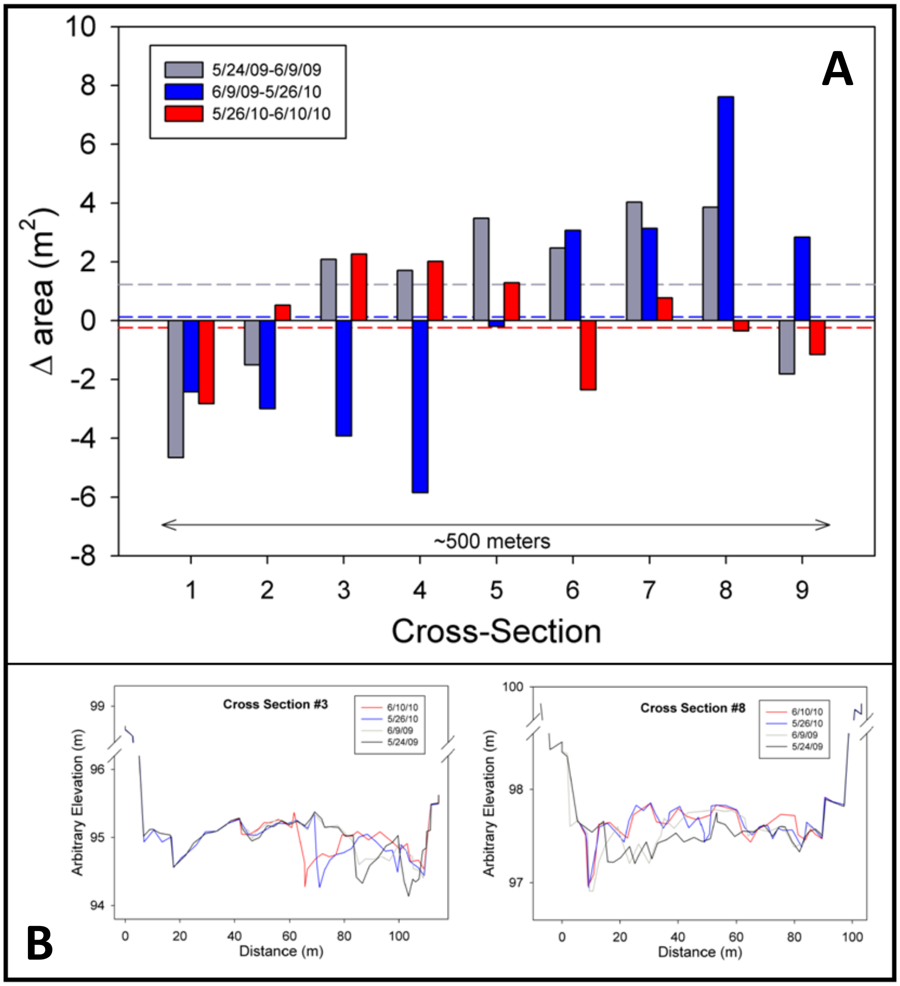

Figure 4.17. A) Changes in cross-sectional area for 9 cross-sections in the modeled braided reach, representing roughly 500 meters. Colors represent channel change occurring between the survey dates shown, in all cases associated with a single flood peak (see Figure 4.3). B) Example channel changes at an upstream and downstream cross-section.

similar to the bed load, with slight surface armoring, whereas the bed material in single-thread reaches is much coarser than the bed load and more reflective of local tributary grain size.

Flow and Sediment Transport Modeling

The results of the bed load sampling suggest the sediment fluxes between reach types are similar, despite drastic differences in scale and cross-stream deviations about the mean depth

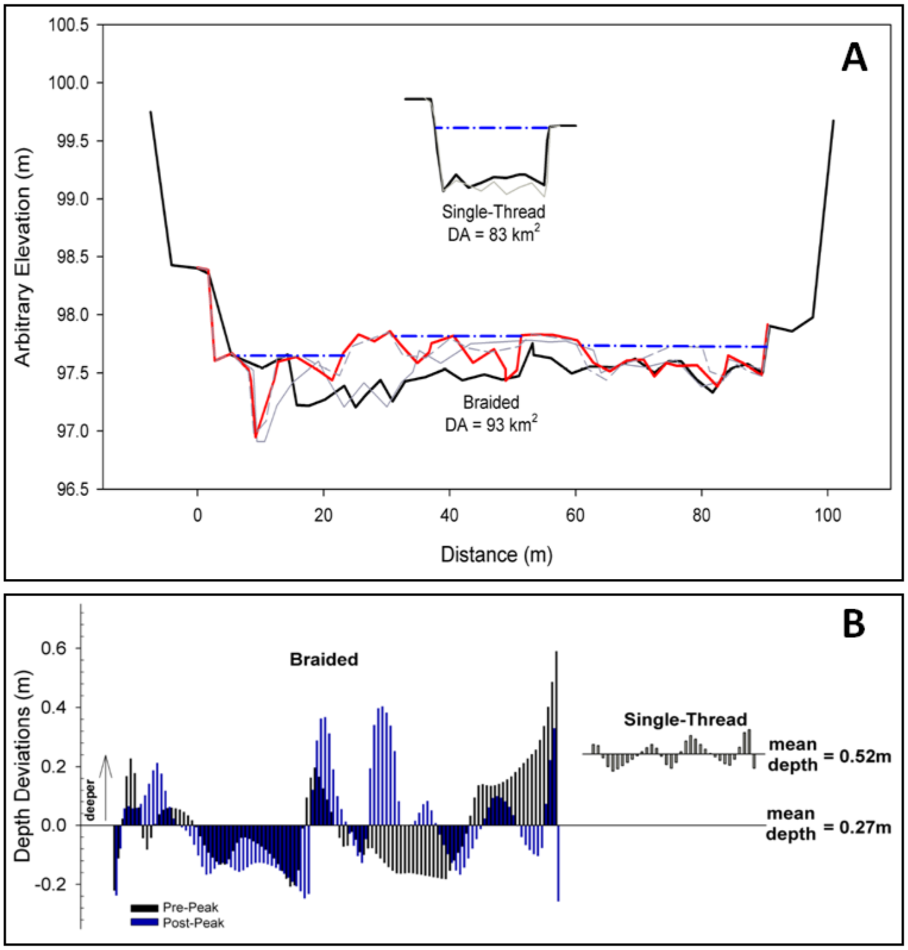

Figure 4.18. A) Example differences in channel geometry between adjacent single-thread and braided reaches. Blue lines are conceptual water surface levels, and line colors represent repeat cross-section surveys. B) Cross-stream depth deviations (vertical lines) shown relative to the mean depth (solid horizontal line labeled at right) for adjacent braided and single-thread reaches.

(Figure 4.16). Figure 4.19 shows the unit discharge and shear stress fields for a flow of 14 cms derived from the FaSTMECH model, with an aerial photo during low flow for reference. The model reproduces the overall flow pattern remarkably well, with good agreement between measured and modeled water-surface elevations (Figure 4.6a). While some of the details of the true flow field are not exact, the primary channel threads are well represented and consistent with field observations, and the modeled flow field represents a reasonable analog for the true flow

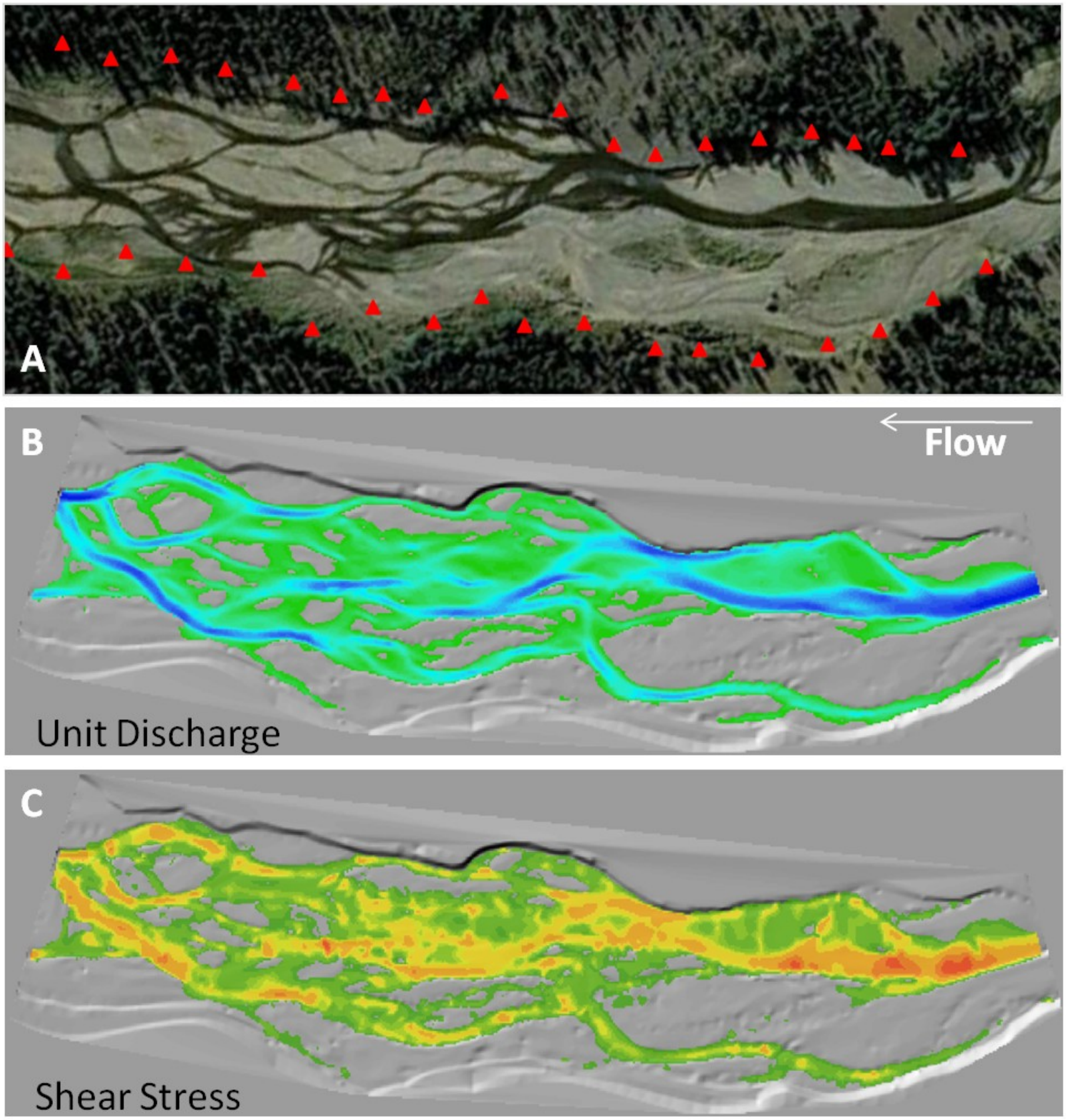

Figure 4.19. A) Aerial photo of study reach taken with surveyed topography at low flow stage. B) Unit discharge and C) shear stress fields derived from FaSTMECH model for a flow of 14 cms. Flow is right to left and modeled reach is approximately 500 m in length.

field. Figure 4.20 shows probability distributions for shear stress extracted from the FaSTMECH model for the two measured flows (10 and 14 cms) compared to stress distributions estimated through velocity measurements in an adjacent single-thread reach for two flows (10 and 12 cms).

While the distributions were derived from different techniques, the magnitude of stresses are consistent between methods and the stress distributions modeled using FaSTMECH in a simple single-thread channels follow the pattern presented here (Segura, 2008; Pitlick et al., 2012). Following previous authors (e.g. Paola, 1996; Nicholas, 2003), we fit these distributions with a two parameter gamma probability density function of the form:

$$f(\tau) = \frac{\alpha\left(\tau/\langle\tau\rangle\right)^{\alpha-1} e^{-\alpha\left(\tau/\langle\tau\rangle\right)}}{\langle\tau\rangle\Gamma(\alpha)} \qquad (18)$$

where Γ is the gamma function, $\tau/\langle\tau\rangle$ is the local shear stress divided by the reach-averaged shear stress, and α is a shape parameter. Also shown on the plots for the braided reach is an exponential distribution (a special case of the gamma distribution where α=1) and, for the single-thread reach, a normal distribution.

In both cases, the gamma distribution is quite adaptable and reasonably fits the data, but with much different shape parameters. This is consistent with previous work (Pitlick et al., 2012) indicating that stress distributions more closely resemble an exponential form in braided reaches versus a more normal distribution in single-thread channels (see also Figure 4.21). Local shear stress in the braided reach can be greater than five times the reach average in isolated locations, while never reaching double the reach average in the single-thread reach (Figure 4.20). As a result, braided reaches are dominated by large areas of the bed experiencing relatively low shear stresses, decreasing non-linearly such that small areas of the bed experience quite high stresses. By contrast, velocity measurements show that single-thread reaches have a more symmetric stress distribution reflecting the relatively uniform channel boundary. Yet the measurements also show very low stresses near the banks, and some small zones of high stress that may be 50% greater than average (Figure 4.20).

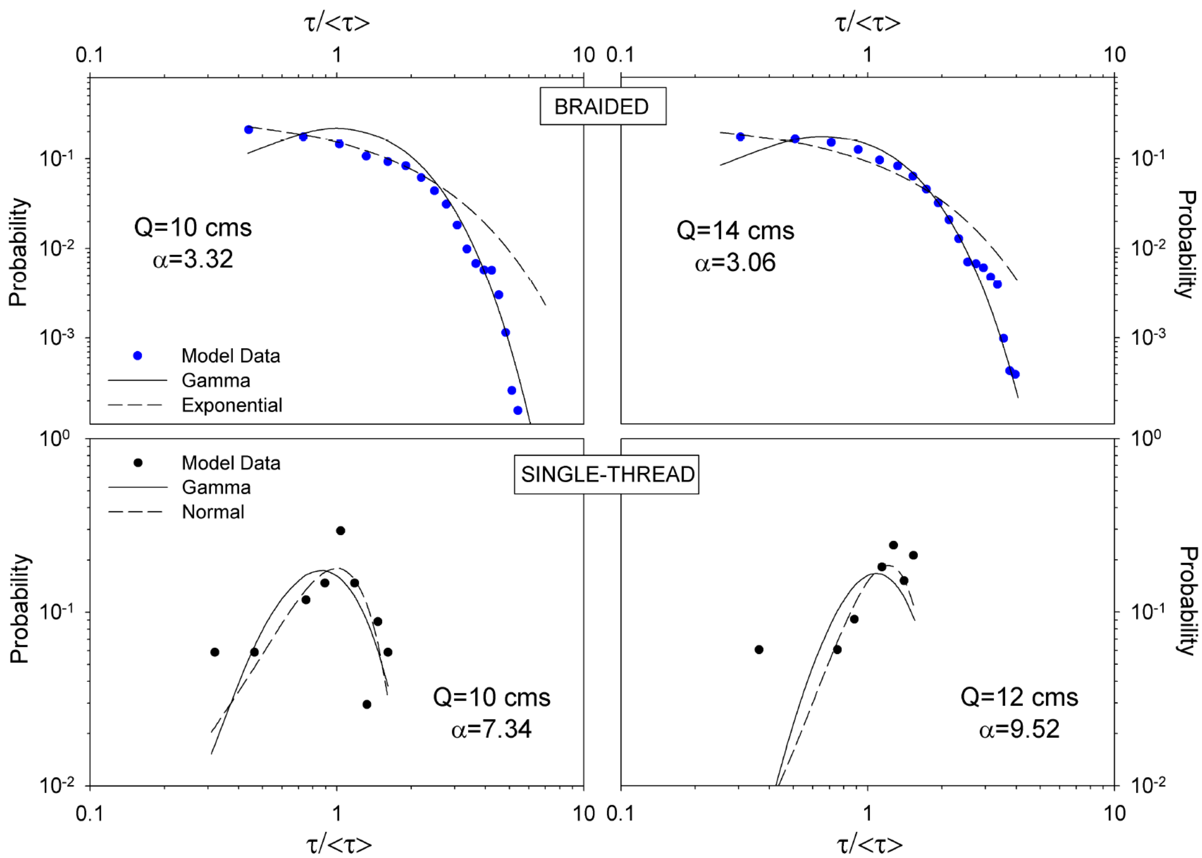

Figure 4.20. Modeled stress distributions for braided and single-thread reaches, fit with different probability density functions. Individual α values for the gamma distribution are shown. Probabilities are based on the modeled data bin sizes.

The response of modeled stress fields to changes in discharge between reach types is shown in Figure 4.21, here plotted on a linear scale. In this case the stress distribution is presented as the fractional width of the channel bed occupied by a given stress bin, such that the area under the curve represents the total channel width – in other words the y-axis is simply the probability of a given stress times reach-averaged width. As discharge increases the stress distribution generally shifts up in the braided reach, indicating that an increase in wetted width is the primary adjustment at these discharges (Figure 4.21a). In fact in the model runs and field surveys, average depth and water-surface elevations change very little, of order several centimeters, while average wetted width increases from about 40 to 60 m as discharge increases from 10 to 16 cms. The result of an increase in flow is therefore to simply increase the number of threads conveying water and sediment. On the other hand, in the sinlge-thread reach changes in discharge are simply accommodated by changes in depth and velocity, and stress distributions shift right in this case (Figure 4.21b). Modeled bed load fluxes reflect these stress distributions as transport in the braided reach tends to favor zones of very high shear stress that occupy a small portion of the total width (Figure 4.22a). Alternatively, in single-thread reaches sediment transport is dominated by relatively wide areas of moderate stress (Figure 4.22), although in some cases at lower flow a narrow zone may account for most of the transport. These results suggest bed load transport in single-thread reaches is distributed more evenly across the channel boundary, whereas zones of convergent flow and channel migration may dominate transport in braided reaches. In fact the modeled high stress zones were typically areas of active erosion where flow converges to a dominant thread near the upstream boundary (Figure 4.17).

Despite the differences in stress distributions, total sediment fluxes modeled between channel patterns are remarkably similar and consistent with field measurements of bed load flux and grain size (Figure 4.23). This result was obtained assuming that the reference shear stress was approximately equal between reaches (τ_r=30 N/m^2), a reasonable approximation given that the surface grain size and slope of this particular single-thread reach (D_{50}=36mm; S=0.009) is nearly identical to that of the braided reach (D_{50}=32mm; S=0.009). The similarity between modeled and measured grain sizes is expected given the weak grain size dependency for the

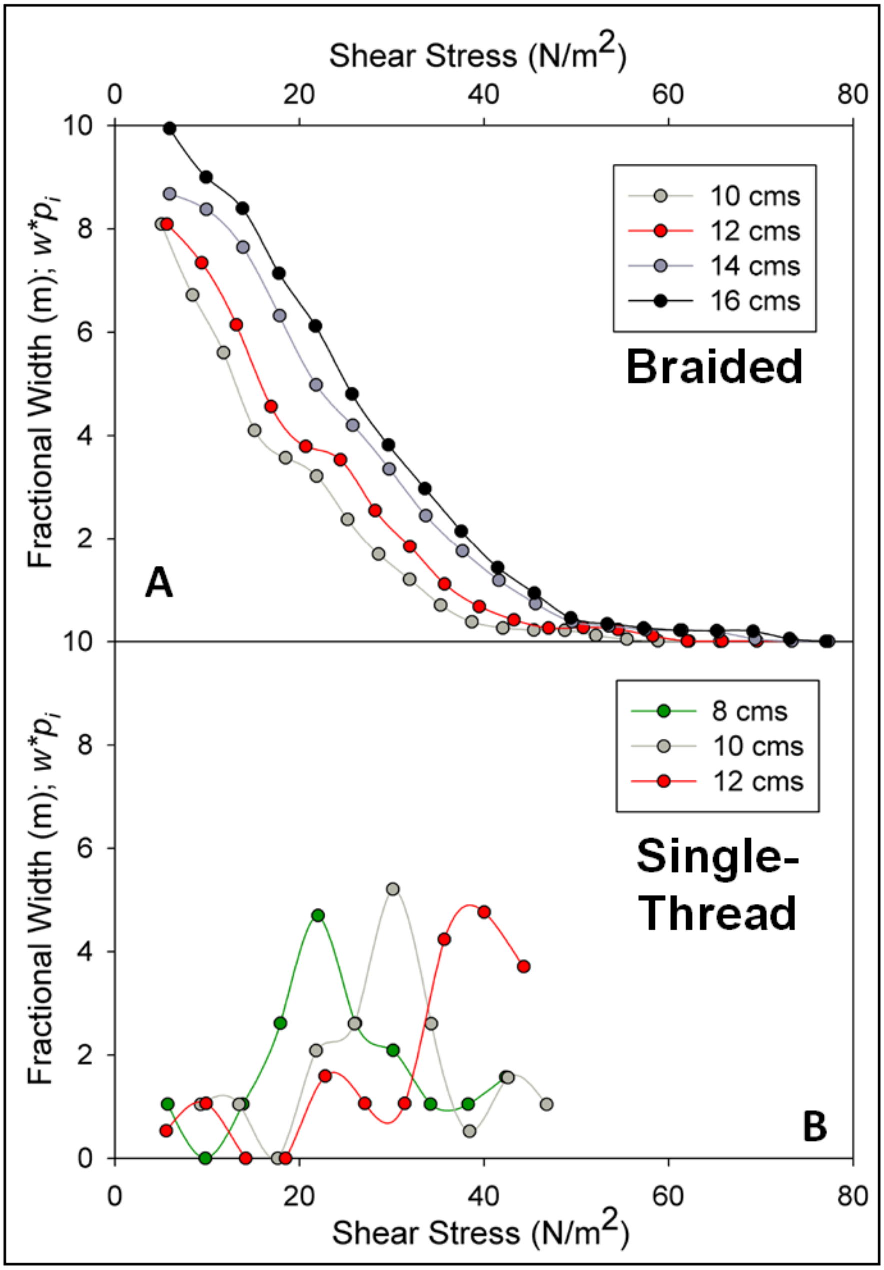

Figure 4.21. Modeled stress distributions for braided versus single-thread reaches, here plotted as a function of fractional width such that the area under the curve equals the total active channel width.

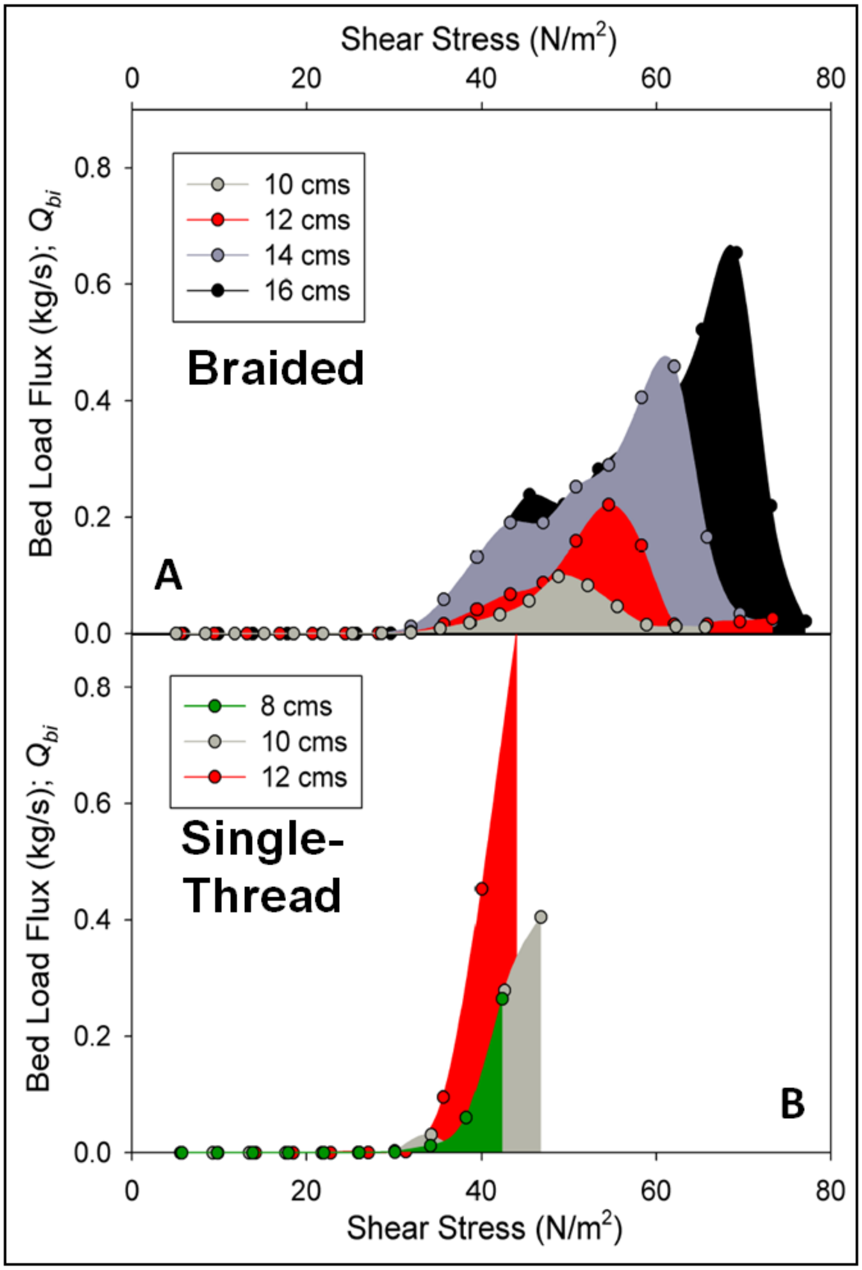

Figure 4.22. Modeled bed load flux as a function of shear stress for several discharges in braided versus single-thread reaches. The area under the curve is equivalent to the total bed load flux.

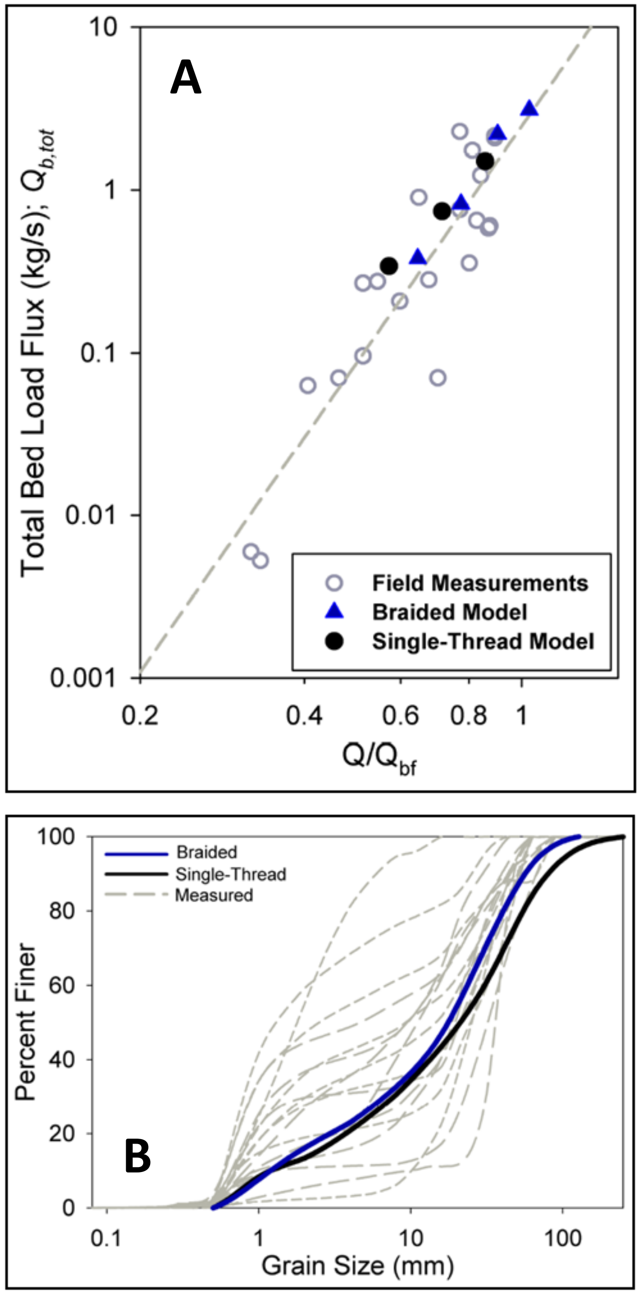

Figure 4.23. A) Modeled versus measured bed load flux. B) Modeled versus measured bed load median grain size.

subsurface hiding function, and consistent with the measured size similarity between bed load and subsurface bed material – particularly in the braided reach (Figure 4.16).

DISCUSSION

The results of this study confirm that sediment supply is a major factor dictating transitions between channel patterns, but that locally channel pattern may be strongly influenced by bank strength or related constriction by bedrock or alluvial fans. The unique erodibility and composition of Paleozoic conglomerates and Eocene volcaniclastic rocks contribute very high amounts of sediment to streams in the region, resulting in some of the highest bed load transport rates in the Rocky Mountains of the Western U.S and the relatively rare occurrence of braided channels. The bed material grain size varies considerably between these rock types, but braided reaches tend to be finer-grained or less armored than single-thread reaches at a given slope. In fact, braided streams in this region are not particularly steep as suggested by Leopold and Wolman (1957), but the grain size effect results in all of them plotting above the braiding criterion given in equation 4 with μ'=1 (Eaton et al., 2010). This general result is consistent with the classic Lane (1955) relation, whereby bed load flux can be expressed as:

$$Q_b \propto \frac{QS}{D} \qquad (19)$$

which is essentially:

$$Q_b \propto Q^* S \qquad (20)$$

but that Q* has a stronger dependence on grain size. It follows that streams with large Q* and steeper slopes should have higher bed load fluxes, and therefore plot higher on the Q*-S plot, as the braided streams do. While this linkage between sediment supply and channel pattern has long been implicit, here for the first time we present a single-thread – braided discriminant function based on sediment concentration, and verified with field data. The function presented in equation 16 is theoretically based in that it is based on equations for flow and sediment transport (Millar, 2005), coupled with an analytically derived stability criterion widely associated with braiding (w/h=50) (Eaton et al., 2010). Importantly, there is no definitive explanation as to why the optimization used by Millar (2005) is correct, and optimality theory has long been questioned (e.g. Griffiths, 1984); yet in light of the slope-minimization criterion used this approach provides a basis for a minimum slope or minimum concentration threshold.

Braided streams clearly discriminate from single-thread reaches based on sediment concentration, but the results also suggests that single-thread channels can absorb wide variations in sediment supply simply through changes in streambed sediment textures or bed state which enhance or limit sediment transport rates (e.g. Mueller and Pitlick, chapter 1; Dietrich et al., 1989). At some point, however, changes in bed sediment texture cannot counter-act the effects of ever increasing sediment supply (Eaton and Church, 2009), thereby leading to aggradation and channel steepening, and potentially the transition to a braided channel pattern. Eaton et al. (2010) discuss that the plotting position in Q*-S space likely reflects to a large degree the bed state (Church, 2006) whereby changes in sediment supply are reflected through fining and increased mobility. Field and flume studies have demonstrated this in the transient case, where as sediment supply is increased there is an associated fining of the surface material (increasing Q*), as well as aggradation and a potential increase in slope (Lisle and Church, 2002) or braiding (Marti and Bezzola, 2009; Pryor et al., 2011). Alternatively as sediment supply rate is stepped down, enhanced armoring is associated with degradation and a return to a single-thread pattern.

In Sunlight Creek transitions in channel pattern appear to be dominated by nature of sediment inputs from tributary fans, likely altering bank strength. Single-thread reaches are typically bound by coarse fan inputs, which inhibit widening by fortifying the banks and effectively increasing μ' in equation 4. These types of channel transitions due to bank strength have long been recognized for braided streams in New Zealand (Schumm, 1979; Carson, 1984b). But in Sunlight Creek the bed sediment also coarsens in single-thread reaches, implying reduced transport rates despite apparent sediment continuity with adjoining braided reaches. Part of the explanation could lie in the transient state of the bed during transport as in the above flume studies. As supply from upstream increases, the bed may become finer grained and smoother enhancing transport, but as flow wanes the bed is winnowed of fine material. As a result, surface pebble counts may not accurately reflect the bed state during transport events. Observations at both of our bed load sampling sites show strips of enhanced transport associated with the passage of bed load sheets much finer than the surface material. During high flows the bed of single-thread reaches became very mobile, particularly near the channel center, while near the banks coarser material remained intact. Recent flume studies have shown such a response is possible, where coarse inactive zones along the channel edges existed due to near-wall boundary shear stress reduction, even at the highest bed load transport rates (Nelson et al., 2009). Alternatively fine patches of stronger transport expanded and retracted in response to supply rate, linking both bank stability near the coarse boundary to grain size modulated sediment mobility in the thalweg (Nelson et al., 2009; Venditti et al., 2010).

Ultimately the transitional nature of channel pattern in Sunlight Creek is consistent with being near the braiding threshold. Both modeled and measured bed load fluxes suggest that near equilibrium sediment conveyance likely occurs between reach types, and the braided reach showed little net aggradation or degradation over three flood events. While bed load fluxes in single-thread reaches are modulated strongly by armoring or bed state, braided reaches are weakly armored and spatial variation in flow hydraulics comes to dominate the transport signal. Flow modeling supports this view and is consistent with previous workers, illustrating that braided channels exhibit an exponential or gamma stress distribution where the majority of sediment transport occurs over a very small portion of the bed. In this case, zones of intense transport can likely be maintained through channel migration, bar growth and dissection typical of braided streams and rivers (e.g. Ashmore, 1991).

These differences in flow hydraulics between reaches illustrates the importance of planform as a dominant degree of freedom in braided streams, and common approaches investigating stable channel form typically ignore the planform component (Griffiths, 1984). Thus while changes in bed state or channel slope are clearly important (as in equation 20), sediment flux from braided reaches does not follow from simple 1-D flow considerations. For example, the Toklat River in Alaska has a sediment concentration 10 times greater than other braided streams for a given Q*, but it is only twice as steep (Figure 4.12). In fact the experimental study of Ashworth et al. (2007) shows this exact result, whereby an order of magnitude increase in sediment supply only resulted in a doubling of slope, but a strong increase in the rate of avulsion and channelization. This follows from previous field and flume studies that show a similar correlation between the degree of braiding intensity and sediment supply (Germanoski and Schumm, 1993; Chew and Ashmore, 2001), where the nature of flow variability due to channel switching and migration may come to be at least as important as channel slope. As a result, any implications about sediment supply on Q*-S plots should perhaps be limited to single-thread reaches, and considerations of bed load flux from braided streams should focus on assessing spatial and temporal variations in flow properties (e.g. Nicholas, 2003; Bertoldi et al., 2009).

CONCLUSIONS

This study takes advantage of a unique opportunity, where the fundamental controls on channel pattern can be isolated in a broad area dominated by similar climate and measurements of bed load flux area available for more than 50 streams. While high sediment loads are an oft-cited characteristics of braided streams, here we quantify this component and present the first discriminant function for single-thread versus braided channels in terms of sediment concentration. From this perspective several general conclusions on regional braided channel formation are reached:

1. Braided streams in the greater Yellowstone region are associated with specific rock types that result in copious amounts of bed load sized material delivered to these streams. As a result, braiding is regionally common in these rock types, but generally absent from the rest of the Rocky Mountains in the western U.S., showing that persistent high supply from these particular lithologies is a prerequisite for braiding.

2. Discrimination of channel patterns is well achieved using the Eaton et al. (2010) function based on slope, discharge, grain size, and bank strength. Following that approach, we present a sediment concentration braiding – single-thread discriminant relation as a function of dimensionless discharge, appropriately classifying 50 of 53 pattern types. It is thus possible to quantify and verify a sediment supply threshold for pattern transitions that has remained largely out of reach.

3. Many of the braided reaches in this study appear to be near a sediment supply threshold and downstream changes in tributary grain size and bank strength have a strong influence on

longitudinal channel pattern. Nevertheless, modeling and measurements suggest sediment continuity is maintained between reach types, and that both represent equilibrium forms.

4. 2-dimensional variability in flow properties in braided reaches may become equal to or dominate over changes in slope in response to high sediment supply. The resilience of single-thread channels to sediment perturbations appears strongly dependent on the degree to which textural changes can modulate variations in sediment supply, but changes in channel planform provides a further mechanism whereby sediment transport capacity can adjust downstream through fluvial systems.

REFERENCES

Aalto, R., Dunne, T., and Guyot, J.L. 2006. Geomorphic controls on Andean denudation rates. *J. of Geology*, **114**: 85-99.

Ahnert, F. 1970. Functional relationships between denudation, relief, and uplift in large mid-latitude drainage basins. *Am. J. Sci.,* **268**: 243-263.

Andrews, E.D. 1984. Bed-material entrainment and hydraulic geometry of gravel-bed rivers in Colorado. *Geol. Soc. Am. Bull.*, **95**(3): 371-378.

Anisimov, O., van den Berg, J., Lovanov, V., and Kondratiev, A. 2008. Predicting changes in alluvial channel patterns in North-European Russia under conditions of global warming. *Geomorphology*, **98**: 262-274.

Ashmore, P. and Sauks, E. 2006. Prediction of discharge from water surface width in a braided river with implications for at-a-station hydraulic geometry. *Water Resources Research* **42**: W03406. DOI: 10.1029/2005WR003993

Ashmore, P.E. 1991. How do gravel-bed rivers braid? *Canadian Journal of Earth Sciences* **28**(3): 326-341.

Ashworth, P.J., Best, J.L. and Jones, M.A. 2007. The relationship between channel avulsion, flow occupancy and aggradation in braided rivers: insights from an experimental model. *Sedimentology*, **54**: 497-513.

Attal, M. and Lave, J. 2006. Changes of bedload characteristics along the Marsyandi River (central Nepal): Implications for understanding hillslope sediment supply, sediment load evolution along fluvial networks, and denudation in active orogenic belts. *in* Willett, S.D., Hovius, N., Brandon, M.T., and Fisher, D., eds., *Tectonics, Climate, and Landscape Evolution: Geological Society of America Special Paper 398*, doi: 10.1130/2006.2398(09), pp. 143–171.

Attal, M., and Lave, J. 2009. Pebble abrasion during fluvial transport: experimental results and implications for the evolution of the sediment load along rivers. *Journal of Geophysical Research*, **114**: F04023, doi:10.1029/2009JF001328.

Barton, G.J., McDonald, R.R., Nelson, J.M., and Dinehart, R.L. 2005. Simulation of flow and sediment mobility using a multidimensional flow model for the White Sturgeon critical-habitat reach, Kootenai River near Bonners Ferry, Idaho. *U.S. Geol. Surv. Scientific Investigations Report 2005-5230*, 54p.

Berenbrock, C. and Tranmer, A.W. 2008. Simulation of flow, sediment transport, and sediment mobility of the lower Coeur d'Alene River, Idaho. *U.S. Geol. Surv. Sci. Invest. Rep. 2008-5093*, 164 pp.

Bertoldi, W., Ashmore, P., and Tubino, M. 2009. A method for estimating the mean bed load flux in braided rivers. *Geomorphology* **103**: 330-340. DOI: 10.106/j.geomorph2008.06.014

Bertoldi, W., Zanoni, L., and Tubino, M. 2010. Assessment of morphological changes induced by flow and flood pulses in a gravel bed braided river: the Tagliamento River (Italy). *Geomorphology*, **114**: 348-360.

Bradley, W.C. 1970. Effect of weathering on abrasion of granitic gravel, Colorado River (Texas). *Geological Society of America Bulletin*, **81**: 61-80.

Braudrick, C.A., Dietrich, W.E., Leverich, G.T., and Sklar, L.S. 2009. Experimental evidence for the conditions necessary to sustain meandering in coarse-bedded rivers. *Proceedings of the National Academy of Sciences* **106**(40): 16,936-16,941. DOI: 10.1073/pnas.0909417106

Buffington, J. M., and Montgomery, D.R. 1999. Effects of sediment supply on surface textures of gravel-bed rivers. *Water Resour. Res*., **35**: 3523– 3530.

Carroll, A.R., Chetel, L.M., and Smith, M.E. 2006. Feast to famine: sediment supply control on Laramide basin fill. *Geology*, **34**: 197-200.

Carson, M.A. 1984a. The meandering-braided river threshold: a reappraisal. *Journal of Hydrology* **73**: 315–334.

Carson, M.A. 1984b. Observations on the meandering-braided river transition, the Canterbury Plains, New Zealand: Part one. *New Zealand Geographer,* **40**(1): 12-19.

Castro, J.M. and Jackson, P.L. 2001. Bankfull discharge recurrence intervals and regional hydraulic geometry relationships: patterns in the pacific northwest, USA. *J. Am. Wat. Res. Assoc.,* **37**(5): 1249-1262.

Charlton, F.G., Brown, P.M, and Benson, R.W. 1978. The hydraulic geometry of some gravel rivers in Britain. *Hydraulics Research Station Report*, **IT 180**, Wallingford, England.

Chatanantavet, P., Lajeunesse, E., Parker, G., and Malverti, L., 2010, Physically based model of downstream fining in bedrock streams with lateral input: Water Resources Research, v. 46, W02518, doi: 10.1029/2008WR007208.

Chetel, L.M., Janecke, S.U., Carroll, A.R., Beard, B.L., Johnson, C.M., and Singer, B.S. 2011. Paleogeographic reconstruction of the Eocene Idaho River, North American Cordillera. *Geological Society of America Bulletin*, **123**(1/2): 71-88, doi: 10.1130/B30213.1.

Chew, L.C. and Ashmore, P.E. 2001. Channel adjustment and a test of rational regime theory in a proglacial braided stream. *Geomorphology*, **37**: 43-63.

Church, M. 1992. Channel morphology and typology: *in* Carlow, P. and Petts, G.E., eds., *The Rivers Handbook*, p. 126-143, Blackwell Scientific Publications, Oxford.

Church, M. 2006. Bed material transport and the morphology of alluvial river channels. *Annu. Rev. Earth. Planet. Sci.*, **34**: 325-354.

Church, M. 2011. The Shields number is a granular bed state parameter. Abstract EP23D-05 presented at 2011 Fall Meeting, AGU, San Francisco, Calif., 5-9 Dec.

Church, M., D. Ham, M. Hassan, and O. Slaymaker. 1999. Fluvial clastic sediment yield in Canada: scaled analysis. *Canadian Journal of Earth Sciences*, **36**:1267-1280.

Church, M., D.G. McLean, and J.F. Wolcott.1987. River bed gravels: Sampling and analysis. In *Sediment Transport in Gravel-Bed Rivers*, edited by C.R. Thorne, J.C. Bathurst, and R.D. Hey, pp. 43-88, John Wiley, New York.

Church, M., Hassan, M. A. and Wolcott, J. F. 1998. Stabilizing self-organized structures in gravel-bed stream channels: Field and experimentalobservations. *Water Resour. Res*., **34**: 3169–3179.

Church, M., Kellerhals, R., and Day, T.J. 1989. Regional clastic sediment yield in British Columbia. *Canadian Journal of Earth Sciences*, **26**(1): 31-45.

Clark, G.M. and Woods, P.F. 2001. Transport of suspended and bedload sediment at eight stations in the Coeur d'Alene River basin, Idaho. *U.S. Geol. Surv. Water Open-File Rep., 00-472,* 26 pp.

Clayton, J.A. and Pitlick, J. 2007. Spatial and temporal variations in bed load transport intensity in a gravel bed river bend. *Water Resources Research* **43**, W02426, doi: 10.1029/2006WR005253.

Conaway, J.S. and Moran, E.H. 2004. Development and calibration of a two-dimensional hydrodynamic model of the Tanana River near Tok, Alaska. *U.S. Geol. Surv. Open File Report 2004-1225*, 13p.

Crosato, A., and Mosselman, E. 2009. Simple physics-based predictor for the number of river bars and the transition between meandering and braiding. *Water Resources Research* **45**(3), W03424. DOI:10.1029/2008WR007242

Curran, J.H., Meyer, D.F., and Tasker, G.D. 2003. Estimating the magnitude and frequency of peak streamflows for ungaged sites on streams in Alaska and conterminous basin in Canada. *U.S. Geol. Surv. Water Resour. Invest. Rep., 03-4188*, 101 p.

Davies, N.S. and Gibling, M.R. 2011. Evolution of fixed-channel alluvial plains in response to Carboniferous vegetation. *Nature Geoscience* **4**: 629-633. DOI: 10.1038/ngeo1237

Dethier, D. 2001. Pleistocene incision rates in the western United States calibrated using Lava Creek B tephra. *Geology,* **29**: 783-786.

Dietrich, W. E., Kirchner, J. W., Ikeda, H. and Iseya, F. 1989. Sediment supply and the development of the coarse surface layer in gravel-bedded rivers. *Nature*, **340**: 215– 217.

Digital Geology of Idaho, Idaho State University: geology.isu.edu/Digital_Geology_Idaho/. Accessed between 3/08-10/11.

Dühnforth, M., Densmore, A.L., Ivy-Ochs, S., and Allen, P.A. 2008. Controls on sediment evacuation from glacially modified and unmodified catchments in the eastern Sierra Nevada, California. *Earth Surface Processes and Landforms*, **33**(10): 1602-1613.

Eaton, B.C. and Church, M. 2007. Predicting downstream hydraulic geometry: a test of rational regime theory. *Journal of Geophysical Research*, **112**: F03025, doi: 10.1029/2006JF000734.

Eaton, B.C. and Church, M. 2009. Channel stability in bed load-dominated streams with nonerodible banks: inferences from experiments in a sinuous flume. *J. Geophys. Res.*, **144**, F01024.

Eaton, B.C., Church, M., and Millar, R.G. 2004. Rational regime model of alluvial channel morphology and response. *Earth Surf. Proc. Landforms*, **29**: 511-529.

Eaton, B.C., Millar, R.G., and Davidson, S. 2010. Channel patterns: Braided, anabranching, and single-thread. *Geomorph,.* **120**: 353-364.

Edwards, T.K. and Glysson, G.D. 1999. Field methods for measurement of fluvial sediment. In: *Techniques of Water-Resources Investigations of the U.S.Geological Survey, Book 3, Applications of Hydraulics*, Chapter C2, 89 p.

Emmett, W.W, Burrows, R.L., and Chacho, E.F. 1996. Coarse-particle transport in a gravel-bed river. *International Journal of Sediment Research* **11**(2): 8-21.

Emmett, W.W. and Wolman, M.G. 2001. Effective discharge and gravel-bed rivers. *Earth Surf. Process. Landforms*, **26**: 1369-1380.

Emmett,W.W. 1975. The channels and waters of the Upper Salmon River area, Idaho, U.S. Geological Survey Professional Paper 870-A, 116pp.

Erwin, S.O., Schmidt, J.C., and Nelson, N.C. 2011. Downstream effects of impounding a natural lake: the Snake River downstream from Jackson Lake Dam, Wyoming, USA. *Earth Surf. Process. Landforms,* 10.1002/esp.2159.

Ferguson, R. I. 2003. The missing dimension: Effects of lateral variation on 1-D calculations of fluvial bedload transport. *Geomorphology*, **56**: 1-14.

Ferguson, R., Hoey, T, Wathen, S., and Werritty, A. 1996. Field evidence for rapid downstream fining of river gravels through selective transport. *Geology*, **24**(2): 179-182.

Ferguson, R.I. (2012) River channel slope, flow resistance, and gravel entrainment thresholds. *Water Resources Research*, in press.

Ferguson, R.I. 1996. Hydraulics and hydraulic geometry. *Progress in Physical Geography*, **10**(1): 1-31.

Ferguson, R.I., Cudden, J.R., Hoey, T.B., and Rice, S.P. 2006. River system discontinuities due to lateral inputs: generic styles and controls. *Earth Surface Processes and Landforms*, **31**: 1149-1166, doi:10.1002/esp.1309.

Fredsoe, J. 1978. Meandering and braiding of rivers. *Journal of Fluid Mechanics* **84**(4): 609–624.

Germanoski, D. and Schumm, S.A. (1993) Changes in braided river morphology resulting from aggradation and degradation. *Journal of Geology*, **102**: 451-466.

Green, G.N., and Drouillard, P.H. 1994. The Digital Geologic Map of Wyoming in ARC/INFO Format. *U.S. Geol. Surv. Open-File Rep. 94-0425*.

Griffiths, G.A. 1983. Stable-channel design in alluvial rivers. *Journal of Hydrology*, **65**: 259-270.

Griffiths, G.A. 1984. Extremal hypotheses for river regime: an illustion of progress. *Water Resources Research,* **20**(1): 113-118.

Griffiths, G.A. 1989. Conversion of braided gravel-bed rivers to single-thread channels of equivalent transport capacity. *Journal of Hydrology (N.Z.)*, **28**(1): 63-75.

Harenberg, W.A. 1980. Using channel geometry to estimate flood flows at ungaged sites in Idaho. *U.S. Geological Survey Water Resour. Invest. Rep., 80-32*, 39 p.

Harrison, J.E. and Grimes, D.J. 1970. Mineralogy and geochemistry of some Belt rocks, Montana and Idaho. *U.S. Geol. Surv. Bull.*, **1312-0**, 49pp.

Harvey, A.M. 1991. The Influence of sediment supply on the channel morphology of upland streams: the Howgill Fells, northwest England. *Earth Surf. Processes Landforms* **16**: 675–684.

Harvey, A.M. 2001. Coupling between hillslopes and channels in upland fluvial systems: implications for landscape sensitivity, illustrated from the Howgill Fells, northwest England. *Catena* **42**: 225-250.

Hey, R.D. and Thorne, C.R. 1986. Stable channels with mobile gravel beds. *J. Hydraul. Div., ASCE*, **112**: 671–689.

Hoffman, D.F. and E.J.Gabet. 2007. Effects of sediment pulses on channel morphology in a gravel-bed river. *GSA Bulletin* **119**: 116-125.

Holnbeck, S.R. 2005. Sediment transport investigations of the Upper Yellowstone River, Montana, 1999 through 2001: Data collection, analysis, and simulation of sediment transport. *U.S. Geol. Surv.Sci. Invest. Rep. 2005-5234*, 69 pp.

Hortness, J.E. and Berenbrock, C. 2004. Estimating the magnitude of bankfull flows for streams in Idaho. *U.S. Geol. Surv. Water Resour. Invest. Rep., 03-4261*, 37 pp.

Horton, T.W., Chamberlain, C.P., Fantle, M., and Blum, J.D. 1999. Chemical weathering and lithologic controls of water chemistry in a high-elevation river system: Clark's Fork of the Yellowstone River, Wyoming and Montana. *Wat. Resour. Res.,* **35**: 1643-1655.

Jarrett, R.D. 1984. Hydraulics of high-gradient streams. *J. Hydraul. Eng.*, **110**: 1519-1539.

Jerolmack, D.J., Reitz, M.D., and Martin, R.L. 2011. Sorting out abrasion in a gypsum dune field. *Journal of Geophysical Research*, **116**: F02033, doi:10.1029/2010JF001821.

Jones, M. L. and Seitz, H.R. 1980. Sediment transport in the Snake and Clearwater Rivers in the vicinity of Lewiston, Idaho. *U.S. Geol. Surv. Open File Rep*., 80-690, 179 pp. (1980).

Kellerhals, R. , Neill, C.R., and Bray, D.I. 1972. Hydraulic and geomorphic characteristics of rivers in Alberta. *River Engineering and Surface Hydrology Rep.*, **72-1**, Research Council of Alberta, Canada.

King, J. G., Emmett, W.W., Whiting, P.J, Kenworthy, R.P., and Barry, J.J. 2004. Sediment transport data and related information for selected coarse-bed streams and rivers in Idaho. *U.S. Forest Service Gen. Tech. Rep. RMRS-GTR 131*, 26 pp.

Kirchner, J.W. et al. 2001. Mountain erosion over 10 yr, 10 k.y., and 10 m.y. time scales. *Geology*, **29**: 591-594.

Kirchner, J.W., Dietrich, W.E., Iseya, F. and Ikeda, H. 1990. The variability of critical shear stress, friction angle, and grain protrusion in water-worked sediments. *Sedimentology*, **37**: 647-672.

Kleinhans, M.G. 2010. Sorting out river channel patterns. *Progress in Physical Geography,* **34(**3): 287-326.

Kleinhans, M.G. and van den Berg, J.H. 2010. River channel and bar patterns explained and predicted by an empirical and a physics-based method. *Earth Surface Processes and Landforms*, **36**(6): 721-738.

Knighton, A.D. 1998. Fluvial Forms and Processes - a new perspective. Arnold, London, 383 pp.

Kodama,Y. 1994. Downstream changes in the lithology and grain size of fluvial gravels, the Watarase River, Japan: evidence of the role of abrasion in downstream fining. *Journal of Sedimentary Research*, **A64**(1): 68–75.

Kondolf, G.M., Piegay, H., and Landon, N. 2002. Channel response to increased and decreased bedload supply from land use change: contrasts between two catchments. *Geomorph.*, **45**, 35-51.

Krumbein, W.C. 1941. The effects of abrasion on the size, shape and roundness of rock fragments. *The Journal of Geology*, **49**(5): 482-520.

Kuelegan, G.H. 1938. Laws of turbulent flow in open channels. *J. Res. Natl. Bur. Stand.*, **21**: 707-741.

Kuelegan, G.H. 1938. Laws of turbulent flow in open channels. *J. Res. Natl. Bur. Stand.*, **21**: 707-741.

Lamb, M.P., Dietrich, W.E., and Venditti, G. 2008. Is the critical Shields stress for incipient motion dependent on channel-bed slope? *Journal of Geophysical Research*, **113**: F02008, doi: 10.1029/2007JF000831.

Lane, S. 1955. The importance of fluvial morphology in hydraulic engineering. *Proc. Am. Soc. Civ. Eng*., **81**, Paper 745.

Lawlor, S, M. 2004. Determination of channel-morphology characteristics, bankfull discharge, and various design-peak discharges in western Montana. *U.S. Geological Survey Scientific Investigations Report 2004-5263*, 19p.

Legleiter, C., Lawrence, R.L., Fonstand, M.A., Marcus, W.A., and Aspinall, R. 2003. Fluvial response a decade after wildfire in the northern Yellowstone ecosystem: a spatially explicit analysis. *Geomorphology*, **54**: 119-136.

Legleiter, C.J., Harrison, L.R., and Dunne, T. 2011b. Effect of point bar development on the local force balance governing flow in a simple, meandering gravel bed river. *Journal of Geophysical Research*, **116**, F01005, doi 10.1029/2010JF001838.

Legleiter, C.J., Kyriakidis, P.C., McDonald, R.R., and Nelson, J.M. 2011a. Effects of uncertain topographic input data on two-dimensional flow modeling in a gravel-bed river. *Water Resources Resarch*, **47**, W03518, doi: 10.1029/2010WR009618.

Leopold, L.B. and Maddock, T. Jr. 1953. The hydraulic geometry of stream channels and some physiographic implications, *U.S. Geological Survey Professional Paper 252*, 57p.

Leopold, L.B. and Wolman, M.G. 1957. River channel patterns: braided, meandering, and straight. *U.S. Geol. Surv. Prof. Paper 282-B*, 51p.

Leopold, L.B., Wolman, M.G. and Miller, J.P. 1964. Fluvial Processes in Geomorphology. New York: W. H. Freeman & Co.

Lewin, J. and Brewer, P.A. 2001. Predicting channel patterns, *Geomorphology*, **40**: 329-339.

Lewin, J. and Brewer, P.A. 2002. Laboratory simulation of clast abrasion. *Earth Surface Processes and Landforms*, **27**: 145-164.

Link, P.K. and Hackett, W.R., eds. 1988. Guidebook to the Geology of Central and Southern Idaho. *Idaho Geological Survey Bulletin*, **27**: 319pp.

Lisle, T.E. 1995. Particle size variations between bed load and bed material in natural gravel bed channels. *Water Resources Research*, **31**: 1107-1118.

Lisle, T.E. and M. Church. 2002. Sediment transport-storage relations for degrading, gravel bed channels, *Water Resour. Res.*, **38**: 1219, doi:10.1029/2001WR001086.

Logan, B.L., McDonald, R.R., Nelson, J.M., Kinzel, PJ., and Barton, G.J. 2011. Use of multidimensional modeling to evaluate a channel restoration design for the Kootenai River, Idaho. *U.S. Geol. Surv. Scientific Investigations Report 2010-5213*, 68p.

Love, J.D. 1973. Harebell Formation (Upper Cretaceous) and Pinyon Conglomerate (uppermost Cretaceous and Paleocene), northwestern Wyoming. *U.S. Geol. Surv. Prof. Paper 734-A*, 53pp.

Love, J.D., and Christiansen, A.C. 1985. Geologic Map of Wyoming: U.S. Geological Survey Special Geologic Map, scale 1:500,000.

Madej, M.A., Sutherland, D.G., Lisle, T.E. and Pryor, B. 2009. Channel responses to varying sediment input: A flume experiment modeled after Redwood Creek California. *Geomorphology*, **103**: 507-519.

Marti, C. and Bezzola, G.R. 2009. Bed load transport in braided gravel-bed rivers. In *Braided Rivers: Process, Deposits, Ecology and Management*, Sambrook-Smith, G.H., Best, J.L., Bristow, C.S., Petts, G.E., and Jarvis, I. Eds. John Wiley and Sons.

Matmon, A. *et al*. 2003. Erosion of an ancient mountain range, the Great Smoky Mountains, North Carolina and Tennessee. *Am. J. Sci*. **303**: 817– 855.

Megahan W.F., Potyondy J.P. and Seyedbagheri K.A. 1992. In *Watershed Management: Balancing Sustainability and Environmental Change*, R.J. Naiman, ed. Springer-Verlag, New York, pp. 401–414.

Métivier, F. and Barrier, L. 2012. Alluvial landscape evolution: what do we know about metamorphosis of gravel-bed meandering and braided streams. In *Gravel-bed Rivers: Processes, Tools, Environments*, Church, M., Biron, P.M., and Roy, A. Eds. John Wiley and Sons.

Meyer, G.A. and Leidecker, M.E. 1999. In *Guidebook to the Geology of Eastern Idaho*. Hughes, S.S. and Thackray, G. D., eds., Idaho Mus. of Nat. Hist., Pocatello, pp. 219– 235.

Meyer, G.A., Pierce, J.L., Wood, S.H., and Jull, A.J.T. 2001. Fire, storms, and erosional events in the Idaho batholiths. *Hydrol. Proc.,* **15**, 3025-3038.

Millar, R.G. 2005. Theoretical regime equations for mobile gravel-bed rivers with stable banks. *Geomorphology* **64**: 207–220.

Millar, R.G. and Quick, M.C. 1998. Stable width and depth of gravel-bed rivers with cohesive banks. *Journal of Hydraulic* Engineering, 124(10): 1005-1013.

Miller, K.A. 2003. Peak-flow characteristics of Wyoming streams. *U.S. Geol. Surv. Water Resour. Invest. Rep., 03-4107*, 79 pp.

Montgomery, D.R. and Brandon, M.T. 2002. Topographic controls on erosion rates in tectonically active mountain ranges. *Earth Planet. Sc. Lett.,* **201**: 481-489.

Moon, S. et al. 2011. Climatic control of denudation in the deglaciated landscape of the Washington Cascades. *Nature Geosci.,* **4**: 469-473.

Morel, P., von Blanckenburg, F., Schaller, M., Kubik, P.W. and Hinderer, M. 2003. Lithology, landscape dissection and glaciations controls on catchment erosion as determined by cosmogenic nuclides in river sediment (the Wutach Gorge, Black Forest). *Terra Nova* **15**: 398-404.

Mueller, E. R., Pitlick, J. and Nelson. J. M. 2005. Variation in the reference Shields stress for bed load transport in gravel-bed streams and rivers. *Water Resources Research*, **41**: W04006, doi:10.1029/2004WR003692.

Mueller, E.R. and Pitlick, J. 2005. Morphologically based model of bed load transport capacity in a headwater stream. Journal of Geophysical Research - Earth Surface, **110**: F02016, doi:10.1029/2003JF000117.

Murray, A.B. and Paola, C. 2003. Modelling the effect of vegetation on channel pattern in bedload rivers. *Earth Surface Processes and Landforms* **28**: 131-143.

Nanson, G.C. and A.D. Knighton.1996. Anabranching rivers: their cause, character and classification, *Earth Surface Processes and Landforms* **21**: 217-239.

Nelson, J. M., J. P. Bennett, and S. M. Wiele. 2003. Flow and sediment transport modeling, in Tools in Fluvial Geomorphology, edited by G. M. Kondolf and H. Piegay, pp. 539–576, John Wiley, Hoboken, N. J.

Nelson, P.A., Venditti, J.G., Dietrich, W.E., Kirchner, J.W., Ikeda, H., Iseya, F., and Sklar, L.S. 2009. Response of bed surface patchiness to reductions in sediment supply. *Journal of Geophysical Research*, **114**, F02005, doi: 10.1029/2008JF001144.

Nelson, W.H. & Pierce, W.G. 1968. Wapiti formation and Trout Peak trachyandesite northwestern Wyoming. *U.S. Geol. Surv. Bull. 1254-H*, H1-H11.

Nicholas, A.P. 2000. Modelling bedload yield in braided gravel bed rivers. *Geomorphology* **36**: 89-106.

Nicholas, A.P. 2003. Investigation of spatially distributed braided river flows using a two-dimensional hydraulic model, *Earth Surf. Proc. Landforms*, **28**: 655-674.

Osterkamp, W.R. 1978. Gradient, discharge, and particle-size relations of alluvial channels in Kansas, with observations on braiding. *American Journal of Science*, **278**: 1253-1268.

Paola, C. 1996. Incoherent structure: Turbulence as a metaphor for stream braiding, In *Coherent Flow Structures in Open Channel Flows*, Ashworth PJ, Bennett SJ, Best JL, McLelland SJ (eds), Wiley: Chichester, 705–723.

Park, C.C. 1977. World-wide variations in hydraulic geometry exponents of stream channels: an analysis and some observations. Journal of Hydrology, **33**: 133-146.

Parker, G, Wilcock, P.R., Paola, C., Dietrich, W.E., and J. Pitlick, J. 2008. Physical basis for quasi-universal relations describing bankfull hydraulic geometry of single-thread gravel bed rivers. *Journal of Geophysical Research*, **112**: F04005, doi:10.1029/2006JF000549.

Parker, G. 1976. On the cause and characteristic scales of meandering and braiding in rivers. *J. Fluid Mech.* **76**, 457– 478.

Parker, G. 1978. Self formed rivers with stable banks and mobile bed: Part II, the gravel river. *J. Fluid Mech.*, **89**(1): 27– 148.

Parker, G. 1979. Hydraulic geometry of active gravel rivers. *Journal of the Hydraulics Division, Am. Soc. Civ. Eng.*, **105**: 1185– 1201.

Parker, G. 1990. Surface-based bedload transport relation for gravel rivers, *J. Hyd. Res.*, **28**: 417-435.

Parker, G. 1991. Selective sorting and abrasion of river gravel. I: theory. *Journal of Hydraulic Engineering*, **117**(2): 131-149.

Parker, G., and Klingeman, P.C. 1982. On why gravel bed streams are paved, *Water Resources Research*, **18**(5): 1409-1423.

Parrett, C. and Johnson, D.R. 2004. Methods for estimating the flood frequency in Montana based on data through water year 1998. U.S. Geol. Surv. Water Resour. Invest. Rep., 03-4308, 101 pp.

Pelton, J. R., and R. B. Smith. 1982. Contemporary vertical surface displacements in Yellowstone National Park, *J. Geophys. Res.*, **87**(B4): 2745–2761.

Perg, L.A., Anderson, R.S., and Finkel, R.C. 2003. Use of cosmogenic radionuclides as a sediment tracer in the Santa Cruz littoral cell, California, USA. *Geology*, **31**(4): 299-302.

Pierce, K.L. & Morgan, L.A. 1992. The track of the Yellowstone hot spot–volcanism, faulting and uplift. *Geol. Soc. Am. Mem.* **179**: 1–53.

Pierce, K.L. 2003. Pleistocene glaciations of the Rocky Mountains. *Dev. Quat. Sci.* **1**: 63-76.

Pierce, K.L. and Morgan, L.A. 1992. The track of the Yellowstone hot spot–volcanism, faulting and uplift. *Geol. Soc. Am. Mem.,* **179**: 1–53.

Pitlick, J. and Cress, R. 2002. Downstream changes in the channel geometry of a large gravel bed river. *Water Resour. Res.*, **38**: 1216, doi:10.1029/2001WR000898.

Pitlick, J., Mueller, E.R., and Segura, C. 2012. Differences in sediment supply to braided and single-thread channels: what do the data tell us? Chapter 35 in *Gravel-bed Rivers:*

Processes, Tools, Environments, Church, M., Biron, P.M., and Roy, A. Eds. John Wiley and Sons.

Pitlick, J., Mueller, E.R., Segura-Sossa, C., Cress, C., and Torizzo, M. 2008. Relation between flow, surface-layer armoring, and sediment transport in gravel-bed rivers. *Earth Surface Processes and Landforms*, doi: 10.1002/esp.1607.

Pizzuto J. 1992. The morphology of graded gravel rivers: a network perspective. *Geomorphology*, **5**: 457-474.

Pizzuto, J.E. 1995. Downstream fining in a network of gravel-bedded rivers. *Water Resources Research*, **31**: 753-759.

Portenga, E.W. and Bierman, P.R. 2011. Understanding Earth's eroding surface with ^{10}Be. *GSA Today,* **21**: 4-10.

Pryor, B.S., Lisle, T., Sutherland Montoya, D., and Hilton, S. 2011. Transport and storage of bed material in a gravel-bed channel during episodes of aggradation and degradation: a field and flume study. *Earth Surface Processes and Landforms*, doi: 10.1002/esp.2224

Recking, A. 2009. Theoretical development on the effects of changing flow hydraulics on incipient bed motion. *Water Resources Research*, **45**: W04401.

Rice, S. 1999. The nature and controls of downstream fining within sedimentary links. *Journal of Sedimentary Research*, **69**: 32-39.

Ryan, S. E., and Emmett, W.W. 2002. The nature of flow and sediment movement in Little Granite Creek near Bondurant, Wyoming. *U.S. Forest Service Gen. Tech. Rep. RMRS-GTR-90*, 48 pp.

Ryan, S.E. 2007. The role of geology in sediment supply and bedload transport patterns in coarse grained streams. In *Advancing the Fundamental Sciences: Proceedings of the Forest Service National Earth Sciences Conference*. Furniss, M., Clifton, C., and Ronnenberg, K. Eds. PNW-GTR-689, 383-390, U.S. Department of Agriculture, Forest Service, Portland, OR.

Ryan, S.E., Porth, L.S., and Troendle, C.A. 2005. Coarse sediment transport in mountain streams in Colorado and Wyoming, USA. *Earth Surface Processes and Landforms*, **30**: 269-288.

Schaller, M., von Blanckenburg, F., Hovius, N., and Kubik P.W. 2001. Large-scale erosion rates from in situ-produced cosmogenic nuclides in European river sediments. *Earth Planet. Sci. Lett.,* **188**: 441-458.

Schiefer, E., Slaymaker, O., and Klinkenberg, B. 2001. Physiographically controlled allometry of specific sediment yield in the Canadian Cordillera: a lake sediment-based approach. *Geogr. Ann.*, **83** A(1-2): 55-65.

Schumm, S.A. 1963. The disparity between present rates of denudation and orogeny. *U.S. Geol. Surv. Prof. Paper 454-H*, 13pp.

Schumm, S.A. 1979. Geomorphic thresholds: the concept and its applications. *Transactions of the Institute of British Geographers,* **4**(4): 485-515.

Schumm, S.A. 1985. Patterns of alluvial rivers. *Annual Review of Earth and Planetary Sciences,* **13**: 5–27.

Segura C. 2008. Effects of sediment transport on benthic organisms in a mountain river, CO. Dissertation, University of Colorado, Boulder, CO; 176 pp.

Segura, C., McCutchan, J.H., Lewis, W.H. Jr., and Pitlick, J. 2011. The influence of channel bed disturbance on algal biomass in a Colorado mountain stream. *Ecohydrology*, **4**(3): 411-421.

Sklar, L.S., Dietrich, W.E., Foufoula-Georgiou, E., Lashermes, B., and Bellugi, D. 2006. Do gravel bed river size distributions record channel network structure? *Water Resources Research*, **42**: W06D18, doi:10.1029/2006WR005035.

Smith, N.D. and Smith, D.G. 1984. William River: An outstanding example of channel widening and braiding caused by bed-load addition. *Geology* **12**: 78-82.

Sternberg, H. 1875. Untersuchungen Über Längen-und Querprofil feschiebeführender Flüsse, *Zeitschrift für Bauwesen*, **25**: 483-506.

Syvitski, J. P. M. and Milliman, J.D. 2007. Geology, geography, and humans battle for dominance over the delivery of fluvial sediment to the coastal ocean. *J. Geology*, **115**: 1-19.

Syvitski, J. P. M. and Milliman, J.D. 2007. Geology, geography, and humans battle for dominance over the delivery of fluvial sediment to the coastal ocean. *J. Geol.,* **115**: 1-19.

Tal, M. and C. Paola. 2007. Dynamic single-thread channels maintained by the interaction of flow and vegetation. *Geology* **35**(4): 347-350. DOI: 10.1130/G23260A.1

Thompson, S.M. 1985. Transport of gravel by flows up to 500 m^3/s, Ohau River, Otago, New Zealand. *Journal of Hyraulic Research* **23**(3): 285-303.

Torizzo, M. and J. Pitlick, J. 2004. Magnitude-frequency of bed load transport in mountain streams in Colorado. *J. of Hydrology*, **290**: 137-151.

Tucker, G.E. and Slingerland, R.S. 2006. Predicting sediment flux from fold and thrust belts. *Basin Research,* **8**: 329-349.

Tunnicliffe, J., Hicks, D.M., Walsh, J., and Duncan, M. 2010. Parameterising spatial variability in shear stress and bed-surface grain size in braided channels. Gravel Bed Rivers VII, Tadoussac, Quebec, Canada.

Turowski, J.M., Rickenmann, D., and Dadson, S.J. 2010. The partitioning of the total sediment load of a river into suspended load and bedload: a review of empirical data. *Sedimentology*, **57**: 1126-1146.

U.S. Geological Survey National Water Information System (NWIS) raw discharge and sediment transport data. Accessed between 1/2008-7/2011.

van den Berg, J.H. 1995. Prediction of alluvial channel pattern of perennial rivers. *Geomorphology* **12**: 259-279.

Venditti, J.G., Dietrich, W.E., Nelson, P.A., Wydzga, M.A., Fadde, J., and Sklar, L. 2010. Effect of sediment pulse grain size on sediment transport rates and bed mobility in gravel bed rivers. *Journal of Geophysical Research*, **115**, F03039, doi: 10.1029/2009JF001418.

von Blanckenburg, F. 2006. The control mechanisms of erosion and weathering at basin scale from cosmogenic nuclides in river sediment. *Earth Planet. Sci. Lett*., **242**: 224-239.

Walling, D.E. 1983. The sediment delivery problem. *Journal of Hydrology*, **65**: 209-237.

White, W. R., Bettess, R. and Paris, E. 1982. Analytical approach to river regime. *Journal of the Hydraulics Division*, Proceedings of ASCE, **108(**HY10): 1179-1193.

Whiting, P.J. and Dietrich, W.E. 1990. Boundary shear stress and roughness over mobile alluvial beds. *J. Hydraul. Div. Am. Soc. Civ. Eng.*, **116**: 1495-1511.

Whiting, P.J., Stamm, J.F., Moog, D.B., and Orndorff, R.L. 1999. Sediment-transporting flows in headwater streams. *GSA Bulletin*, **111**(3): 450-466.

Wiberg, P.L. and Smith, J.D. 1991. Velocity distribution and bed-roughness in high-gradient streams. *Water Resour. Res*., **27**: 825-838.

Wilcock, P.R. and Crowe, J.C. 2003. Surface-based transport model for mixed-size sediment, *J. Hyd. Eng.*, **129**(2): 120-128.

Williams, G. P., and D. L. Rosgen. 1989. Measured total sediment loads (suspended loads and bedloads) for 93 United States streams. *U.S. Geol. Surv. Open File Rep. 89-67*, 128 p.

Williams, R.P and Krupin, P.J. 1984. Erosion, channel change, and sediment transport in the Big Lost River, Idaho. *U.S. Geol. Surv. Water Resour. Invest. Rep., 84-4147*, 87 p.

Wolman, M.G. 1954. A method of sampling coarse river-bed material, *Trans. Amer. Geophys. Union, 35*, 951-956.

Wolman, M.G. and Miller, J.P. 1960. Magnitude and frequency of forces in geomorphic processes. *J. Geol.*, **68**: 54-74.

Worl, R.G., Link, P.K., Winkler, G.R., and Johnson, K.M., eds. 1995. Geology and mineral resources of the Hailey 1º x 2º quadrangle and western part of the Idaho Falls 1º x 2º quadrangle, Idaho. *U.S. Geological Survey Bulletin 2064-C.*

Zelt, R.B. 2001. Channel characteristics and large organic debris in adjacent burned and unburned watersheds a decade after wildfire. *Proc. 7th Federal Interagency Sedimentation Conference, Reno, NV*, X-57-64.

Zelt, R.B. and Wohl, E.E. 2004. Channel and woody debris characteristics in adjacent burned and unburned watersheds a decade after wildfire, Park County, Wyoming. *Geomorphology*, **57**: 217-233.

Zienteck et al. 2005. Spatial databases for the geology of the Northern Rocky Mountains – Idaho, Montana, and Washington. *U.S. Geological Survey Open-File Report 2005-1235*.